

Factors Governing Accumulation of
Oil and Gas in Stratigraphic Traps

Thesis by
L. de Witte

In Partial Fulfillment of the Requirements
for the Degree of Doctor of Philosophy

California Institute of Technology

Pasadena

1950

ACKNOWLEDGMENTS

The author wishes to make acknowledgments to:

Dr. J. P. Buwalda, who supervised the research work on this project.

Dr. G. W. Potapenko for suggestions on the writing of the thesis.

Mr. R. von Huene and Mr. W. J. P. Otto for valuable aid in the preparation of the samples.

Mr. E. Offeman of the Baroid Sales Division, in Los Angeles, for lending several pieces of Baroid equipment for use in the experiments carried out.

ABSTRACT

This thesis is a study of those characteristics of sedimentary rocks, that determine their capability to function as cap rocks for petroleum accumulations.

The function of the cap rock is to prevent the oil from upward migration. The active upward forces on the oil (or gas) are due to the buoyancy of the oil (or gas) on water. The forces opposing upward migration of the oil are due to the capillary retention of the water in the cap rock. For any oil trap it is necessary that the capillary forces in the cap rock are larger than the buoyancy of the accumulating oil on the subsurface waters.

For a given combination of oil or gas and subsurface water, the magnitude of the capillary retention forces on the water in the cap rock is given by the displacement pressure of that rock.

An outline is given of the theories, relating the displacement pressure to the basic characteristics of the rock, such as permeability, porosity, interstitial surface area and the Kozeny constant.

The displacement pressure for a given rock is directly proportional to the interfacial tension between the water and the non-wetting phase. The buoyancy of the oil or gas on the water depends upon the density difference between the non-wetting phase and the water. The variations of densities and interfacial tensions with temperature and pressure are discussed and graphical relations are given between these quantities and the depth of the accumulation in question.

Displacement pressures for various types of sandstones were determined from experimental studies of the capillary pressure versus saturation relationships. From the experimentally determined

displacement pressures, permeabilities and porosities, the interstitial surface area and the Kozeny constants for the various rocks were computed.

It was found that the interstitial surface areas could be correlated with the electrochemical formation coefficients of the sediments in question, which were measured in the course of another research project by this author. This correlation indicates the possibility of a subsurface method for the determination of displacement pressures, using the S. P. curves of electrologs.

Different types of stratigraphic traps are described and the relative positions of the cap rocks are considered for the various cases.

A schematic example is given of the location of a "permeability pinch-out" type of stratigraphic trap by computation of the displacement pressures from electrologs of drill holes in the vicinity.

TABLE OF CONTENTS

<u>PART</u>	<u>TITLE</u>	<u>PAGE</u>
	Acknowledgments	
	Abstract	
	Introduction	1
I	Migration and accumulation of oil in general	3
II	Theoretical considerations on the migration of oil into a porous medium, completely saturated with water	9
III	Densities of oil and gas. Oil-water and oil-gas interfacial tensions	25
IV	Experimental procedure	32
V	Description of samples and experimental results	36
VI	Applications of subsurface determinations of displacement pressures	45
	References	49

INTRODUCTION

The purpose of this thesis is to investigate some of the inherent characteristics of sediments which enable them to become caprocks, for trapped accumulations of oil and gas.

We assume that in the geologic history of most commercial-size oil pools the source rock, carrier bed, reservoir rock and trap relationship exists. However, regardless of whether the oil migrated as such or whether organic fluids accumulated in the trap and the final stages of conversion to oil, occurred in the same places where the oil now is found, the requirements for the caprock to initially block the passage of oil or to keep the oil in place after it was formed, will be essentially the same.

In structural oil traps the relations between reservoir rocks and caprock are often relatively simple. Where structural closure exists, mostly a large thickness of beds has been involved in the formation of the structure. In the vertical succession of beds, sooner or later a bed with the necessary properties to act as caprock, will be present. This is especially true for the anticlinal or dome shaped structures with quaquaversal dips. For fault traps, the problem of finding suitable caprocks on all sides of the structure already is far more complicated, unless the fault gauge zones are "tight" enough to retain the oil. Our analysis may then be applied to the fault zone to find whether or not this is the case.

The most interesting application of analysis of sediments on their suitability to serve as caprocks, is to the case of stratigraphic traps. The types of stratigraphic traps (see later) vary from truncated strata and depositional pinch-outs, where trapping of oil depends upon the properties of the overlying or adjoining rocks, to the permeability

pinch-out type where the oil is retained by changes in the reservoir rock itself.

In classifying rocks as to their ability to serve as caprocks, it is obvious that layers with absolutely no permeability will always serve effectively to retain oil.

By and large the greatest number of caprocks, however, is of a different type. These rocks will be permeable to water, although their specific permeability may be low. In addition, they will be preferentially water wetted and because of their capillary retention of water, they will resist displacement of water by a non-wetting phase. Thus when 100% water wetted they will block the passage of oil, until the pressure of the oil overcomes the capillary forces retaining the water. Practically all sediments, even unconsolidated sandstones, have such a "threshold pressure," or "displacement pressure." In most cases, however, this pressure is very low and is soon offset by the buoyancy of the oil. Only rocks with a high enough displacement pressure to withstand the buoyancy caused by columns of tenths or hundreds of feet of oil will be effective as caprocks for commercial accumulations of oil or gas.

In this thesis an outline is given of the theory of capillary behavior of porous solids, relating the displacement pressures to some of the basic characteristics of the porous rocks, and experimental attempts are made to correlate some of these properties in order to enable us to determine the displacement pressure by sub-surface geological methods.

PART IMigration and accumulation of oil in general

In this work we will accept the general idea of a source rock - carrier bed - trap relationship in the history of the formation of the larger part of the commercial oil pools.

The most likely source beds are dark shales or marls and in some cases, bituminous limestones. This has been demonstrated both on grounds of their organic content and their frequent relationships to commercial oil accumulations. It is recognized, however, that not all dark shales or marls are actual source beds (1).

From the shales the oil is driven into the more permeable carrier beds by compaction. Beckstrom and van Tuyl (2) demonstrated conclusively that compaction is a completely effective means of removing oil from shales. Actual migration of oil from shales into sandstones was shown experimentally by E. T. Thomas (3), who also brought out the following important conclusions: (a) Oil moves more readily into water wetted, than into dry sand; (b) Oil moves fastest in the direction of greatest pressure decline (this is, in most cases, upward). The mechanism of the migration of the oil from the source beds into the more permeable sands is based on the differential compaction. While sandstones will decrease only 2% in volume, due to a burial to a depth of 4000 feet, a clay will lose close to 45% of its original volume for the same depth of burial. A detailed description of shale compaction with depth of burial was given by Athy (4). The squeezing out of oil by compaction pre-assumes that the oil is formed as such before too great a depth of burial is reached and the larger part of compaction has taken place.

An alternative hypothesis was formulated by Fash (5), namely, that the formation of oil is not completed and only a preliminary product, neokerogen, has been formed by the time squeezing by compaction has stopped. This neokerogen reaches the porous media in a decomposed, partly gaseous stage and disperses in all directions, "travelling as films on the surfaces of the sedimentary particles and along crystal surfaces inside the particles and accumulate in traps, where they are subjected to the catalytic effect of the surfaces of the sediments, with which they are in contact." In the trap the main transformation to petroleum occurs.

It is not clear what factors govern the accumulation of the decomposition products in traps, in other words, what kind of traps would be required to halt the migration of the films, on the surfaces and through the crystal-lattices of the sedimentary particles.

We will therefore only work with the assumption that oil as such, or a very similar product, reaches the porous media mainly in the liquid state, after being squeezed out of the shales by compaction.

The reasons for assuming the oil to be mainly in the liquid state were summarized by Russell (6) who compared rock pressures and temperatures at depth with the vapour pressures of the various hydrocarbon compounds usually present in oil. Russell showed that for the oil fractions to occur as vapours in appreciable quantities they must be above their critical temperatures, and even then a large portion would remain dissolved in the liquid, heavier fractions.

There is, however, no important qualitative difference between the migration and accumulation of oil, and that of gas.

The migration of oil to its final place of accumulation has been the subject of many papers and discussions and also of considerable

experimentation, of which some of the most important ones will be referred to later.

The most widely accepted idea of oil migration is the hydraulic theory as described most thoroughly by J. L. Rich (7,8).

This theory postulates moving underground water as the primary cause of the migration of oil and gas. The migration may take place either directly in the porous reservoir rock to the place where the oil is trapped, or through so-called carrier beds, which are very permeable horizons between the source and the place where the oil is found (9).

The hydraulic theory, although closely fitting the field evidence in many cases, is liable to convey a physical misconception, namely, that the moving water is carrying the oil or forcing it ahead of it. A more correct picture is that the oil and gas, as well as the water, are all moving under the same pressure gradient. This pressure gradient may be due to differences in hydrostatic head of the underground water or to lateral differences in compaction or any other cause. Once a pressure gradient is established, all fluids will move at velocities corresponding to the relative permeabilities, to the different fluids, which again depend on their partial saturations.

The relationships of relative permeabilities to saturation for liquid-gas mixtures were established by Wyckoff and Botset (10), and for oil-water mixtures by Leverett (11) for the case of unconsolidated sands. Leverett and Lewis (12) worked out the relations for gas-oil-water mixtures also for unconsolidated sands, while Botset (13) found that for gas-liquid mixtures the flow through consolidated sand gave very nearly the same characteristics.

Fig. 1 gives the saturation - relative permeability relationship

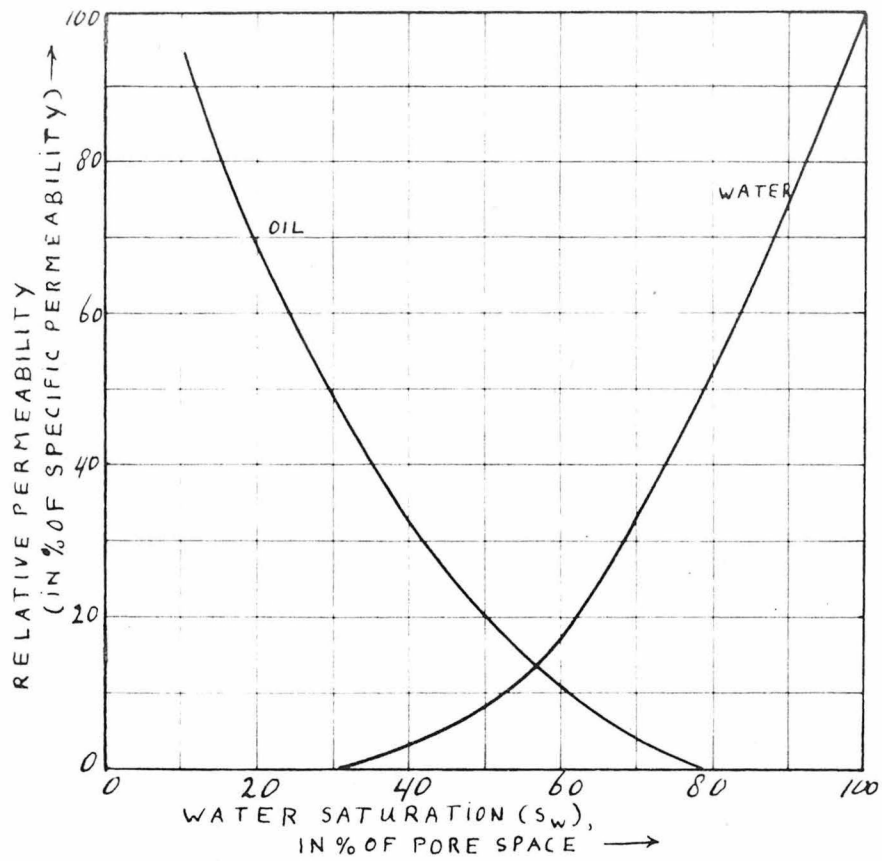


Fig. 1 (LEVERETT, 1939)

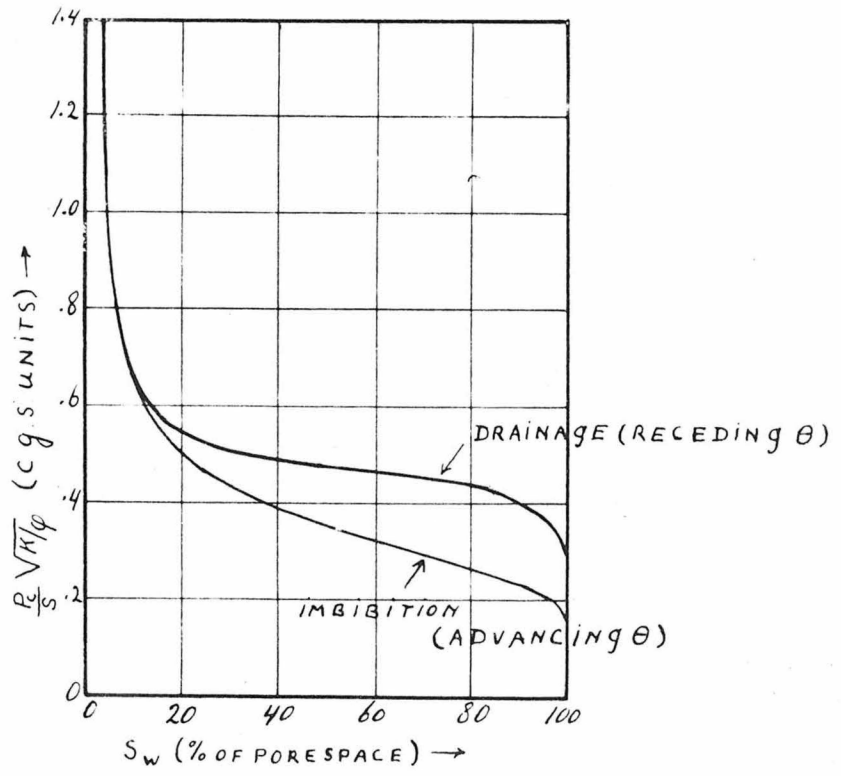


Fig. 2 (LEVERETT, 1941)

for an oil-water mixture in unconsolidated sands as taken from Leverett's paper (14).

In the above cited papers it was shown that for small saturations of a particular component of the mixture its relative permeability goes to zero, or in other words, the component will no longer move. The saturation at which for practical purposes this zero relative permeability is reached depends upon the pressure gradient and the characteristics of the sand. For larger saturations the relative permeabilities increase, and, of course, they equal the specific permeability at 100% saturation for any particular component.

With these characteristics in mind we can explain many features of the migration of mixtures of oil, water and/or gas as observed in the field or in the laboratory. We must remember, however, that the above relationships are only valid for steady flow of homogenous mixtures and cannot serve to evaluate the phenomena that occur when a water saturated medium is invaded by one of the mixtures in question.

Through a carrier bed with constant permeability the flow will continue unobstructedly as long as the pressure gradient continues to exist. If, however, the permeable bed pinches out either by truncation, successive overlapping or by a change in facies, we must consider a different medium being invaded by a fluid mixture. The question arises here, whether all components of the mixture are capable of penetrating the new medium or whether one or more of the components will be "screened out" at the boundary. For a continuous facies change we actually have to consider an infinite succession of such boundaries. If screening out occurs, the oil and/or gas will accumulate at the boundary and we have a so-called stratigraphic trap.

Before analyzing the factors involved in the screening out of oil and the formation of a stratigraphic trap, we want to consider one question regarding the migration of the fluid mixtures through the carrier beds, which has caused some confusion in the past.

As shown in fig. 1 the relative permeability to oil becomes zero when the oil saturation becomes smaller than approximately 20% in unconsolidated sands, while in consolidated sandstones this value will generally be even higher. However, in many beds that are considered to be carrier beds between the source rocks and the place of accumulation of oil we do not find any trace, of the migrating oil, left. By what mechanism was this oil removed?

In this case the diagrams of the articles cited before are of little or no help, as the oil is removed by very minute quantities, at a rate too low to be measured by the apparatus employed for the construction of the relative permeability graphs. Where oil is flushed completely from a carrier bed it is almost certain that free gas was present with the moving water for a considerable period of time. The oil will collect at the interface between the gas and the water and move as a thin film coating the gas bubbles. There is no steady flow of oil, the minute oil particles moving corresponding to a fraction of the total amount of gas bubbles that migrates per unit time. This process may go on till the last oil is removed. The gas may be removed by solution after it stops being supplied from a source.

This influence of gas on removal of oil remnants was already accurately described by Dodd (15) in 1922, who termed the secondary migration of trapped oil under the influence of gas, "rejuvenated migration." He also states that by this rejuvenated migration, in the

course of time most, if not all, of the oil would be removed. This is the only case in which the term "carrying" of the oil by another fluid can be properly applied. As long as there is enough oil present to form continuous flow in a fine network of channels, it will move under any pressure gradient at a rate corresponding to its relative permeability. After being transported through the carrier bed, accumulation of the oil may be affected by screening out, where the flow of water continues, or where the waterflow is slowed down or stopped, oil may accumulate in the higher part of the structure under the effect of gravity. In both cases the characteristics of the overlying rock must be such that oil is prevented from migration into them, under the existing pressure differentials.

PART IITheoretical considerations on the migration of oil
into a porous medium, completely saturated with water

The problem of infiltration of a water saturated porous medium by an oil-water mixture is rather complicated. Basically, however, the mechanism is much the same as that in the case of pure oil infiltrating a medium one hundred per cent saturated with water, as the flow of the water does not change the phase relations and merely defines part of the pressure gradient. We will, therefore, concentrate upon the invasion of a 100% water saturated porous medium by a non-wetting fluid, assuming that the porous solid is preferentially water wetted.

Water in a saturated porous medium exhibits a capillary pressure. The magnitude of this pressure is equal to the pressure at the base of a column of water, of a height equal to the height to which the water would rise in the capillary interstices against the force of gravity above an adjacent free water level. Or, in other words, in the equilibrium position the gravitational pressure of the water column just balances the capillary pressure under which the water-air interface tends to advance. To penetrate a water saturated porous medium, one has to overcome this same capillary pressure. One has to drive back the water against its tendency to advance in the capillary interstices. The minimum pressure that is necessary to cause a continuous penetration into the water saturated porous medium, is called the displacement pressure.

As capillary pressure is caused by interfacial tension, displacement pressure must always be defined for a given combination of fluids. In our case displacement pressure will always be used to indicate

the pressure of displacement of water, by oil, unless otherwise indicated.

In order to relate the displacement pressures to other characteristics of a sand, we will have to analyze more fully the capillary behavior of porous media. The first thorough analysis of capillary behavior in porous media was made by M. C. Leverett (16). At several points in the following discussion we will use some of Leverett's derivations and conclusions.

We will first discuss the over-simplified case, where the porous medium is represented by a bundle of straight cylindrical capillary tubes.

This assumption gives a rather close approximation for an extremely well-sorted sand consisting of well-rounded grains. Such a sand would have a distribution of pores of equal size which lateral dimensions might be represented by an equivalent circular section.

This representation was used by Bartell and Osterhof (17), who used measurements of displacement pressures for the computation of interfacial contact angles and adsorption tensions. The material used by them consisted of finely ground pure silica, smaller than 350 mesh, and compacted into a porous membrane. As displacement pressure, they measured the minimum pressure necessary to prevent water from advancing in the capillary pores of the membrane, the pores of the membrane being filled with air. This arrangement measures a displacement pressure corresponding to an "advancing contact angle," which means that the pressure is measured which just prevents the liquid, which wets the solid material preferentially, from advancing. (The contact angle is defined as the angle made between the interface of the wetting and the non-wetting fluid, and the solid walls.) As was pointed out by the same authors later (18), there is a distinct difference between advancing and receding contact angle in many

cases. The receding contact angle is established when the porous medium is first saturated with the liquid that wets it preferentially and then pressure is applied to displace this liquid from the interstices against its capillary tendency, to retain its advanced position in the interstices. The receding contact angle method of determining displacement pressures was used later by Bartell and Whitney (19) for determination of adhesion tensions and seemed to give more consistent results. As will be shown later, there is a definite relationship between the interfacial contact angle and the displacement pressure. The distinction between receding and advancing contact angles makes, therefore, that the displacement pressure is not uniquely defined. In the case of infiltration of a watersand by oil, however, we always deal with a receding contact angle, and unless otherwise defined, our displacement pressures will always refer to receding contact angles.

To facilitate better understanding of the factors involved in capillary phenomena, we want to summarize, at this point, some of the basic relationships.

All capillary phenomena are directly related to surface and adhesion tensions, and the tendency always prevails to reach a condition of minimum free surface energy.

One of the most important theorems on capillary behavior is the following: The excess of pressure on one side of a film of constant interfacial tension, over that on the other side, is equal to $S (1/R_1 \pm 1/R_2)$ where S is the interfacial tension and R_1 , R_2 are the principal radii of curvature of the film at the point in question (20). The positive or negative sign allotted to the curvatures depends upon whether the center of curvature lies on one side of the film or on the

other, and is mostly established by convention.

This theorem relates the pressure across an interface to the interfacial tension and the curvature of the interface. In the case of two fluids within a porous medium, the pressure across the interface is termed the "capillary pressure." When the capillary pressure is zero, the curvature is zero and the interface is a plane. Such interface is often referred to as a "free liquid surface."

One of the best known capillary phenomena is the capillary rise of liquids, in circular tubes of small diameters, above a free liquid surface. The magnitude of this capillary rise can be related to the interfacial tension for the combination of fluids under consideration, the radius of the capillary tube and the interfacial contact angle, made with the walls of the tube (21).

The derivation of the relationship is based on the following considerations: The interfacial tension exists throughout the interface with an equal magnitude and tends to keep the interface as small as possible at a given set of conditions. To maintain this tension at the contact line of the walls with the interface, the walls must exert a force per unit length, on the interface which equals the interfacial tension. (Compare, for instance, a rope under tension fastened to a wall. The wall exerts the same force on the rope as the tension within the rope.) For a circular tube of radius r the total force exerted by the walls on the liquid at the interface is $2 \pi r s$, and the total vertical force on the liquid column $2 \pi r s \cos \theta$ if θ is the interfacial contact angle.

This force must equal the force exerted by gravity on the liquid column above the free liquid surface.

Equating the two forces leads directly to the expression:

$$S = \frac{r H d g}{2 \cos \theta}$$

where r is the tube radius, d the density difference between the two fluids, θ the interfacial contact angle with the solid material of the walls of the tube, and H is the height above the free liquid surface, when the fluid within the tube is in capillary equilibrium. (H refers to the lowest point of the interface.) $H d$ represents here the pressure differential across the interface (in g/cm^2) and is therefore identical with the capillary pressure. Corresponding to this capillary pressure, the interface has a fixed curvature, in the above equilibrium position.

We are now able to analyze more clearly the relation between the displacement pressure and the capillary pressure. Assume again a porous block completely saturated with water. At its boundary the curvature of the liquid surface is zero and the capillary pressure is zero. We now mount this block so that a pressure differential can be applied across it, lengthwise, for instance by applying a pressure via a fluid (air or oil) above it, while keeping the pressure below it constant. As we increase the pressure above the block, the pressure across the fluid interface at the upper boundary increases and correspondingly the curvature of the interface increases. In this way we can increase the exterior pressure differential and thereby the capillary pressure across the interface and the interface curvature, until the force exerted by the exterior pressure equals the force due to the interfacial tension. Any increase of pressure above this point will cause the fluid to flow. This critical capillary pressure is the displacement pressure corresponding to the receding interfacial contact angle. The curvature that is reached at this point is the minimum interfacial curvature with which the two fluids can be contained

together within this particular porous medium.

If we can compare the porous medium to a bunch of vertical capillary tubes, we see that the critical capillary pressure, or the displacement pressure, is equal to the gravitational pressure differential in the equilibrium position of capillary rise in a tube.

Bartell and Osterhof, using this analogy, used the formula

$$S = \frac{r H d g}{2 \cos \theta}$$

derived for the capillary tubes, in the case of the porous membrane, substituting the displacement pressure π for the gravitational pressure $H d g$ thus having:

$$S = \frac{r \cdot \pi}{2 \cos \theta}$$

From this formula, r (the equivalent radius of the pores) can be calculated if θ is known, or vice versa.

We see that according to the above derivation π is inversely proportional to r and that for a porous medium, strictly speaking, we can only sharply define the displacement pressures if all pores have the same equivalent radius. For a normal sandstone or other porous sediment, we have a wide range of pore sizes and irregularly shaped pores. Fortunately not all large pores are mutually inter-connected, and neither are the small ones. Therefore, for a reasonably homogenous sandstone penetration in a given direction will have to make use at least of part of the smaller pores. The displacement pressure is the pressure at which continuous flow will take place through the specimen, using the easiest continuous path in a given direction. This makes that even for very badly sorted sandstones the displacement pressures are still defined within a fairly narrow range of values.

As pointed out by Leverett (16), the comparison of an average

sandstone with a bundle of straight capillary tubes is over-simplified and leads, in most cases, to erroneous results. In the case of sandstones we certainly cannot speak any longer about any one equivalent radius of the pores, and even assuming a fixed distribution of equivalent radii does not give the complete picture, as it does not take into account the irregular shapes and inter-connections of the pores. Leverett therefore suggests to abandon the representation by parallel straight capillary tubes completely, and focused attention instead on the relationships between capillary pressure, interfacial curvature and the relative saturation of the different fluid components. The treatment of these relationships by Leverett is of great importance in the theoretical evaluation of the displacement pressure, in terms of the basic characteristics of the rocks in question. We will summarize in short, therefore, the results of Leverett's work.

Part of the derivations are made for a vertical column of porous solid, preferentially wetted by one fluid (forming zero contact angle with the solid) and partly saturated with a second fluid of smaller density. The fluids may be taken as respectively, water and oil.

Use is made again of the relationship between capillary pressure and interfacial curvature:

$$P_c = S \left(\frac{1}{R_1} + \frac{1}{R_2} \right)$$

An additional formula is derived for the vertical distribution of capillary pressure, in the following manner:

Consider a large porous mass, preferentially wetted by water in which two fluids such as oil and water are distributed in the manner required for capillary equilibrium. Suppose a small volume of water ΔV

is transferred from the level h , to the level $h + dh$. Since equilibrium exists, the change in free energy due to the infinitesimal displacement of V will be zero ($dF = 0$). dF , however, consists of two parts, which therefore must be equal and of opposite sign:

- a) The change in free energy of ΔV by the rise in the gravitational field:

$$\frac{\partial F}{\partial h} = \rho_w \cdot g \cdot \Delta V \quad \left(\begin{array}{l} \rho_w = \text{density of water} \\ g = \text{acceleration of gravity} \end{array} \right)$$

- b) The change of free energy of ΔV passing from a level h where the pressure of the water is P_w to a level $(h + dh)$

$$\text{where the water pressure is } (P_w + dP_w) : \quad \frac{\partial F}{\partial P_w} = \Delta V$$

We have therefore:

$$dF = \left(\frac{\partial F}{\partial h} \right) dh + \left(\frac{\partial F}{\partial P_w} \right) dP_w = \rho_w \cdot g \cdot \Delta V \cdot dh + \Delta V dP_w = 0$$

$$\text{or } -dP_w = \rho_w g dh \quad \dots (1)$$

A similar derivation may be made for the oil, which gives:

$$-dP_o = \rho_o g dh \quad \dots (2)$$

The capillary pressure P_c across the water-oil interface is by definition

$P_c = P_o - P_w$, whence differentiating:

$$dP_c = dP_o - dP_w \quad \dots (3)$$

Combination of expressions (1), (2) and (3) gives:

$$dP_c = (\Delta \rho_{wo}) g dh \quad \dots (4)$$

where $\Delta \rho_{wo}$ is the density difference between water and oil.

As shown before, there is a definite minimum value for the capillary pressure across the interface between the two fluids within the porous medium, equal to the displacement pressure. For all larger values of P_c we find the relation between P_c and h by integrating equation (4),

so that we obtain:

$$P_c = (\Delta \rho_{wo})g h = S \left(\frac{1}{R_1} + \frac{1}{R_2} \right) \dots (5) \text{ for } P_c \quad \text{where}$$

is the displacement pressure for water by oil for the particular porous medium under consideration.

It should be emphasized that equation (5) was derived without any assumptions regarding the fluids or the porous medium, except that they are isothermal and in capillary equilibrium. A corollary of equation (5) is that all interfaces in any particular two-fluid system have the same curvature and capillary pressure at the same horizontal level, if they are in capillary equilibrium.

Assuming a hypothetical level of zero curvature and zero capillary pressure, which would coincide with a free liquid surface outside the porous medium, the zone of 100% water saturation will for a given porous medium, always extend to the same elevation above the hypothetical zero level. At the top of this zone of 100% water saturation the capillary pressure will be equal to the displacement pressure, for that particular two-fluid system.

After establishing the relationship between capillary pressure (or curvature) and height, it remains to find the relation between curvature and saturation in order to find the vertical distribution of the fluids in the sand column.

Although we are, in our case, not interested in any static fluid distribution, the relationship between curvature and saturation in terms of normal characteristics of the sand in question, will fix automatically the relation between the displacement pressure (which is just one point on the curvature-saturation graph) and these sand characteristics.

The curvature of the oil-water interface is apart from its thermodynamic relation to capillary pressure and height, a geometric quantity determined by the dimensions of the interstices in which it exists, the contact angle of the interface with the solid and the proportions of the fluid phases present.

Work by W. O. Smith (22) and others has shown that the curvature saturation function is not single valued over its entire range. There is a considerable hysteresis loop in the function. The reasons for this behavior are derivable from the geometry of the system as discussed in detail by Smith. There also are good indications that the two branches of the hysteresis loop correspond respectively to the establishment of a receding or an advancing contact angle.

Leverett determined the saturation - curvature relationship experimentally for clean, unconsolidated sands. He used both imbibition and drainage to obtain the saturation gradients. Corresponding to imbibition (advancing contact angle) one branch of the curves was obtained, while drainage (receding contact angle) gave the other branch of the hysteresis loop. The receding contact angle curve gives higher values of capillary pressure for a given saturation than the advancing contact angle curve.

The most important result of Leverett's work, as far as our problem is concerned, is that regardless of the degree of sorting or the character of the sands, the same curves were obtained for the curvature - saturation relationship, when plotted in the dimensionless form

$$\frac{\Delta \rho g h}{s} \cdot \left(\frac{K}{\phi} \right)^{1/2} \text{ against } S_w \text{ or } \frac{P_c}{s} \cdot \left(\frac{K}{\phi} \right)^{1/2} \text{ against } S_w \text{ (both are}$$

exactly equivalent according to equation (5)). Here K is the permeability

and φ is the fractional porosity. K must be expressed in c.g.s. units, consistent with the other variables of the group.

Fig. 2 gives the relationship as determined by Leverett (23) for clean, unconsolidated sands. With clean sands are meant sands void of clayey and amorphous materials.

The replacement pressure is the largest capillary pressure found for 100% water saturation and is determined from the largest value of

$$\frac{P_c}{S} \left(\frac{K}{\varphi} \right)^{1/2} \text{ for 100\% water saturation on the receding contact angle}$$

(drainage) curve. This maximum value is the same for all clean sands and has a value of .3 in fig. 2. To find the displacement pressure for any clean, unconsolidated sand, we may use, therefore, the following procedure: Determine the porosity and permeability (one c.g.s. unit of permeability = 1.014×10^8 darcies); find the interfacial tension for the oil-brine combination in question (approximately 35 dynes/cm) and apply the formula:

$$\pi = 0.3 S (K/\varphi)^{-1/2} \dots (6)$$

If clayey or hydratable material is present, the water is held by other than capillary forces only. The tendency seems to be, a decrease of the constant in formula (6), for increases in content of hydratable material. The decrease of the constant does not mean, however, that π decreases with increasing amount of clayey material, as the latter decreases the permeability very strongly, while practically not changing the porosity.

The capillary behavior in porous media has been elaborated upon in a recent paper by Rose and Bruce (24) who extended the principles outlined earlier, to consolidated porous rocks and derived several new relationships between the fundamental characteristics of those rocks and

their capillary properties.

The following paragraph gives an outline of their analysis, which they start with Leverett's equation for the capillary retention relation:

$$j(S_w) = \frac{P_c}{S} \left(\frac{K}{\varphi} \right)^{1/2} \dots (7) \text{ where } j(S_w) \text{ is a dimensionless}$$

function of the wetting phase saturation.

It can be shown from the Poiseuille and Darcy equations for permeability that the term $(K/\varphi)^{1/2}$ is equal to the average pore radius of the porous medium under consideration. Hence Leverett's equation conforms with the basic expression for capillary rise in circular tubes, in that it combines the same variables in a simple relationship.

Starting with the equation $P_c = d g h = \frac{2S}{r}$ for capillary rise in spherical tubes, Carman (25) showed that to evaluate capillary rise in more complex systems, such as random-packed non-spherical sand grains, we can replace the radius r , by twice the hydraulic radius. The latter is defined as the ratio of porosity, φ , to the surface area of the grains, A , in units of bulk volume. This leads to the relation:

$$\frac{\overline{P_c}}{S} = \frac{d g h}{S} \frac{A}{\varphi} \dots (8)$$

The connection between equations (7) and (8) becomes evident by considering the Kozeny equation (26, 27) which expresses the specific surface area in terms of permeability and porosity.

Rose and Bruce rearranged this equation as follows:

$$A = \varphi \left\{ \frac{\varphi}{K} \right\}^{1/2} (1/k)^{1/2} \dots (9)$$

where k is the so-called "rock textural constant". Equation (9) is the

expression for streamline motion through granular beds.

Combining (9) and (8) we have:

$$\frac{\bar{P}_c}{S} = \left(\frac{K}{\phi}\right)^{1/2} \left(\frac{1}{k}\right)^{1/2} \text{ or } \frac{\bar{P}_c}{S} \left(\frac{K}{\phi}\right)^{1/2} = (1/k)^{1/2} \dots (10a)$$

Remembering that (8) is the expression for capillary rise and that for circular tubes h is measured to the lowest point of the meniscus, above the free liquid surface, while \bar{P}_c is the pressure differential across the interface (or meniscus) we see, that \bar{P}_c is the capillary pressure, corresponding to the highest point of 100% water saturation, as in the case of the circular tube. In other words, \bar{P}_c in equation (10a) equals the displacement pressure π .

Rewriting (10a) gives us:

$$\frac{\pi}{S} (K/\phi)^{1/2} = (1/k)^{1/2} \dots (10b)$$

where the displacement pressure $\pi = \lim_{S_w \rightarrow 1} P_c$.

Equation (10b) shows that for consolidated systems the constant of equation (6) which was found to be approximately equal to 0.3 for unconsolidated clean sand, equals the square root of the reciprocal Kozeny constant.

$$\text{That is } \lim_{S_w \rightarrow 1} j(S_w) = (1/k)^{1/2}$$

The Kozeny constant is related to the specific surface area by equation (9), which gives:

$$k = \frac{\phi^3}{K A^2} \quad \text{or with } A^1 = A/\phi$$

$$k = \frac{\phi}{K (A^1)^2} \dots (11) \quad \text{where } A^1 \text{ is the inter-}$$

stitial surface area in cm^2 per cm^3 pore volume.

Equation (8) applied to porous media gives the direct relation between the displacement pressure and the specific surface area per bulk-volume.

$$\frac{\pi}{S} = A/\varphi = A^1 \quad (12)$$

Equation (10b) showed the relationship between the displacement pressure and Kozeny's constant.

For clean unconsolidated sands the value of k is about 5.5 .

Rose and Bruce showed that k depends very strongly on the fine fraction (\approx clay content) of the sands.

They found for a clay percentage of 5.9 a value of $k = 31.2$ and for a clay percentage of 8.5 and 11.6 respectively, $k = 155.0$ and $k = 400.0$.

This indicates that the Kozeny constant k can be used as a measure of the extent to which the sediment behaves as an argillaceous rock.

This suggests that k may be related to the factors determining the magnitude of the electrochemical potentials which are established when solutions of different salinities are brought into contact with each other within the interstices of the sediments.

These potentials are also dependent on the relative position of the sediment in the sandstone shale series. The factor that identifies this position is the electrochemical "formation coefficient." This factor is at a minimum for clean sands and at a maximum for purely argillaceous shales.

A description of the characteristics of the above mentioned electrochemical potentials and the precise definition of the formation coefficient are given in another thesis by this author (28).

The purpose of the experimental part of this thesis will be to determine whether any of the constants related to the displacement pressure, can be correlated with the electrochemical formation coefficients.

Such correlation, if established, will furnish a means of determining the displacement pressure by subsurface geological methods.

Before describing the experimental procedure and results, two other factors governing the accumulation and final distribution of oil and gas, in reservoir, have to be analyzed.

These factors are the interfacial tension, S , and the density difference between the wetting phase and the non-wetting phase, $\Delta \rho$.

The displacement pressure for any given rock and an water-oil combination, is directly proportional to the interfacial tension, S , while $\Delta \rho$ is the factor governing the buoyancy of the oil, which forms the counterpart of the capillary forces.

Both factors enter, as well, in the trapping of the oil and gas, under a caprock as in the final distribution of the wetting and non-wetting phases, in the porous reservoir rock.

If the force of buoyancy caused by the density difference between the brine and the oil is larger than the displacement pressure of the caprock, the trap will leak, permitting oil to infiltrate the caprock. During this infiltration buoyancy must remain larger than the displacement pressure, until a minimum oil saturation in the caprock is reached, at which the relative permeability of the rock to oil is larger than zero. Until this point is reached no continuous flow of oil can occur. Once the minimum saturation is established, however, the oil will flow under any

pressure gradient and it will migrate out of the trap.

It is of primary importance, therefore, to know the magnitude of oil and gas densities and of the interfacial tensions, under reservoir conditions.

A discussion of the variations of these quantities with temperature and pressures, which will enable us to estimate their magnitude at depth, is given in Part III of this thesis.

PART IIIDensities of oil and gas.Oil-water and oil-gas interfacial tensions.

The variations with temperature and pressure of density difference and interfacial tension between oil or gas and oil field brines, will be analyzed in the following paragraphs. They will be presented in terms of variations with depth, assuming a constant temperature gradient with depth and an average rock pressure.

The analysis will be carried out in the following order:

1. Density variations of natural gases with depth.
2. Surface tension of oil field brines against natural gas and its variation with depth.
3. Density of crude oils and its variation with reservoir temperatures and pressures.
4. Oil-water interfacial tension.

1. Density variations of natural gases with depth.

To facilitate analysis of the variation of densities and interfacial tensions with depth, we will assume an average temperature gradient of 1° F per 60 feet of depth and an increase in rock pressure of 4 p.s.i. per 10 feet.

If reservoir pressures and temperatures deviate considerably from the conditions resulting from the above assumptions, the relations derived later have to be used step by step.

Fig. 3 shows the variation of temperatures and pressures with depth, corresponding to the above assumptions.

To find the variation of gas density with depth we cannot simply apply the gas law of Boyle, which holds true only for ideal gases.

25A

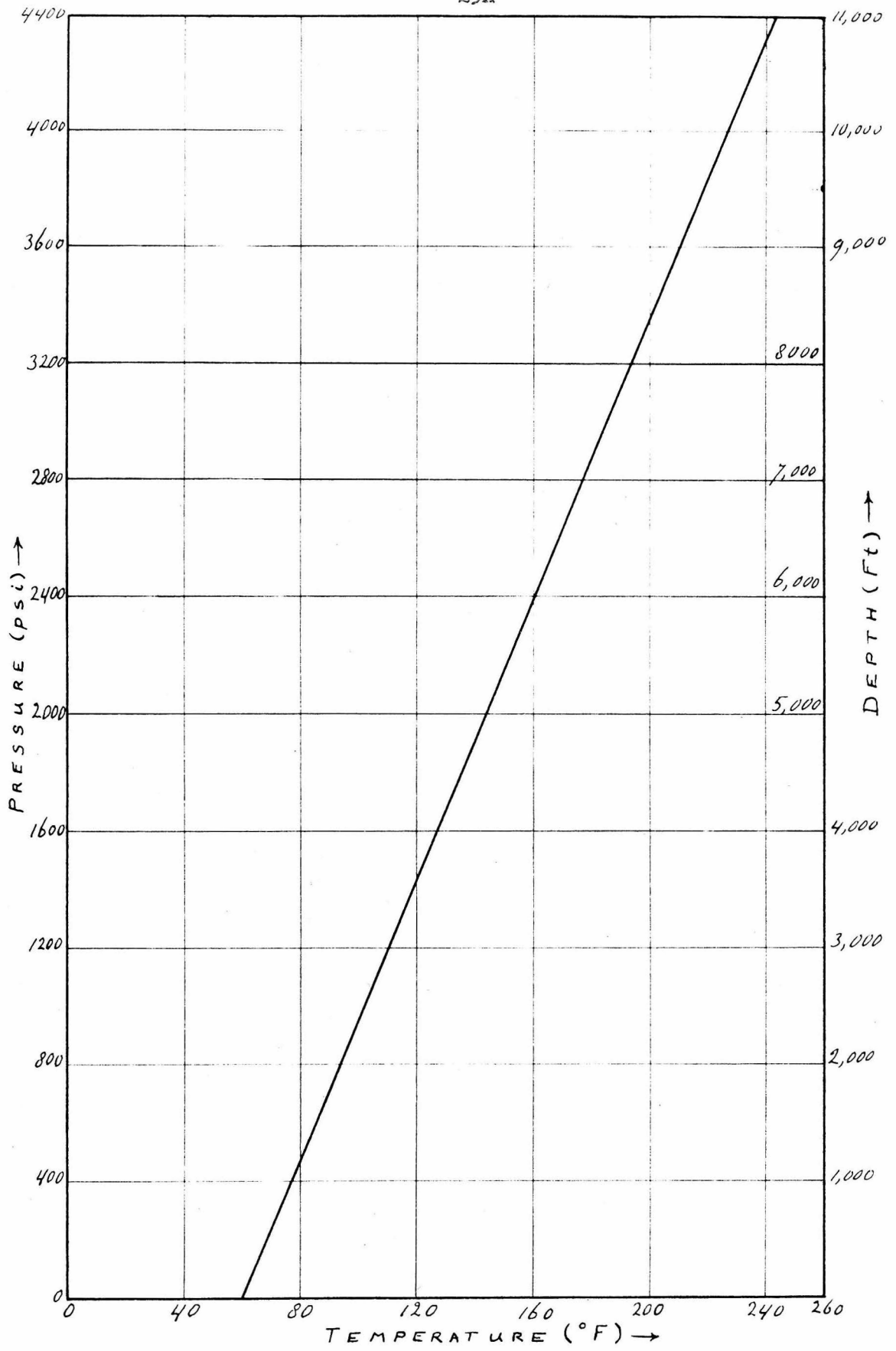


Fig. 3

Deviations from Boyle's law are taken into account by applying an experimentally determined correction factor to the value of the volume, V , found for a given quantity of gas at elevated temperature and pressure.

The density then is inversely proportional to the corrected volume.

The correction factors as mentioned above were given by Sage and Lacey (28) for pressures up to 3000 psi and temperatures ranging from 70° F to 220° F.

These data were extended by Standing and Katz (29) to pressures up to 10,000 psi and temperatures up to 300° F. The latter authors furthermore found that many types of gases give smooth relationships between their pseudo-critical conditions and their gravity (compared to air). All gases whose pseudo-critical temperatures and pressures fit a certain set of gravity curves, have the same density for a given temperature, pressure and gas gravity, independent of their composition. This simplification makes it possible to construct charts giving gas density as a function of temperature, pressure and gas gravity. (Gas gravity = specific gravity of gas / specific gravity of air.)

Such charts were made up by Standing and Katz for hydrocarbon gases containing more than 83% of combined methane, heptanes and heavier fractions. This includes most of the natural gases.

From these charts fig. 4 has been prepared giving gas density (in g/cm^3) as a function of depth, for gas gravities ranging from .6 to 1.0 .

For gases containing more than 3% nitrogen and larger fractions of ethane, propane and butanes, the densities deviate from the relation presented in fig. 4 and have to be calculated with the use of the extended

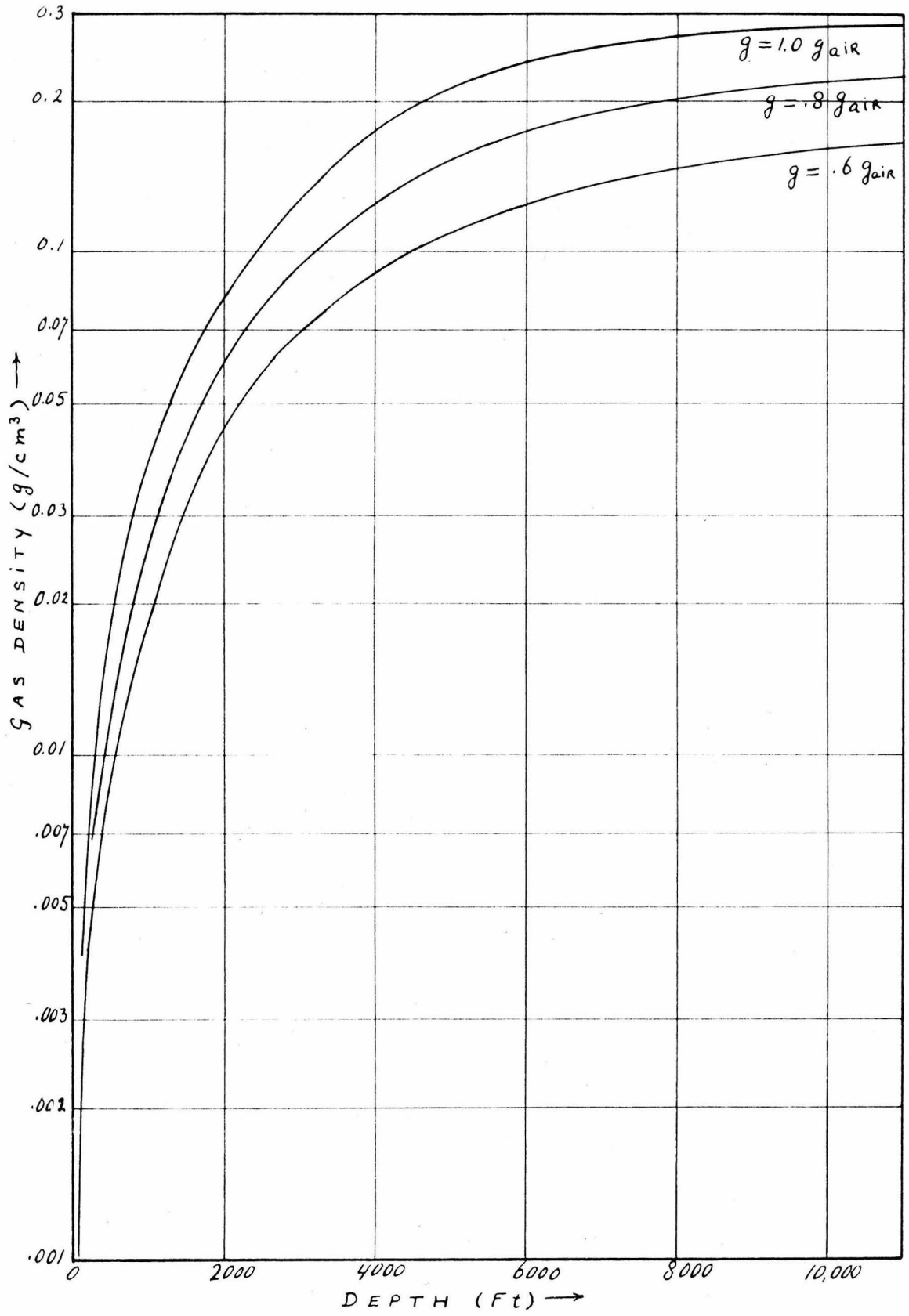


Fig. 4

compressibility correction factor chart given by Standing and Katz.

For our purposes, however, fig. 4 gives a good representation of the magnitude of density variation with depth for most saturated natural gases.

2. Surface tension of oil field brines against natural gas and its variation with depth.

The behavior of the surface tension of water against natural gas at elevated temperatures and pressures was investigated by Hocott (30).

Fig. 5 gives the results of these investigations for a gas consisting mostly of methane, with some ethane and propane, as given by Hocott. The curve for 225° F is extrapolated.

From the relations presented in figs. 3 and 5, curve (a) of fig. 6 has been prepared giving the water-gas interfacial (surface) tension as a function of depth.

For studies of the equilibrium distribution of gas and water in a gas reservoir-sand the ratio $\frac{\Delta \rho}{S}$ is one of the most important factors.

in this case is the density difference between the brine ($\rho \approx 1.1 \text{ g/cm}^3$) and the natural gas. For a gas of 0.8 gravity $\Delta \rho$ has been calculated from fig. 4 and $\frac{\Delta \rho}{S}$ is given in fig. 6, curve (b). To make the latter relation applicable in reservoir computations we have to assume that the interfacial tension between water and a relatively dry gas does not differ greatly from that between water and a "wet" gas.

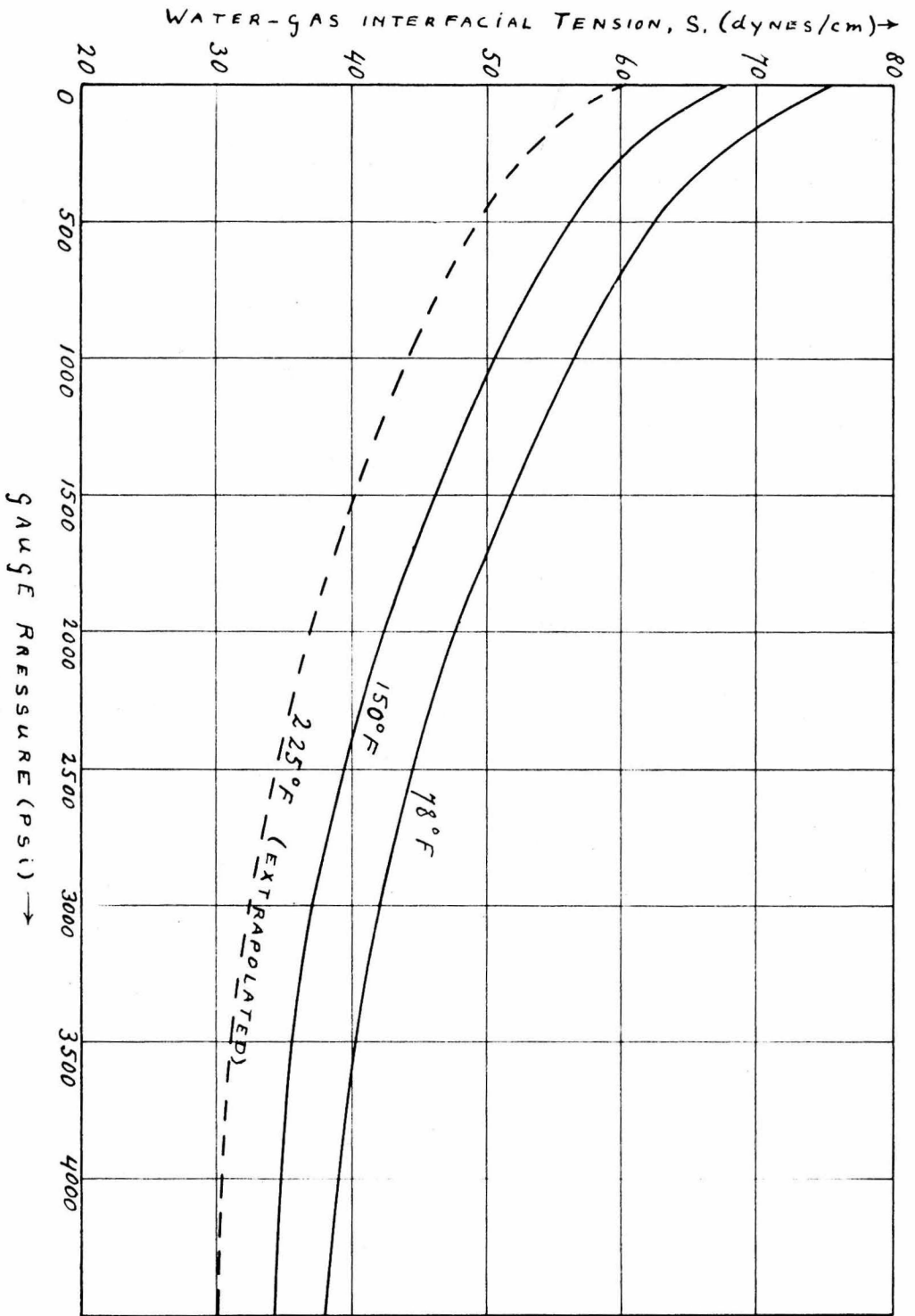


Fig. 5

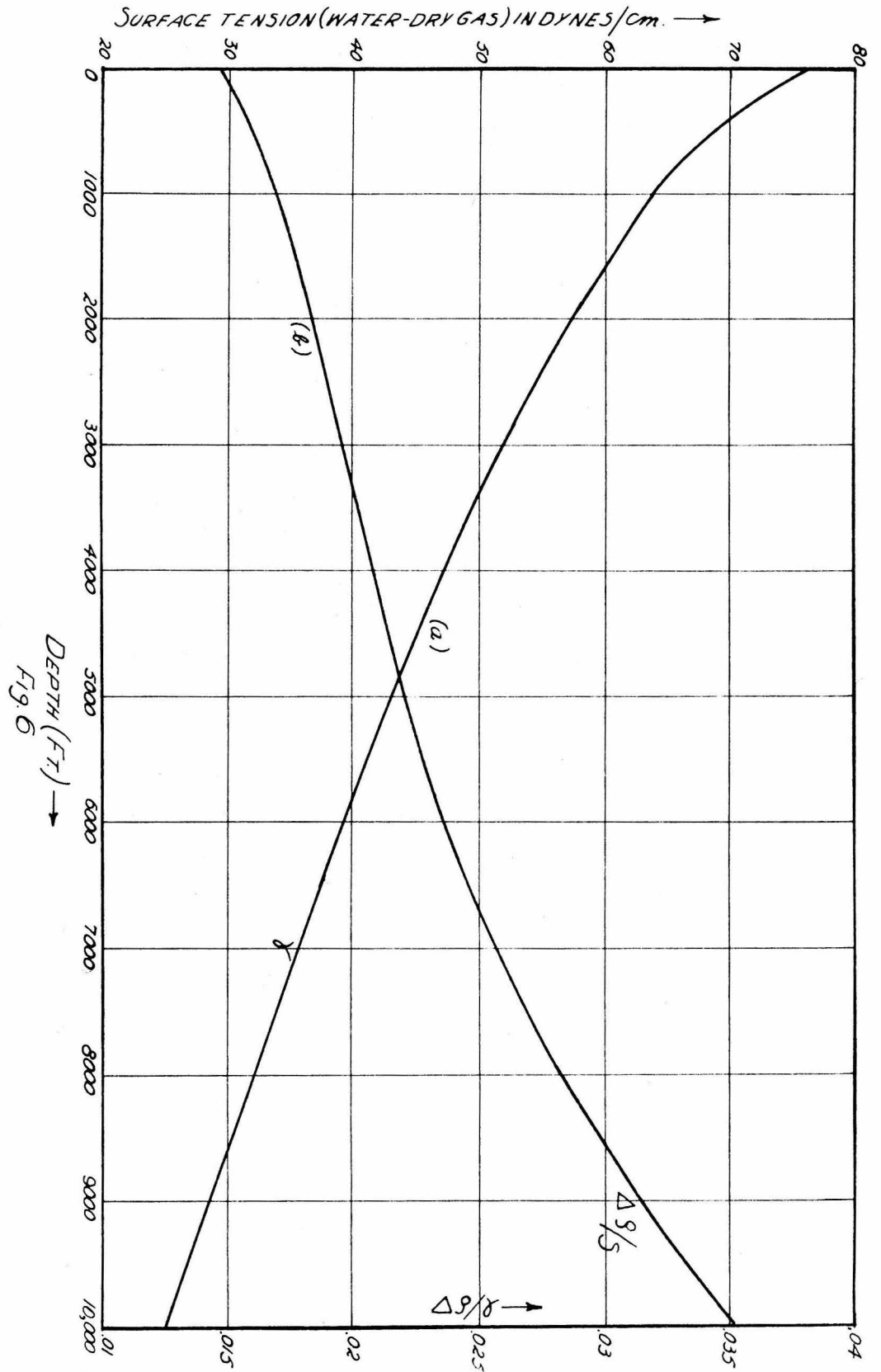


Fig. 6

3. Density of crude oils and its variation with reservoir temperatures and pressures.

The variation of the density of crude oils with temperature and pressure is very much complicated by the solution of gas in the oil. Especially the lighter hydrocarbon gases, such as methane and ethane, cause large changes in oil density, when they are dissolved in the oil in sufficient quantities.

Therefore the density of a given crude oil can only be computed if the methane and ethane content at the depth in question is known. The computation may be carried out following a method outlined by Standing and Katz (31). This method consists of first determining a hypothetical surface density, which would represent the gravity of the oil under surface conditions, if all of the methane and ethane dissolved at depth would remain in solution. This hypothetical density is then corrected for the effects of temperature and pressure. The corrected value equals the actual density at the depth under consideration.

The difficulty in obtaining a generalized relation between oil densities and reservoir temperatures and pressures, is caused by the fact that the crude oil at depth is not generally saturated with the lighter hydrocarbon gases (methane and ethane).

If complete saturation did exist, the amounts of methane and ethane in solution, at various temperatures and pressures, could be calculated from the experimental data assembled by Sage, Lacey and co-workers (32, 33, 34). These data include experimental determinations of the amounts of methane and ethane dissolved in various oils at reservoir temperatures and bubble-point pressures. With the aid of these values, the oil densities could be easily computed following the

method of Standing and Katz, for the case of complete saturation.

As the actual saturation varies from case to case, no general rule can be laid down for the variation of crude oil density with depth. In specific cases, however, the densities may be computed following the above principles.

Fig. 7 shows two examples of such computations. Curve (a) represents a crude of 25.7° A.P.I. gravity which does not contain methane nor ethane. Curve (b) shows the density variation for a crude oil containing 5% methane and 15% ethane at a depth larger than 7000 feet and being saturated with methane closer to the surface.

4. Oil-water interfacial tension.

The data on oil-water interfacial tensions are extremely scarce. Livingston (32) found the following generalities for the interfacial tension between reservoir brines and "dead-oil": At 70° F oils with viscosity higher than 7 centipoises gave an average of 21.3 dynes/cm interfacial tension. Oils with a viscosity smaller than 4 centipoises gave an average of 19 dynes/cm. This indicates that changes with the character of the crude oil are not too important. In general higher viscosity crudes have higher interfacial tensions.

For the variation of interfacial tension with temperature, Livingston gives an average decrease of 0.15 dynes/cm per ° F increase in temperature.

The average value for all crudes tested at 70° F was found by him as 20.4 dynes/cm.

However, under reservoir conditions, the pressures are generally above the saturation pressures for the prevailing temperatures

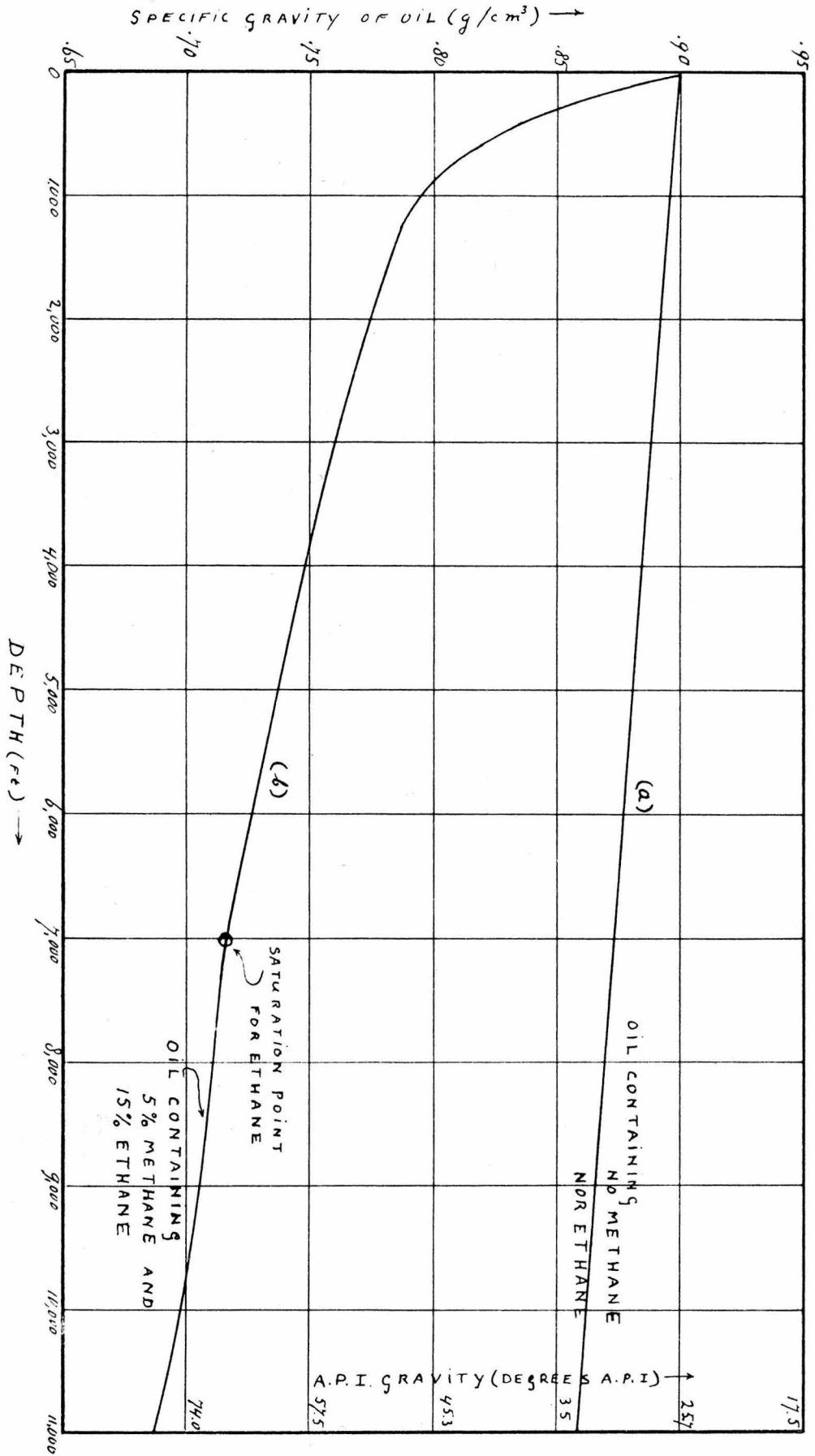


Fig. 7

and the oil is saturated with natural gas, so that conclusions reached for dead oil do not apply.

Hocott (30) found that variations in pressures above and below the saturation pressure, at a given temperature, have relatively little influence on the interfacial tension. Hocott's measurements were made for oils in equilibrium saturation with natural gas, at various pressures, for a given reservoir temperature. Unfortunately no measurements were made for one given oil at various temperatures.

The curves obtained by Hocott are represented in fig. 8. On these curves we have indicated points corresponding to the temperature for which the curves were plotted and the pressure that would prevail at a depth at which such temperature would occur according to the depth - temperature - pressure relationship of fig. 3. The points are indicated by small triangles.

The gravity of the crudes used for the experiments from which curves I, II and III of fig. 8 were obtained was respectively 33.5, 36.9 and 41.3° A.P.I.

This means they are essentially all high gravity oils, and neglecting differences in the interfacial tensions due to the variations in the character of these oils will cause relatively small errors. The position of the three triangular points shown in fig. 8 gives us therefore the approximate trend of the relationship between pressure, depth or corresponding temperature and the interfacial tensions for crude oils completely or nearly saturated with natural gas at elevated temperatures. In fig. 8 this trend has been indicated by a straight line through the three points.

We note from fig. 8 that at low pressures, the variations in pressure or in the amounts of gas dissolved have a much greater influence

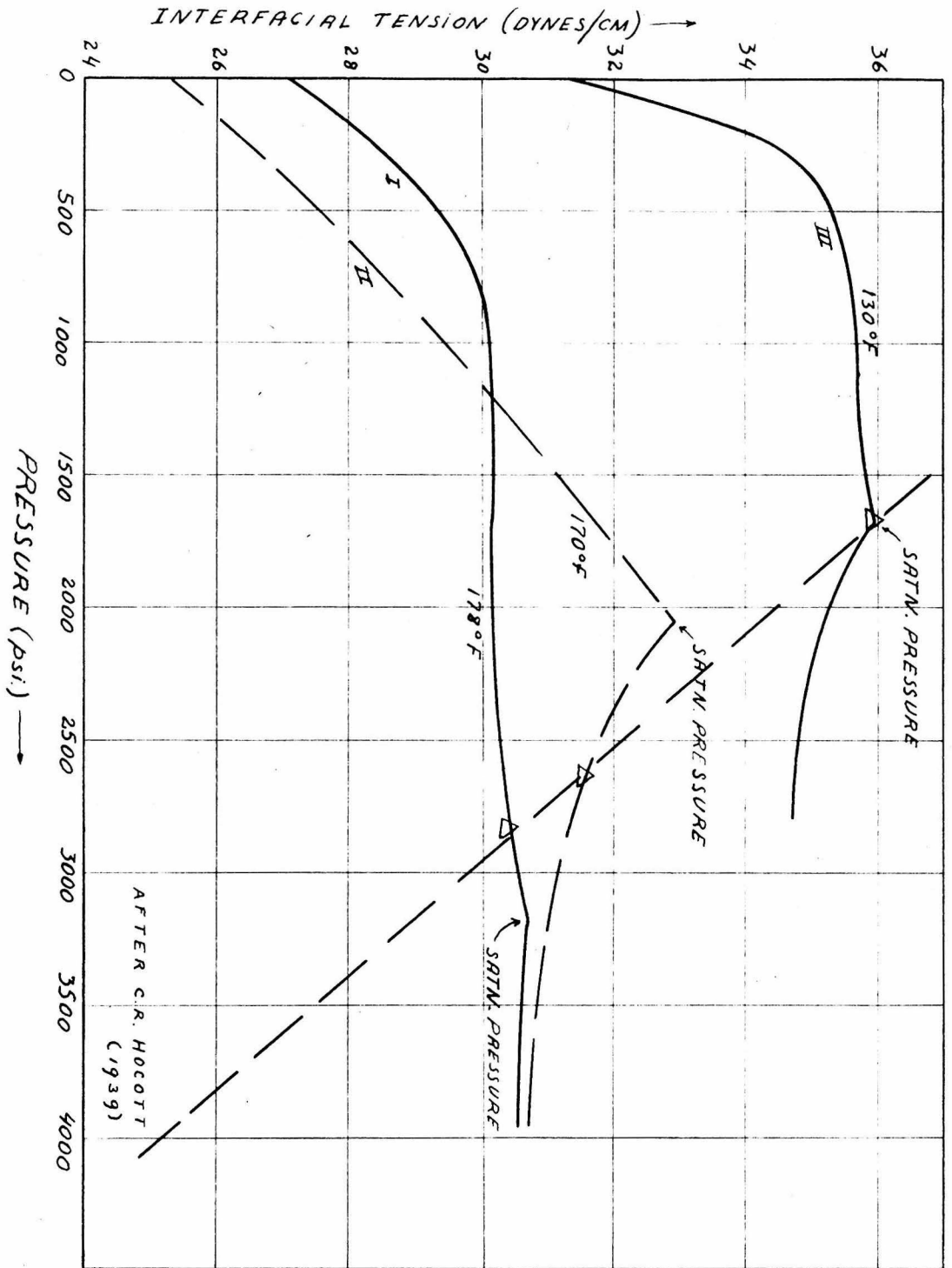


Fig. 8

AFTER C.R. HOCOTT
(1939)

on the interfacial tension. For pressures below 1200 p.s.i. (or at depths below 3000 feet) the interfacial tension decreases rapidly for decreasing amounts of gas dissolved. It is known that in the same range of pressures the surface tension of crude oils decreases with increasing amounts of gas dissolved. These two trends are in agreement with Antonow's rule which states that for mutually saturated solutions the interfacial tension approximately equals the difference between the two surface tensions. It was shown, however, by Livingston (35) that for crude oil water systems Antonow's rule cannot be applied to compute the oil-water interfacial tensions.

The decrease in interfacial tension with decreasing amounts of gas dissolved in the range of low pressures will explain in part the differences in absolute values of the interfacial tensions as found by Livingston and by Hocott. At atmospheric pressure and 130° F Hocott finds for a 41.3° A.P.I. gravity oil, an interfacial tension of 31 dynes/cm. For the same temperature Livingston finds values of the interfacial tension of the order of 12 dynes/cm.

As Hocott's experiments seem to represent more closely reservoir conditions we will use the trend established by his data to represent roughly the variation of interfacial tension at depth. For the range of lower pressures we have to take into account the decrease of the interfacial tension due to the decrease in amounts of gas dissolved. The overall variation of interfacial tension with depth following the above relations is represented schematically in fig. 9.

From figs. 6 and 9 we note that at large depths (10,000 feet) the interfacial tension water-oil and the interfacial tension water-natural gas, approach each other very closely.

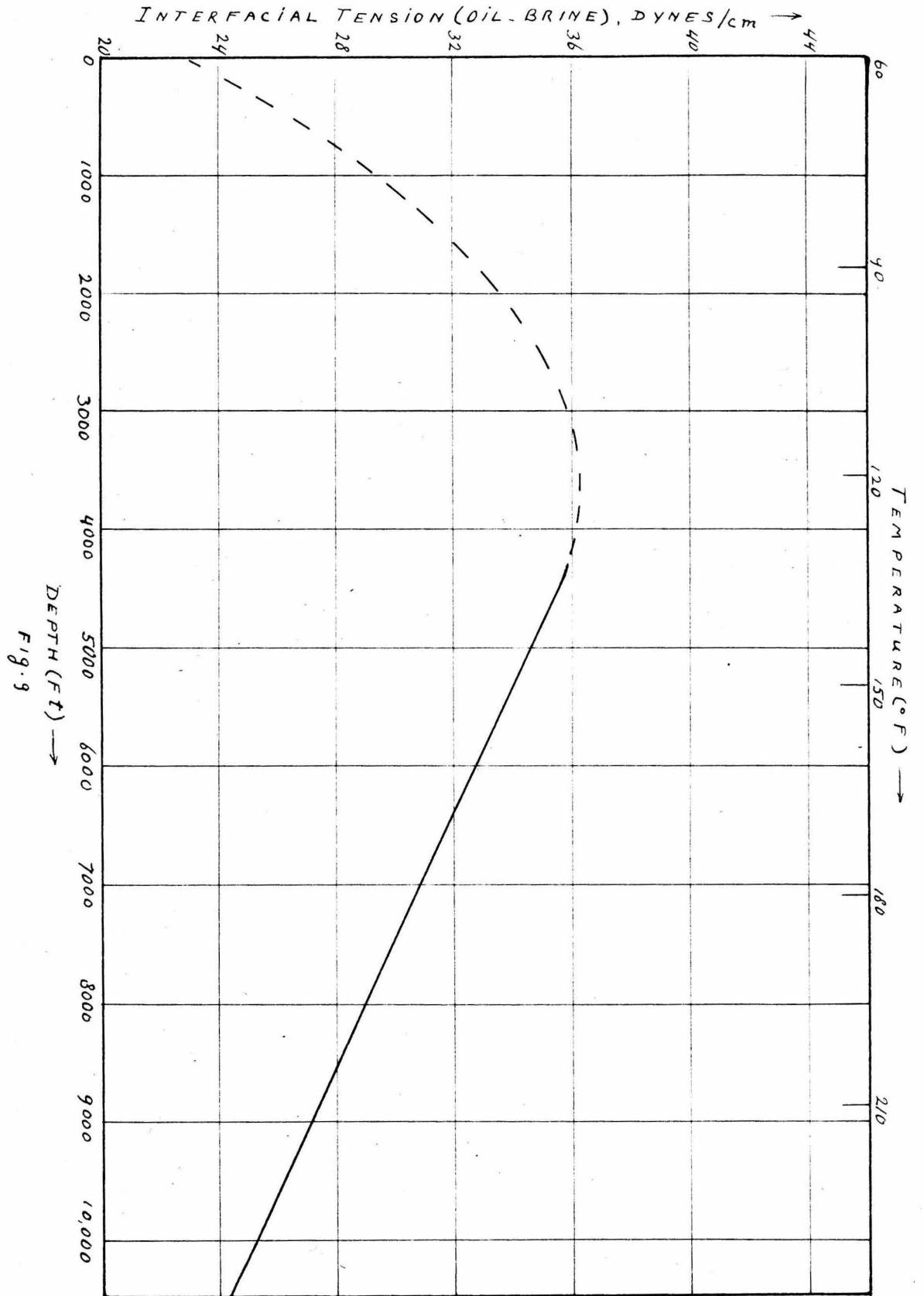


Fig. 9

PART IVExperimental procedure

The purpose of the experimental part of this thesis, is to measure displacement pressures of porous rocks and compare them with data compiled from research on self-potentials of similar rocks.

To measure the displacement pressures, a cylindrical core of approximately 2.8" diameter and 2" height is mounted in the bottom part of the cylinder of a baroid wall building tester. The core is then flushed with CO₂ gas to remove the air from the interstices. Thereupon water is forced through. All trapped CO₂ gas will dissolve in the water. This flushing is continued until the electrical resistivity of the core (measured with a four electrode system) does no longer change. A second check is made by comparison of the resistivity of the influent and effluent water. When the latter are equal, no more CO₂ is going into solution, which means that no more CO₂ is present in the core.

After the core is thus 100% saturated with water, the permeability to water is measured and also the porosity (as the weight difference between the wet and the dry core, divided by the bulk volume).

Oil (30° A.P.I. gravity) is then poured in the upper part of the cylinder to a height of approximately 1/2" and pressure is applied, using a nitrogen bottle with regulating valves.

It was initially attempted to measure the displacement pressure directly as the minimum pressure at which water would be effluent from the core. It was found, however, that this point is difficult to determine, as oil will enter some large pores first and displace some water before complete infiltration takes place.

To avoid this difficulty the apparatus was adjusted to measure the capillary pressure - saturation relationship for each core. The displacement pressure is then defined as $\pi = \lim_{S_w \rightarrow 1} P_c$.

The baroid wall building tester was adapted for capillary measurements in the following manner: (See fig. 10)

The holder (H) shown in fig. 10a was replaced by a holder (H^1) which is shown schematically in fig. 10b.

In addition an insert (I) was machined to fit with a sliding fit inside H^1 , resting with its flange on the inside shoulders of H^1 and just clearing the bottom of H^1 to allow fluid passage.

In the insert I a high grade circular porous disc is fitted, which has a controlled pore size of approximately 1 micron. The disc is secured in place by castolite casting resin and a circular groove is cut in the resin, to hold an "O"-seal gasket, which fits against the lower rim of the baroid cylinder. The castolite is a thermo-setting resin, which is cured for approximately 35 minutes at 170° F. It makes a very tight bond with the porous material, but a rather poor one with the brass of the insert. The "O"-seal gasket, however, prevents any leakage between the resin and the brass, and the only passage for effluent fluids is through the porous disc. The bottom of the insert is perforated by symmetrically placed small holes (1/16"). Water passing through these holes collects in the small clearing between H^1 and the bottom of I and drains off through the little tube inserted in the center of H^1 .

The porous plate (Coors #740 porcelain) when water wetted has a displacement pressure of more than 40 psi. Thus by increasing the gas pressure on the oil we may increase the confining pressure on the oil

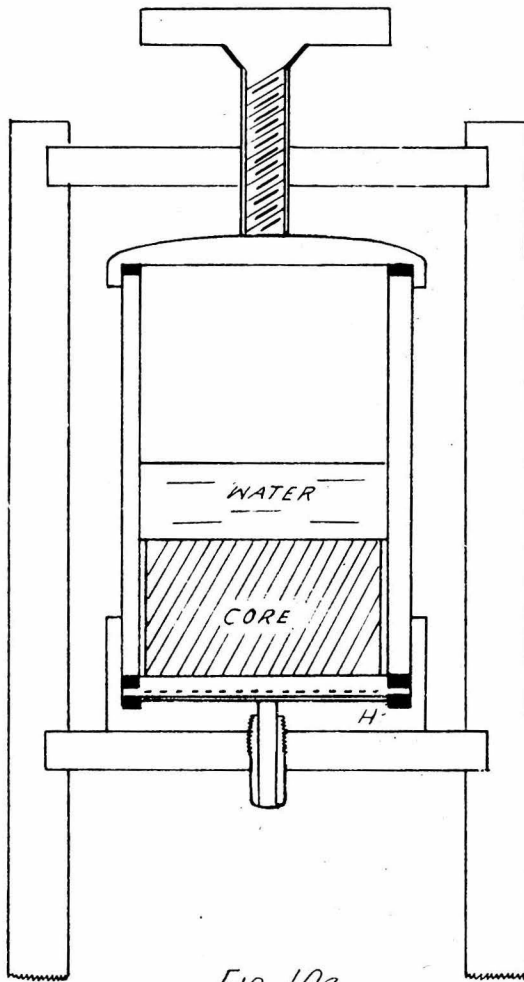


Fig. 10a

BAROID WALL BUILDING TESTER
WITH SAMPLE MOUNTED
IN CYLINDER

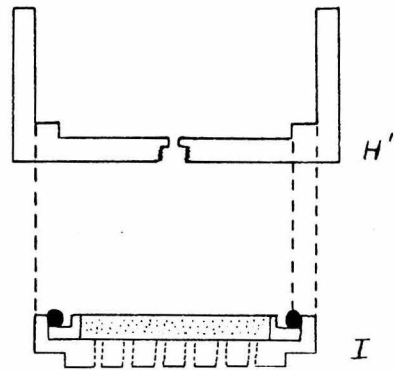


Fig. 10b
ADAPTORS

to 40 psi. The water, on the other hand, can freely move through the permeable porcelain. In this way we can establish any differential pressure between the oil and water up to 40 psi, the water remaining at atmospheric pressure. The pressure differential across the oil-water interface is in effect the capillary pressure. To any pressure thus established corresponds a fixed water-saturation, which is measured by subtracting the amount of effluent water from the amount originally present, or by weighing.

To insure operation of this mechanism we must establish a continuous water path between the core and the porcelain. Forcing the core directly onto the porcelain might result in breakage of the latter. Therefore a thin layer of powdered Coors porcelain was spread between the core and the porcelain. A small amount of cold water putty was mixed in with the porcelain powder, to provide a better bond with the sandstone and the porous disc. In this way a good continuous path for the water was maintained, preventing formation of an oil sheet between the core and the porcelain, while the compressibility of the intermediate layer protected the porcelain from physical damage.

The samples used, were outcrop samples of the following formations:

- Pico sandstone (Lower Pliocene, Southern California)
- Modello shaley sandstone (Upper Miocene, Southern California)
- Saugus, landlaid sandstone (Pleistocene, Southern California)
- Berea "clean" sandstone* (Lower Mississippian, Ohio)
- Mezozoic dense sandstone (Jurassic ?, Redlands, California)

*Obtained by courtesy of the production department of the Union Oil Company, Whittier, California.

Of the first four groups, sieve analysis were made using divisions between 16 and 250 mesh/inch. In addition, thinsections were prepared of these samples and analyzed by the point counter method described by Chayes (36).

The interfacial tension between the oil and water used in the experiments was determined by measurements of the displacement pressure of a fritted glass disc. The measurements were made by connecting the glass tube of a fritted glass gas-disperser, via a pressure regulating valve to a nitrogen bottle. Before pressure was applied the disperser was immersed in water, which would imbibe the disc and partly fill the tube of the disperser. Then pressure was applied and gradually increased in very small steps of the order of 0.05 p.s.i. The pressure was measured by a 0 - 15 p.s.i. gage. The minimum pressure at which gas would escape through the disc was registered as the displacement pressure for nitrogen gas, which for all practical purposes is equivalent to the displacement pressure for air, π_{a-w} . After this measurement was made the disc was imbibed fully with water again, and oil was injected into the partly water filled tube of the disperser below the water-air interface. The oil would collect at the surface of the water and form a clean oil-water interface, free of gas bubbles. The procedure was then repeated using the nitrogen pressure to force the oil against the water-saturated fritted glass disc and the displacement pressure for oil, π_{o-w} , was measured.

As the displacement pressures for porous membranes are directly proportional to the interfacial tension (see page 14) and the interfacial tension air-water is a known quantity (namely 72 dynes/cm) we can easily compute the oil-water interfacial tension. For the 30° A.P.I. gravity oil the following results were obtained: $\pi_{a-w} = 3.86$ psi $\pi_{o-w} = 1.2$ psi.
This gives for the interfacial tension: $S = \frac{1.2}{3.86} \times 72 = 22.4$ dynes/cm.

PART VDescription of samples and experimental resultsA. Berea sandstone

Sample description:

Average porosity: 27.1%

Average permeability to water: 25. m. darcies

Sieve analysis:

	Mess/inch	mm (opening)	% by weight
Larger than:	16	.991	1.13
" "		.420	.635
" "	80	.177	65.9
" "	120	.125	19.85
" "	170	.088	6.87
" "	210	.070	4.22
" "	250	.061	.662
Smaller than:	250	.061	.855

Point counter thinsection analysis:

Classification	% of total volume
Quartz	62.7
Porespace	28.1
Calcite	7.0
finer (clay)	1.5
Mica (white)	0.5
Feldspar	<u>0.2</u>
Total	100.0

The porespace as determined with the point counter method is 28.1% of the total volume, as compared to 27.1% found as average porosity from determinations by imbibition with water. The difference in this case is probably due to the closed, non-effective pore space, which appears in the thinsections as open space, but does not effect the imbibition by water.

The capillary pressure versus water saturation relations are given for two samples in fig. 11.

$$\text{We see that } \pi = \lim_{S_w \rightarrow 1} P_c = 0.6 \text{ psi}$$

The irreducible or bound water saturation is approximately 0.18 .

B. Pico sandstone (from outcrop near Sunland, California)

Sample description:

Average porosity: 37.6%

Average permeability to water: 354 m. darcies

Sieve analysis:

	Mess/inch	mm (opening)	% by weight
Larger than:	16	.991	9.31
" "		.420	37.54
" "	80	.177	26.3
" "	120	.125	7.91
" "	170	.088	7.06
" "	210	.070	9.0
" "	250	.061	1.725
Smaller than:	250	.061	1.485

37A

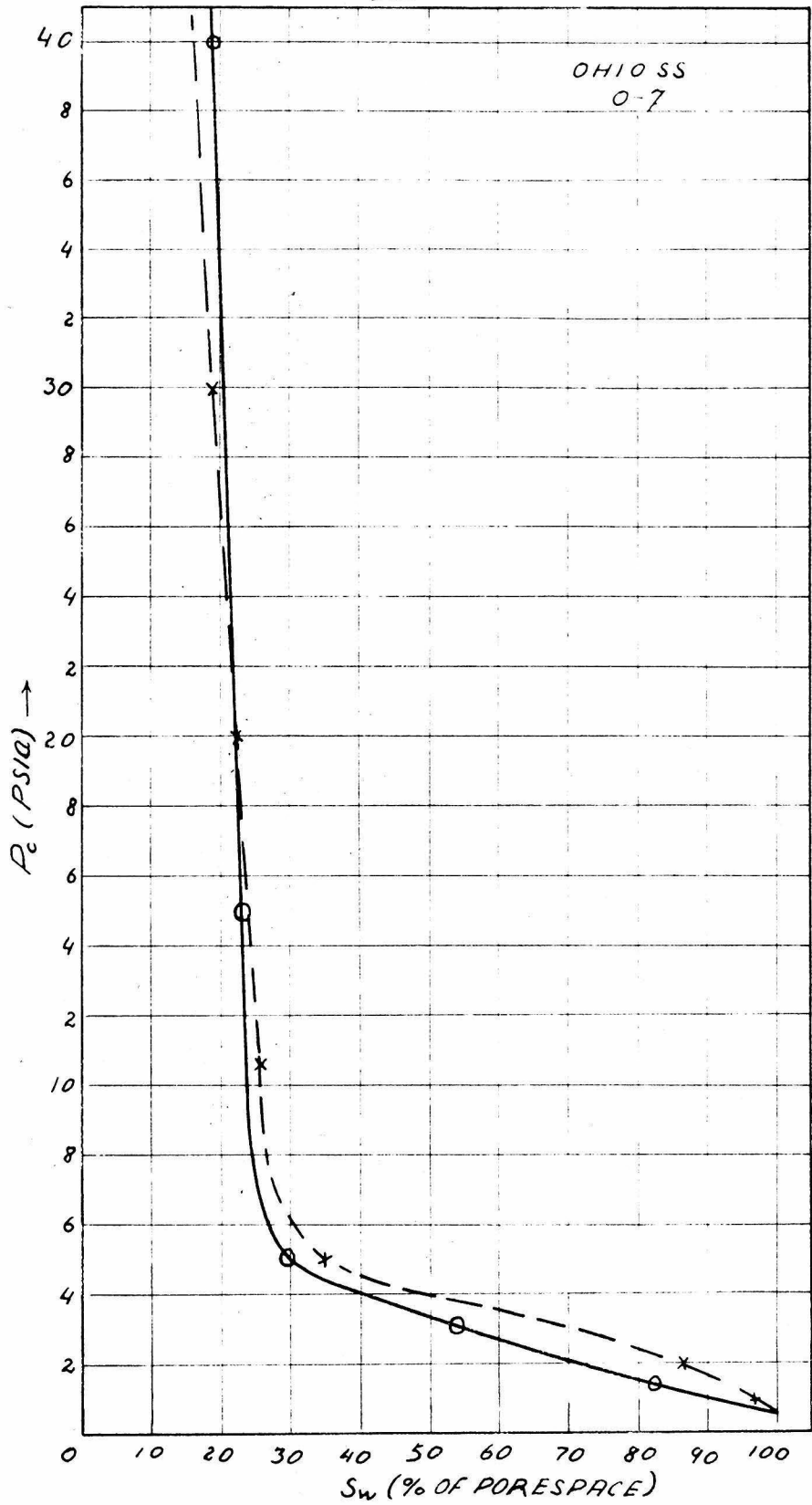


FIG 11

Point counter thinsection analysis:

Classification	% of total volume
Quartz	43.6
Porespace	38.6
Limonite	6.75
Feldspar	5.46
Mica	2.58
Accessories	1.01

The capillary pressure versus water saturation relations are shown for two samples of the Pico sandstone, in fig. 12 and fig. 13.

We find for the displacement pressure the values of $= 0.5$ and $= 0.4$, respectively, and for the bound water content 0.27 and 0.26 expressed, as a fraction of the total porespace.

It must be pointed out that of necessity, the sieve and thin-section analyses are not made from the same specimen, for which the capillary relations are established. For this case, however, the displacement pressure for nitrogen gas was measured directly on the specimen of which the thinsection was made. We obtained a value $p_{air} = 1.25$ psi. This gives for the displacement pressure for oil, approximately $\frac{30}{78} \times 1.25 = 0.49$ psi, which checks well with the above results.

C. Saugus sandstone

Sample description:

Average porosity: 11.7%

Average permeability to water: 2.48 m. darcies

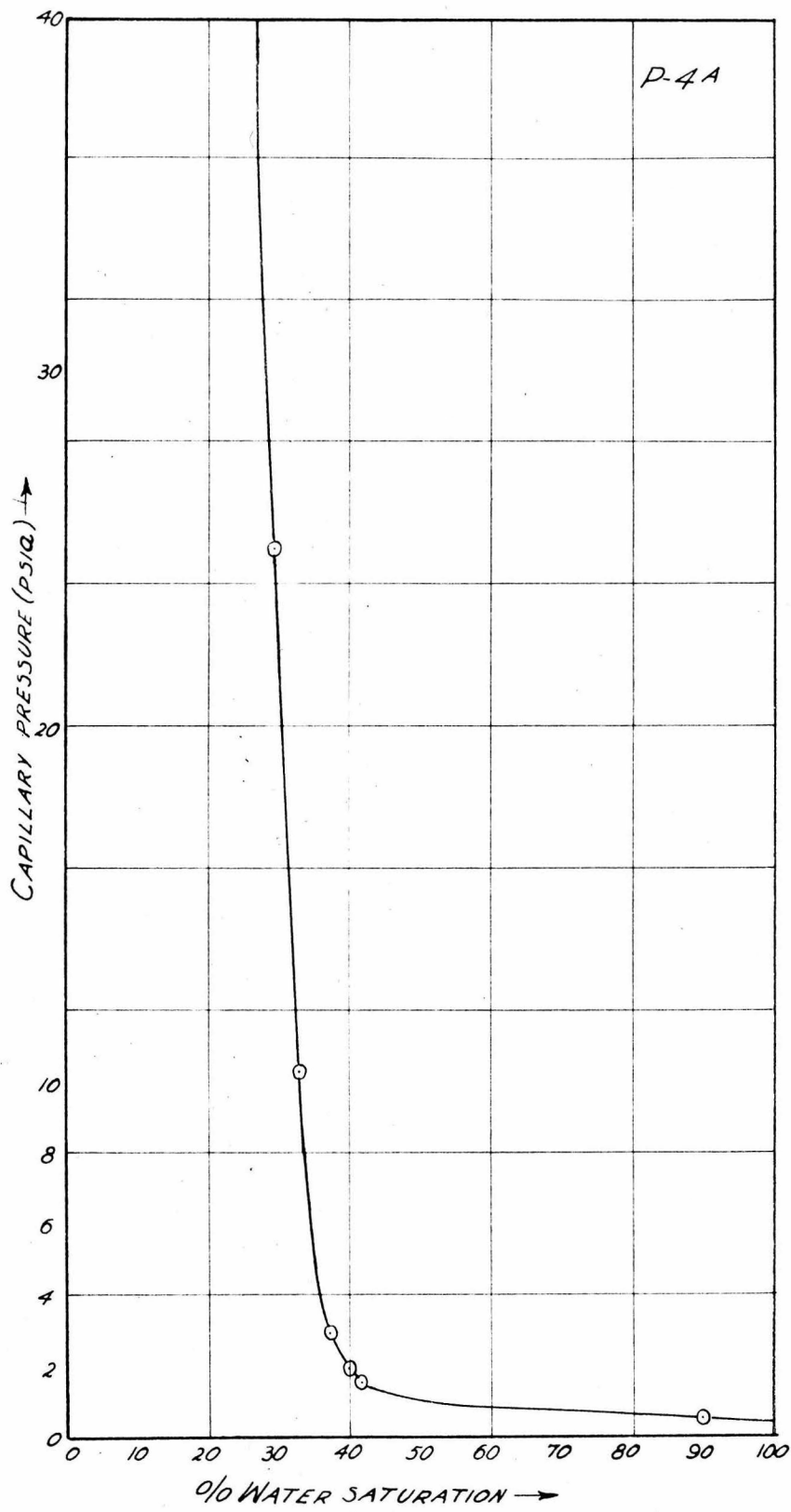
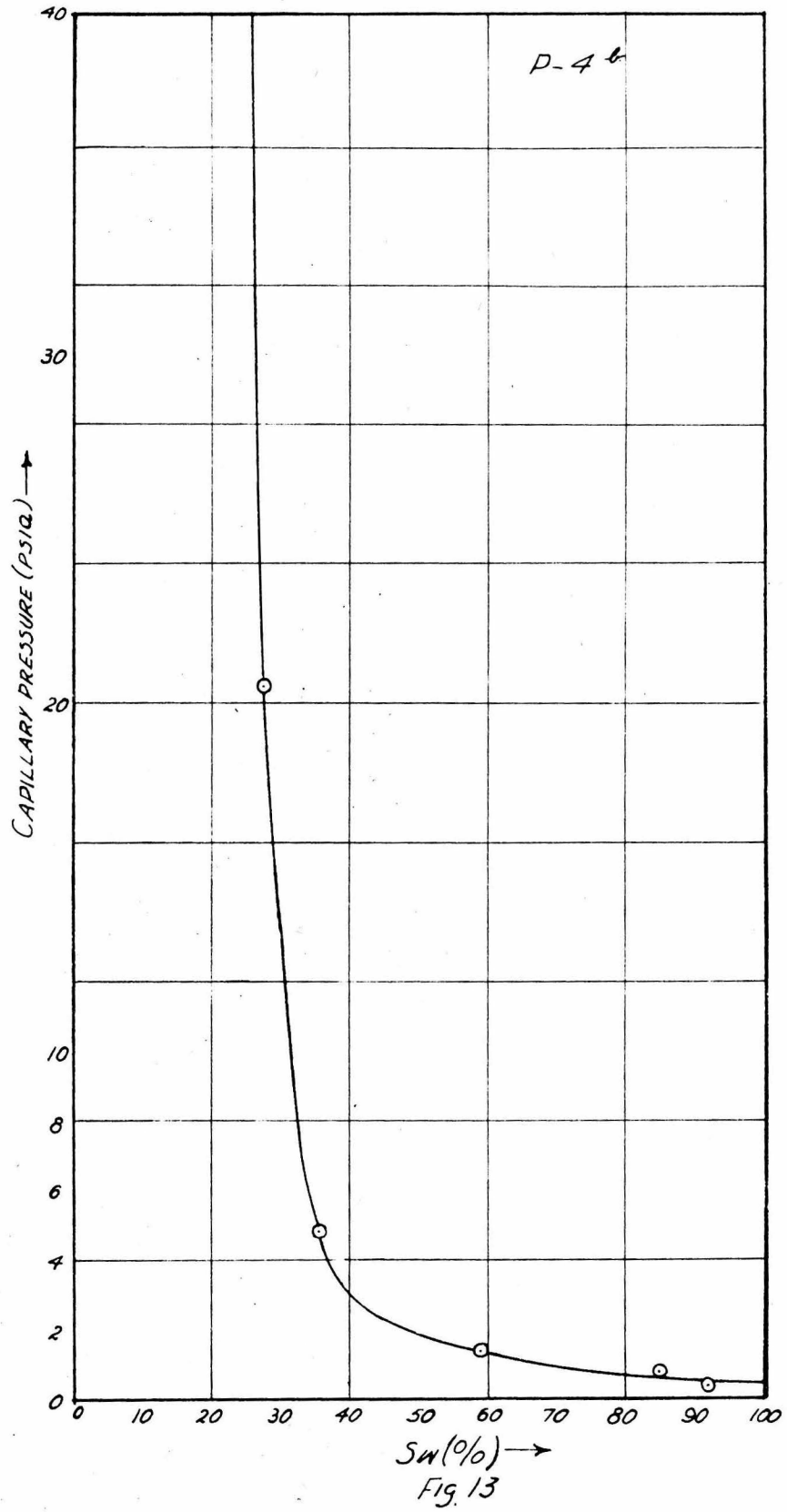


Fig. 12



Sieve analysis:

	Mess/inch	mm (opening)	% by weight
Larger than:	16	.991	20.1
" "		.420	35.0
" "	80	.177	28.1
" "	115	.131	6.8
" "	170	.088	3.4
" "	210	.070	3.2
" "	250	.061	0.7
Smaller than:	250	.061	2.7

Point counter thinsection analysis:

Classification	% of total volume
Quartz	34.2
Porespace	25.*
Calcite	19.8
Fines	9.6
Feldspar	6.9
Mica	3.6
Accessories	<u>0.9</u>
Total	100.0

The capillary characteristics are given in fig. 14.

We find $\pi = \lim_{S_w \rightarrow 1} P_c = 3.8 \text{ psi}$

The bound water content is approximately 60.2%.

*This value is not at all representative as because of the poor cementation of the sandstone, the thinsection was badly torn.

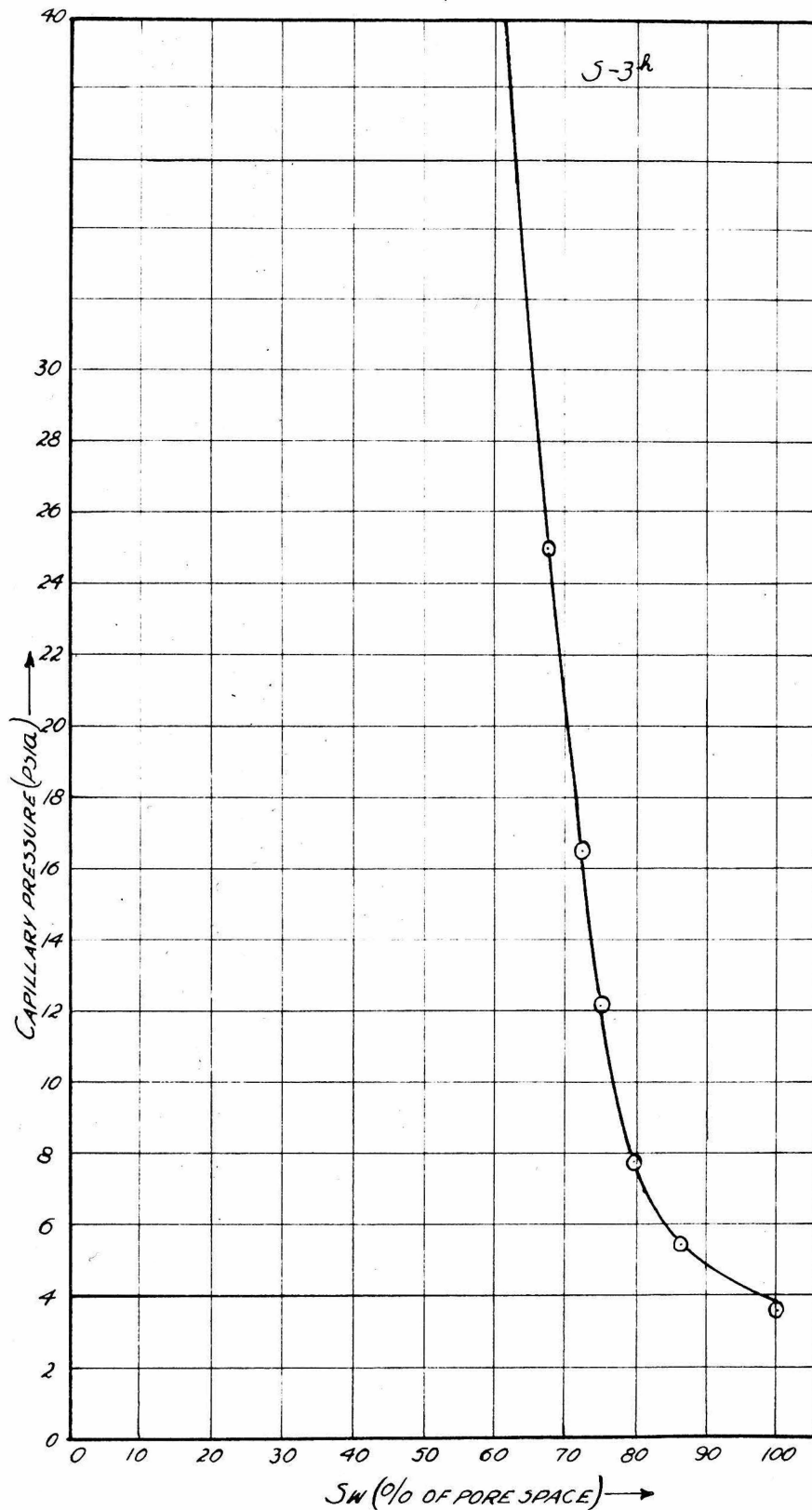


Fig. 14

D. Modello shaley sandstone

Sample description:

Porosity: 15.04%

Permeability to water: 1.47 m. darcies

Sieve analysis:

	Mess/inch	mm (opening)	% by weight
Larger than:	16	.991	1.12
" "		.420	12.3
" "	80	.177	41.7
" "	115	.131	19.33
" "	170	.088	7.39
" "	210	.070	7.06
" "	250	.061	7.94
Smaller than:	250	.061	4.16

Point counter than section analysis:

Classification	volume %
Quartz	47.
Porespace	15.3
Feldspar	6.64
Mica (primary and secondary)	11.16
Fines	16.7
Accessories (including calcite)	<u>3.3</u>
Total	100.0

The capillary pressure versus water saturation relationship is given in fig. 15.

$$\pi = \lim_{S_w \rightarrow 1} P_c = 2.2 \text{ psi}$$

and the bound water content, $C_w = .675$.

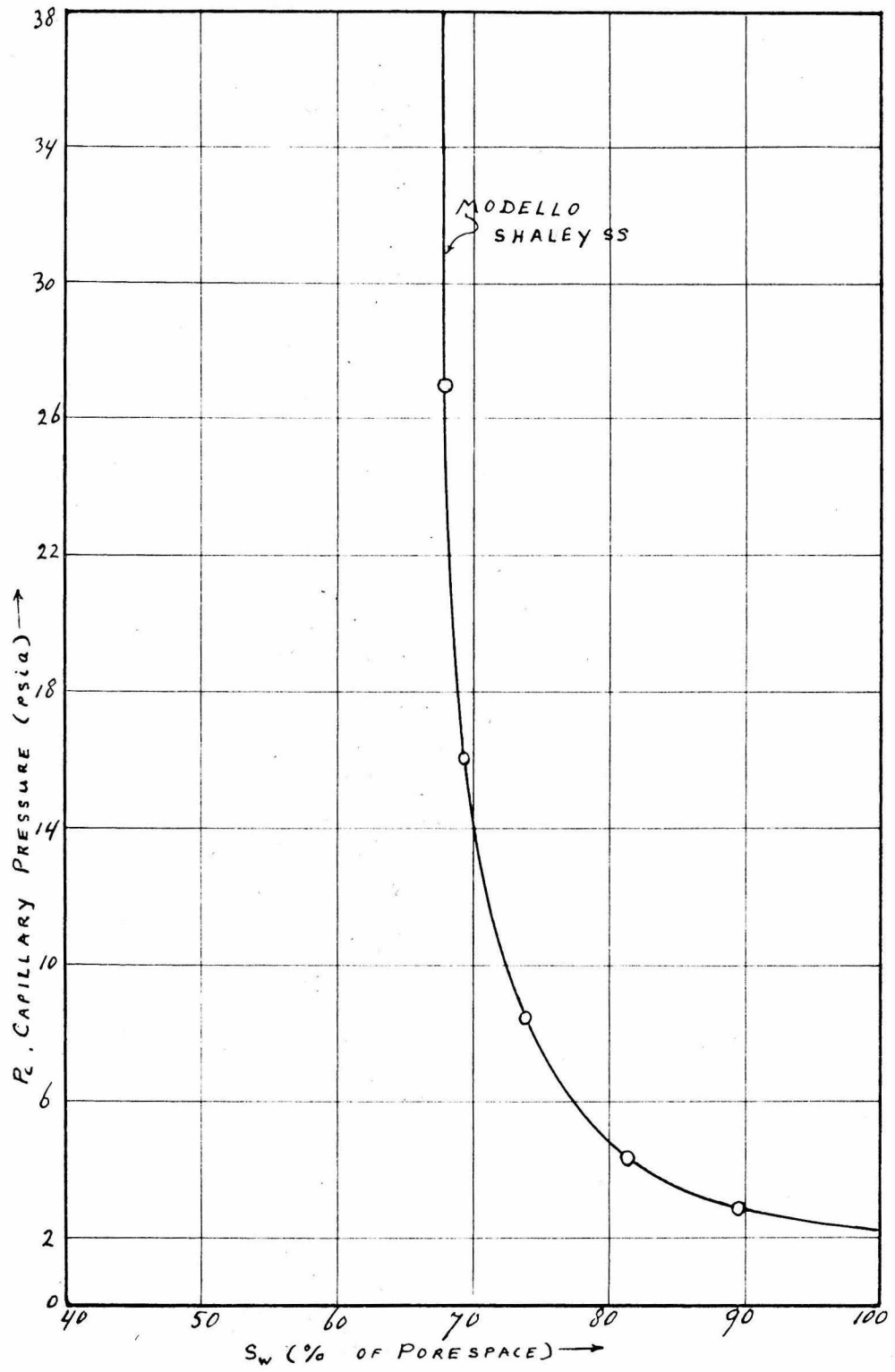


Fig. 15

E. Finally fig. 16, curve (a), gives the same relations for a dense Mesozoic (Jurassic?) sandstone. We find $\pi = 5.4$ p.s.i. and $C_w = .45$.

Fig. 16, curve (b), shows the capillary pressure - saturation graph for a Modello sandstone. Here we have

$$\pi = 1.25 \text{ p.s.i. and } C_w = 0.48 .$$

The Kozeny constants for these various rocks can be calculated from equation (10b) using the measured values of the displacement pressure π , the permeability K , and the fractional porosity ϕ .

From equation (12), the interstitial surface areas A^i per unit of porespace and A , per unit of bulk volume are calculated, using the measured values of π and ϕ . In both equations (10b) and (12) the value of $S = 22.4$ dynes/cm as was determined in part IV (page 35) is substituted.

The measured and computed quantities are listed in Table A. Also given are the electrochemical formation coefficients for the various sandstones which were measured in the course of another research project by this author (28).

We notice from the data given in Table A, that a fairly good correlation exists between the interstitial surface area per unit of bulk volume and the electrochemical formation coefficient. Fig. 17 represents this correlation graphically.

The scattering in the points as shown in fig. 17 is probably partly due to experimental inaccuracies, and partly caused by the fact that the samples on which the capillary measurements were made are not exactly identical to the ones for which the electrochemical potentials were measured.

The large differences in character, composition, age and origin of the samples used, gives good assurance that the graph of fig. 17 represents a universal relationship for sediments of the shale sandstone series.

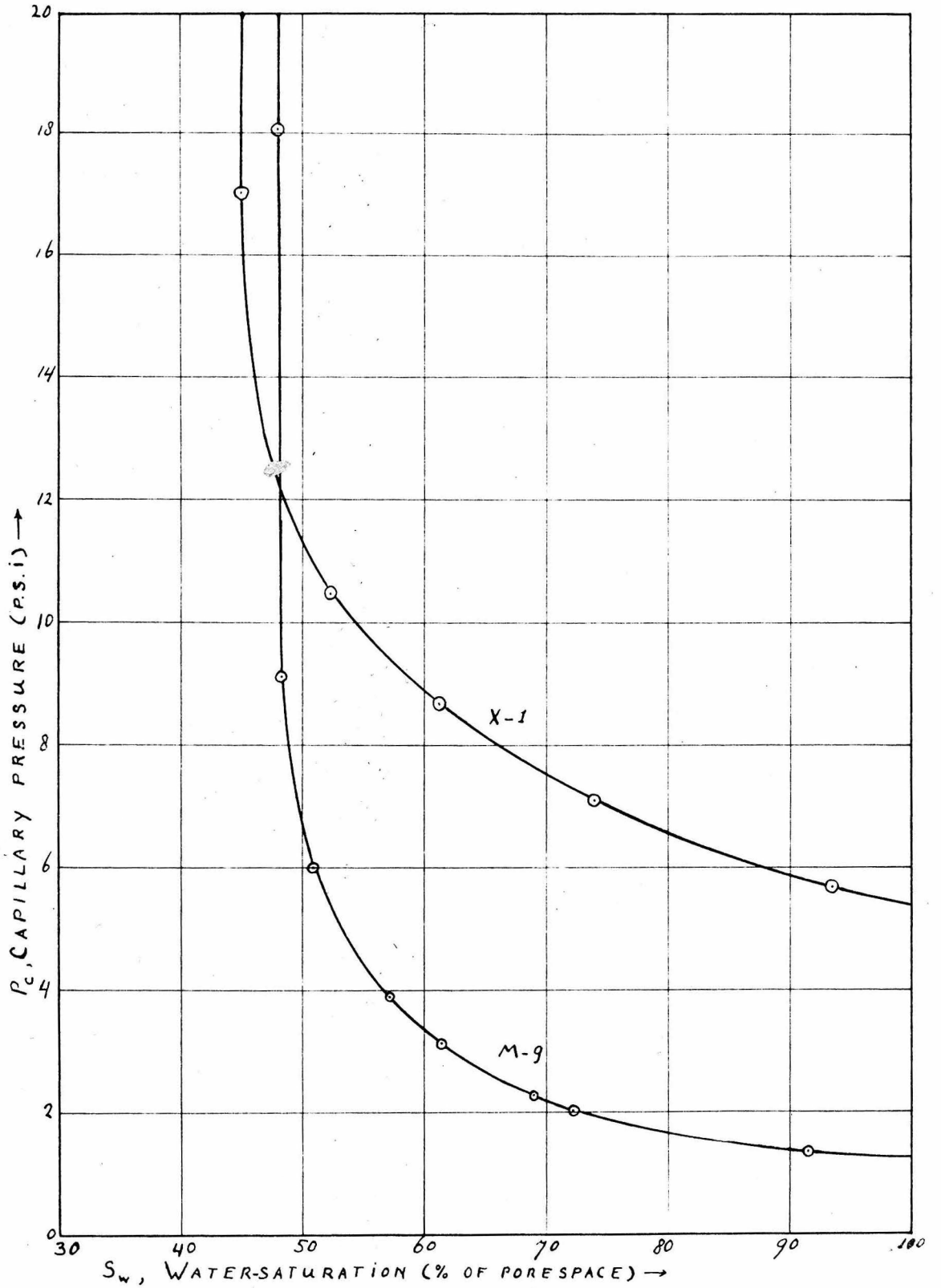


Fig. 16

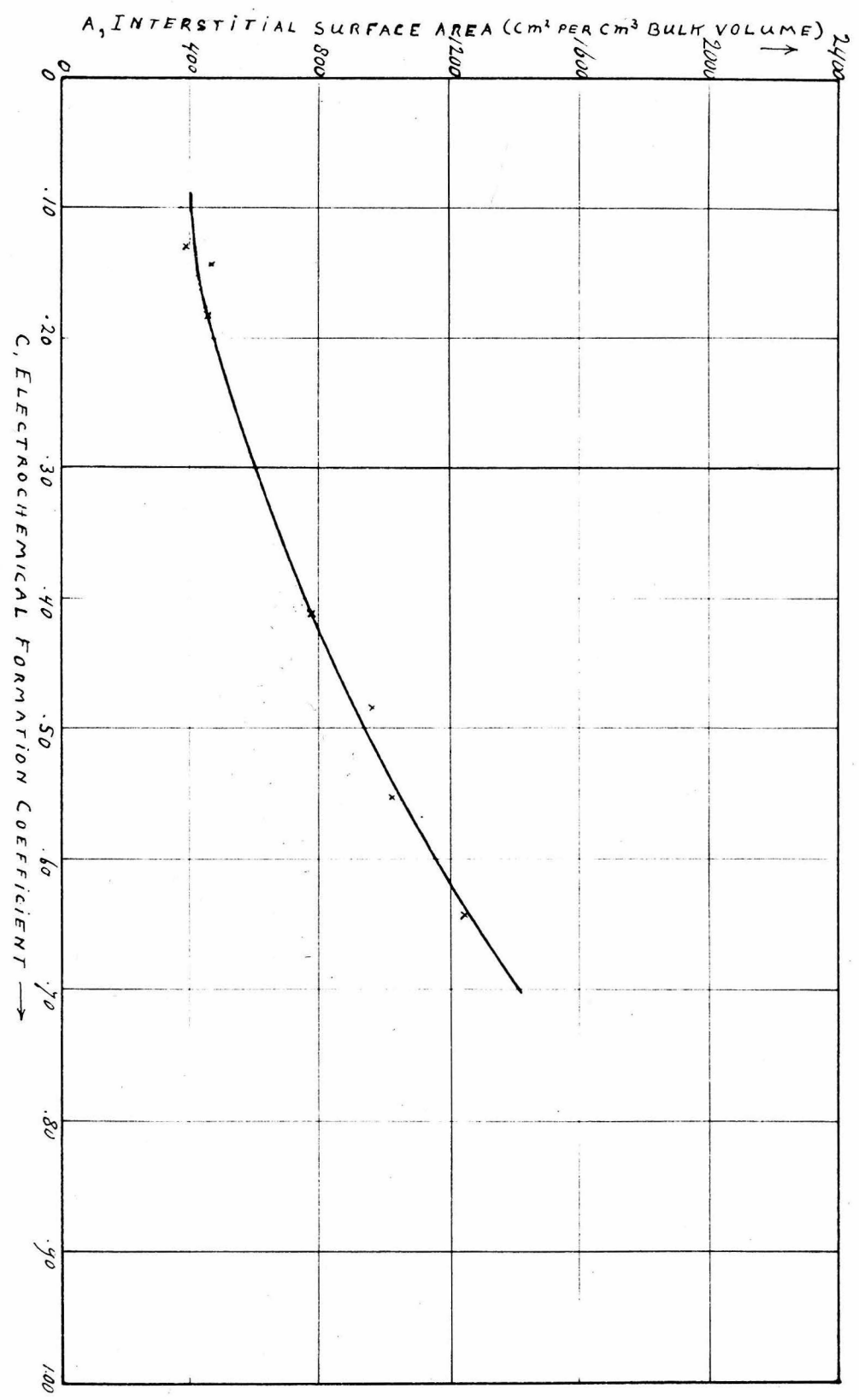


Fig. 17

TABLE A

Sample No.	π p.s.i.	π dynes/cm ²	fractional porosity	K milli-darcys	K c.g.s. units	$\frac{\pi(K)}{S(\phi)^2}$ c.g.s. units	k	A' cm ²	A cm ²	C formation coefficient
Berea ss O-7	0.6	41,400	.254	25	2.462×10^{-10}	.0577	300	1850	470	0.142
Pico ss P-4a	0.45	31,000	.333	318	3.14×10^{-9}	.1339	55.9	1380	460	0.181
Pico ss P-4b	0.45	31,000	.284	390	3.85×10^{-9}	.1608	38.6	1380	393	0.126
Saugus ss S-3h	3.80	262,400	0.106	2.62	2.59×10^{-11}	.1828	50	11700	1241	0.64
Modello shaley ss M-4	2.2	152,000	0.150	1.47	1.45×10^{-11}	.0668	224	6790	1020	0.55
Mesozoic dense ss X-1	5.4	372,000	0.058	0.015	1.48×10^{-13}	.0265	1420	16600	964	0.477
Modello ss M-9	1.25	86,200	0.202	35	3.46×10^{-10}	.1590	39.6	3840	777	0.410

NOTE: 1 p.s.i. = 69,000 dynes/cm²

1 darcy = 9.8692×10^{-9} c.g.s. units of permeability

S = 22.4 dynes/cm

The large calcite content of the Saugus sandstone (see thin-section analysis) may well indicate that the relation also holds true for calcareous sediments.

Rose and Bruce (24) have shown that a rough correlation exists between the bound water content C_w and the interstitial surface area per unit pore volume.

Table B gives the values for C_w , C and A^1 for the sandstones that were investigated.

TABLE B

<u>Sample</u>	<u>No.</u>	<u>C_w</u>	<u>C</u>	<u>A^1 (cm² per cm³ pore volume)</u>
Berea ss	O-7	0.18	0.142	1850
Pico ss	P-4a	0.27	0.181	1380
Pico ss	P-4b	0.255	0.126	1380
Saugus ss	S-3h	0.63	0.64	11700
Modello shaley ss	M-4	0.675	0.55	6790
Mesozoic ss	X-1	0.45	0.477	16600
Modello ss	M-9	0.48	0.41	3840

We see that for these samples the correlation between C_w and A^1 is not very good.

There seems to be some correlation between C_w and C . It appears however, that the character of the rock minerals other than their surface area per unit volume seems to have a larger effect on C_w than on C . In general the presence of argillaceous materials will increase C_w more, percentagewise, than they increase the interstitial surface area.

From the values of k , and C listed in Table A it is apparent that no direct correlation exists between the Kozeny constant and the electrochemical formation coefficient. This means that probably the correlation found by Rose and Bruce, between the amount of clay in a

sandstone and the Kozeny constants applies only to sandstones which differ in clay content but do not vary to any important extent in other characteristics such as the overall composition of the non-argillaceous parts, the sorting and the cementation. This explanation is supported by the data for the Pico and Modello sandstones. Table A shows that within each group k is larger for the sample with the higher formation coefficient. However, comparison between the groups indicates that no general correlation exists.

Table C shows a listing of the amount of fines as determined from sieve analysis and the Kozeny constants of various samples. The fines being taken as the material < 250 mesh.

TABLE C

<u>Sample</u>	<u>No.</u>	<u>fines (weight %)</u>	<u>k</u>
Berea ss	O-7	1.63	300
Pico ss	P-4b	2.59	38.6
Saugus ss	S-3h	2.69	30
Modello shaley ss	M-4	5.1	224

We see that for these widely varying specimen no correlation is obtained between the amount of fines and the Kozeny constant. It is realized, however, that the weight percentage of fines depends very strongly on the maximum size taken as the limit of the fine fraction. For instance taking 200 mesh as the upper limit would result in very different percentages.

For this reason it seems that the information obtained by sieve analysis is not of great value in determining the characteristics of sediments with respect to the behaviour of fluids contained in their interstices.

Part VIApplications of subsurface determinations of
displacement pressures

As pointed out in the introduction to this thesis, the most interesting application of displacement pressure determinations are as an aid in the location of stratigraphic traps.

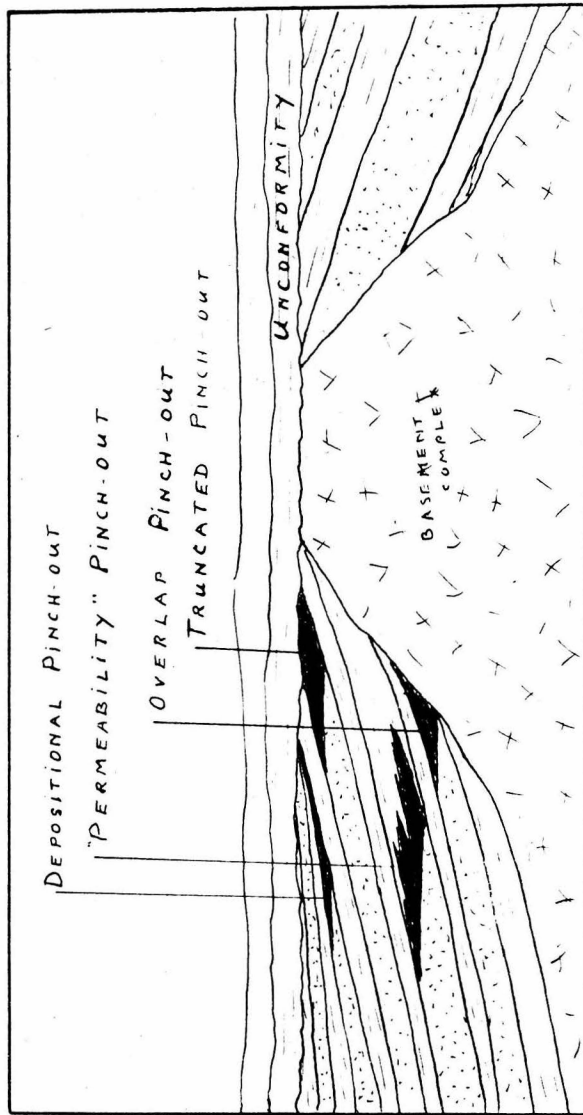
The stratigraphic traps may be divided into four groups:

- a) Depositional pinch-outs, caused by gradual thinning up-dip of all members of the formation.
- b) Truncated pinch-outs, where the beds of a formation are truncated by an overlying series of sediments.
- c) Overlap pinch-outs, occurring on regional unconformities or at the base of marine overlap of a basement complex.
- d) Permeability pinch-outs, caused by a lateral change in facies of a rock unit.

Fig. 18 gives an illustration of the mode of occurrence of these various traps.

In all cases the traps are caused by "impermeable" rocks overlying or bordering the porous reservoir rocks. In cases a, b, c, there is mostly a sharp contact between the two units. In the case of the permeability pinch-out the facies change is gradual.

Whether or not the trap has the required properties to hold a commercial accumulation of oil or gas depends upon the geometric



TYPES OF STRATIGRAPHIC TRAPS

Fig. 18

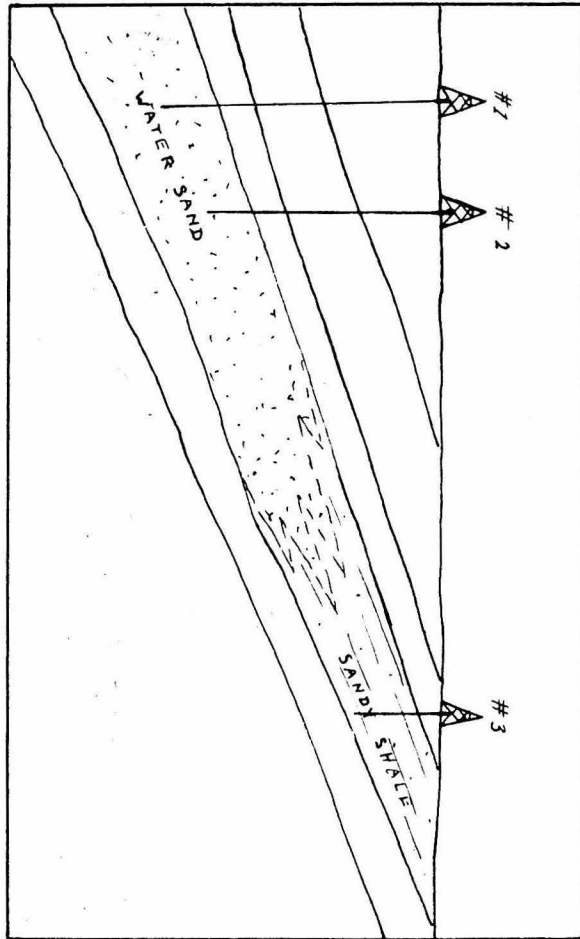
dimensions of the traps and the displacement pressure of the capping formation.

In the course of geological and geophysical exploration for oil reservoirs, unconformities and overlaps of the types a, b and c can be found by existing methods of exploration. The permeability pinch outs cannot be detected so easily.

However, to determine whether or not the capping formation has the right properties we have to use information from outcrops or drill holes. If the caprock outcrops we can determine its properties directly. If no outcrops are present or the rocks change laterally in facies we have to rely upon drill hole information and make extrapolations or interpolations from the data assembled from the existing holes.

As electrologs are run in practically all exploratory holes, they are the natural tool to be used for the required determinations. The computation of the displacement pressures from the electrochemical formation coefficients which in turn are determined from the self potential curves of electrologs introduces a rapid means of obtaining the necessary information.

To illustrate the proposed usage of this method more specifically, an example is given in fig. 19 of the location of a permeability pinch-out trap. Wells 1 and 2 show a watersand at the depth of the formation in which we are interested. The electrochemical formation coefficient is larger in case 2 than in case one, showing lateral variation of the sand. Well three shows a tight shaley sand with a high formation coefficient. Interpolation between wells 2 and 3 enables us to determine at which point the displacement pressure of the formation becomes large enough to screen out a commercial quantity of oil.



LOCATING OF A "PERMEABILITY" PINCH-OUT TRAP

Fig. 19

At this point it remains to consider the quantitative relationship between displacement pressures and the size of accumulations of oil or gas that can be obtained.

If we have an oil density of 0.80 g/cm^3 and a brine density of 1.1 g/cm^3 , the density difference between the water and the oil,

$\rho_{wo} = 0.3 \text{ g/cm}^3$. Therefore the total upward force acting on 1 cm^3 of oil will be 0.3g . This force is counteracted by the capillary forces in the caprock.

A displacement pressure of 1 p.s.i. is the equivalent of 70.31 g/cm^2 . This means that a displacement pressure of 1 p.s.i. is sufficient to prevent upwards migration of a column of $\frac{70.31}{0.3} = 234 \text{ cm} = 7.68 \text{ feet}$ of oil.

$$\text{In general } H = \frac{2.3 \pi}{\rho_{wo}} \dots \dots \dots (13)$$

where H is the height of accumulated oil in feet and π is the displacement pressure of the caprock in p.s.i. and ρ_{wo} is given in g/cm^3 .

The same relation holds for accumulations of gas, with ρ_{wg} , the density difference between the water and the gas substituted for

$$\rho_{wo}$$

To determine ρ_{wo} the approximate surface gravity and content of light hydrocarbons of the oil must be estimated from data of producing fields in the region in question. If no such data are available, average values have to be assumed. The estimate of the subsurface density of the oil is then made using fig. 7 and/or the procedure outlined by Standing and Katz (31).

If the electrochemical formation coefficient is found from electrologs, we obtain the interstitial surface area per unit bulk volume, A , from fig. 17. The displacement pressure, π , is then found

from the formula

$$\frac{\pi}{S} = \frac{A}{\varphi}$$

where φ is the fractional porosity, which also may be found from electrologs (37).

The interfacial tension, S , is estimated from the relations shown in figures 5 and 9, for the depth to the horizon in question.

The possible oil or gas accumulation is determined using equation (13). Whether or not the possible accumulation is commercial depends amongst other factors, on the size of the trap and the porosity and connate water content of the reservoir rock, that is the total amount of oil that can be expected after the height of the accumulation has been determined.

REFERENCES

1. P. D. Trask and H. W. Patnode, Source Beds of Petroleum. A.A.P.G. publication, (1942), Tulsa.
2. R. C. Beckstrom and F. M. van Tuyl: Compaction as a Cause of the Migration of Petroleum. Bull. A.A.P.G. XII, (1928), 1049.
3. E. T. Thomas: The Effect of Pressure on the Migration of Oil. Bull. A.A.P.G. VIII, (1924), 527.
4. L. F. Athy: Compaction and Oil Migration. Bull. A.A.P.G. XIV, Part 1, (1930), 25.
5. R. H. Fash: Theory of Origin and Accumulation of Petroleum. Bull. A.A.P.G. 28, Part 2, (1944), 1510.
6. W. L. Russell: Is Geologic Distillation of Petroleum Possible? Bull. A.A.P.G. XIII, (1929), 75.
7. John L. Rich: Moving Underground Water as a Primary Cause of the Migration and Accumulation of Oil and Gas. Economic Geology, 16 No. 6 (1921), 347.
8. John L. Rich: Further Notes on the Hydraulic Theory of Oil Migration and Accumulation. Bull. A.A.P.G. VII, (1923), 213.
9. John L. Rich: Function of Carrier Beds in Long-distance Migration of Oil. Bull. A.A.P.G. XV, Part 2, (1931), 911.
10. R. D. Wyckoff and H. G. Botset: The Flow of Gas-Liquid Mixtures through Unconsolidated Sands. Physics 7 (1936), 325.
11. M. C. Leverett: Flow of Oil-Water Mixtures through Unconsolidated Sands. A.I.M.E. Transactions 132 (1939), 149.

12. M. C. Leverett and W. B. Lewis: Steady Flow of Gas-Oil-Water Mixtures through Unconsolidated Sands. A.I.M.E. Transactions 142 (1941), 107.
13. H. G. Botset: Flow of Gas-Liquid Mixtures through Consolidated Sands. A.I.M.E. Transactions 136 (1940), 91.
14. M. C. Leverett. op. cit. pg. 168, fig. 12.
15. H. V. Dodd: Some Preliminary Experiments on the Migration of Oil up Low-Angle Dips. Economic Geology, 17, No. 4 (1922), 274.
16. M. C. Leverett: Capillary Behaviour in Porous Solids. A.I.M.E. Transactions 142 (1941), 152.
17. F. E. Bartell and H. J. Osterhof: The Work of Adhesion between Solid and Liquid Phases. Zeitschrift fur Phys. Chemie 130 (1927), 715.
18. F. E. Bartell and H. J. Osterhof: Three Fundamental Types of Wetting. Adhesion Tension as the Measure of Degree of Wetting. Jn. Phys. Chem. 34 (1930), 1399.
19. F. E. Bartell and Ch. E. Whitney: Adhesion Tension (a receding contact angle, pressure of displacement method). Jn. Phys. Chem. 36 (1932), 3115.
20. Champion and Davy: Properties of Matter, 99 - 101, New York, (1937) Prentice Hall.
21. Champion and Davy: op. cit. pg. 113.
22. W. O. Smith: The Final Distribution of Retained Liquid in an Ideal Uniform Soil. Physics 4 (1933), 425 - 438. See also other references at the end of Leverett's paper (16).
23. M. C. Leverett: op. cit. (16), Fig. 4, Pg. 161.

24. W. Rose and W. A. Bruce: Evaluation of Capillary Character in Petroleum Reservoir Rock. *Pet. Tech.* May, 1949, (T.P. 2594) p. 127
25. P. C. Garman: Capillary Rise and Capillary Movement of Moisture in Fine Sands. *Soil Science* 52 (1942), 1 - 14.
26. J. Kozeny: Uber Kapillare Leitung des Wassers in Boden. *Sitz-b. Akad. Wiss. Wien. Math-nature. K.I.*, 136, (1927) 27 - 306.
27. J. Kozeny: Ground Water Movement. *Wasserkraft und Wasserwirtschaft* (1927) 22, 67, 86.
28. B. H. Sage and W. N. Lacey: Formation Volumes and Energy Characteristics of the Gas Cap Material from Kettleman Hills Field. *Drilling and Production Practice* (1936), 158 - 170. *Am. Petr. Inst. Publication.*
29. M. B. Standing and D. L. Katz: Density of Natural Gases. *A.I.M.E. Transactions* 146 (1942), 140.
30. G. R. Hocott: Interfacial Tension between Water and Oil under Reservoir Conditions. *A.I.M.E. Transactions* 132 (1939), 184.
31. M. B. Standing and D. L. Katz: Density of Crude Oils, Saturated with Natural Gas. *A.I.M.E. Transactions* 146 (1942), 159.
32. B. H. Sage, D. C. Webster and W. N. Lacey: Mixtures of Methane and Crude Oil. *Jn. of Industrial and Engineering Chemistry*, 28 (1936), 984.
33. B. H. Sage, D. C. Webster and W. N. Lacey: Solubility of Methane in Four Light Hydrocarbons. *Industrial and Eng. Chemistry*, 28 (1936), 1045.
34. B. H. Sage, J. A. Davies, J. E. Sherborne and W. N. Lacey: Ethane - Crystal Oil System. *Industrial and Eng. Chemistry* 28 (1936), 1328.

35. H. K. Livingston: Surface and Interfacial Tensions of Oil-Water Systems in Texas Oil Sands. *Petroleum Technology*, November, 1938.
36. F. Chayes: A Simple Point Counter for Thinsection Analysis. *The American Mineralogist*, 34 (Jan. - Feb., 1949), Pg. 1.
37. L. de Witte: Infiltration of Drilling Fluids in Relation to Quantitative Analysis of Electrologs. Thesis. California Institute of Technology, 1950.
38. L. de Witte: Experimental Studies on the Characteristics of Electrochemical Potentials in Drill Holes. Thesis. California Institute of Technology, Pasadena, (1950).

EXPERIMENTAL STUDIES ON THE CHARACTERISTICS OF
THE ELECTROCHEMICAL POTENTIALS ENCOUNTERED IN DRILL HOLES

Thesis by

Leendert de Witte

In Partial Fulfillment of the Requirements
For the Degree of
Doctor of Philosophy

California Institute of Technology
Pasadena, California
1950

ABSTRACT

This thesis describes the results of experimental studies on the characteristics of the electrochemical potentials encountered in drill holes and registered by electrologging apparatus.

The experiments were carried out by bringing samples of sediments into contact with two solutions of different salinities on opposite sides and measuring the difference in potentials between the solutions.

The following conclusions were drawn from the measurements thus obtained:

The potentials are independent of the amount of material involved. They are proportional to the logarithm of the concentration ratio of the two solutions. The potentials decrease slowly with time.

There is no sharp demarcation between the electrochemical behavior of sandstones and shales, but rather there exists a complete continuity in the potentials exhibited across sediments of the sandstone shale series.

This continuity is explained using the concept of "apparent ion mobilities".

To classify sediments according to their electrochemical behavior, the electrochemical formation coefficient, C , is introduced. Dense argillaceous shales have a formation coefficient of 1. Inert clean sands have $C = 0$. It is

shown however that in practice sands may very seldom be considered inert.

A correlation exists between the formation coefficient and the ratio of the amount of conductive solids or argillaceous materials over porosity (see references 8 and 13). The influence of temperature on self potentials is computed theoretically and confirmed experimentally.

It is pointed out that dense formations may give considerable self potential kicks on electrologs. This conclusion is confirmed by measurements of the potentials across quartzites.

The general conclusions concerning the character of the electrochemical potentials are extended to the self potentials across calcareous formations.

The application of the analysis of the electrochemical potentials to electrolog interpretation is outlined. Also the possibility of electrochemical testing of sediments as a new tool in surface geology is indicated.

ACKNOWLEDGMENTS

The author wishes to make acknowledgments to:

Dr. S. Frankel, Dr. R. M. Badger and Dr. G. W. Potapenko, with whom various aspects of the problem were discussed.

Mr. W. Otto and Mr. R. von Huene for valuable advice in the preparation of the samples used.

Mr. J. N. Harris for suggestions for the construction of the measuring circuits.

TABLE OF CONTENTS

<u>PART</u>	<u>TITLE</u>	<u>PAGE</u>
	INTRODUCTION	1
I.	EXPERIMENTAL EQUIPMENT AND PROCEDURE	9
II.	PRELIMINARY MEASUREMENTS	17
III.	POTENTIALS ACROSS SEDIMENTS OF THE SANDSTONE SHALE SERIES	24
IV.	THE VARIATIONS OF SELF POTENTIALS WITH TEMPERATURE	33
V.	SELF POTENTIALS OF DENSE ROCKS AND OF LIMESTONES The Influence of Compaction on the Self Potentials	46
VI.	APPLICATIONS OF THE ANALYSIS OF ELECTROCHEMICAL POTENTIALS ACROSS SEDIMENTS	48
	REFERENCES	55

INTRODUCTION

Since the early days of commercial application of electrologging, attempts have been made to relate the spontaneous potentials registered on the electrologs to some of the basic characteristics of the formations traversed, such as porosity and permeability, and (or) to the composition of the connate waters and drilling fluids.

In spite of the many theories and hypotheses put forward on this subject, the spontaneous or self potential curves still defy in many cases any quantitative analysis.

One of the first attempts to explain the presence of spontaneous potentials in drill holes was made by C. and M. Schlumberger and E. O. Leonardon. In their first paper (1) they attributed the potentials almost entirely to electro-filtration effects. Drilling mud, under its own hydrostatic pressure infiltrates the porous formations. This gives rise to so-called "streaming potentials" between the mud and the formations. Such potentials depend on the surface characteristics of the porous medium and are proportional to the pressure difference across the medium in which the infiltration takes place. They are independent of the porosity of the formation. Although these basic characteristics were recognized and clearly stated in the above quoted paper, the authors nevertheless used the term "porosity diagram" for the self-potential log.

After the publication of this first paper it soon became apparent that spontaneous potentials often occurred in cases where no pressure difference existed between the mud and the formation waters. This phenomenon was explained in a second paper by the same authors (2), as the effect of other electrochemical processes of which the most important were the diffusion or liquid junction potentials. Apart from these, contact potentials of unknown nature, existing at the boundaries between pervious and impervious formations were recognized as influencing the S.P.'s (self potentials).

Furthermore, they showed experimentally that the combined effect of the boundary and diffusion potentials could be expressed as:

$$E_t = K \log_{10} \frac{R_2}{R_1} \quad (1)$$

where R_1 and R_2 are the resistivities of the connate water and the mud respectively.

Their experiments were carried out using a coarse siliceous sand and a plastic gray clay and solutions of sodium chloride. For this combination they found $K \approx 17$.

Regarding the diffusion potential set up at the contact between the coarse porous layer and the mud (or free electrolyte) the following description was given:

"There is a contact between sweet and salt water in a medium where the pores have large dimensions, and where the

mobility of the ion is not appreciably hindered, by the presence of the porous material. Experience shows that the electromotive force is the same as though the contact took place directly between the two fluids alone."

Regarding the nature of the boundary potentials at the contacts with the impervious rock no statements were made.

This uncertainty and many other difficulties encountered by subsequent investigators in attempts to explain the electrochemical S. P.'s has been mostly due to the failure to recognize the continuity in the geologic series of sedimentary rocks. Coarse sands and fine argillaceous shales are physically only extremes in a completely continuous series of sediments. It is therefore logical to expect that in all physical characteristics the same principles underlie the behavior of sands and of shales. Factors that may be important in the behavior of shales may be negligible in the case of coarse sands and vice versa, but in principle they are present and in between the two extremes there will be a continuous gradation of the characteristics. In studies of sedimentation and lithology these facts have been considered obvious and are universally recognized. Yet in the studies of electrochemical phenomena most authors have only considered "clean sands" and "pure clays or shales" and treated them as two entirely different media that have nothing whatsoever in common.

Thus, although the above authors realized that coarse sands do not influence the mobility of the ions in their interstitial water to any appreciable extent, they did not assume that shales might have a very noticeable influence on those mobilities, and that in shaley sands and siltstones this influence might vary from the one extreme to the other with the lithologic variations of those sediments.

The first attempt to correlate the S.P. kicks with the character of the sediments, beyond the classification of sands and shales was made by S. J. Pirson (3).

Pirson explains the S.P. curves by considering the potential differences between the solid frame-work of the rocks and the surrounding liquids, due to the preferential adsorption of ions from the solutions by the rock.

These electrochemical or thermodynamic potentials (E) are independent of the salinity of the connate water, but strongly dependent on the character of the rocks and the mud salinity.

Shales having a strong preferential adsorption of Cl ions would give large voltages. Pure sands exhibit the same phenomena, but to a much lesser extent. In this way shales would be the main sources of the potentials observed on S.P. logs. The magnitude of the S.P. kick would be mostly indicative of the amount of clay present in the sediment.

Diffusion potentials and electro filtration potentials are considered by Pirson as secondary phenomena, which will mostly only change the magnitude of the "shale-potential" kicks.

Although several objections may be raised against Pirson's theory, it has the distinction of recognizing the importance of the influence of the character of the sands on the magnitude of the S.P. kicks.

The main objection to Pirson's theory is that it does not properly account for the influence of the connate water salinity on the magnitude of the self potentials.

The idea that shales are the main seat of the natural potentials was originated by W. D. Mounce and W. M. Rust (4) who showed experimentally that shales placed in contact with solutions of different salinities at opposite sides exhibited potentials of a magnitude comparable to those found in oil wells between the two solutions. They also noticed that pure sands did not have this characteristic, or only to a negligible extent.

An important contribution to the understanding of the shale potentials was made recently by M. R. J. Wyllie of the Gulf Research and Development Co. (5).

Wyllie conducted extensive experiments on the potentials across shale barriers between solutions of different salinity. As in all afore-mentioned experiments, NaCl solutions of various concentrations were used.

Wyllie showed that the potential across a shale barrier can be represented by $E = K \log \frac{a_1}{a_2}$ (2)

where a_1 and a_2 are the ionic activities of the two solutions.

For dilute solutions these may be replaced by the conductivities or the inverse values of the resistivities.

K was found to be close to 59.15 at 25° C, which corresponds to the value of the constant of the Nernst equation for a metal in contact with electrolyte solutions:

$$E = \frac{RT}{F} m \log \frac{a_1}{a_2} \quad (3)$$

where R is the gas content, F the Faraday, T the absolute temperature, and $m = 1/\log_{10} e$ (e = base of natural logarithm).

Wyllie assumes therefore that the shale acts like a sodium electrode, in the sense that sodium ions are able to diffuse through the shale from one solution to the other, while the high negative charges on the shale particles repel the chloride ions. This causes the less saline solution to become positive with respect to the more saline solution. Wyllie also recognizes the diffusion or "boundary" potentials in the case where saline interstitial water within a sand is in contact with less saline mud.

In the cell, Mud / Interstitial water in the porous beds / Shale / Mud (see Fig. 1) the diffusion potential and

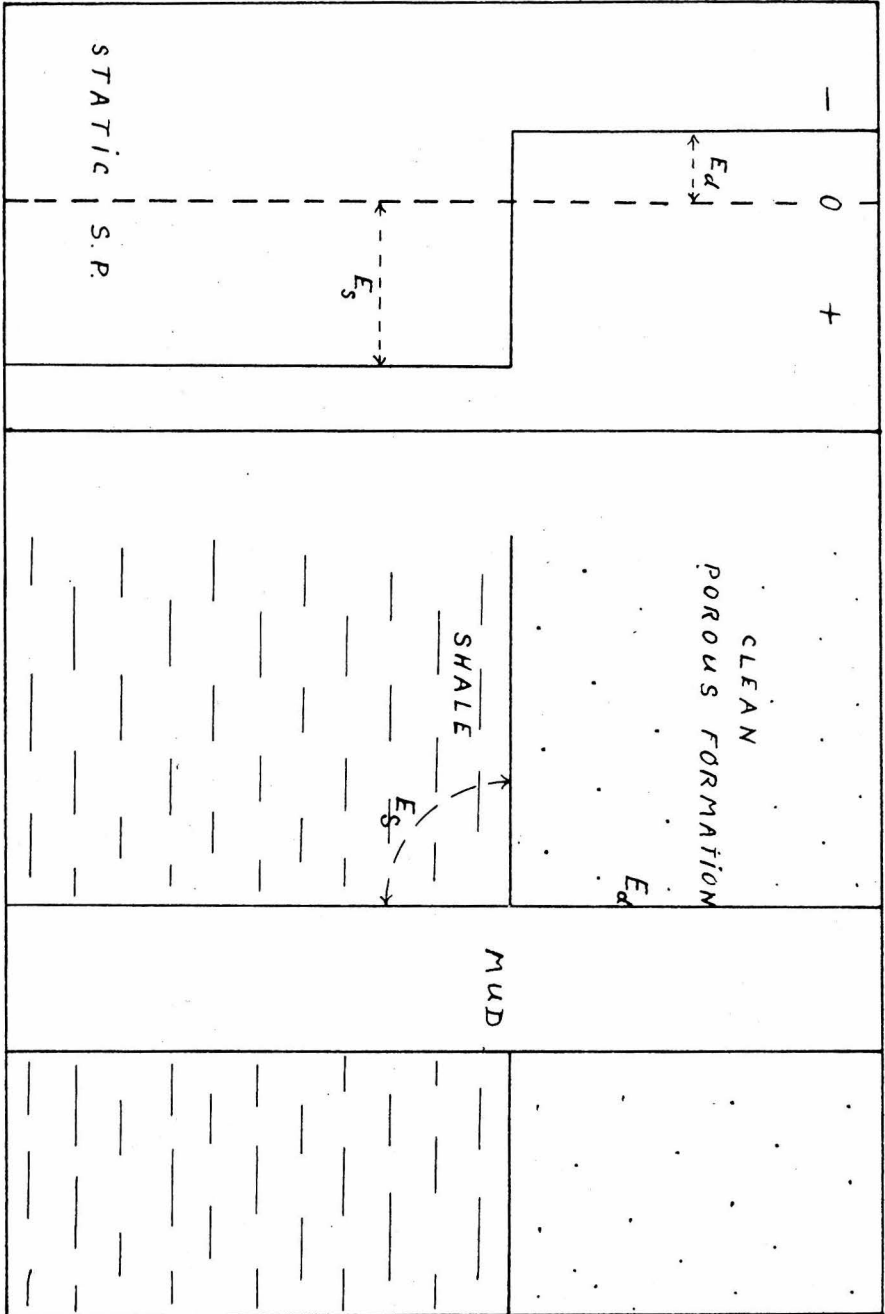


Fig. 1

the shale potential act in the same direction. The total E.M.F. of the cell equals therefore the algebraic sum of the two potentials. As for NaCl solutions, the diffusion potential may be represented by $E_d = 11.5 \log \frac{a_1}{a_2}$, the total E.M.F. for the cell (E_t) becomes

$$E_t = 59.15 \log \frac{a_1}{a_2} + 11.5 \log \frac{a_1}{a_2} = 70.65 \log \frac{a_1}{a_2} \quad (4)$$

This formula is a good representation of the electrochemical component of the S.P. curve in cases where very clean sandstones are in contact with dense argillaceous shales. In practice such conditions will seldom be found.

It must be pointed out here that the E.M.F. existing across the mud - sandstone - shale - mud cell is not necessarily equal to the potential difference measured on the S.P. log. Actually the E.M.F. gives rise to a sustained current flow, the so-called S.P. current and the S.P. log registers the ohmic drop in the mud column due to this current. For thick beds of low resistance, this ohmic drop is very nearly equal to the static E.M.F. In all other cases it is smaller. The relations governing the relative magnitude of the ohmic potential drop, as a function of formation thicknesses and resistivities have been very accurately and completely described by H. G. Doll (6).

The actual E.M.F. which would be equal to the S.P. measured on the logs if the effect of the S.P. current could

be neglected (for instance if insulating plugs were placed in the mud column) was termed by Doll the "static S.P."

In a later paper (7) Doll treated the self potentials of shaley sands by representing these by a series of thin clean sand layers interbedded with layers of pure argillaceous material. Although the calculated results seem to be in qualitative agreement with the S.P. logs of shaley sands, the assumptions are geologically untenable.

The main object of this thesis is to show experimentally the relations between the magnitude of the static S.P. and the character of the sediments involved.

Important conclusions are reached regarding the nature of the electrochemical phenomena and some possibilities of practical application of the observed relationships are pointed out.

PART I

EXPERIMENTAL EQUIPMENT AND PROCEDURE

The measurements of electrochemical potentials across sediments were carried out, using samples of approximately the following dimensions:

Height 1" ; Length $1\frac{1}{2}$ " ; Width 2".

These were mounted with zophar wax in a small catheter tray of $1\frac{1}{4}$ " x 8" x $2\frac{1}{4}$ ", leaving on each side a volume of approximately 240 cm^3 , which were filled with the solutions to be used.

The solutions were made up by mixing c.p. NaCl with distilled water.

Two solutions of different NaCl concentration would be poured in the end sections of the tray simultaneously so that imbibition of the sample would take place equally from both sides.

As soon as imbibition was completed, the potential measurements were started. The change of the potentials with time were measured over periods of several days, the measurements being spaced according to the rate of change in the potentials.

The circuit used for the measurements is represented schematically in Fig. 2.

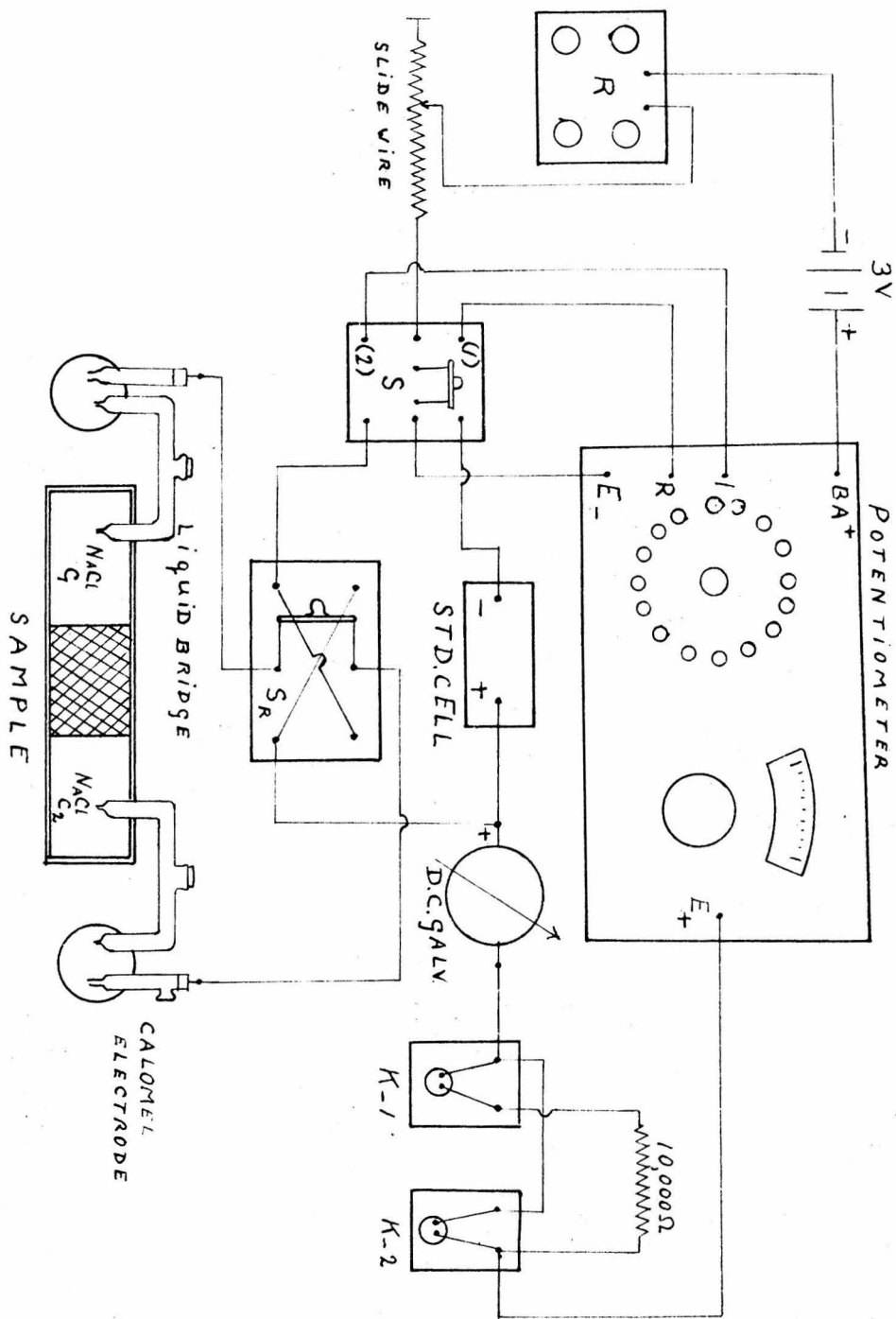


Fig. 2

The solutions on each side were connected to small beakers containing identical solutions by means of two liquid bridges with capillary end tips, also filled with the same solutions. In the two small beakers two calomel half-cell electrodes were placed. The electrodes were saturated KCl fibre-tip electrodes of the type used with the Beckman pH meters (Beckman #270 electrodes). Care was taken to prevent pollution of the KCl by NaCl, while the pollution of the solutions in contact with the sample by KCl from the electrodes was minimized by the use of the liquid bridges.

The potentiometer arrangement used was a Leeds and Northrup type K students' potentiometer in combination with a Rubicon high sensitivity spotlight galvanometer (type 3418).

This galvanometer has an internal resistance of 3800 ohms, a sensitivity of 0.0006 micro amperes per mm scale division, a period of 4 seconds and an external critical damping resistance of 55,000 ohms. The accuracy of the measurements depended somewhat on the total resistance of the sample and the liquid bridges, but was always better than 0.5 V.

The current through the potentiometer was delivered by two 1.5 Volt dry batteries in series, and adjusted to a value of 0.01 ampere by a four dial rheostat and a slide

wire. The smallest divisions of the rheostat were .1 ohm, which means that using the rheostat alone the voltage across the potentiometer, to be checked against the standard cell voltage, could be adjusted only with an accuracy of .5 m Volt. As both the standard cell calibration and the potentiometer dial setting permit a better accuracy, the slide wire was added in series with the rheostat. The wire consisted of 6 ft. of no. 18 copper coated steel wire with a total resistance of .15 ohm or approximately .002 ohm per inch. This permitted adjustment of the voltage across the potentiometer, when checking against the standard cell, to .01 m Volt. Variations of the position of the movable contact of the slide wire of less than one inch gave galvanometer deflections which could no longer be read. Therefore using the slide wire to vary the resistance, the current adjustment depended only on the accuracy of the potentiometer setting and the galvanometer zero reading.

The standard cell had a voltage of 1.01598 Volt. Both the standard cell and the batteries were packed with glass wool in a tin can to insure equithermic conditions for all parts. The tin cans in turn were packed with glass wool in wooden boxes to keep temperature variations at an absolute minimum.

Before a measurement was started, current was allowed to pass through the potentiometer for approximately one half hour, to stabilize the battery output. Then the potenti-

ometer dials were set at the value equal to the standard cell voltage and the current through the potentiometer adjusted until the galvanometer gave zero deflection, which indicated that the current had the value of 0.01 ampere. While checking against the standard cell, two tap keys K_1 and K_2 were used (see Fig. 2). When K_1 was tapped a protecting resistance of 100,000 ohm was connected into the galvanometer circuit. Coarse adjustment was made using K_1 and thereafter fine adjustment was made using K_2 , thus omitting the 100,000 ohm resistance. For accurate zeroing of the galvanometer by means of the resistance slide wire K_2 could be locked.

When the current was adjusted, the switch S was placed in position (2) connecting the E.M.F. to be measured to the potentiometer circuit. The potentiometer dials were set at zero. Then K_1 was tapped and the deflection noted. The galvanometer was then zeroed by varying the dial setting on the potentiometer and from the latter the E.M.F. was read directly in millivolts. If increasing the potentiometer voltage from its zero starting point would increase the galvanometer deflection, switch S_p would be placed in reverse position. In this way when making the readings, the positive side of the unknown E.M.F. would always be connected to the galvanometer.

After each measurement, the liquid bridges were taken out of the tray and placed across two small beakers containing solutions identical to those in the bridges. This was done

to prevent air from entering the capillary ends of the bridges, which would break the fluid contact continuity for subsequent readings. The tray was then closed by a snugly fitting lid to prevent evaporation of the solutions. The electrodes were taken out of the solutions, wiped off with tissue paper and sealed with their protective rubber caps and sleeves.

The salinity ratio of the NaCl solutions could be determined by measuring the resistivities using a four electrode A.C. circuit described in another thesis by this author (8). A more convenient method however was to measure the liquid junction potential between the two solutions. This was done in the following manner:

The liquid bridge containing solution C_1 was placed on one side in a small beaker filled with the same solution and on the other side in a beaker containing solution C_2 .

The fluid level of C_2 was placed momentarily slightly above that of C_1 so that fluid would flow through the bridge toward C_1 . This pulls up the liquid junction in the capillary end of the bridge, to obtain "cylindrical symmetry" of the boundary layer which improves stability of the liquid junction potential (9).

The potential between the solutions in the two beakers was then measured as the liquid junction potential, using the half cell calomel electrodes as described before.

To study the influence of temperature on the magnitude of the self potentials, the tray and specimen were heated in a water bath to approximately 185°F. For these elevated temperatures a different type electrode had to be chosen, as the #270 Beckman electrodes do not function properly above 45°C (113°F).

The electrodes used were Beckman #1170-71, sleeve type calomel electrodes.

The normal temperature range for these electrodes is -5° to 60°C. However, if carefully checked and constantly kept filled with saturated KCl they may be used up to temperatures just below the boiling point of water.

The electrodes were inserted directly in the solutions on both sides of the specimen. The liquid bridges were not used in this case, to avoid excessive difficulties in the control of the temperature of the system and the evaporation of the solutions. The evaporation of the solutions in the tray was minimized by keeping the tray covered by its lid. The temperature of the solutions was measured with a thermometer graduated in °F.

Pollution of the solutions by KCl from the electrodes might be the source of errors. The electrodes were therefore taken out of the solutions directly after each measurement and during the measurements the outflow of KCl was minimized by keeping the rubber stoppers in the filling holes of the electrodes. Readings of the E.M.F. and the temperature were

made before and during the heating of the system.

After a reading was made at the highest temperature at which the system could be maintained in the thermic equilibrium, the system was allowed to cool slowly. Successive measurements of the E.M.F. and prevailing temperature were then made until room temperature was reached. In this manner reliable measurements were obtained over the temperature range from 65° to 185°F, which corresponds very well to the range of temperatures normally occurring in oil wells.

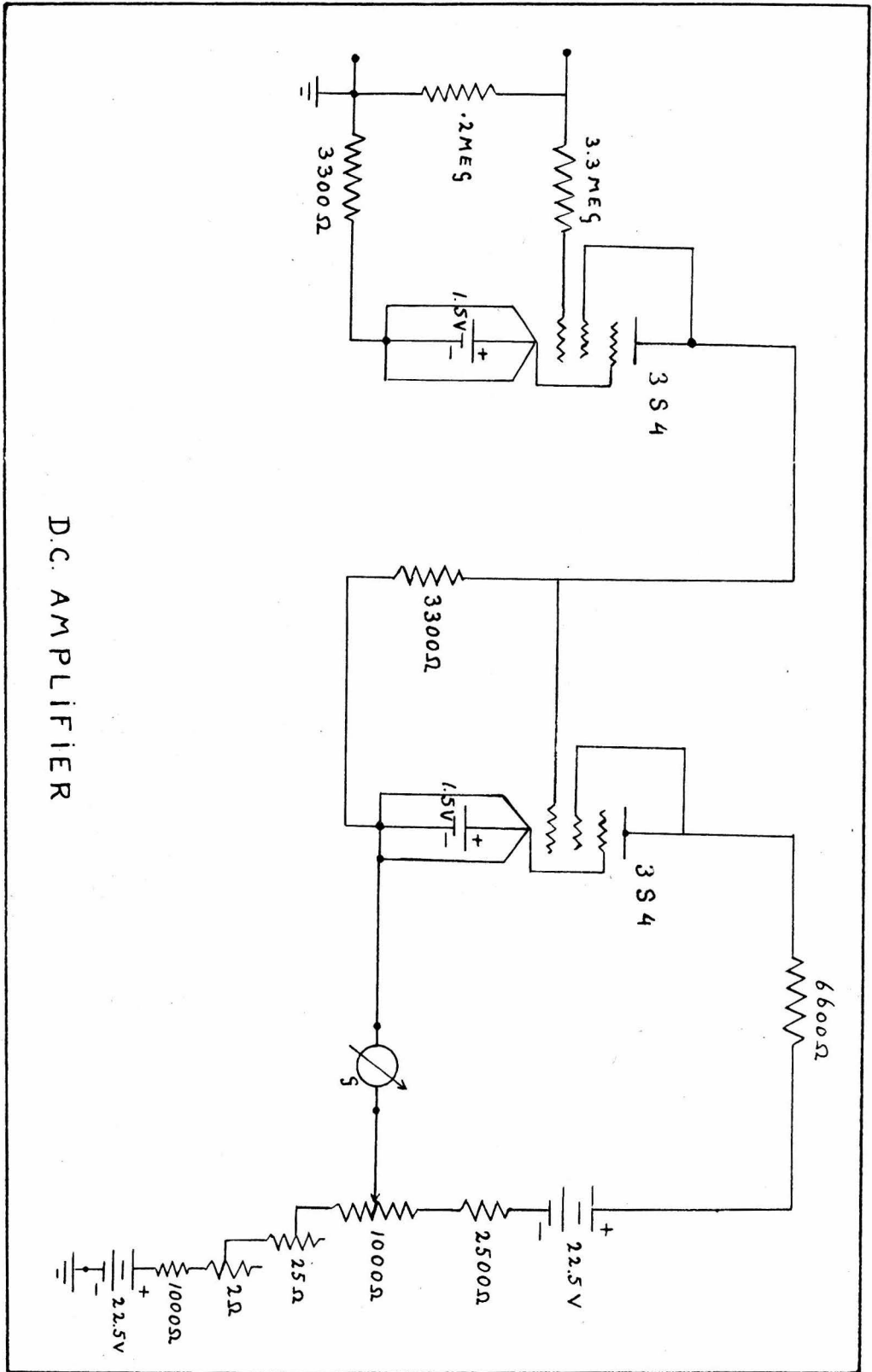
To measure the E.M.F. across specimens of high resistivity (25,000 Ω resistance across the specimen) a D.C. current amplifier was used. (The amplifier circuit is represented in Fig. 3.) Current amplification was especially necessary for the measurements on dense limestones, marbles, and quartzites, all of which have very low permeabilities and high resistivities.

The specimens used for the self potential determinations were mostly sediments taken from outcrops. Some black shales obtained from cores from a depth of approximately 8000 ft. were also used.

The samples were either cut with a diamond saw and air-dried or cut with a rotary wire brush.

The latter procedure was used for all the less consolidated sediments.

For several limestone samples the following determinations were made:



D.C. AMPLIFIER

Fig. 3

1. Porosity: Determined by imbibition with water and measuring the difference between wet and dry weight.

2. Insoluble residue: A weighed sample was dissolved in 20% HCl. The insoluble residue was weighed and computed as weight percentage of total.

3. Clay fraction: From the insoluble residue the clay fraction was determined by pipette analysis, as the fraction of particles with a diameter less than 5 microns. For the analysis the residue was mixed with 400 cc of 0.01 N. sodium carbonate. The mixing was done with a high speed soil dispersion mixer.

After the mixing the dispersed residue was allowed to settle for 1 hour and 14 minutes (this was the settling time for particles of 5 micron diameter, for a depth of 10 cm). Then 20 cc of sample was withdrawn by pipette from a depth of 10 cm below the surface of the fluid. This fraction was boiled dry in a beaker and weighed. The total clay fraction was then found as $\frac{400}{20} = 20$ times the weighed fraction. All weighing was done using a sensitive chain balance which could be read to 0.1 milligram.

PART II

PRELIMINARY MEASUREMENTS

A. Determination of influence of the quantity of materials involved.

To determine whether or not the amount of material used in the experiments influences the magnitude of the electrochemical potentials the following test was made.

A block of Saugus ss was divided into two parts. From these parts were cut one sample of 10 x 8 x 5 cm (volume = 400 cm³) and one sample of 5.9 x 5.7 x 3.5 cm (volume = 118 cm³).

The larger sample was placed in a large tray which was filled up with 625 cm³ of NaCl solution on each side of the sample.

The smaller sample was mounted in a small tray and 110 cm³ of NaCl was poured into the tray at each side of the sample.

The solutions at corresponding sides of the two samples were identical. The ratio of the salt concentrations on opposite sides of the sample was 5.7.

The E.M.F. across the samples upon completion of imbibition of the salt solutions was measured for both cases at a temperature of 69°F.

The reading for the potential across the sample in the large tray was 24.6 m Volt.

Across the small sample a potential of 25.2 m Volt was obtained. The difference in the readings is probably mostly due to small differences in the composition and (or) texture of the samples and to experimental inaccuracies. It is obvious however that the amounts of material involved do not govern the magnitude of the potentials across the samples, as long as the samples are large enough to give a good statistical representation of all components and characteristics of the rock from which they are taken.

B. Comparison of methods of determination of the concentration ratio between the solutions on opposite sides of the samples.

To determine the concentration ratio between the salt solutions on both sides of the sample the following methods can be used:

1. Weighing of the amounts of NaCl and distilled water used in the preparation of the solutions.
2. Measurement of the resistivities of the solutions.
3. Measurement of the liquid junction potential, E_d , between the two solutions, when they are brought into contact with each other in an inert porous medium or inside a capillary tube.

It was shown by Wyllie (5) that the electrochemical potentials across shale barriers depend more directly on the activities of the solutions involved than on their concentrations. The potentials were found to be directly proportional to the logarithm of the ratio of the activities of the salt solutions.

As the liquid junction potentials are also proportional to this same parameter, it is preferable to use method no. 3.

In the interpretation of self potential data from electrologs, the resistivity ratio is used instead of the ratio of activities. This is based on the well-known fact that resistivities of salt solutions are nearly inversely proportional to their concentrations, and that for dilute solutions the differences between the ratios of the activities and the concentrations of the two solutions may be neglected.

To obtain some idea of the validity of these approximations, two solutions were prepared and comparison was made between the three parameters: $\log \frac{C_1}{C_2}$, $\log \frac{R_2}{R_1}$, and $\log \frac{a_1}{a_2}$ (as determined from the liquid junction potential).

The following results were obtained:

$$\begin{array}{lll} C_1 = 15,300 \text{ ppm} & C_2 = 510 \text{ ppm} & \log \frac{C_1}{C_2} = 1.477 \\ R_1 = 40 \Omega \text{ cm} & R_2 = 990 \Omega \text{ cm} & \log \frac{R_2}{R_1} = 1.394 \\ E_d = -17.0 \text{ m Volt} = 11.6 \log \frac{a_1}{a_2} & & \log \frac{a_1}{a_2} = 1.461 \end{array}$$

We see that using the resistivities instead of the activities may introduce some error.

As the measurement of the liquid junction potential requires no extra apparatus and can be done in a few minutes, method no. 3 was used for all measurements referred to hereafter.

C. Relation between the activity ratio of the solutions and the magnitude of the electrochemical potential.

As mentioned before, Wyllie has shown by extensive experiments that the E.M.F. across a shale barrier may be represented by $E = K \log \frac{a_1}{a_2}$ (2)

The question arises whether this relation also holds for sediments, which are neither pure shales nor inert clean sands.

This was tested again using a sample of Saugus ss. Assuming equation (2) to hold true, we can calculate K from one measurement of E_d and the corresponding E.M.F. Knowing K we may compute the E.M.F. that should be obtained for any other value of E_d or $\log \frac{a_1}{a_2}$. The results are shown in Table A.

Table A

E_d (m Volt)	$\log \frac{a_1}{a_2}$	E.M.F. (m Volt)	
		calculated	measured
-8.15	0.702		23.6
-21.54	1.857	62.4	61.0
-4.3	0.371	12.5	12.7
-14.7	1.269	42.5	43.1

The data presented in Table A show that for all practical purposes equation (2) may be applied also to sediments that are intermediate between sands and shales.

The measurements were carried out at temperatures ranging from 77 to 81°F and in the computations the effects of the small temperature variations are neglected.

D. E.M.F. across a shale barrier.

To check whether our method of measuring the electrochemical potentials across sediments gave similar results to those obtained by the investigations of Wyllie, who used a different method of mounting the specimen and bringing the solutions in contact with the specimen, the E.M.F. across a pure argillaceous shale was measured.

$$\text{Wyllie had found } E \approx 59.15 \log \frac{a_1}{a_2} \quad (3a)$$

Using equation (3a) we can compute the E.M.F. for any value of $\log \frac{a_1}{a_2}$ (obtained from measurement of E_d) and compare the computed E.M.F. with the potential difference across the shale. The results of our measurements are shown in Table B.

Table B

E_d (m Volt)	$\log \frac{a_1}{a_2}$	temp. (°F)	E.M.F. (m Volt)	
			calculated	measured
-11.6	1.0	73	59.15	60.9
-16.8	1.45	72	85.9	84.3
-15.0	1.29	73	76.4	75.5

The results show that our method of measurement is equivalent to the one used by Wyllie.

E. The effect of time on the E.M.F. across sediments.

All measurements made of the E.M.F. across any type of rock showed a decrease of the absolute potential difference with time. Fig. 4 shows some typical graphs of the magnitude of the E.M.F.'s versus time. The sign of the potentials is established arbitrarily in the same direction as the potentials found in drill holes, that is for shales the less saline solution is positive. For inert sandstone the less saline solution is negative (same sign as that of the liquid junction potential). A negative potential will become larger negative with time.

We see from Fig. 4 that the slope of the first part of the curves varies from rock to rock. There seems to be some indication that the decline is steeper in the more porous rocks and less steep in the tight formations.

After the first twelve hours the decrease becomes very uniform and almost negligible.

F. Effects of temperature

The electrochemical potentials across rocks are dependent upon temperature. However, the variation with temperature is not the same in all cases. As the effect of temperature on the potentials has an important bearing on the actual nature

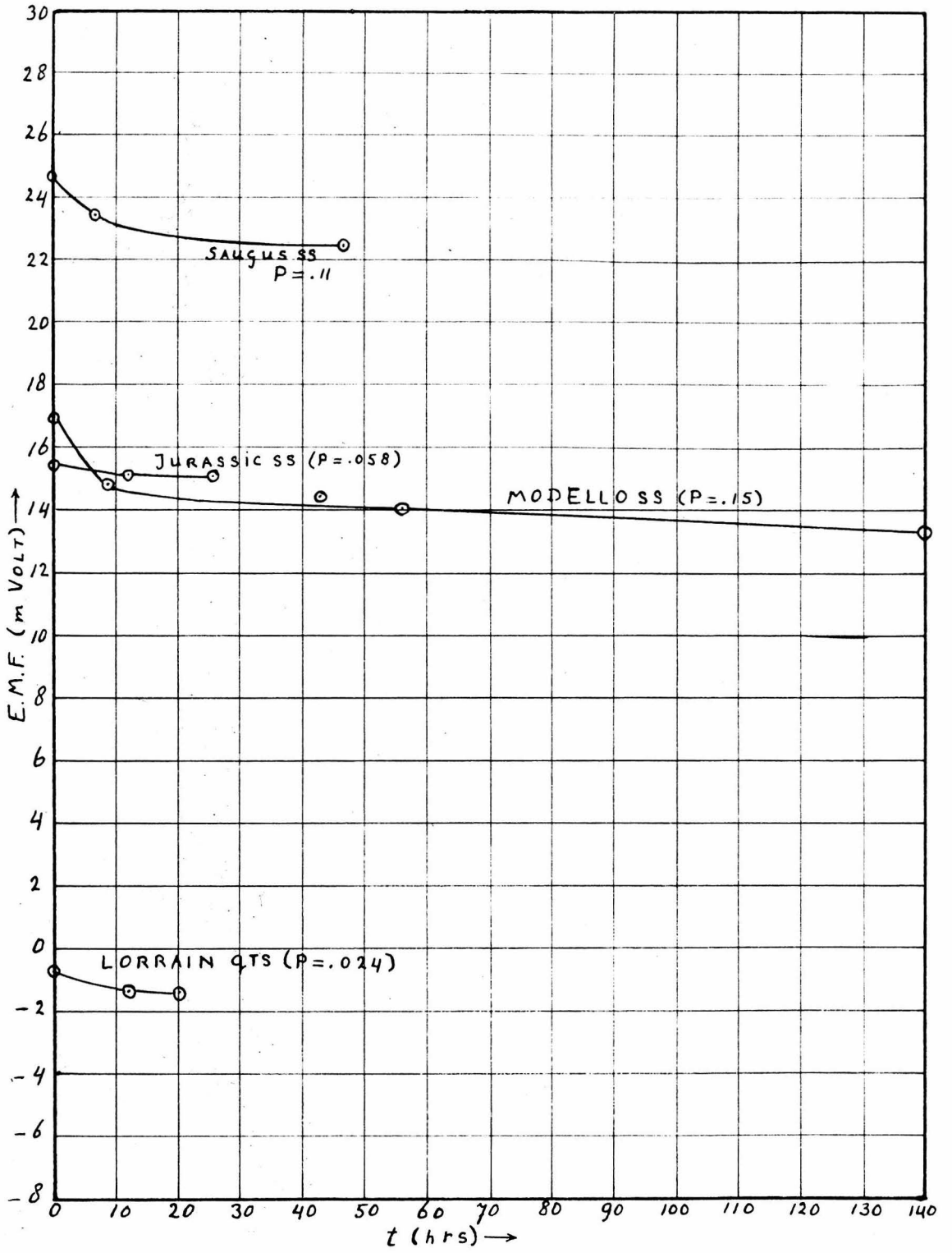


Fig. 4

of the potentials, the experimentally and theoretically obtained data on these variations will be discussed later in a separate section. At the present it suffices to state that the variations are small enough so that the changes in the measurement of potentials due to fluctuations in the room temperature may be neglected in most cases.

PART III

POTENTIALS ACROSS SEDIMENTS OF THE SANDSTONE SHALE SERIES

As pointed out in the introduction to this thesis, there exists a continuous series of sediments between pure quartz sands and argillaceous shales, if classified according to the texture and lithologic composition. It is expected therefore that these sediments also show continuity in their other physical properties, such as the electrochemical potential across them, when placed in contact with salt solutions of different concentrations.

To prove that such continuity does exist, measurements were made on a large number of specimens of sandstones, siltstones, shaley sands, and sandy shales. As was expected, values of self potentials were found ranging over the entire interval between those for inert clean sands and those for pure shales.

To be able to classify sediments according to their electrochemical behavior, the following parameters are now introduced:

1. The absolute self potential (A.S.P.). This quantity is defined as the electrochemical potential across the sediment at any arbitrary concentration contrast of the solutions in contact with the sediment, as-

suming always the more saline solution to be at zero potential. This means that if the more saline solution is positive with respect to the less saline solution the A.S.P. is negative. This will be the case for very pure sands. For most other sediments of the sandstone shale series the A.S.P. is positive.

2. The electrochemical formation constant, k , which is defined by the equation:

$$\text{A.S.P.} = k \log \frac{a_1}{a_2} \quad (5)$$

where a_1 and a_2 are the activities of the more saline and less saline solution respectively.

k always has the same sign as the absolute self potential and is at a given temperature, characteristic for a given rock, as long as we use solutions containing a given type of ions.

For NaCl solutions, we have for inert clean sand, at 25°C, $k = -11.5$, and for a pure argillaceous dense shale $k = 59.15$.

3. To ascribe sediments of the sandstone shale series a fixed place in this series, based on their electrochemical behavior, we introduce the "electrochemical formation coefficient" or "formation coefficient", C . This quantity is defined by the relation:

$$C = \frac{k_{25} + 11.5}{70.65} \quad (6)$$

where k_{25} is the electrochemical formation constant for the rock in question, for NaCl solutions at 25°C. For inert clean sandstones $C = 0$, and for pure shales $C = 1.0$.

From the definition of k we see that we may write:

$$k = \frac{11.5}{(E_d)_{25}} \times \text{E.M.F.} \quad (7)$$

$(E_d)_{25}$ denotes the diffusion potential between the solutions in question at 25°C.

Using relations (6) and (7), the formation coefficients have been determined for a number of widely varying sediments. The results are listed in Table C.

Table C

Description of sample	C	Description of sample	C
Pico (lower Pliocene) ss quartzitic	0.126	Mint Canyon shaley siltstone	0.444
Berea (Mississippian) ss	0.142	Modelo ss (San Fernando)	0.472
Mint Canyon friable ss	0.167	Mesozoic dense ss	0.477
Mint Canyon ss	0.244	Martinez (Eocene) ss	0.484
Coconino (land-laid) ss	0.252	Modelo shaley ss (upper Miocene)	0.592
Pico (lower Pliocene) siltstone	0.282	Saugus (Pleistocene, land-laid) calcareous ss	0.640
Modelo ss (Castaic)	0.350	Jurassic gray slate	0.896
Modelo sandy shale	0.430	Black shale	1.0

We see from the data given in Table C that the sediments of the sandstone shale group form indeed a continuous series with respect to their electrochemical behavior, with inert clean sands at one end and pure argillaceous shales at the other extreme. We see however that normally sands cannot be

considered to be clean, in the sense of being inert electrochemically. This is well demonstrated by the coefficients of the Berea ss and the quartzitic Pico ss.

From resistivity measurements described elsewhere (8) it was found that a correlation exists between the amounts of conductive solids present in the rocks and the electrochemical formation coefficient.

It was also found by this author (10) that a correlation exists between the formation coefficient and the total interstitial surface area per unit of bulk volume of the rocks. One of these relations is a logical consequence of the other as the conductive solids are mostly the minerals that are in the colloidal state and have a much larger interstitial surface area per unit volume than any of the other minerals present.

We now want to consider the nature of the absolute self potentials. Wyllie explained those of inert clean sands as being simple liquid junction potentials and those of the pure shales as being "sodium electrode potentials."

This abstract separation makes it difficult to understand the continuity of the potentials throughout the sandstone shale series.

We will therefore first discuss the basic character of both potentials, giving due consideration to the factors they have in common.

The liquid junction potential arises when two solutions of different ion content are brought into contact with each other. In our case, the solutions will differ mainly in concentration only and for simplicity's sake we will limit our discussions to the potentials due to the presence of two NaCl solutions of different concentration.

When two such solutions are brought into contact with each other, for instance in the interstices of an inert, porous medium, ions from the more concentrated solution will diffuse into the more dilute solution. For NaCl solutions the Cl ions diffuse more rapidly than the Na ions.

Shortly after the contact of the two solutions is established, an electric charge will set up across the boundary as more negative ions than positive ions cross the contact. The dilute solution will therefore become negatively charged with respect to the more concentrated solution. This charge will retard the migration of negative ions and accelerate the migration of positive ions, until a dynamic equilibrium is reached, at which both migrate at the same speed, or rather at which equal numbers of positive and negative ions diffuse into the dilute solution, per unit time.

The magnitude of the potential across the boundary at which this dynamic equilibrium is reached is given for NaCl solutions by the equation:

$$E_d = \frac{RT}{F} \frac{(v - u)}{(v + u)} \ln \frac{a_1}{a_2} \quad (8)$$

where v and u are the ionic mobilities of the chloride ions and sodium ions respectively, and a_1 and a_2 being the mean activities of respectively the more saline and the less saline solution.

If we arbitrarily consider the concentrated solution again at zero potential, the potential of the dilute solution becomes:

$$E = \frac{RT}{F} \frac{(u - v)}{(u + v)} \ln \frac{a_1}{a_2} \quad (9)$$

At 25°C $v_{Cl} = 76.3$ and $u_{Na} = 59.6 \Omega^{-1} \text{cm}^2$

or $\frac{u - v}{u + v} = 0.20$ and $T \frac{(u - v)}{(u + v)} = 59.6$

The constant factor $\frac{R}{F \log_{10} e} = 1.98 \times 10^{-4}$ practical units.

This leads to $E_d = -11.5 \log \frac{a_1}{a_2}$ m Volts.

When diffusion takes place across a shale barrier, the chloride ions are prevented from migration by the negative charge on the shale lattice, therefore in equation (8) we can make the chloride ion mobility equal to zero, which gives:

$$E_s = \frac{RT}{F} \ln \frac{a_1}{a_2} \quad (10)$$

It is obvious that the actual ion mobility of the chloride ions does not change, only the "apparent mobility" of the chloride ions in the establishment of the boundary potentials across the shale barrier, is zero.

Equation (10) is the same expression as the Nernst equation for monovalent metals in contact with solutions contain-

ing ions of the metal, as was pointed out by Wyllie.

The above presentation however eliminates the impression that two entirely different processes are involved in the establishment of the shale potential and of the simple liquid junction or diffusion potential.

As in the case of the liquid junction potential, equilibrium is reached for the shale potential when the migration of both ion types occurs at the same rate. This means equilibrium is reached when the migration of the sodium ions has been halted completely, too.

For all intermediate members of the sandstone shale series, we must conclude that the physical effects of the rock framework on the solutions influence the migration of the ions. The magnitude of the resulting potentials is such that the negative ions must be retarded or (and) the rate of migration of the positive ions increased.

This results in an analytical expression of the form:

$$E = \frac{RT}{F} \frac{\alpha^+ u - \alpha^{n-} v}{\alpha^+ u + \alpha^{n-} v} \ln \frac{a_1}{a_2}$$

or

$$E = \frac{RT}{F} \frac{(u - \alpha v)}{(u + \alpha v)} \ln \frac{a_1}{a_2} \quad (11)$$

where $0 < \alpha < 1$

α depends upon the texture and composition of the solid rock and can be directly related to the electrochemical formation coefficient, C .

Possible ways in which the solid framework could influence the apparent mobilities of the ions in the solutions

were discussed with Dr. S. Frankel.

Based on suggestions by Dr. Frankel, a very plausible mechanism was worked out, which will be explained, using the illustration as given in Fig. 5.

Fig. 5 represents a portion of a thin section of Pico sandstone. We note that some of the interstices are interconnected by open passages, indicated by "O", while other connecting passages are filled with fines, marked with "F". These fines are mostly clay minerals and comprise in general the conductive solids present in the rock. The correlation between c and the amount of conductive solids indicates that the latter must have a direct bearing on the magnitude of the electrochemical potentials. This occurs in the following manner: Through the open passages, both Cl^- and Na^+ ions can diffuse, at rates corresponding to their mobilities. Through the passages blocked by fines, however, only the Na^+ ions can migrate, while the Cl^- are prevented by the negative charge on the clay particles from passing through. The passages filled with fines act therefore as miniature shale-barriers. The presence of the clay passages causes the overall rate of migration of the Na^+ ions to be larger in comparison to the rate of diffusion of the Cl^- ions, across the boundary between the solutions, than in the case of a free liquid junction. This means that the apparent mobility of the Na^+ ions is increased or that of the Cl^- ions is decreased. The extent of increase or decrease in the apparent



Fig. 5
THIN SECTION OF PICO SANDSTONE (X100)

mobilities depends upon the number of passages filled with fines in proportion to the number of free passages. This explains very clearly the relation between the electrochemical formation coefficient and the amount of conductive solids, if the latter is expressed as a fraction of total pore space.

The method by which the amount of conductive solids is determined was described in another thesis by this author (8). The correlation is shown in Fig. 6.

The above interpretation shows that the apparent mobilities are completely statistical quantities. As pointed out before, the electrochemical formation coefficient is therefore only defined for samples of a rock large enough to give a good representation of the statistical characteristics of the rock.

As was shown on page 20 the expression

$$E = K \log \frac{a_1}{a_2}$$

gives a good approximation for the potentials across sediments of the sandstone shale series. This means that for the range of concentrations used in our experiments (1 N to 0.01 N) the variation of the relative ion mobilities with concentration are small enough to be neglected.

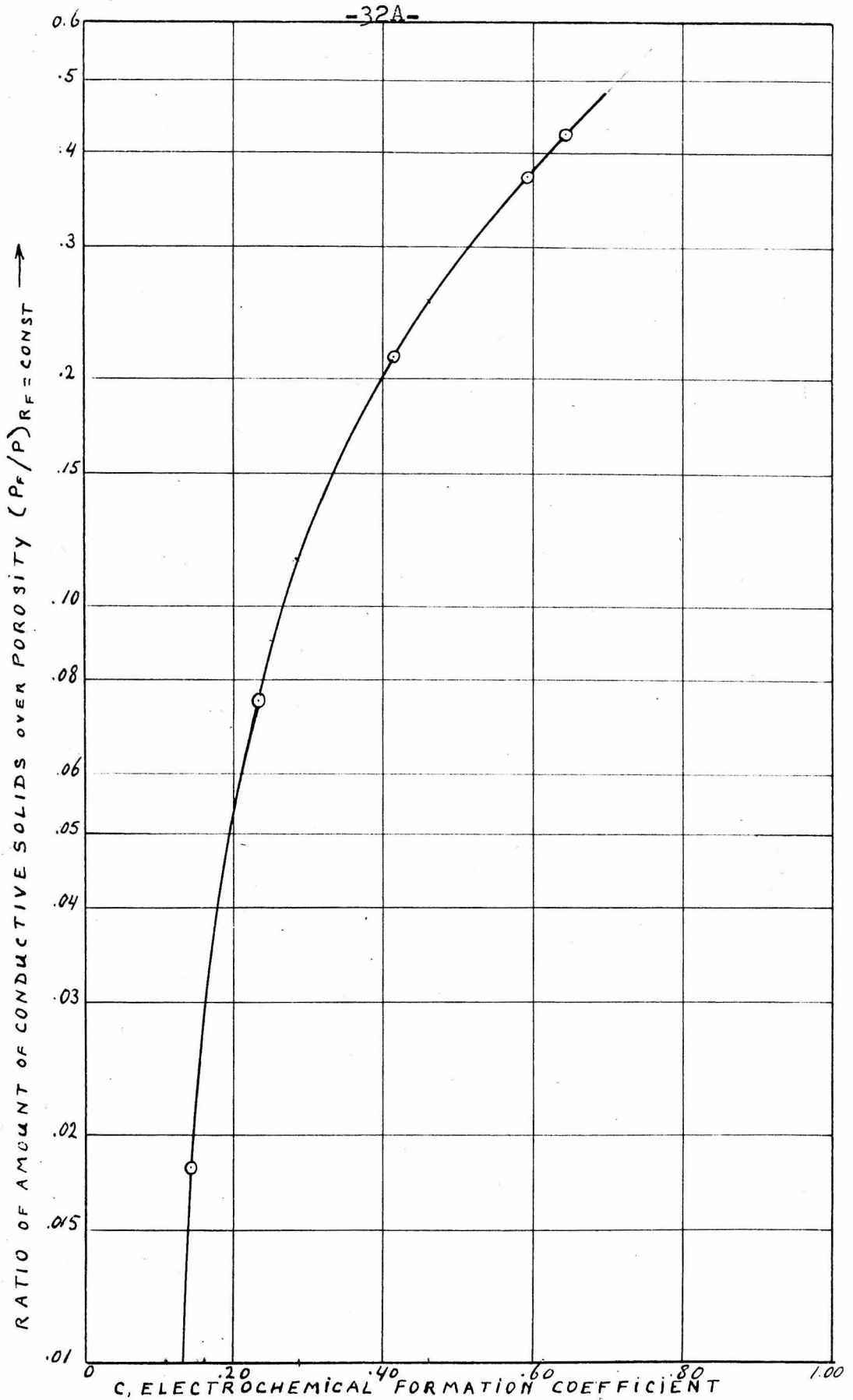


Fig. 6

PART IV

THE VARIATIONS OF SELF POTENTIALS WITH TEMPERATURE

From equations (9), (10) and (11) it is obvious that the electrochemical potentials vary with temperature.

The potentials across a shale barrier (equation (10)) are directly proportional to the absolute temperature if we assume that the effect of temperature on the mean activities of the two solutions in question is the same and therefore cancels out in the factor $\ln \frac{a_1}{a_2}$.

For the liquid junction potentials and all the potentials of the intermediate members of the shale sandstone series, the dependence upon temperature is more complicated. This is caused by the fact that the ion mobilities vary with temperature.

Table D shows values of the Cl^- and the Na^+ ion mobilities as given in the Physikalisch Chemische Tabellen (11) for various temperatures. Also listed are various other quantities that enter into equation (9).

Table D

Temperature			l_{Cl}	l_{Na}	$\frac{l_{\text{Cl}} - l_{\text{Na}}}{l_{\text{Cl}} + l_{\text{Na}}}$	$T \frac{l_{\text{Cl}} - l_{\text{Na}}}{l_{\text{Cl}} + l_{\text{Na}}}$
$^{\circ}\text{F}$	$^{\circ}\text{C}$	$^{\circ}\text{K}$	$\text{Ohm}^{-1}\text{cm}^2$	$\text{Ohm}^{-1}\text{cm}^2$		
32	0	273	41.3	26	.227	62
64	18	291	65.4	43.45	.202	58.8
77	25	298	76.3	50.9	.199	59.5
122	50	323	116	82	.172	55.5
167	75	348	160	116	.159	55.4
212	100	373	207	155	.144	53.6
262	128	401	264	203	.131	52.4
313	156	429	318	249	.122	52.1

We see from Table D that the overall effect of temperature on the liquid junction potentials is a slow decrease for increasing temperature. It should be pointed out that with our selection of the sign of the potentials this means that the liquid junction potentials become smaller negative with increasing temperature. This tendency becomes of importance when potential differences between solutions in contact with adjacent formations are compared.

The actual changes in the electrochemical potentials, with variations in temperature, are best represented by computing the electrochemical formation constant k , as a function of temperature. k equals the absolute self potential when $\log \frac{a_1}{a_2} = 1$. Using equation (10) we have

$$k = \frac{RT}{F} m \frac{l_{Na} - \alpha l_{Cl}}{l_{Na} + \alpha l_{Cl}} \quad \text{with } 0 \leq \alpha \leq 1$$

or $k = .198 \beta T$ with $\beta = \frac{l_{Na} - \alpha l_{Cl}}{l_{Na} + \alpha l_{Cl}}$ (12)

if the A.S.P. is expressed in m Volts.

Values of k as a function of temperature are shown in Fig. 7. The liquid junction potentials are represented by the k values for inert clean sands.

Variation with temperature of the electrochemical potentials for all the intermediate members of the sandstone shale series may be computed in the same manner as for the liquid junction potentials, using equation (10).

Table E gives $\beta = \frac{l_{Na} - \alpha l_{Cl}}{l_{Na} + \alpha l_{Cl}}$ and $T\beta$

for various temperatures and different values of α .

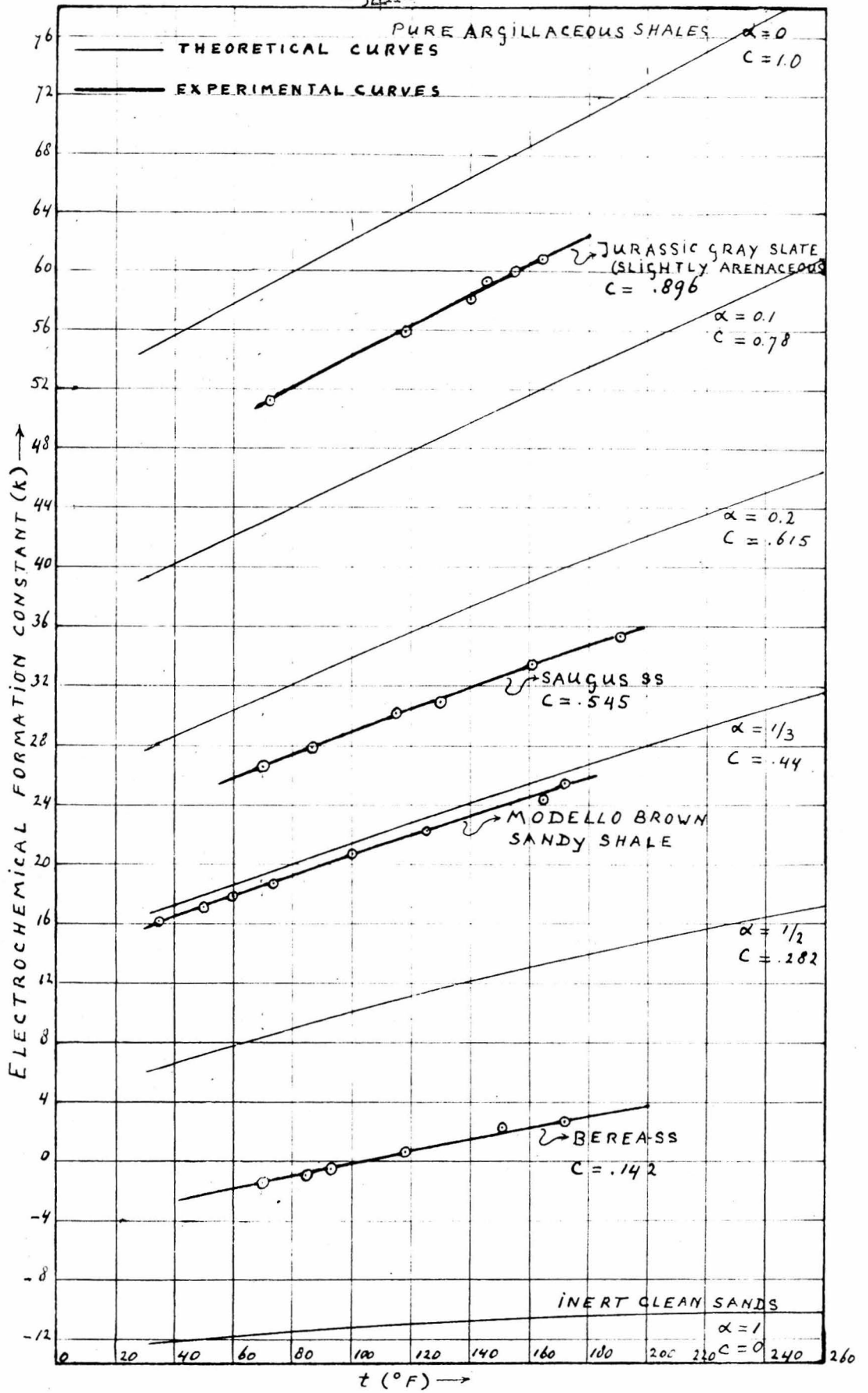


Fig. 7

Table E

Temperature		$\alpha = 1/2$		$\alpha = 1/3$		$\alpha = 0.2$		$\alpha = 0.1$	
$^{\circ}\text{F}$	$^{\circ}\text{K}$	β	$T\beta$	β	$T\beta$	β	$T\beta$	β	$T\beta$
32	273	.115	31.2	.307	84	.514	140.5	.728	198.5
64	291	.141	41	.332	96.5	.536	156	.739	214.8
77	298	.143	42.6	.334	99.5	.539	159.7	.739	220.2
122	323	.173	55.4	.359	116	.558	180	.751	242.5
167	348	.184	64	.370	129	.568	197.8	.758	263.8
212	373	.1995	77.4	.392	146.5	.579	216	.765	286
262	401	.211	85	.395	150.8	.588	235.8	.770	309
313	429	.2204	94.6	.402	172.8	.593	254.5	.772	332

From the values of $T\beta$ we can compute the corresponding values of k , using equation (11). The k 's thus computed are represented as a function of temperature for $\alpha = 1, 1/2, 1/3, 0.2$ and 0.1 by the theoretical curves in Fig. 7.

Fig. 7 also shows four curves for k as a function of temperature, computed from experimental data, using equation (7). These relations are represented by solid lines.

The theoretical relations shown in Fig. 7 have been plotted with the aid of equation (12) and the values for the ion mobilities listed in Table D assuming α to be independent of temperature. The latter assumption is equivalent to the assumption that the effective ion mobilities in a clay membrane will change with temperature in the same way that they do in free solution. Establishment of the validity of the assumption would be subject to a detailed theoretical analysis of the principles governing ion mobilities in clay membranes. The close agreement between the experimental data and the graphs computed from equation (12) suggest however that no

serious errors are introduced by assuming α to be independent of temperature.

The effect of temperature on the absolute self potentials may be summarized as follows:

For pure shales the potentials are proportional to the absolute temperature.

For all other sediments the temperature effect depends upon the absolute temperature, the ion mobilities at the prevailing temperatures and the electrochemical formation coefficient.

For inert clean sands ($C = 0$; $\alpha = 1$) the effect due to variation of ion mobilities is slightly larger than that directly due to the increase in absolute temperature and of opposite sign. The overall effect of temperature is a slow decrease of the magnitude of the negative potentials with increasing temperatures.

For all relatively clean sands ($C < .30$) the effect due to the variation of ion mobilities becomes rapidly larger for increasing C 's. The slope of the curve giving the A.S.P. or the electrochemical formation constant as a function of temperature becomes steeper.

For less clean sands, shaley sands and sandy shales ($.30 < C < 1.0$) the effect of temperature due to changes in ion mobilities becomes smaller and smaller and the direct effect of the increase in absolute temperature becomes relatively more predominant. The slope of the curve representing

the A.S.P. versus temperature still becomes steeper for increasing values of C. The increase in potential expressed as a percentage of the potential at 60°F however becomes much smaller than in the case of the sands having a formation coefficient of approximately .30. This last point may be illustrated by the following example:

Using for simplicity's sake values of k instead of the absolute self potentials, we have for $\alpha = 1/2$ ($C \approx .28$):

$$(k)_{t=60^{\circ}\text{F}} = +7.6 \quad \text{and} \quad (k)_{t=212^{\circ}\text{F}} = 15.2$$

which means an increase in k or in the A.S.P. of 100% for a temperature increase from 60°F to 212°F.

For $\alpha = .1$ ($C \approx .78$) we have:

$$(k)_{t=60^{\circ}\text{F}} = 42 \quad \text{and} \quad (k)_{t=212^{\circ}\text{F}} = 56.5$$

which indicates an increase in the A.S.P. of less than 35% for the same increase in temperature from 60°F to 212°F.

The above conclusions have an important bearing on the analysis of static self potentials as found from electrologs. The latter are equal to the difference between the A.S.P. of the shales and those of adjacent permeable formations encountered in drill holes (See Fig 1). Wyllie, assuming the absolute potentials of the permeable formations to be equal to the simple liquid junction potentials, used the formula:

$$E_{\text{total}} = 2.303 \frac{RT}{ZF} \left(1 + \frac{u - v}{u + v} \right) \log \frac{f_{mf}}{f_c} \quad (13)$$

where 2.303 is the conversion factor introduced by using the

logarithm to the base 10 instead of the natural logarithm; z is the valency of the ions and ρ_{mf} and ρ_c are respectively the resistivity of the mud filtrate and of the connate water.

The potentials as calculated from equation (13) correspond to the differences in k values between the curve for $\alpha = 0$ and the curve for $\alpha = 1$ in Fig. 7. It is readily seen from Fig. 7 that for all practical cases, where the sands may not be assumed to be electrochemically inert the effect of the temperature on the static S.P.'s is much smaller.

This will be illustrated again by an example:

Assume $\log \frac{\rho_{mf}}{\rho_c} = 1$ so that $k = A.S.P.$

we then find at $60^\circ F$ the static S.P. for an inert sand equals 71 m Volts and at $212^\circ F$ the static S.P. for the same case equals 85.5 m Volts, with means an increase of 14.5 m Volts.

For a sand with a formation coefficient of $C = .28$ ($\alpha \approx 1/2$) we have at $60^\circ F$ S.P. = 51.3 m Volts and at $212^\circ F$ S.P. = 59.8 m Volts, which correspond to an increase of 8.5 m Volts.

If we consider the increase in terms of a percentage of the S.P. value at $60^\circ F$ the contrast becomes less marked. We find for the two cases respectively an increase of 20.4% and 16.5% of the S.P. value at $60^\circ F$.

PART V

SELF POTENTIALS OF DENSE ROCKS AND OF LIMESTONES

The Influence of Compaction on the Self Potentials

In parts III and IV of this thesis, it was shown that for sediments of the sandstone shale series the self potentials are not governed directly by the porosity or permeability of the formations but by effects of the solid framework on the apparent mobilities of the ions.

It was also suggested that the greater part of the effect of the solid framework on the apparent ion mobilities is due to the presence of argillaceous material or conductive solids in the interstices of the rock. The argillaceous materials, because of the negative charge on their particles, decrease the apparent mobilities of the negative ions in the solutions.

It is a known fact however that most crystal lattices have surface charges due to unbalanced valencies. As shown by experiments on cataphoresis, finely ground quartz particles exhibit negative surface charges and will move under the influence of an electric field.

It might therefore be possible that if the pores in a rock are small enough, the small surface charges of crystal lattices other than those of the conductive solids may become of importance in determining the apparent mobility of the negative ions. Such effects, if present, might cause large positive

A.S.P.'s for dense limestones and other tight rocks like quartzites.

To check on this possibility, measurements were made on two types of quartzites.

The first specimen was a metamorphic pure quartzite, namely a sample of Lorrain quartzite from Bell Lake, Ontario. From measurements of the resistance across the specimen it was found that the formation factor* was approximately 300. The electrochemical measurements gave $k = 1.22$ and $C = 0.147$.

The second sample was a gray quartzite formed mainly by siliceous cementation. The formation factor in this case was found to be approximately 600. This quartzite gave $k = 43.74$ and $C = 0.218$.

We see that the absolute self potentials for these very dense quartzites are small and compare in magnitude to those of relatively clean sandstones. The Lorrain quartzite has a porosity of .024 and the gray quartzite is even less porous. It must be concluded from the obtained values of C that even for the exceedingly small pores of these quartzites the effect of the negative charge on the quartz crystal lattices on the apparent ion mobilities is still very small.

It is believed however that the effect though small is present, as in the case of the Lorrain quartzite the compo-

*For rocks containing little or no conductive solids, the formation factor may be defined as the ratio of the resistivity of the rock saturated with an electrolyte, over the resistivity of that electrolyte. The formation factor is usually denoted by F .

sition was practically 100% quartz and no conductive solids could be detected at all. The electrochemical formation coefficient of 0.147 indicates that $\alpha \approx 0.7$ which means that the apparent chloride ion mobility is only 0.7 times the value of the normal chloride ion mobility. This would mean statistically that in 3 out of 10 pores the chloride ions are prevented from migration.

From the results of the above measurements it is clear that the static S.P.'s for the quartzite beds in contact with shales are of the same magnitude as the static S.P.'s of permeable and porous sandstones in contact with shales. This fact rules out the conventional assumption that dense formations do not give S.P. kicks. It is true that because of the high resistivity of the quartzite beds, the ohmic potential drop in the formation, due to the S.P. current may not be neglected and the actual S.P. kick as registered on an electrolog will be smaller than the static S.P. Doll (6) calculated the magnitude of the deviations from the static S.P. for various ratios of the formation resistivity over the mud resistivity and various thickness of the formations, expressed in terms of the hole diameter.

These computations show that for thick beds the actual S.P. kicks for highly resistive quartzite beds will still be considerable.

For example, assuming $\frac{R_{mf}}{R_w} = 10$ and $R_{mf} = R_m$

(where R_{mf} , R_w and R_m are respectively the resistivities of the mud filtrate, the connate water and the drilling mud) we find from Doll's data the following values:

For $F = 600$ we have $R_t = FR_w = 60 R_m$ if R_t denotes the formation resistivity.

If the bed thickness $d = 8d_0$ (where d_0 is the hole diameter) the S.P. kick equals 0.63 times the static S.P. For $d = 32d_0$ the S.P. kick equals 0.94 times the static S.P.

For a hole with a diameter of 10" a bed thickness of $32d_0$ is less than 27 ft., which is not regarded as a thick bed, in most cases. Still we find the S.P. kick for a quartzite bed of that thickness is very nearly the same as the S.P. kick for a permeable water sand, assuming that in both cases the ratio of the mud filtrate resistivity to the connate water resistivity is the same.

It should be realized however that in a dense formation with very fine pores a small amount of conductive solids will suffice to block a large percentage of the available passages and therefore create a high absolute self potential. This is illustrated by the dense Jurassic sandstone (see Table C) which has a formation coefficient of 0.477, while the percentage of conductive solids is estimated to be of the same order as for most of the Pico sandstones ($C = 0.126$ to 0.282).

The above described behavior of the self potentials of dense formations is of great importance to the understanding of the self potentials of limestones. In calcareous forma-

tions, dense and porous zones will alternate in an unpredictable manner. The theory that dense formations give no self potential kicks has been found in practice completely unreliable, and often the self potential log of calcareous formations is regarded as practically of no use for purposes of interpretation of formation characteristics and fluid contents.

If the solid framework of a pure limestone can be regarded again as practically inert in the establishment of electrochemical potentials in its interstices, the magnitude of the self potentials across calcareous rocks would depend again on the presence of clay particles and the proportion of the latter to the porosity of the rocks.

The fact that the limestone framework is inert if no clay particles are present was proven by measurements which will be discussed in one of the following paragraphs. The amount of clay present in limestones can be determined by analysis of the insoluble residues. This would offer a convenient method of checking the correlation between the magnitude of electrochemical potentials across limestones and the amount of clay particles present. It must be realized however that not all of the clay particles present in a rock take an active part in the establishment of the electrochemical potentials. Only those particles blocking or partly obstructing the passages in which diffusion takes place influence the potentials. In poorly cemented sandstones this will comprise most of the

clay fraction. In well cemented sandstones and even more so in limestones a large unknown fraction of the clay particles will be surrounded completely by inert rock and will be of no importance in the establishment of the electrochemical potentials. This leads to the conclusion that there will be no direct correlation between the absolute self potentials and the total clay fraction of sediments as determined from insoluble residues and mechanical analysis.

On the other hand the amounts of conductive solids as determined by resistivity measurements include only those particles that take part in current conduction and are therefore capable of providing passage to the positive ions and blocking the negative ions in diffusion processes.

The above conclusions will be illustrated by experimental data obtained on three limestone samples. Table F gives the results of the electrochemical measurements, porosity determinations, and the pipette analyses of the insoluble residues. The clay fraction was taken as the total amount of particles with a diameter smaller than 5 microns.

Table F

Description of sample	Porosity, P (vol%)	Insoluble residue (weight%)	Clay fraction (P _c) (weight%)	P _f /P	Formation coefficient, C
Red limestone	8.0	2.16	0.694	.087	0
Gray dolomitic limestone	16.7	0.67	0.423	.0254	.037
Dense gray limestone	0.6	0.332	0.195	.324	.297

We see from Table F that no consistent correlation exists between the ratio of the clay fraction and porosity and the electrochemical formation coefficient, although the dense limestone with a high factor, P_f/P , also has a relatively high formation coefficient.

No resistivity data were available on these limestones so that the correlation between the electrically determined amounts of conductive solids and the formation coefficients could not be checked.

Another outstanding fact that can be noted from Table F is that pure limestones are "cleaner" than clean sands, that is, they give much lower formation coefficients. The red limestone of Table F was found to be completely inert, electrochemically. Dense limestones, if pure, will have a low A.S.P. and when in contact with shales, considerable S.P. kicks may be registered on an electrolog. From the example of the dense limestone shown in Table F it is evident, however, that an extremely small fraction of clay particles will suffice to make the absolute self potentials of dense limestones relatively high, and accordingly the S.P. kicks on the electrologs will become small.

An example of an electrolog showing an S.P. kick in front of a dense limestone of the same magnitude as the kicks in front of porous limestones was given by LeRoy and Grain (12) in their book on subsurface geologic methods. The phenomenon was termed by these authors an unexplained anomaly.

Influence of Compaction on the Self Potentials

The increase of the absolute self potentials with increase in density applies as well to shales as to any other type of rock. This means that a poorly compacted shale which still contains a portion of free water will have a lower formation coefficient than a dense shale or slate. This accounts in part for the low formation coefficient of the Modelo sandy shales, which was found to be only 0.43.

A very striking example of the influence of compaction on the self potentials was found by measuring the A.S.P. across loosely packed pure Bentonite clay. The formation coefficient for this clay was only 0.426.

In the light of these data, it becomes very clear why the experiments made by the Schlumbergers (2) gave static potentials following the relationship

$$S.P. = 17 \log \frac{C_1}{C_2}$$

If the sand used in their experiments had a formation coefficient equal to zero, the formation constant for the clay would be 17, which gives $C = 0.404$.

A result of the effect of compaction on the shale potentials will be that the S.P. kicks on electrologs for poorly consolidated formations will be lower in general than those for well consolidated strata.

The effect of compaction on the A.S.P.'s of sands will be much less than in the case of shales. This results from

the large differential compaction between sands and shales. Sands when buried under an overburden of 4000 ft. will decrease in volume only approximately 2% due to compaction. For the same depth of burial, clays decrease approximately 44% in volume (14). A more important factor governing the S.P.'s of sands is the amount of cementation. As explained before, a sand with a given amount of conductive solids will give a higher A.S.P. when tightly cemented than when only slightly cemented.

It must be realized that compaction is an irreversible process. A shale once compacted will maintain its density when brought close to surface by later erosion of the overburden. Correspondingly, dense slates and shales which are now found in surface outcrops still have high formation coefficients. As an example we may use the Jurassic slates taken from a surface outcrop, which had a formation coefficient of 0.896.

PART VI

APPLICATIONS OF THE ANALYSIS OF
ELECTROCHEMICAL POTENTIALS ACROSS SEDIMENTS

A. Application to Electrolog Interpretation.

In the computation of fluid contents of formations from resistivity logs, some quantities are involved that cannot be solved from resistivity data only. The most important of these unknown quantities is the connate water salinity or resistivity. Another unknown is the amount of conductive solids in the porous formation.

We have seen that both these quantities enter in the determination of the magnitude of the absolute self potentials and the S.P. kicks on electrologs.

The relations between resistivities, connate water salinity and amounts of conductive solids in reservoir rocks were first treated by Patnode and Wyllie (13) and have been elaborated upon by this author in a before-mentioned thesis (8).

At the present we will not enter into the details of these relations but merely outline the proposed use of the S.P. curve in the interpretation of the resistivity logs.

The role of the conductive solids in the determination of the resistivity of a water sand will be represented by

a parameter N . It can be shown that

$$N = f (R_i, R_t, R_{mf}, R_w) \quad (14)^*$$

where R_i , R_t , R_{mf} and R_w are respectively the resistivities of the infiltrated zone of the water sand, the undisturbed formation, the mud filtrate and the connate water.

R_i and R_t can be determined from the resistivity log and R_{mf} can be measured separately.

This means that for a given water sand we can plot N as a function of R_w .

A second relation between these quantities is furnished by the S.P. log.

From the S.P. log the magnitude of the differential kick in front of the shales and sands can be measured.

This value must be corrected for bed thickness and formation resistivity, as outlined by Doll (6), to obtain the static self potential, $(SP)_s$.

We then may write

$$(SP)_s = K_t \log \frac{R_{mf}}{R_w} \quad (16)$$

where K_t depends upon the electrochemical formation constant of the formation in question and the temperature.

*The actual relationships are (Reference 8, p. 102, equation 6-18)

$$\frac{1}{N} = \frac{R_t}{R_w(R_i - R_t)} - \frac{R_i}{R_{mf}(R_i - R_t)} \quad (15)$$

and $\frac{P_f}{P} = \frac{R_f}{N}$ where P_f is the fraction of conductive solids per unit bulk volume of rock, P is the fractional porosity and R_f is the bulk resistivity of the conductive solids.

In general we have for the absolute self potentials of the shales:

$$(A.S.P.)_{\text{shale}} = (k_t)_{\text{shale}} \log \frac{R_{mf}}{R_w}$$

and for the formation in question:

$$(A.S.P.)_{\text{formation}} = (k_t)_{\text{formation}} \log \frac{R_{mf}}{R_w}$$

where k_t is the electrochemical formation factor at the prevailing temperature.

For the differential static S.P. we obtain:

$$(SP)_s = ((k_t)_{\text{shale}} - (k_t)_{\text{formation}}) \log \frac{R_{mf}}{R_w} \quad (17)$$

From (16) and (17) we see that:

$$K_t = (k_t)_{\text{shale}} - (k_t)_{\text{formation}} \quad (18)$$

In Fig. 8 the variations of k_t with temperature are given for various values of the formation coefficient, C.

Assuming that the shales are dense argillaceous shales ($C = 1$) and using equation (18) and the data from Fig. 8, we can find any given temperature, t_1 , the values of K_{t_1} as a function of the formation coefficient C of the formation in question, using equation (18). If the shales are sandy or poorly compacted, their formation coefficient should be determined in the laboratory from core samples, and the corresponding curve for $(k_t)_{\text{shale}}$ can be found by interpolation in Fig. 8. Using the values of $(k_t)_{\text{shale}}$ thus determined, K_t may be computed as a function of C in exactly the same manner as in the case where $C_{\text{shale}} = 1$.

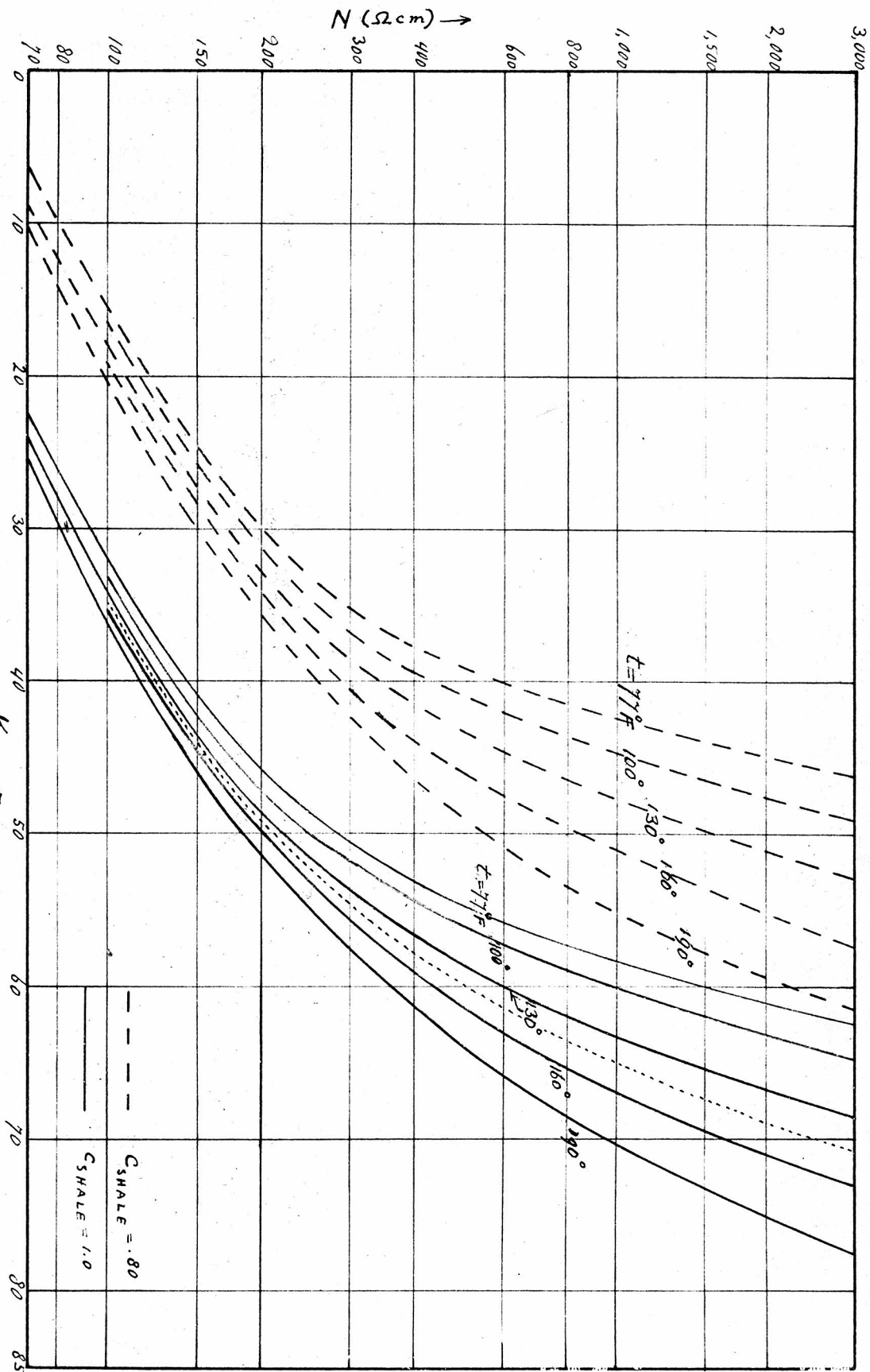


Fig. 8

The relation between K_t and C can be combined with the relation between C and the amount of conductive solids or N , which was given in Fig. 6,* to compute the relationships between N and K_t at various temperatures. Curves representing these relations are shown in Fig. 8, for $C_{\text{shale}} = 1$ and for the case where $C_{\text{shale}} = .80$.

Finally using the corrected $(SP)_s$, equation (17) and the data from Fig. 8 we can make a second plot of N as a function of R_w .

At the intersection point of the two plots of N versus R_w , the ordinate and abscissa are respectively the true values of N and of R_w .

The interpretation procedure may be summarized as follows:

- 1) From the resistivity data find N as a function of R_w (using equation (15)).
- 2) For the temperature of the formation in question and the prevailing value of C_{shale} , interpolate the graph for K_t as a function of N , using the curves of Fig. 8.
- 3) Measure the S.P. kick on the log and correct it to obtain the static self potential, $(SP)_s$.
- 4) Using the interpolated graph found under 2) and the values of $(SP)_s$ determined under 3), make a second

*The ordinate in Fig. 6 was given in terms of $\frac{Pf}{P} = \frac{R_f}{N}$ (see footnote on page 49). R_f is nearly a constant and in the plot of Fig. 6 the value of $R_f = 33 \Omega \text{ cm}$ was used.

plot of N as a function of R_w with the aid of the equation

$$(SP)_s = K_t \log \frac{R_{mf}}{R_w}$$

- 5) Find the intersection point of the graph made under 1) and the graph obtained under 4).
- 6) Read the values of R_w and N corresponding to this intersection point as the true values of the connate water resistivity and the parameter N .

Numerical example.

The following is a numerical example taken from an electrolog of a well in the Los Angeles Basin. Sand thickness $d = 50$ ft. Formation temperature 145°F . C_{shale} assumed to be 1.0. $d_o = 9"$. S.P. = 35 m V.

$$R_m \approx R_{mf} = 2.42 \Omega \text{ m} \quad R_t/R_m = 1.9$$

$$R_i/R_m = 6 \text{ (as determined from the resistivity log)}$$

The above values give $R_t = 4.6 \Omega \text{ m}$ and $R_i = 14.6 \Omega \text{ m}$.

For $R_t/R_m = 1.9$ and $d/d_o = 67$ $SP = (SP)_s$

Equation (15) gives:

$$1/N = \frac{R_t}{R_w(R_i - R_t)} - \frac{R_i}{R_{mf}(R_i - R_t)}$$

or $\frac{1}{N} = \frac{.46}{R_w} - .603$

From this relation N is plotted as a function of R_w . The resulting graph is shown in Fig. 9, curve (a). (Note: as all resistivities in equation (15) are given in $\Omega \text{ m}$'s

the computed values of N are also in Ωm , in contrast to the N values given in Fig. 8 which are in Ωcm .)

For $C_{shale} = 1$ and $t = 145^{\circ}F$ we have found the corresponding relation between K_t and N by interpolation between the curves of Fig. 8 (see dotted curve in Fig. 8).

$$\text{From } (SP)_s = K_t \log \frac{R_{mf}}{R_w}$$
$$\text{we obtain } 35 = K_t \log \frac{2.42}{R_w}$$

From this we can find K_t as a function of R_w and using the interpolated graph for K_t versus N we can compute again N as a function of R_w .

Some computed points are listed below.

R_w (m)	K_t	N (m)
.2	32.4	93
.3	38.6	120
.4	44.8	155
.5	51.1	228
.6	57.8	400
.7	65	970

Using these values a second plot is made of N versus R_w (see Fig. 9, curve (b)).

For the intersection point we find:

$$R_w = .34 \Omega m \quad \text{and} \quad N = 1.3 \Omega m.$$

B. Application to Surface Geology

As the electrochemical formation coefficient is characteristic for any given sedimentary rock unit, electrochemical testing of samples could be applied in many surface geological problems.

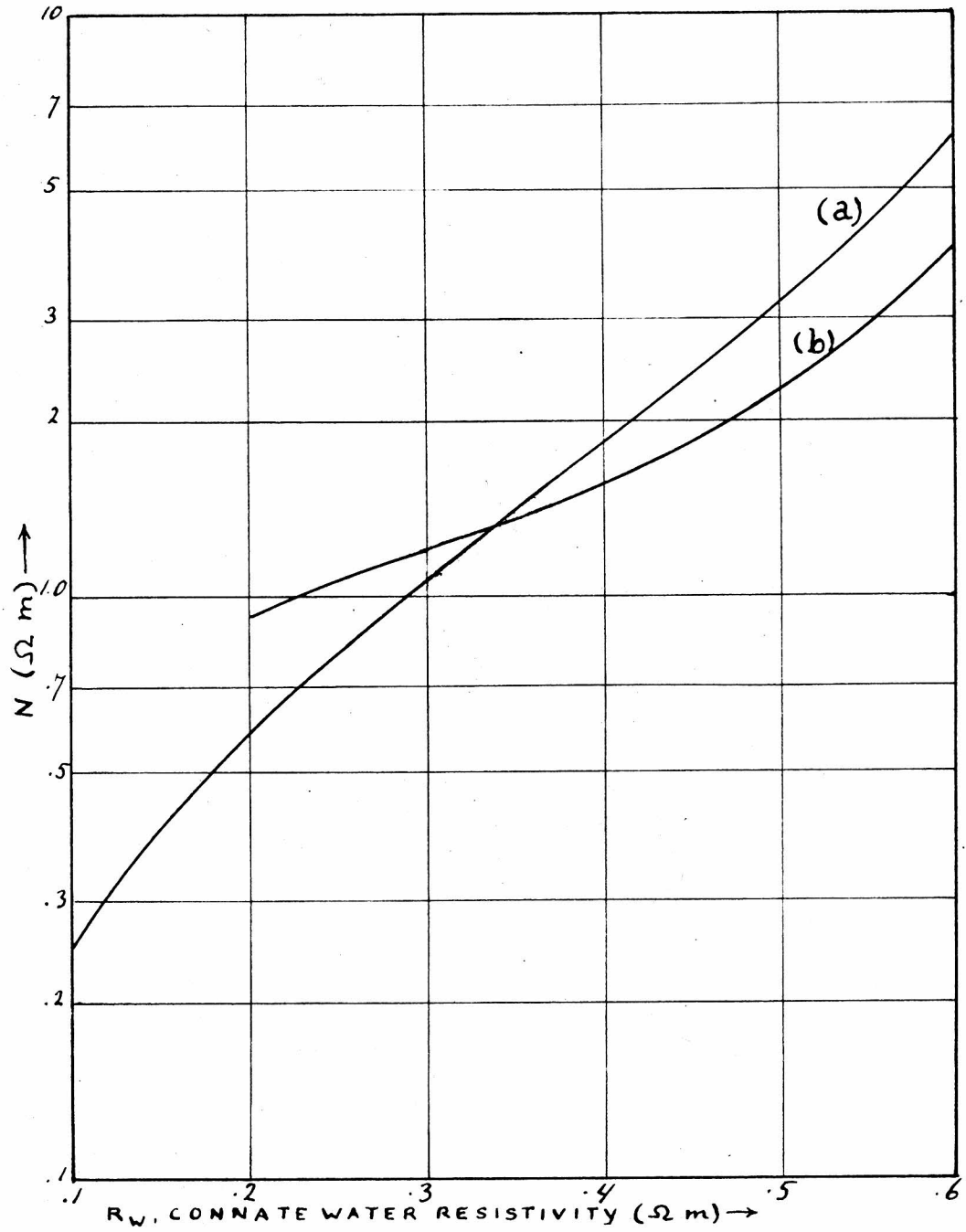


Fig. 9

For instance, identification of a certain bed by measurement of its formation coefficient may help in tracing certain horizons where outcrops are few.

Displacements on faults may be measured by sampling beds on each side, determining the formation coefficients and finding the offset in the series.

Finally, at unconformities where sandstones of one formation lie against sandstones of another formation, electrochemical testing may be used to locate the contact where other methods fail. A striking illustration of the applicability of electrochemical testing to the latter type of problem was found in distinguishing between Mint Canyon and Martinez sandstones in the Elizabeth's Lake Canyon area (near Castaic, California). The Martinez sandstones are older and marine, while the Mint Canyon sandstones are landlaid. Both rocks however are derived from the same source material, have the same tan color, and weather in the same fashion. Visual inspection fails completely in most cases to distinguish between the units, when trying to locate the contact.

Electrochemical tests showed that the formation coefficients of the lower Mint Canyon sandstone beds varied between .15 and .25, while the upper Martinez sandstones gave values between .45 and .55.

It is realized that these tests serve only to distinguish between similar looking facies. This is, however, where an additional aid in identification is needed most.

REFERENCES

1. C. and M. Schlumberger and E. G. Leonardon: Electrical Coring; a Method of Determining Bottomhole Data by Electrical Measurements. A.I.M.E. Transactions 110, (1934), 237-272.
2. C. and M. Schlumberger and E. G. Leonardon: A New Contribution to Subsurface Studies by Means of Electrical Measurements in Drill Holes. A.I.M.E. Transactions 110, (1934), 273-289.
3. S. J. Pirson: A Study of the Self Potential Curve. Oil and Gas Journal, October 4, 1947.
4. W. D. Mounce and W. M. Rust: Natural Potentials in Well Logging. A.I.M.E. Transactions 164, (1945), 288.
5. M. R. J. Wyllie: A Quantitative Analysis of the Electrochemical Component of the S.P. Curve, Petroleum Technology, January, 1949, 17.
6. H. G. Doll: The S.P. Log. Theoretical Analysis and Principles of Interpretation. Petroleum Technology, September, 1948.
7. H. G. Doll: The S.P. Log in Shaley Sands. Presented at Los Angeles meeting of the A.I.M.E., October 20-21, 1949.
8. L. de Witte: Infiltration of Drilling Fluids in Relation to Quantitative Analysis of Electrologs in Drill Holes. Thesis, California Institute of Technology (1950).

9. E. A. Guggenheim: A Study of Cells with Liquid-Liquid Junctions. Journal American Chemical Society, 52 (1930), 1333.
10. L. de Witte: Factors Governing Accumulation of Oil and Gas in Stratigraphic Traps. Minor thesis, California Institute of Technology (1950).
11. Landolt, Börnstein, Roth, Scheel: Physikalisch Chemische Tabellen. Zweiter Ergänzungsband, 2^{er} Teil, p. 1062. Eg. band III, p. 2059.
12. L. W. LeRoy and H. M. Crain: Subsurface Geologic Methods. Fig. 135, p. 325. Department of Publications, Colorado School of Mines, Golden, Colorado (1949).
13. H. W. Patnode and M. R. J. Wyllie: The Presence of Conductive Solids as a Factor in Electric Log Interpretation. San Antonio (Texas) meeting A.I.M.E., Petroleum Branch, October 5-7, 1949.
14. L. F. Athy: Compaction and Oil Migration. Bulletin A.A.P.G. 14 (1930) Part I, 25.

STUDIES ON INFILTRATION OF POROUS FORMATIONS
BY DRILLING FLUIDS IN RELATION TO THE
QUANTITATIVE ANALYSIS OF ELECTROLYTES IN DRILL HOLES

Thesis by
Leendert de Witte

In partial fulfillment of the requirements
for the degree of
Doctor of Philosophy

California Institute of Technology
Pasadena, California

1950

ACKNOWLEDGMENTS

The author wishes to make acknowledgments to:

Dr. G. W. Potapenko under whose supervision the research was carried out.

Dr. W. R. Smythe and Dr. W. Magnus with whom some theoretical aspects of the problems were discussed.

Dr. F. W. Maxstedt and Mr. R. C. Serviss for valuable advice on construction of the measuring circuits.

Mr. R. von Huene and Mr. W. J. P. Otto for aid in the preparation of the samples.

Mr. E. Offeman of the Baroid Sales Division in Los Angeles, for furnishing several pieces of Baroid equipment used in the experimental investigations.

ABSTRACT

This thesis presents a discussion of a method, by which certain characteristics of the infiltrated zones around bore holes can be made to good use in determining the fluid content and the formation factor, of the horizons in which we are interested.

To obtain the necessary field data a new combination of electrode spacings is proposed, namely a short lateral spacing, with two normal spacings. It is shown that apparent resistivities, obtained with these spacings, enable us to obtain the true resistivity, the resistivity of the invaded zone and the diameter of the latter.

To be able to use the invaded zone resistivity in the determination of the formation factor and fluid contents a group of laboratory experiments were carried out, using consolidated sandstone samples and drilling muds or liquids having the properties of the mud filtrate. The sandstones were invaded by the muds or their equivalent filtrates for different conditions of initial fluid contents. Then the resistivity changes were measured by a four electrode arrangement coupled to an amplifier-rectifier circuit and a sensitive test meter.

For the case of oil and gas sands the displacement of the non-wetting phase by water is treated analytically using the concept of relative permeabilities of the reservoir rocks and the results are compared with the experimental data.

From measurements on coresamples the actual resistivity profiles in the infiltrated zones of formations were computed. These showed that in all cases the resistivity of the invaded zone may be approximated by a constant.

The relations between resistivities of rocks and their fluid contents are considered in the light of experimental results and several new formulae are introduced, governing these relations.

Finally the water saturations of the invaded zones of oil and gas horizons are correlated with the water saturations of the undisturbed formations.

A brief outline is given of the computation of fluid contents and formation factors of porous rocks from the measured values of infiltrated zone- and true resistivities, using the new resistivity formulae and data obtained from analysis of the self potential curve of electrologs.

TABLE OF CONTENTS

PART	TITLE	PAGE
	Acknowledgments	
	Abstract	
	Introduction	1
I	Derivation of Relations between Actual Resistivities and Apparent Resistivities	3
II	Computation of the True Resistivity of Formations and the Resistivity of the Infiltrated Zone	24
III	Experimental Equipment	39
IV	Experimental Procedure	60
V	Theory of the Displacement of the Non-Wetting Phase by Water during Radial Infiltration	65
VI	Basic Relations between Resistivities and Fluid Contents of Porous Rocks and their Application to Electrolog Interpretation	83
VII	Experimentally Determined Characteristics of the Infiltrated Zones of Permeable Formations	105
	References	126
	Appendix	

INTRODUCTION

Quantitative analysis of electric well logs, or electrologs, has as its main purpose the determination of the relative saturation of the fluids, contained in the formations traversed. The fluids in which we are mainly interested are oil and gas.

To be able to interpret the resistivity measurements given on electrologs into terms of fluid content of the formations, we must know the basic relations between the content and character of interstitial fluids and the resistivity of the rock. Important factors in these relations are the effect of the solid framework of the rock on the electrolytic conduction of current by its interstitial water and the amount of "conductive solids" present in the rock. This means that essentially there are four unknown parameters governing the formation resistivities, namely: The saturation of oil or gas, the conductivity of the interstitial water, the "cell constant" due to the inert framework, and the amount of conductive solids present.

In order to attempt to solve for these quantities, we must first of all determine the true resistivity of the formations in question. Additional information can be obtained from determination of the true resistivity of the zones of porous formations immediately surrounding the drill holes which have been invaded by the filtrate of the drilling fluids, displacing part or all of the initially present interstitial fluids. Finally, important information can be gained from analysis of the self potential measurements which are made simultaneously with the resistivity measurements in electrologging practice.

This thesis outlines a method of computing the true resistivities of the undisturbed formations and the invaded zones from the apparent resistivities measured on the electrolog.

Furthermore, experimental studies were made on the basic relations between the resistivities, the fluid content, and the rock characteristics of the formations.

Finally, the displacement of the interstitial fluids by the mud filtrate upon invasion and the resulting relations between resistivities of the infiltrated zones and those of the undisturbed formations are studied both theoretically and experimentally.

No attempt is made to outline all of the work done and literature published on the subject of electrolog interpretation. Previous work by other investigators is only quoted where it has a direct bearing on the experiments and analyses reported in this thesis.

Because of the many factors involved in the interpretation of resistivity measurements in drill holes, the research was limited in most cases to the bare essentials and therefore this work should be regarded strictly as a reconnaissance type investigation of the problems involved in quantitative analyses of electrologs.

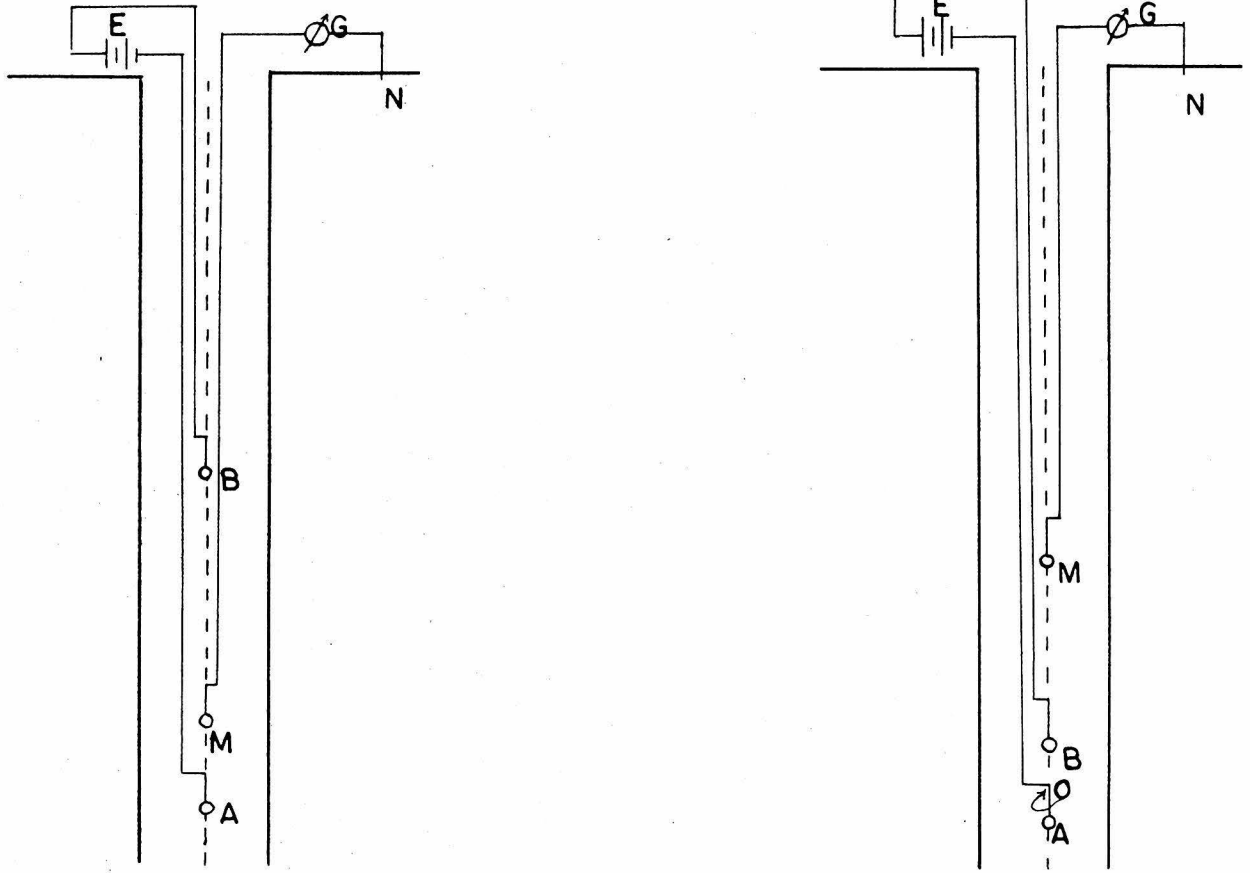
PART I

Derivation of Relations Between Actual Resistivities
and Apparent Resistivities*

Nomenclature

- R_a = apparent resistivity
 R_m = mud resistivity
 R_1 = resistivity of infiltrated zone
 R_t = true resistivity of formation
 R_w = resistivity of interstitial water
 ρ_w = resistivity of infiltrating liquid
 r_0 = radius of drill hole
 d_0 = diameter of drill hole
 r_1 = radius of infiltrated zone
 d_1 = diameter of infiltrated zone
 AM = spacing of electrodes in normal arrangement (See Fig. I-1)
 AO = spacing of electrodes in lateral arrangement (See Fig. I-1)
 S_w = water saturation as a fraction of porespace
 S_o = oil saturation as a fraction of porespace
 S_g = gas saturation as a fraction of porespace
 I = modified bessel function of first kind, of order zero ($I \cong I_0$)
 K = modified bessel function of second kind, of order zero ($K \cong K_0$)
 I_n = modified bessel function of first kind, of order n
 K_n = modified bessel function of second kind, of order n

* A historical review of the development of these relations is given on Pages 5 and 6.



NORMAL-ELECTRODE ARRANGEMENT - LATERAL
Fig. I-1

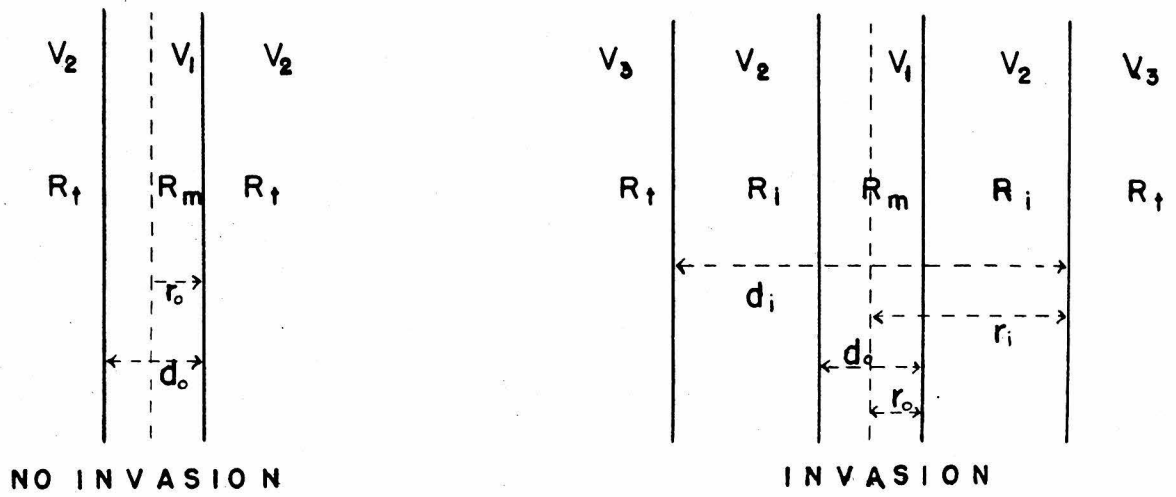


Fig. I-2

r = distance from origin

s = $\frac{AM}{F_0}$ for normal arrangement of electrodes

s_1 = $\frac{AM}{F_0}$ for lateral arrangement of electrodes

s_2 = $\frac{PM}{F_0}$ for lateral arrangement of electrodes

Physical Description of the Problem

When measuring resistivity in a drill hole (see Fig. I-1) the current is sent between two current electrodes and the potential difference is measured between two potential electrodes. For the normal arrangement one current electrode and one potential electrode are at the surface, which for theoretical purposes is considered to be at infinity. For the lateral arrangement, two current electrodes and one potential electrode are in the hole and the second potential electrode is at infinity (zero potential) or two potential electrodes and one current electrode are in the hole and the other current electrode at the surface.

To calculate the potential distribution due to the current between the current electrodes, all electrodes in the hole are assumed to be dimensionless (point electrodes) and located on the central axis of the drill hole.

Further assumptions are that the wall of the hole is cylindrical, and that invasion if present is equal in all radial directions.

This means that in the case of no invasion we have two media of constant resistivity and with cylindrical boundaries. In the case of invasion we have three media with two cylindrical boundaries and it is

normally assumed that the resistivity of the invaded zone is also a constant. We will later inspect the limitations of this latter assumption and see that the behavior of the resistivity in the infiltrated zone is of primary importance to our interpretation.

Fig. 1-2 represents schematically the conditions for which we want to calculate the potential distribution caused by axial point electrodes.

If we calculate the potential distribution due to one electrode, we can find the distribution for any number of axial current electrodes by mere superposition, so we will limit our derivations to the case of one electrode on the axis.

Historical Review of the Development of the Theory of Resistivity Logging

The theory of resistivity logging as outlined above was largely developed in Russia.

In 1933, only shortly after electrologging became generally accepted as commercially useful, V. A. Fock (3) worked out the basic theory of the relations between apparent and true resistivities. However, his treatment was limited to the case of no invasion.

Some years later the research department of the Schlumberger Corporation, in Paris, extended the theory to include the effects of invasion and started the computation of master curves (7). The results of this work were not published until 1947. In 1938 the complete theory with many examples of computation procedures was published in a book by L. M. Alpin (4), written in the Russian language.*

Another book, by V. N. Dakhnov (5), also in Russian, was published

* The dielectric analogy of the case of no invasion is treated by Smythe in his book on static and dynamic electricity. (1)

in 1941. Dakhnov's work is based mostly on the theory as outlined by Alpin, and describes several methods of the use of these theories in the interpretation of electrologs.

Some of the more important conclusions of Dakhnov's work were reviewed by Hubert Guyod in a series of articles in the Oil Weekly of 1947 and 1948.

The most complete set of data on the apparent resistivity relationships was published in 1947 by the Schlumberger Corporation (7) in the form of a booklet containing assemblies of resistivity departure curves for use in quantitative interpretation of electrologs.

In this thesis no attempt is made to outline the previous work done on the theory of electrologging. Only the parts that are necessary to understand the proposed method of obtaining additional data from electrologging are described.

Derivation of the Potential Distribution in the Case of No Invasion

The primary condition on which all following derivations are based is that at no point of the system under consideration there can be accumulation of charge. This means that for any volume element the total current coming in must equal the total outgoing current.

If we consider such volume element, enveloped by a surface A (see Fig. I-3) we can express the above condition analytically by:

$$\iint_A \mathbf{y} \cdot \mathbf{n} dA = 0$$

where $\mathbf{y} \cdot \mathbf{n}$ is the component of the current density \mathbf{y} normal to the surface.

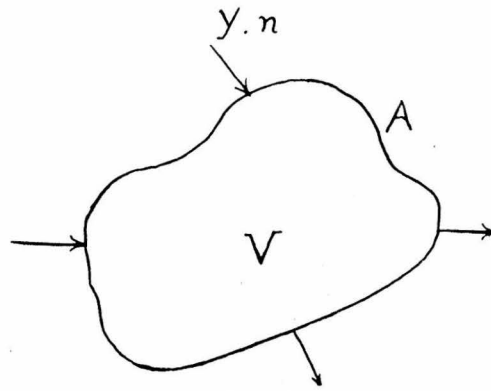


Fig. I-3

By Green's theorem:

$$\iint_A \mathbf{y} \cdot \mathbf{n} dA = \iiint_V \nabla \cdot \mathbf{y} dV = 0 \quad (1-1)$$

This holds for any volume so that $\nabla \cdot \mathbf{y}$ must be zero.

By Ohm's law:

$$\mathbf{y} = \sigma \mathbf{E} = \frac{1}{R} \mathbf{E} \quad (1-2)$$

where σ is the conductivity, R is the resistivity and \mathbf{E} is the field strength. The field strength, \mathbf{E} , can be expressed as:

$$\mathbf{E} = -\nabla V$$

where V is the potential. Substituting into (1-2) gives:

$$\nabla \cdot \mathbf{y} = \nabla \cdot \left(-\frac{1}{R} \mathbf{E} \right) = -\nabla \cdot \left(\frac{1}{R} \nabla V \right) \quad (1-3)$$

When R is a constant we can write:

$$\nabla \cdot \mathbf{y} = -\frac{1}{R} \nabla^2 V = 0 \quad \text{or} \quad \nabla^2 V = 0 \quad (1-4)$$

which is Laplace's equation.

We know that for no invasion R is a constant in both media and in the case of invasion that R_1 is also a constant, so that we may use Laplace's equation for the potential distribution in both cases.

As all the boundaries in our system have cylindrical symmetry, we want to use cylindrical coordinates. Equation (1-4) then becomes:

$$\frac{1}{r} \frac{\partial}{\partial r} \left(R \frac{\partial V}{\partial r} \right) + \frac{1}{r^2} \frac{\partial^2 V}{\partial \varphi^2} + \frac{\partial^2 V}{\partial z^2} = 0$$

$$\frac{\partial^2 V}{\partial r^2} + \frac{1}{r} \frac{\partial V}{\partial r} + \frac{1}{r^2} \frac{\partial^2 V}{\partial \varphi^2} + \frac{\partial^2 V}{\partial z^2} = 0$$

Let $V = R(r) \Phi(\varphi) Z(z)$

Then we have:

$$\Phi Z \left(\frac{d^2 R}{dr^2} + \frac{1}{r} \frac{dR}{dr} \right) + \frac{RZ}{r^2} \frac{d^2 \Phi}{d\varphi^2} + R\Phi \frac{d^2 Z}{dz^2} = 0$$

Dividing by V and multiplying by r^2 :

$$\frac{r^2}{R} \left(\frac{d^2 R}{dr^2} + \frac{1}{r} \frac{dR}{dr} \right) + \frac{1}{\Phi} \frac{d^2 \Phi}{d\varphi^2} + \frac{r^2}{Z} \frac{d^2 Z}{dz^2} = 0 \quad (1-5)$$

Here $\frac{1}{\Phi} \frac{d^2 \Phi}{d\varphi^2} = 0$, as V is independent of φ , and hence:

$$-\frac{1}{Z} \frac{d^2 Z}{dz^2} = \frac{1}{R} \left(\frac{d^2 R}{dr^2} + \frac{1}{r} \frac{dR}{dr} \right)$$

This holds for all values of z and r so that obviously both sides must be equal to the same constant.

$$\text{Let } \frac{1}{Z} \frac{d^2 Z}{dz^2} = -k^2$$

This gives $\frac{d^2 Z}{dz^2} + k^2 Z = 0$, so that $Z = A \sin kz + B \cos kz$.

Equation (1-5) now becomes:

$$\frac{r^2}{R} \left(\frac{d^2 R}{dr^2} + \frac{1}{r} \frac{dR}{dr} \right) - k^2 r^2 = 0.$$

$$\text{or } r^2 \frac{d^2 R}{dr^2} + r \frac{dR}{dr} - (k^2 r^2 + 0^2) R = 0$$

Let $kr = v$ then:

$$v^2 \frac{d^2 R}{dv^2} + v \frac{dR}{dv} - (v^2 - 0^2) R = 0 \quad (1-6)$$

This is the modified Bessel equation of zero order.

Its solutions are the modified Bessel functions of zero order:

$$R(v) = C I_0(v) + D K_0(v)$$

The general solution of (1-5) then becomes:

$$V = (A \sin kz + B \cos kz) [CI_0(kr) + DK_0(kr)] \quad (1-7)$$

Before solving the constants by applying the boundary conditions of our system we will list some properties of the modified Bessel functions:

$$I_n(v) = j^{-n} J_n(jv) = \sum_{p=0}^{\infty} \frac{(jv)^{n-p}}{p! (n-p)!} \quad (a)$$

$$K_n(v) = -I_n(v) \int \frac{dv}{v I_n(v)^2} \quad (b)$$

From these expressions a series of recurrence formulae have been derived, relating functions of different order and derivatives of the modified Bessel functions. (1)

We will make use of the following:

$$K_0'(v) = -K_1(v) \quad (c)$$

$$I_0'(v) = I_1(v) \quad (d)$$

$$I_n' K_n - K_n' I_n = \frac{1}{v} \quad (e)$$

Also of importance are the extreme values:

$$I_0(0) = 1 \quad I_0(\infty) = \infty$$

$$K_0(0) = \infty \quad K_0(\infty) = 0$$

Finally we will use an expression for the inverse distance from the origin in terms of modified Bessel functions, namely:

$$\frac{1}{r} = \frac{2}{\pi} \int_0^{\infty} \cos kz K_0(kr) dk$$

For the derivation of this expression see appendix (A).

With the aid of the outlined properties of the modified Bessel

functions we will now proceed to determine the constants of our general solution for the potential distribution. We will call the potential in the drill hole V_1 and in the surrounding formation V_2 .

Furthermore we can write $V_1 = V_0 - V'$, where V_0 is due directly to the point source and V' represents the effect of the boundary. As V_1 and V_0 satisfy Laplace's equation, V' necessarily does so too.

We know that V is of the form A/\bar{r} (from the analogy of the potential around a point charge in the dielectric case).

The r-component of the field strength is given by:

$$E_r = -\frac{\partial V}{\partial r} \quad \text{so that} \quad j_r = -\frac{1}{R} \frac{\partial V}{\partial r} =$$

= current density in r direction.

Assuming a small sphere around the electrode with radius ϵ and surface S , we have for the total current:

$$j = - \iint_S \frac{1}{R} \frac{\partial V}{\partial r} dS = -\frac{1}{R} \left(-\frac{A}{\epsilon^2}\right) 4\pi \epsilon^2 = \frac{4\pi A}{R} \left(\frac{\partial V}{\partial r} = \frac{-A}{\epsilon^2}\right)$$

$$\text{Therefore } A = \frac{Rj}{4\pi} \quad \text{and} \quad V_0 = \frac{Rj}{4\pi \bar{r}} \quad (1-8)$$

With $R = R_m$ and substituting the expression for $1/\bar{r}$ this becomes:

$$V_0 = \frac{j R_m}{4\pi \bar{r}} = \frac{j R_m}{4\pi} \times \frac{2}{\pi} \int_0^\infty K_0(kr) \cos(kz) dk$$

V' , satisfying Laplace's equation must be of the form:

$$(A K_0 + B I_0) \quad (C \cos kz + D \sin kz)$$

As the potential on the axis is finite and $K_0(0) = \infty$, A must be zero.

This makes $V' = B I_0 (C \cos kz + D \sin kz)$, or in its most general form:

$$V' = \frac{j R_m}{2\pi^2} \int_0^\infty \psi(k) I_0(kr) (\cos kz + D' \sin kz) dk$$

The constant $\frac{1}{2\pi^2} R$ can be included in $\psi(k)$, but is placed before the integral sign in order to obtain the same type of formula as for V_0 .

For V_2 we must consider that the potential at infinity must be zero so that the I_0 term cancels out and V_2 becomes:

$$V_2 = \frac{1}{2\pi^2} R \int_0^\infty \psi(k) K_0(kr) (\cos kz - E \sin kz) dk$$

For both V_1 and V_2 the additional condition: $V(r, z) = V(r, -z)$ exists.

This means that the coefficients of the sine terms must be zero.

The final expressions for V_1 and V_2 therefore are:

$$V_1 = \frac{1}{2\pi^2} R \int_0^\infty [K_0(kr) + \psi(k) I_0(kr)] \cos kz dk$$

$$\text{and } V_2 = \frac{1}{2\pi^2} R \int_0^\infty \psi(k) K_0(kr) \cos kz dk.$$

We are primarily interested in the potential distribution in the bore hole and therefore we want to find the value of $\psi(k)$. To do this we must make use of the boundary conditions.

First Boundary Condition:

At the bore face, the potential must be continuous, or $(V_1)_{r=r_0} = (V_2)_{r=r_0}$. Using the properties of the Fourier-Bessel integrals we can show that in this case we may equate the integrands directly. This gives:

$$K_0(kr_0) + \psi(k) I_0(kr_0) = \psi(k) K_0(kr_0) \quad (1-9)$$

Second Boundary Condition:

The r-component of the current density must be continuous. Since

$$j_r = \frac{1}{R} \frac{\partial V}{\partial r} \quad \text{we have:}$$

$$\frac{1}{R_m} \left(\frac{\partial V_1}{\partial F} \right)_{r=r_0} = \frac{1}{R_t} \left(\frac{\partial V_2}{\partial F} \right)_{r=r_0}$$

or with $\frac{R_m}{R_t} = T$:

$$\left(\frac{\partial V_1}{\partial F} \right)_{r=r_0} = T \left(\frac{\partial V_2}{\partial F} \right)_{r=r_0} \quad (1-10)$$

Differentiating the expressions for V_1 and V_2 under the integral sign, substituting into (1-10) and equating the integrands gives:

$$K'(kr_0) + \psi(k) I'(kr_0) = T \varphi(k) K'(kr_0) \quad (1-11)$$

From (1-9) we have

$$\psi(k) = \frac{\varphi(k) K(kr_0) - K(kr_0)}{I(kr_0)}$$

Substituting into (1-11):

$$K'(kr_0) + \frac{I'(kr_0)K(kr_0) (\varphi(k)-1)}{I(kr_0)} = T \varphi(k) K'(kr_0) \quad (1-11a)$$

We now use property (e):

$$I'K - K'I = \frac{1}{kr_0}$$

Rearranging (1-11a) and substituting gives:

$$T \varphi(k) K'(kr_0) I(kr_0) = \varphi(k) \left[\frac{1}{kr_0} + K'(kr_0) I(kr_0) \right] - \frac{1}{kr_0}$$

$$\text{or } \varphi(k) = \frac{1}{1 - kr_0 (T-1) I(kr_0) K'(kr_0)} \quad (1-12)$$

Substituting (1-12) in (1-9):

$$\psi(k) = \frac{kr_0 (T-1) K(kr_0) K'(kr_0)}{1 - kr_0 (T-1) I(kr_0) K'(kr_0)}$$

This gives for points on the axis ($I_0(0) = 1$)

$$V_1 = \frac{\gamma R_m}{4\pi F} + \frac{\gamma R_m}{2\pi^2} \int_0^\infty \frac{kr_0(T-1)K(kr_0)K'(kr_0)}{1-kr_0(T-1)I(kr_0)K'(kr_0)} \cos kz \, dk$$

A similar formula was worked out in Smythe's book (2) for the dielectric case.

Let $kr_0 = x$ and let us make the following abbreviations:

$$x K(x) K_1(x) = -x K(x) K'(x) \equiv M$$

$$x I(x) I_1(x) = x I(x) I'(x) \equiv N$$

$$x I(x) K_1(x) = -x I(x) K'(x) \equiv P$$

$$x K(x) I_1(x) = x K(x) I'(x) \equiv Q$$

Obviously $MN = PQ$ and property (e) can now be written as

$$P = 1 - Q \quad \text{or} \quad P + Q = 1$$

Substituting the above definitions:

$$V_1 = \frac{\gamma R_m}{2\pi F} + \frac{\gamma R_m}{2\pi^2} \int_0^\infty \left[\frac{-(T-1) M \cos\left(\frac{x}{r_0} x\right)}{1 + (T-1)(1-Q)} \right] \frac{1}{r_0} \, dx$$

The integrand can be reworked to:

$$\frac{1}{r_0} \frac{M \cos\left(\frac{x}{r_0} x\right) \, dx}{-\left(\frac{1}{T-1}\right) + 1-Q} = \frac{1}{r_0} \frac{M}{\left(\frac{1}{T-1} - 1\right) + Q} \cos\left(\frac{x}{r_0} x\right) \, dx$$

Here $T = \frac{R_m}{R_t}$ so that $\frac{1}{1-T} - 1 = \frac{1}{1 - \frac{R_m}{R_t}} - 1 = \frac{R_t - R_m}{R_t - R_m} = \frac{1}{\frac{R_t}{R_m} - 1}$

Let $\frac{R_t}{R_m} - 1 = e$ then $\frac{1}{1-T} - 1 = \frac{1}{e}$

The final expression for V_1 , substituting the above results, becomes:

$$V_1 = \frac{\gamma R_m}{4\pi F} + \frac{\gamma R_m}{2\pi^2 r_0} \int_0^\infty \frac{M}{\frac{1}{e} + Q} \cos\left(\frac{x}{r_0} x\right) \, dx \quad (1-13)$$

For the normal electrode arrangement, electrode N is at zero potential, so that the measured ΔV equals the potential at M. Electrode B is far

enough away so that its influence may be neglected, and therefore we have to consider only the potential at M due to a single point electrode.

This means $\Delta V_{MN} = V_1$, where ΔV_{MN} is the potential difference measured by the galvanometer in the resistivity logging circuit, between M and the surface electrode N.

However, the resistivity logs are calibrated to read directly in terms of so-called apparent resistivity, R_a . The apparent resistivity is defined as the resistivity of a homogeneous, infinite medium surrounding the electrodes, that would give the same potential at M, due to the current between A and B, for the given electrode spacing, as the potential measured by the galvanometer.

We may write therefore $V_1 = \frac{I R_a}{4 \pi \bar{r}}$ with $\bar{r} = \overline{AM}$. This is of the same form as equation (1-8), which was derived for V_0 .

The equation for R_a becomes:

$$R_a = \frac{V_1}{I} 4 \pi (\overline{AM})$$

As M is a point on the axis, we also have $s = \overline{AM}$. Let $\frac{s}{r_0} = \frac{\overline{AM}}{r_0} = s$.

Then we have from (1-13) and 1-14):

$$R_a = R_m + \frac{2}{\pi} R_m s \int_0^{\infty} \frac{M}{\frac{1}{s} + Q} \cos (sx) dx$$

or $\frac{R_a}{R_m} = 1 + \frac{2}{\pi} s \int_0^{\infty} \frac{M}{\frac{1}{s} + Q} \cos (sx) dx$ (1-15)

For the lateral arrangement (see Fig. I-1) we have either two current electrodes and one pick-up electrode in the hole or two pick-up electrodes and one current electrode. (The second current electrode may either be at a sufficiently large distance in the hole or at the surface so that its influence can be neglected.)

It can be shown that the resulting voltage differences for similar spacings between the electrodes are the same in both cases.*

We will limit our discussion therefore to the case of two relatively closely spaced current electrodes and one pick-up electrode in the hole and the other pick-up electrode at infinity.

The voltage difference between M and N (N has zero potential) may be expressed in this case as:

$$\Delta V = \frac{\int R_M}{4\pi} \left(\frac{1}{AM} - \frac{1}{BM} \right) = (V_1)_A - (V_1)_B$$

Where $(V_1)_A$ and $(V_1)_B$ are respectively the potentials at M due to the point sources A and B.

$$R_M = \frac{(V_1)_A - (V_1)_B}{\int} \frac{4\pi}{\frac{1}{AM} - \frac{1}{BM}}$$

$$\text{Let } AM = s_1, \quad BM = s_2, \quad s_1 = \frac{z_1}{r_0}, \quad s_2 = \frac{z_2}{r_0}$$

$$\overline{OM} = \frac{1}{2} (\overline{AM} - \overline{BM}) = z \quad \text{while } b = \overline{BM} - \overline{AM}$$

$$(V_1)_i = \frac{\int R_M}{4\pi r_0} + \frac{\int R_M}{2\pi^2 r_0} \int_0^\infty \frac{M}{\frac{1}{e} + Q} \cos\left(\frac{s_i}{r_0} x\right) dx \quad \text{with } i = 1, 2$$

$$R_M = \left(\frac{\int R_M}{4\pi s_1} - \frac{\int R_M}{4\pi s_2} \right) \frac{4\pi}{\int \left(\frac{1}{s_1} - \frac{1}{s_2} \right)} + \frac{4\pi}{\left(\frac{1}{s_1} - \frac{1}{s_2} \right)} \cdot \frac{\int R_M}{2\pi^2 r_0} \int_0^\infty \frac{M}{\frac{1}{e} + Q} (\cos s_1 x - \cos s_2 x) dx$$

$$= R_M + \frac{2R_M}{\pi r_0} \cdot \frac{1}{\left(\frac{1}{s_1} - \frac{1}{s_2} \right)} \int_0^\infty \frac{M}{\frac{1}{e} + Q} (\cos s_1 x - \cos s_2 x) dx \quad (1-16)$$

$$= R_M + \frac{z^2}{b} \left(1 - \frac{b^2}{4s^2} \right) \frac{2R_M}{\pi r_0} \int_0^\infty \frac{M}{\frac{1}{e} + Q} (\cos s_1 x - \cos s_2 x) dx \quad (1-16a)$$

* This statement is known as the reciprocity theorem.

A commonly used approximated formula for the lateral arrangement is derived as follows:*

Given one point electrode as current source, we will designate the potentials at the pick-up electrodes M and N respectively as V_M and V_N . The potential difference measured by the lateral arrangement then is

$$V_L = V_M - V_N = \frac{\rho(R_G)_l}{4\pi} \left(\frac{1}{AM} - \frac{1}{AN} \right)$$

where $(R_G)_l$ is the apparent resistivity corresponding to the characteristic volume of the lateral spacing in question.

We now assume that M and N are far from the point source A and the distance between them is small compared to \overline{AO} so that in the region between them the potential decreases approximately linearly with the distance and therefore the fieldstrength in the z-direction (E_z) is a constant.

We then have $V_M - V_N = \Delta z \cdot E_z$ where $\overline{MN} = \Delta z$, $V_M > V_N$ and the positive z direction is the direction from M to N.

We make a second approximation by writing:

$$\frac{1}{AM} - \frac{1}{AN} = \frac{\overline{AN} - \overline{AM}}{\overline{AM} \cdot \overline{AN}} \approx \frac{\overline{MN}}{(\overline{OA})^2} = \frac{\Delta z}{z^2}$$

$$\text{where } \overline{OA} = \frac{1}{2} (\overline{AN} + \overline{AM}) = z$$

This holds true only for $\overline{AM}/\overline{AN} \approx 1$ (or $\overline{OA} \gg \overline{MN}$) and is in general a good approximation for large lateral spacings, e.g. for the conventional 10', 16' or 18' spacings.

* As the physical picture is somewhat easier understood for the case of two pick-up electrodes and one current electrode in the hole, we will make the derivation for this arrangement. The results apply equally well, however, to the alternative arrangement.

Combining the above expressions we have:

$$(R_a)_\ell = \frac{4\pi}{\gamma} \cdot E_z \cdot s^2 \quad \text{with } E_z = -\frac{\partial V}{\partial z} \approx \text{constant.}$$

$$\text{As } V = \frac{\gamma R_m}{4\pi s} + \frac{\gamma R_m}{2\pi^2 r_0} \int_0^\infty \psi(x) \cos\left(\frac{x}{r_0} s\right) dx$$

$$\begin{aligned} E_z &= -\left\{ -\frac{\gamma R_m}{4\pi s^2} - \frac{\gamma R_m}{2\pi^2 r_0} \int_0^\infty \frac{x}{r_0} \psi(x) \sin\left(\frac{x}{r_0} s\right) dx \right\} \\ &= \frac{\gamma R_m}{4\pi s^2} + \frac{\gamma R_m}{2\pi^2 r_0} \int_0^\infty x \psi(x) \sin\left(\frac{x}{r_0} s\right) dx \end{aligned}$$

Substitution of this expression gives for $(R_a)_\ell$:

$$(R_a)_\ell = R_m + \frac{2}{\pi} R_m \frac{s^2}{r_0^2} \int_0^\infty x \psi(x) \sin\left(\frac{x}{r_0} s\right) dx$$

or replacing $\frac{x}{r_0}$ by s :

$$W = \frac{(R_a)_\ell}{R_m} = 1 + \frac{2}{\pi} s^2 \int_0^\infty x \psi(x) \sin(sx) dx$$

If we call the apparent resistivity for a normal arrangement with $\frac{AN}{r_0}$ equal to the $\frac{OA}{r_0}$ of our lateral arrangement ($=s$), $(R_a)_n$ and write $X = \frac{(R_a)_n}{R_m}$ then we have from equation (1-15):

$$X = \frac{(R_a)_n}{R_m} = 1 + \frac{2}{\pi} s \int_0^\infty \psi(x) \cos sx dx$$

$$\text{and } \frac{dX}{ds} = -\frac{2}{\pi} s \int_0^\infty x \psi(x) \sin sx dx + \frac{2}{\pi} \int_0^\infty \psi(x) \cos s x dx$$

$$\text{and therefore } W = X - s \frac{dX}{ds}$$

This permits us to plot the departure curves for the lateral arrangement if we have calculated them for the normal arrangement. For small lateral spacings however it is better to use formula (1-16).

Potential Distribution if Invasion has Occurred

In this case it is assumed that there is an infiltrated zone of radius r_1 and of a constant resistivity R_1 . We will see later exactly what happens to the resistivity in the invaded zone and in how far the latter assumption is justified.

Using the above assumptions we have a three-layer problem, analogous to the two-layer case of non-invasion, but with two more unknowns and two more boundary conditions.

For the potential in the hole we write again:

$$V_1 = V_0 + V' = \frac{\gamma R_0}{2\pi^2} \int_0^{\infty} \left[K_0(kr) + \psi(k) I_0(kr) \right] \cos kz \, dk \quad (1-17)$$

In the infiltrated zone r neither approaches zero nor infinity so that the potential V_2 will be expressed as the general solution containing both K_0 and I_0 .

$$V_2 = \frac{\gamma R_0}{2\pi^2} \int_0^{\infty} \left[\alpha(k) K_0(kr) + \beta(k) I_0(kr) \right] \cos(kz) \, dk \quad (1-18)$$

Finally the potential in the undisturbed formation, as in the case of non-invasion becomes:

$$V_3 = \frac{\gamma R_0}{2\pi^2} \int_0^{\infty} \varphi(k) K_0(kr) \cos kz \, dk \quad (1-19)$$

We now have the following boundary conditions:

1) $V_1 = V_2$ for $r = r_0$

$$\text{or } K_0(kr_0) + \psi(k) I_0(kr_0) = \alpha(k) K_0(kr_0) + \beta(k) I_0(kr_0)$$

$$K_0(kr_0) \left[\alpha(k) - 1 \right] = \left[\psi(k) - \beta(k) \right] I_0(kr_0) \quad (1-20)$$

2) $V_2 = V_3$ for $r = r_1$

$$\text{or } \alpha(k) K_0(kr_1) + \beta(k) I_0(kr_1) = \varphi(k) K_0(kr_1) \quad (1-21)$$

3) Continuity of radial component of current density at first boundary:

$$\frac{1}{R_m} \left(\frac{\partial V_1}{\partial r} \right)_{r=r_0} = \frac{1}{R_1} \left(\frac{\partial V_2}{\partial r} \right)_{r=r_0}$$

which gives:

$$K_0'(kr_0) + \psi(k) I_0'(kr_0) = T_1 \left[\alpha(k) K_0'(kr_0) + \beta(k) I_0'(kr_0) \right]$$

where:

$$T_1 = \frac{R_m}{R_1} \quad K_0'(kr_0) = -K_1(kr_0) \quad \text{and} \quad I_0'(kr_0) = I_1(kr_0)$$

so that

$$-K_1(kr_0) + \psi(k) I_1(kr_0) = T_1 \left[-\alpha(k) K_1(kr_0) + \beta(k) I_1(kr_0) \right] \quad (1-22)$$

4) Continuity of radial component of current density at second boundary:

$$\frac{1}{R_1} \left(\frac{\partial V_2}{\partial r} \right)_{r=r_1} = \frac{1}{R_t} \left(\frac{\partial V_3}{\partial r} \right)_{r=r_1}$$

$$\text{or } -\alpha(k) K_1(kr_1) + \beta(k) I_1(kr_1) = -T_2 \varphi(k) K_1(kr_1) \quad (1-23)$$

where $T_2 = \frac{R_1}{R_t}$.

Thus we have four equations (1-20) through (1-23) with four unknowns, namely $\psi(k)$, $\alpha(k)$, $\beta(k)$, and $\varphi(k)$ which we want to solve for $\psi(k)$, as we are primarily interested in the potential in the hole itself.

We will use the notations:

$$kr_0 = x$$

$$K_0(x) \equiv K$$

$$I_0(x) = I$$

$$K_1(x) = K_1$$

$$I_1(x) \equiv I_1$$

$$\frac{R_1}{R_0} = n$$

$$K(n) \equiv K(nx) \quad I(n) \equiv I(nx) \quad M(n) \equiv M(nx) \quad \text{etc.}$$

$$\psi(k) \equiv \psi \quad \varphi(k) \equiv \varphi \quad \alpha(k) \equiv \alpha \quad \beta(k) \equiv \beta$$

$$\text{From (1-20): } \psi = \frac{(\alpha - 1)K + \beta I}{I} \quad (a)$$

$$\text{From (1-22): } \psi = \frac{T_1 (\beta I_1 - \alpha K) + K_1}{I_1} \quad (b)$$

$$\text{While (1-23) gives: } \varphi = \frac{\beta I_1(n) - \alpha K_1(n)}{-T_2 K_1(n)} \quad (c)$$

From (1-22) and (c):

$$\alpha = \frac{\beta I_1(n) - \alpha K_1(n)}{-T_2 K_1(n)} - \frac{\beta I(n)}{K(n)}$$

$$\alpha = \frac{\beta I_1(n)K(n) - \alpha K_1(n)K(n) + \beta I(n)K_1(n)T_2}{-T_2 K_1(n)K(n)}$$

$$\alpha = \frac{\beta Q_n - \alpha M_n + \beta P_n T_2}{-T_2 M_n}$$

$$\text{or } -T_2 M_n \alpha + \alpha M_n = \beta Q_n + \beta P_n T_2$$

$$M_n(1-T_2)\alpha = \beta(Q_n + P_n T_2)$$

Here we can write:

$$P_n T_2 = Q_n + T_2(1-Q_n) = T_2 - T_2 Q_n + Q_n = T_2 + Q_n(1-T_2)$$

so that we have:

$$M_n(1-T_2)\alpha = \beta [T_2 + Q_n(1-T_2)]$$

$$\text{or } M_n \alpha = \beta \left(\frac{T_2}{1-T_2} + Q_n \right)$$

$$\text{with } \frac{T_2}{1-T_2} = \frac{1}{1/T_2 - 1} = \frac{1}{R_4/R_1 - 1} = \frac{1}{D'} \quad \text{where } D' = \frac{R_4}{R_1 - 1}$$

this gives $\alpha = \frac{1/D' + Q_n}{M_n}$ (d)

Equating (a) and (b)

$$\frac{(\alpha - 1)K + \beta I}{I} = \frac{T_1(\beta I_1 - \alpha K_1) + K_1}{I_1}$$

Substituting α from (d):

$$\beta + \frac{1/D' - Q_n}{M_n} \beta - 1 \frac{K}{I} = \frac{T_1 \beta [I_1 - (1/D' + Q_n) K_1 / M_n] + K_1}{I_1}$$

$$\begin{aligned} \text{or } \beta & \frac{M_n I I_1 + K I_1 (1/D' + Q_n) - T_1 M_n I I_1 + I K_1 (1/D' + Q_n) T_1}{M_n I I_1} \\ & = \frac{K_1}{I_1} + \frac{K}{I} \end{aligned}$$

$$\beta \frac{M_n N + Q(1/D' + Q_n) - T_1 M_n N + T_1 P(1/D' + Q_n)}{M_n N} = \frac{P + Q}{N}$$

and as $P = 1 - Q$ or $P + Q = 1$ we have

$$\beta = \frac{M_n}{(1 - T_1) M_n N + (1/D' + Q_n) (Q + T_1 P)}$$

$$\beta = \frac{M_n}{M_n N (1 - T_1) (1/D' + Q_n) [T_1 + Q(1 - T_1)]}$$

$$\beta = \frac{M_n}{(1 - T_1) [M_n N + (1/D' + Q_n) (1/c + Q)]} \quad (e)$$

$$\text{From (d): } \alpha = \frac{1/D' + Q_n}{(1 - T_1) [M_n N + (1/D' + Q_n) (1/c + Q)]} \quad (f)$$

Substitution of (e) and (f) into (b) gives:

$$\begin{aligned} \psi & = \frac{T_1 [M_n I_1 - (1/D' + Q_n) K_1] + K_1 (1 - T_1) [M_n N + (1/D' + Q_n) (1/c + Q)]}{I_1 (1 - T_1) M_n N + (1/D' - Q_n) (1/c - Q)} \\ & = \frac{T_1 [M_n N - (1/D' + Q_n) P] + P (1 - T_1) [M_n N - (1/D' - Q_n) (1/c - Q)]}{N (1 - T_1) [M_n N + (1/D' + Q_n) (1/c + Q)]} \end{aligned}$$

$$= \frac{1/c [M_2 N - (1/D' + Q_2) P] + P [M_2 N + (1/D' + Q_2) (1/c + Q)]}{N [M_2 N + (1/D' + Q_2) (1/c + Q)]}$$

$$\psi = \frac{1/c M_2 N - P/c D' - P Q_2/c + P M_2 N + P/c D' + P Q/D' + P Q_2/c + P Q Q_2}{N^2 M_2 + N/c D' + N Q/D' + N Q_2/c + N Q Q_2}$$

Using $MN = PQ$ this becomes

$$\psi = \frac{1/c M_2 N + P M_2 N + MN/D' + M N Q_2}{N^2 M_2 + N/c D' + N Q/D' + N Q_2/c + N Q Q_2}$$

$$\psi = \frac{1/c M_2 + P M_2 + M/D' + M Q_2}{N M_2 + 1/c D' + Q/D' + Q_2/c + Q Q_2} \quad (g)$$

This expression can be used directly or can be reworked to take a slightly simpler form:

Letting $D = \frac{R_1}{R_t} - 1$ we have:

$$\frac{1}{D'} = \frac{1}{R_t/R_1 - 1} = \frac{R_1/R_t}{1 - R_1/R_t} = \frac{D+1}{-D} = -(1 + \frac{1}{D})$$

Also using $Q_2 = 1 - P_2$ we obtain for :

$$\psi = \frac{1/c M_2 - M (1 + 1/D) + M(1 - P_2) + P M_2}{N M_2 - 1/c (1 + 1/D) - Q(1 + 1/D) + Q(1 - P_2) + 1/c(1 - P_2)}$$

$$\psi = \frac{M/D - M_2/c + (M P_2 - P M_2)}{1/c D + Q/D + P_2/c + (Q P_2 - N M_2)} \quad (1-24)$$

In the same way as for non-invasion:

$$V_1 = \frac{j R_m}{4 \pi \bar{r}} + \frac{j R_m}{2 \pi^2 R_0} \int_0^{\infty} \psi(k) I_0(kr) \cos(kr \frac{\bar{r}}{R_0}) d(kr_0)$$

On the axis $I_0(kr) = 1$ and $\bar{r} = z$

So for the normal arrangement with $z = \overline{AM}$ and $s = \frac{\overline{AM}}{R_0}$ we have

$$R_2 = \frac{V_1}{j} 4 \pi z = R_m + \frac{2}{\pi} R_m s \int_0^{\infty} \psi(k) \cos(sk) dx$$

$$\text{or } \frac{R_a}{R_M} = 1 + \frac{2}{\pi} s \int_0^{\infty} \psi(k) \cos(sx) dx \quad (1-25)$$

where $\psi(k)$ is given by (1-24).

For the lateral arrangement we obtain in the same manner:

$$\frac{R_a}{R_M} = 1 + \frac{2}{\pi} \frac{1}{(1/s_1 - 1/s_2)} \int_0^{\infty} \psi(k) [\cos(s_1 x) - \cos(s_2 x)] dx \quad (1-26)$$

where $s_1 = \frac{AM}{r_0}$ and $s_2 = \frac{BM}{r_0}$ and $\psi(k)$ again is given by (1-24).

Values of R_a can be obtained by plotting the integrands and finding the area under the curves by using a planimeter. Both integrands converge very fast.

In this way curves can be plotted for R_a as a function of R_t , s , r_1 and R_1 . These curves are often called resistivity departure curves, and a large assembly of them is published under that name by the Schlumberger Well Surveying Corporation (7).

PART II

Computation of the True Resistivity of Formations
and the Resistivity of the Infiltrated Zone

The conventional way of plotting resistivity departure curves is to give R_a/R_m as a function of s for several values of R_t/R_m and d_1/d_0 for a given ratio of R_1/R_m . Instead of using s , the abscissae are mostly in terms of $s/2 = \frac{\Delta H}{2r_0} = \frac{\Delta H}{d_0}$. Fig. II-1 gives a family of these departure curves for the case of no-invasion, for the normal electrode arrangement. Fig. II-2 gives departure curves for the case of invasion, with $r_1 = 2r_0$ and $R_1 = 10 R_m$ also for the normal device. For larger values of r_1 the curves will be shifted upward, as indicated by dotted lines. Fig. II-3 gives the departure curves in the case of invasion for the lateral device.

The present use of resistivity departure curves for determination of R_t is as follows: (6)

An experimental curve is plotted in the same way as the resistivity departure curves, using measurements of R_a from electrologs for different electrode spacings. This curve is compared with master curves made up in series as described above (7), and R_t is found by interpolation between the two closest fitting theoretical curves. As can be easily seen from the shape of the curves in Figs. II-1 to II-3, at least four points will be needed to make an accurate plot of such experimental curve. This means that the logs have to be run with four different normal spacings. Though this is possible with the modern seven conductor cables, it is not yet a universally common practice. Some authors have

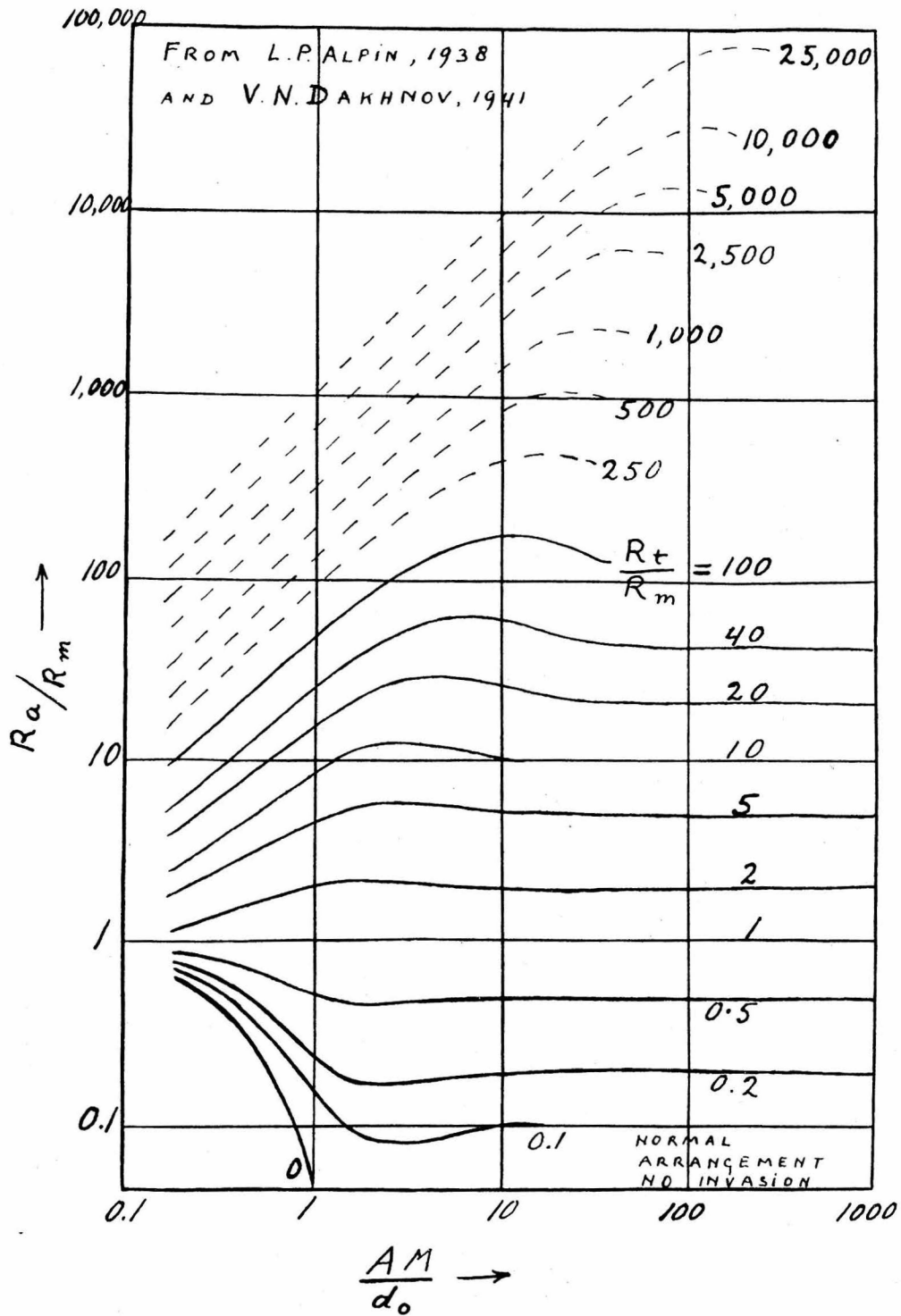


Fig. II-1

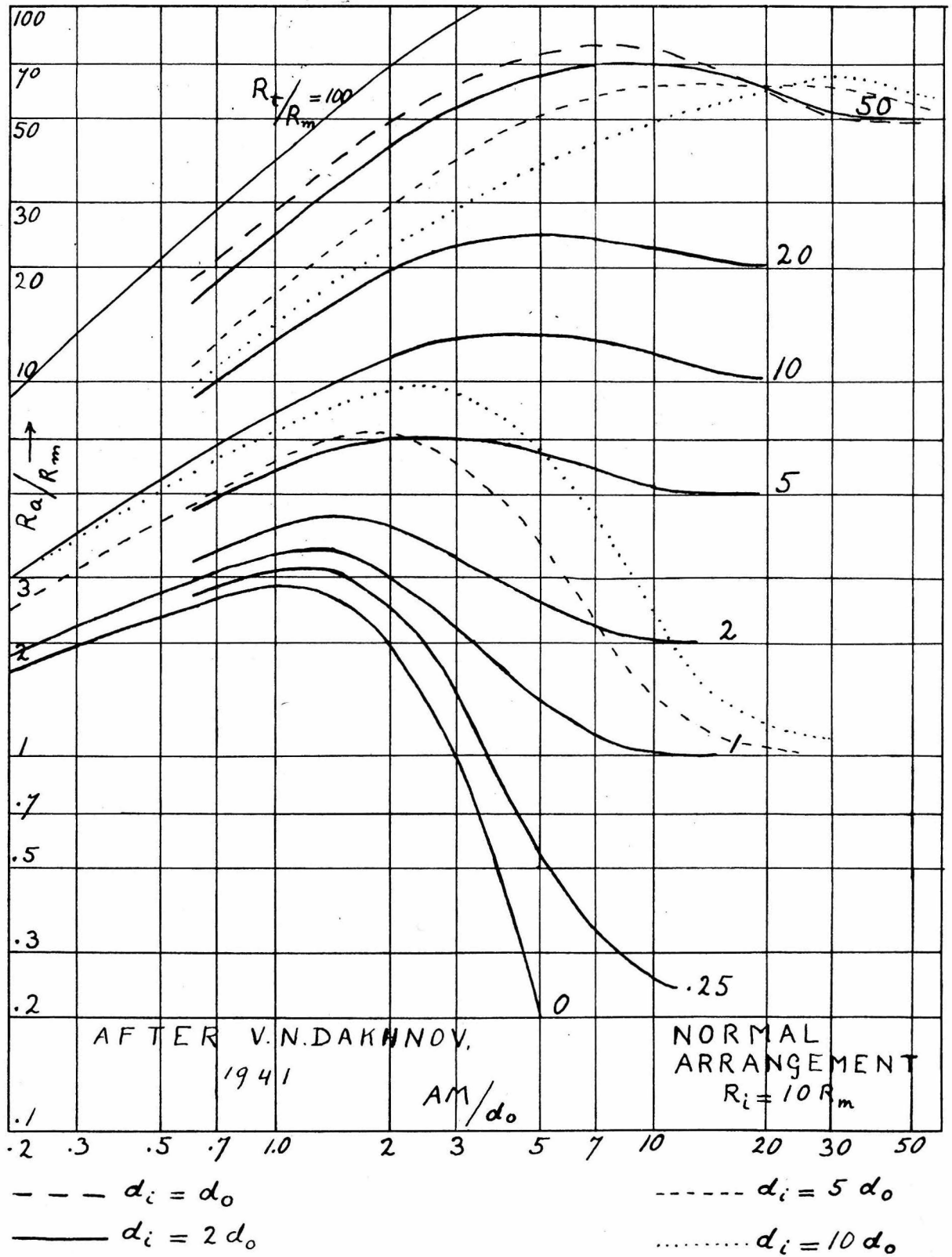


Fig. II-2

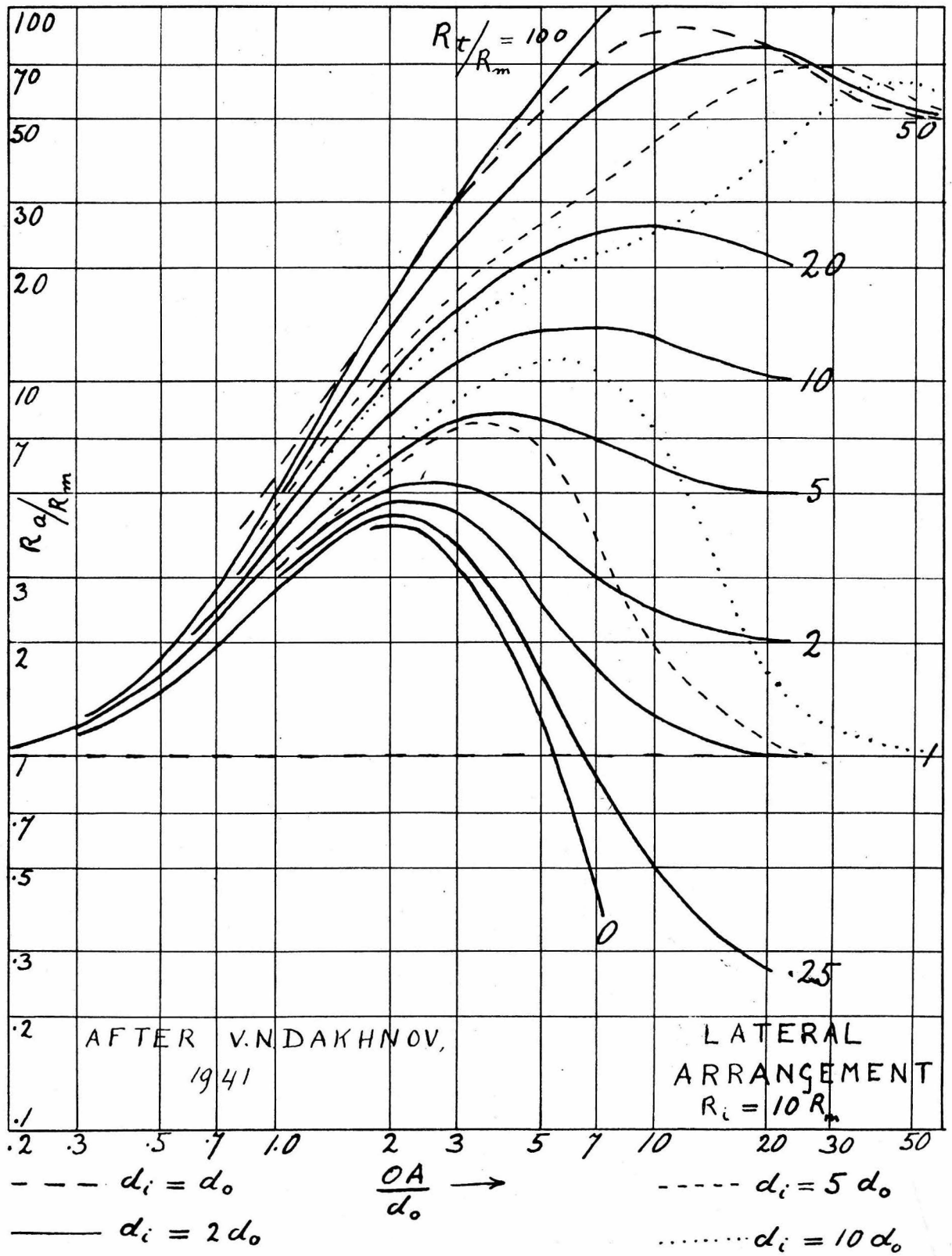


Fig. II-3

claimed that a good determination can be made by using an experimental departure curve constructed with the aid of two points only. Obviously it is utterly impossible to construct a curve whose location and shape is of paramount importance, using two points only. The ambiguity of this situation is clearly demonstrated by Fig. II-4 which gives R_2 as a function of R_3 for different values of R_1 and r_1 . We see that any R_3 gives an infinite number of possible combinations. A second R_3 found for another given electrode spacing will eliminate part of the possibilities, but still leave too many to make the method workable, in most cases.

Alternative Method of Finding R_2 and R_1

For the reasons described above, it appears to be worth while to find a more direct way of interpretation, and we have therefore worked out a new method, which makes use of one lateral and two normal curves.

In order to evaluate R_2 accurately we want a maximum amount of information on the infiltrated zone. More specifically, we want to determine the true resistivity of the infiltrated zone. It is common knowledge that small spacings give information about the resistivities close to the borehole and it has often been stated that the "normal" curve which usually corresponds to a spacing of $10''$ gives a good approximation of the invaded zone resistivity. However, if we look at Fig. II-2, we see that even for the smallest spacings of the normal arrangement the influence of R_3 on the measured R_2 is very large. Fig. II-2 shows that for very small spacings of the lateral device, R_2 is more independent of the resistivity of the formation beyond the infiltrated zone (R_3).

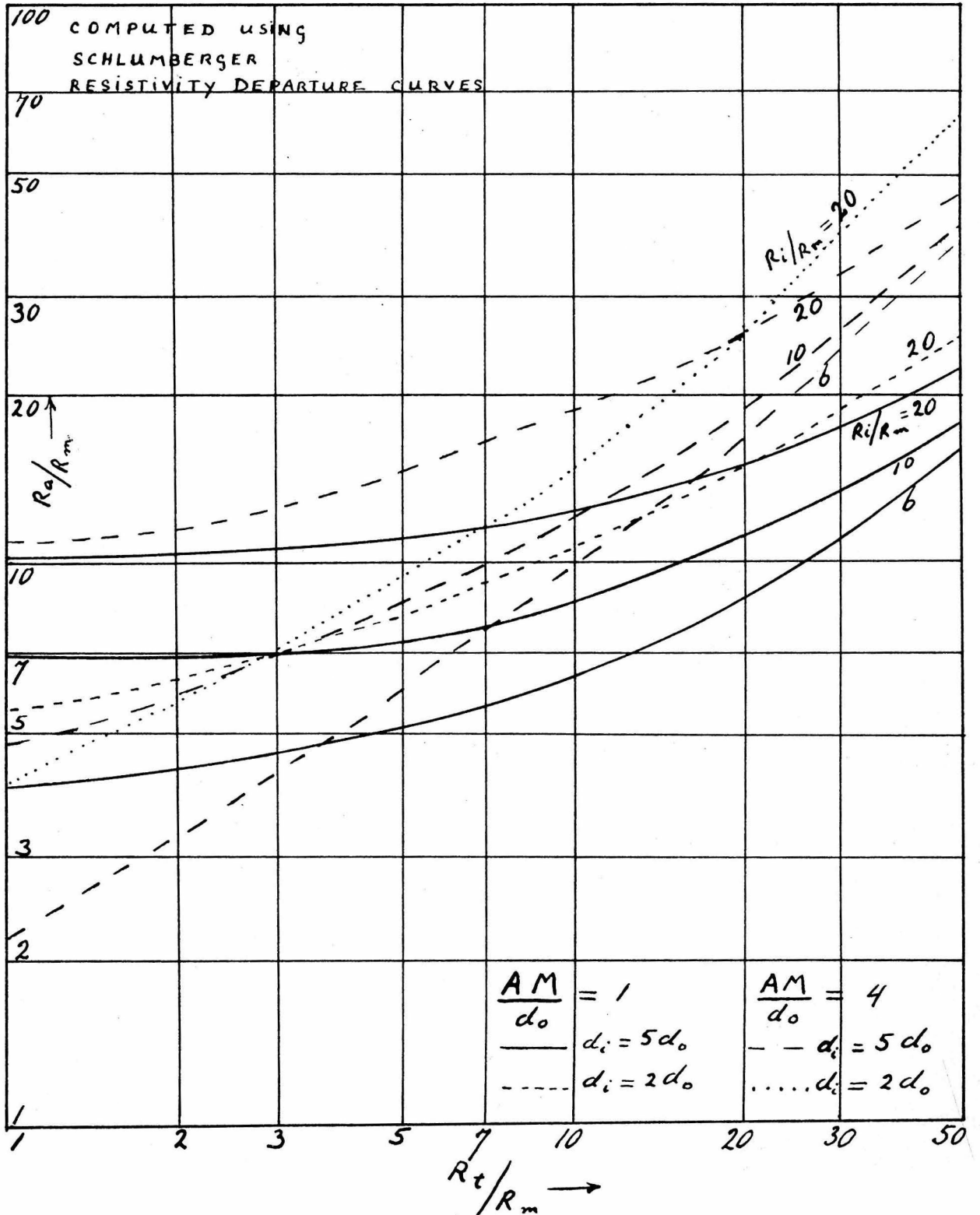


Fig. II-4

It seems therefore advisable to use a small lateral spacing, to obtain data on the infiltrated zone and normal spacings to find the true resistivity of the undisturbed formation.

The optimum lateral spacing to be used, will be the one that gives apparent resistivities which are very nearly equal to the true resistivity of the infiltrated zone and which are as little as possible dependent upon R_t .

The second of these conditions is best fulfilled by the smallest possible lateral spacing. However, most of the apparent resistivities for very small spacings have, for usual ranges of R_t , values, which are lower than the infiltrated zone resistivity, because of the large influence of the borehole itself.

In other words the apparent resistivities that would be obtained for a wide range of values of R_t , varying from very small to very large R_t 's, will not be distributed symmetrically around the true R_t , but the whole group will be shifted towards lower values.

Also small inaccuracies in the determination of the hole diameter, will give larger errors for the extremely small spacings, than for larger ones.

The optimum spacing therefore will be a compromise between the influence of the borehole and the effect of R_t , on the apparent resistivity.

To determine this optimum spacing, the apparent resistivity was computed for a series of small spacings in the range that appeared most promising, and the most effective one was selected.

The computations were carried out for average invasion diameter,

given values of R_1/R_2 and values of R_t/R_2 which covered most of the conditions that are normally encountered.

As stated before, the approximated formula for R_a cannot be used for small lateral spacings. However it is possible to obtain values for $(R_a)_\ell$ (= apparent resistivity for lateral arrangement) from the departure curves for the normal arrangements using the following method of conversion:

Considering the lateral arrangement as consisting of one current electrode A and two potential electrodes M and N we can write:

$$V_M = \frac{J(R_a)_1}{4\pi(\overline{AM})} \quad \text{or} \quad \frac{V_M}{J} = \frac{(R_a)_1}{4\pi(\overline{AM})}$$

$$V_N = \frac{J(R_a)_2}{4\pi(\overline{AN})} \quad \text{or} \quad \frac{V_N}{J} = \frac{(R_a)_2}{4\pi(\overline{AN})}$$

Here $(R_a)_1$ and $(R_a)_2$ are the apparent resistivities corresponding to normal electrode arrangements having respectively the spacing \overline{AM} and \overline{AN} .

Denoting the voltage drop between the potential electrodes of the lateral arrangement and the apparent resistivity for this arrangement respectively by V_ℓ and $(R_a)_\ell$ we have:

$$V_\ell = \frac{J(R_a)_\ell}{4\pi} (1/\overline{AM} - 1/\overline{AN})$$

and as $V_\ell = V_M - V_N$ we can write

$$(R_a)_\ell = 4\pi \frac{V_M - V_N}{J} \frac{1}{(1/\overline{AM} - 1/\overline{AN})}$$

$$= \left[\frac{(R_a)_1}{\overline{AM}} - \frac{(R_a)_2}{\overline{AN}} \right] \frac{1}{(1/\overline{AM} - 1/\overline{AN})}$$

so that

$$\frac{(R_a)l}{R_m} = \left[\frac{(R_a)_1 / R_m}{\overline{AN}/d_o} - \frac{(R_a)_2 / R_m}{\overline{AN}/d_o} \right] \left(\frac{1}{1/(\overline{AM}/d_o) - 1/(\overline{AN}/d_o)} \right) \quad (2-1)$$

For any given lateral arrangement and hole diameter the factor

$$K_g = \frac{1}{1/(\overline{AM}/d_o) - 1/(\overline{AN}/d_o)}$$

can be calculated directly.

The quantities $(R_a)_1/R_m$ and $(R_a)_2/R_m$ are found from the departure curves for the normal device for any given set of conditions (R_1 , d_1 and R_t), under consideration, corresponding to the values of \overline{AM}/d_o and \overline{AN}/d_o .

Using values of $(R_a)_1/R_m$ and $(R_a)_2/R_m$ obtained from the Schlumberger conventional departure curves (7), $(R_a)l/R_m$ has been computed with the aid of equation (2-1) for three values of R_1/R_m , average invasion diameter and several values of R_t/R_m and are shown in Tables II-A, II-B and II-C.

TABLE II-A

$d_1 = 5 d_o$		$\overline{AN}/d_o = 1.75$		$\overline{AN}/d_o = 2.25$	
$R_1 = 6 R_m$		$R_1 = 11 R_m$		$R_1 = 21 R_m$	
R_t/R_m	$(R_a)l/R_m$	R_t/R_m	$(R_a)l/R_m$	R_t/R_m	$(R_a)l/R_m$
30	6.07	55	9.85	105	18.6
6	5.44	11	9.69	21	11.59
1	5.29	1	7.32	1	11.19
.12	5.08	.11	7.3	.1	10.32

TABLE II-B

$d_1 = 5 d_0$		$\overline{AN}/d_0 = 2.75$		$\overline{AN}/d_0 = 3.25$	
$R_1 = 6 R_m$		$R_1 = 11 R_m$		$R_1 = 21 R_m$	
R_t/R_m	$(R_a)_l/R_m$	R_t/R_m	$(R_a)_l/R_m$	R_t/R_m	$(R_a)_l/R_m$
30	7.35	55	12.2	105	29.22
6	7.08	11	11.75	21	20.46
1	5.29	1	10.64	1	14.89
.12	4.8	.11	9.12	.1	15.08

TABLE II-C

$d_1 = 5 d_0$		$\overline{AN}/d_0 = 3.5$		$\overline{AN}/d_0 = 4.0$	
$R_1 = 6 R_m$		$R_1 = 11 R_m$		$R_1 = 21 R_m$	
R_t/R_m	$(R_a)_l/R_m$	R_t/R_m	$(R_a)_l/R_m$	R_t/R_m	$(R_a)_l/R_m$
30	10.0	55	20.8	105	31.6
6	8.34	11	12.87	21	21.4
1	4.86	1	9.18	1	18.8
.12	4.24	.11	9.07	.1	17.7

Similar tables were made up for other small lateral spacings and also for various values of \overline{AN}/d_0 .

From comparison of eight of these tables it was found that the most satisfactory spacing is:

$$\overline{AN}/d_0 = 2.75$$

$$\overline{AN}/d_0 = 3.25$$

As shown in Table I-A, for smaller spacings, the average values of

$(R_a) / R_m$ shift below the actual value of R_1 / R_m .

For spacings larger than the optimum spacing, the effect of R_t becomes more and more pronounced and the average values of $(R_a) / R_m$ are found to be larger than the R_1 / R_m in question.

For increased \overline{MN}/d_0 we find a slightly less regular distribution of $(R_a) / R_m$ with respect to R_1 / R_m .

Using the above determined optimum spacing, we can now make up a series of master curves, representing R_a / R_m as a function of R_1 / R_m for different values of R_t / R_m and for different ratios of the invasion diameter, d_1 , over the hole diameter, d_0 .

These master curves will be called "apparent resistivity curves."

To obtain a complete set of these apparent resistivity curves, the use of the heretofore published resistivity departure curves for the normal electrode arrangements, does not suffice, because of scarcity of data in most ranges.

For instance the Schlumberger departure curves, which form the most complete set published to date, give only three values of R_1 / R_m and four values of d_1 / d_0 . For the computation of the vast majority of our curves we have to go back therefore to the formula, which we derived for (R_a) , and is given by equation (1-26) and as direct computation will be more accurate than the semi-graphical method outlined before, it is advisable to obtain the apparent resistivity curves using equation (1-26) exclusively.

Fig. II-5, gives an example of a set of apparent resistivity curves, for the lateral arrangement.

To obtain a set of master curves which will completely cover all or

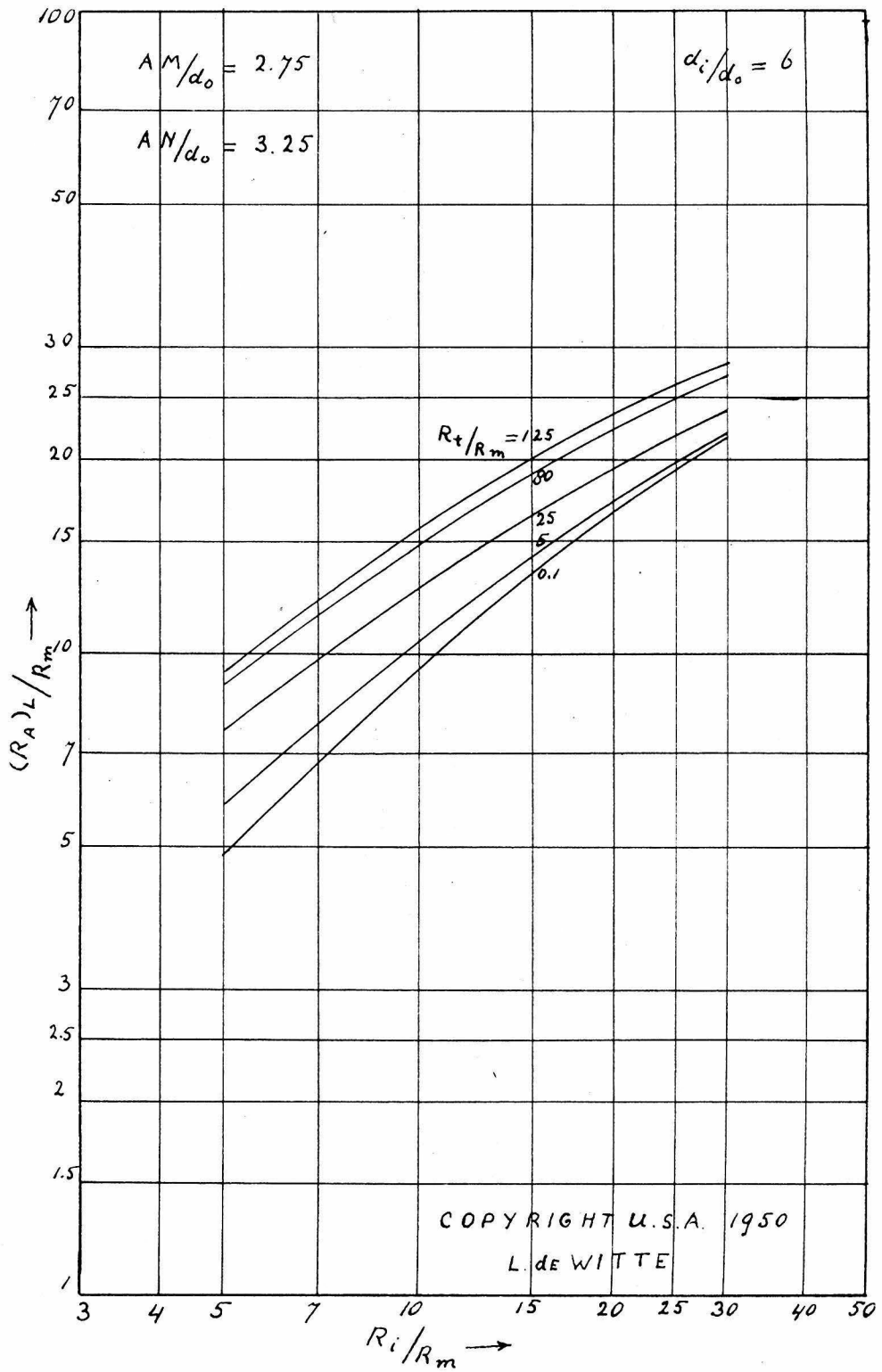


Fig. II - 5

most of the conditions arising in practice, there is one more complication that has to be taken into account, namely the variation in diameter of the drill hole, d_0 .

The average drill hole diameter depends upon the size of bit used for drilling. The bit sizes vary from well to well and are often changed several times during the drilling of each single hole.

Apart from the variations due to different bit sizes used, the actual drill hole diameter will also vary with the character of the formations traversed. Hard, well consolidated formations will mostly give a hole of relatively uniform diameter, slightly larger than the bit size. Poorly consolidated formations will often cave in, which results in enlarging of the hole diameter. Clays, shales and slates usually swell, upon coming into contact with the drilling mud, which is mostly less saline than the formation water. This results in decrease of the hole diameter. Fissile shales on the other hand will cave in very often and the swelling may even aid the fracturing as the expansion is restricted in vertical direction and the resulting curvature tends to split off slices of the material. Limestones, and beds of rocksalt, gypsum and anhydrite, loose material due to solution in the drilling mud, which tends to enlarge the hole diameter.

It is obvious therefore that the actual hole diameter is not a constant in any given hole, but is subject to many changes from one depth to the other. Mostly however any given formation which is more or less homogeneous, will show a constant deviation from the average hole diameter, within its boundaries.

To determine the deviations it has become a common practice to run

a "calliper log,"* either simultaneous with the electrolog or separately.

The calliper log gives the hole diameter as a function of the depth in the well.

Where no calliper log is available we will have to rely upon the average hole diameter, as estimated from the bit size. This however may introduce very serious errors.

To take into account the various sizes of drill holes, different sets of electrodes should be available to fit the most common hole sizes.

For instance one set of electrodes can be made such that $\overline{AM}/d_0 = 2.75$ and $\overline{AN}/d_0 = 3.25$ for a hole with a diameter (d_0) of 8". This will give $\overline{AM} = 22"$ and $\overline{AN} = 26"$.

Similarly another set can be made to fit a 12" hole, resulting in $\overline{AM} = 33"$ and $\overline{AN} = 39"$.

The intermediate sizes of drill holes or the extremely small and large ones and also the deviations from the average hole diameter within one well, can then be taken into account by making up "apparent resistivity charts" for the above electrode spacings and deviating values of d_0 .

Using for example the arrangement with $\overline{AM} = 22"$ and $\overline{AN} = 26"$, a seven inch hole will give ratios of \overline{AM}/d_0 and \overline{AN}/d_0 respectively of 3.14 and 3.61 and for these values a set of apparent resistivity charts may be prepared.

In the same way charts can be made up for other ratios of \overline{AM}/d_0

* The mechanism of the calliper logging device consists of a set of springs which are in contact with the boreface at all times and the expansion or contraction of which acts on a variable resistor or on the motion of an induction coil, which in turn affect changes in a current which are precalibrated in terms of the hole diameter and are registered as such by the logging apparatus.

and \overline{AN}/d_0 corresponding to one of the standard size arrangements and a complete range of values of d_0 . Approximately 10 sets of charts will be required to cover the range of values of d_0 usually encountered in practice. For extreme sizes of drill holes, special arrangements of electrodes should be prepared, to give as nearly as possible: $\overline{AN}/d_0 = 2.75$ and $\overline{AN}/d_0 = 3.25$.

After having determined the lateral spacing to be used, we will now discuss the requirements for the normal spacing from which we want to obtain an approximate value of R_t .

From the conventional resistivity departure curves we easily observe the fact that very large normal spacings, give apparent resistivities that are good approximations to the true resistivity.

However this holds true only for formations that are thick enough, so that the influence of the boundaries at the top and the bottom of the formations may be neglected.

It can be shown that in order to meet this condition, the thickness of the formation must be at least five times the normal spacing used. (8)

For instance in a drill hole of 8" diameter and using a spacing \overline{AN} , equal to 10 d_0 , the effect of the boundaries can only be neglected for beds that are $5 \times 10 \times 8" = 400"$ or approximately 33 ft. thick.

As many commercially important formations have thicknesses much smaller than 33' we want to use the smallest spacing that will still give an apparent resistivity, which is a fair approximation to the true resistivity.

The best compromise between the two factors described above appears to be obtained, by an electrode spacing (\overline{AN}) equal to 5 times the hole diameter.

In the case of an 8" hole, apparent resistivities can be obtained with such spacing, on beds 17 ft. thick or thicker without the necessity of correction for the effect of the formation boundaries. For thinner beds, correction factors may be applied for the boundary effects, as described by Guyod (8).

The lower limit of applicability of such correction factors, is a bed thickness of two times the spacing. In our case this would be a bed of 80" (= 6.7 ft.) thick.

Again standard arrangements may be made up by fitting the actual spacings to the most common hole sizes (8" and 12") and variations of the hole diameters are taken into account by a number of apparent resistivity charts made up for values of \overline{AM}/d_0 , smaller and larger than 5.

Fig. II-6 shows a set of apparent resistivity curves for $\overline{AM}/d_0 = 5$. R'_g denotes the apparent resistivity as measured with the long normal device.

On the proposed master curves for the lateral device the apparent resistivity is given as a function of the true invaded zone resistivity for various values of the true formation resistivities (see Fig. II-5), while for the long normal device the apparent resistivity is given as a function of R_t for various values of R_1 (see Fig. II-6). The reasons for this choice of parameters are that the apparent resistivity for the lateral device in many cases is nearly equal to R_1 and varies only little with R_t while for the long normal device, the apparent resistivities are closer to R_t and are influenced to a much lesser degree by R_1 . Actually all the variables are given as dimensionless quantities in the forms

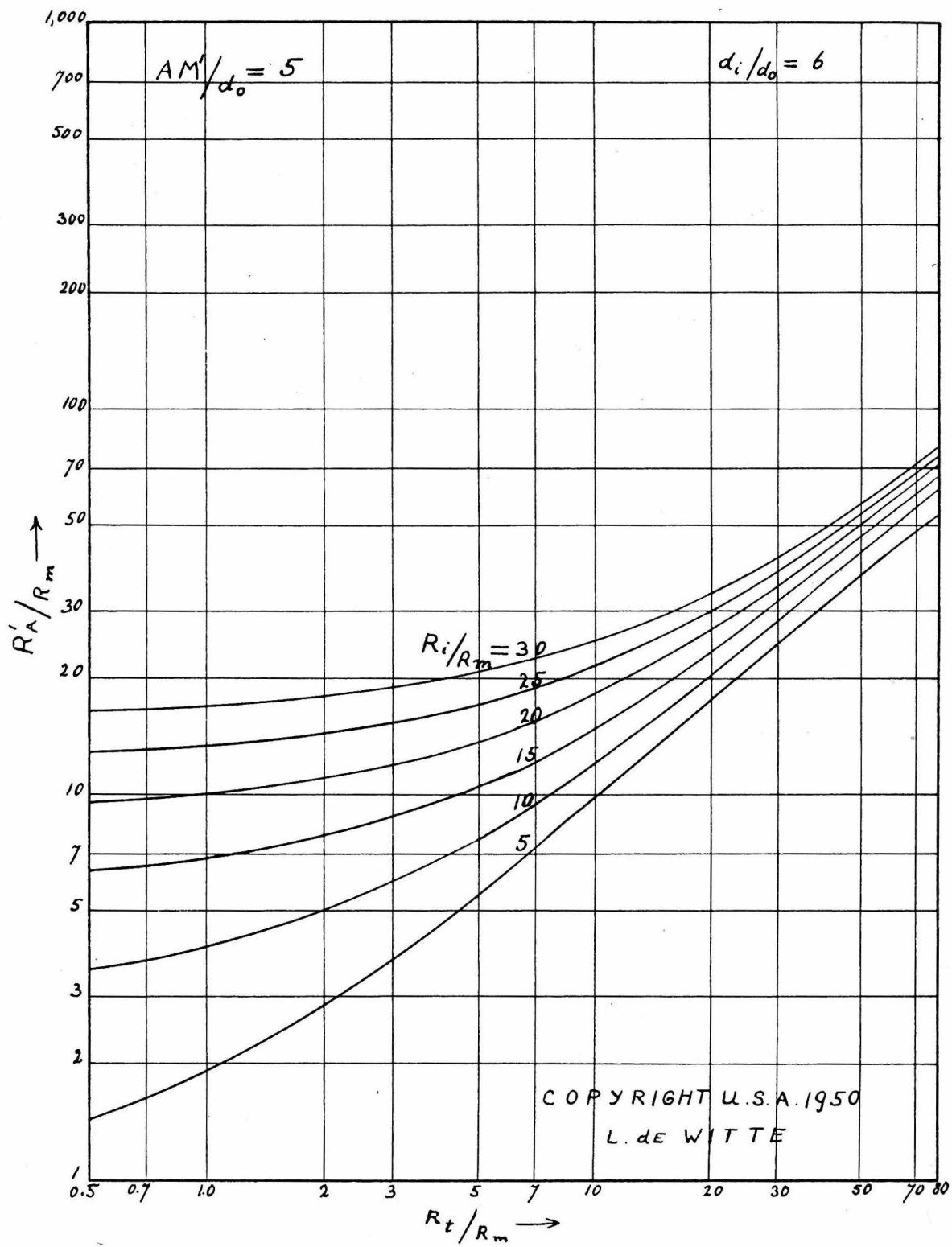


Fig II-6

R_a/R_m , R_l/R_m and R_t/R_m .

The interpretation method to be used with these curves consists basically of the following steps:

1. Take the apparent resistivity obtained with lateral spacing as a first approximation to R_l .

2. For this value of R_l find the R_t corresponding to the apparent resistivity obtained with the long normal device, from the apparent resistivity curves for the ratio of \overline{AM}'/d_o in question.

3. With the obtained value of R_t find a better approximation for R_l using the apparent resistivity curves for the lateral device.

4. This successive approximation is continued till no further substantial changes in the values of R_l and R_t are found.

5. The final values of R_l and R_t thus obtained will be the actual true invaded zone resistivity and true formation resistivity, if the actual invasion diameter equals the invasion diameter given on the set of resistivity charts we used for our determination.

This last condition brings in the necessity for a third curve, for which we have chosen a "short" normal curve.

The spacing for this curve is not critical. Any spacing of either normal or lateral device, that gives an apparent resistivity which is markedly influenced by both the invaded zone resistivity and the true formation resistivity, will suffice.

A good and convenient value is obtained by taking a normal curve of which the spacing \overline{AM} equals the \overline{AM} of the short lateral device already being used. This obviates the necessity for an additional electrode as the apparent resistivity for this normal curve is simply

measured between the first pickup electrode of the lateral device and the surface pickup electrode of the long normal device. We will use therefore $(\Delta H) \approx (\Delta H)_l = 2.75 d_0$ for the standard sondes.

In contrast with the long normal spacing described before we will term this spacing the "short normal spacing," although it is considerably larger than the conventional short normal spacing which is only 10" long and in cases even approaches the 38" conventional normal which is often called the "long normal spacing." For the short normal spacing a group of apparent resistivity charts is made up in the same way as for the long normal spacings (see Fig. II-7).

The function of this short normal curve is to check assumptions regarding the invasion diameter.

The interpretation procedure may be started assuming normal invasion ($d_1 = 6 d_0$). Using the apparent resistivity charts made up for $d_1 = 6 d_0$ we then find a value for R_1 and another for R_t .

With the aid of these values we can then determine the apparent resistivity that one should obtain for the short normal spacing, using the apparent resistivity charts for that spacing.

If this theoretical value checks with the actually measured value, the assumption regarding the infiltration diameter is right. However if the theoretical and actual values for the short normal apparent resistivity are not equal we must correct our assumption regarding d_1 as indicated in Table II-D. Table II-D only shows the direction in which the actual infiltration diameter varies from the assumed diameter, but not the magnitude of the corrections. The correction procedure is best illustrated by an example:

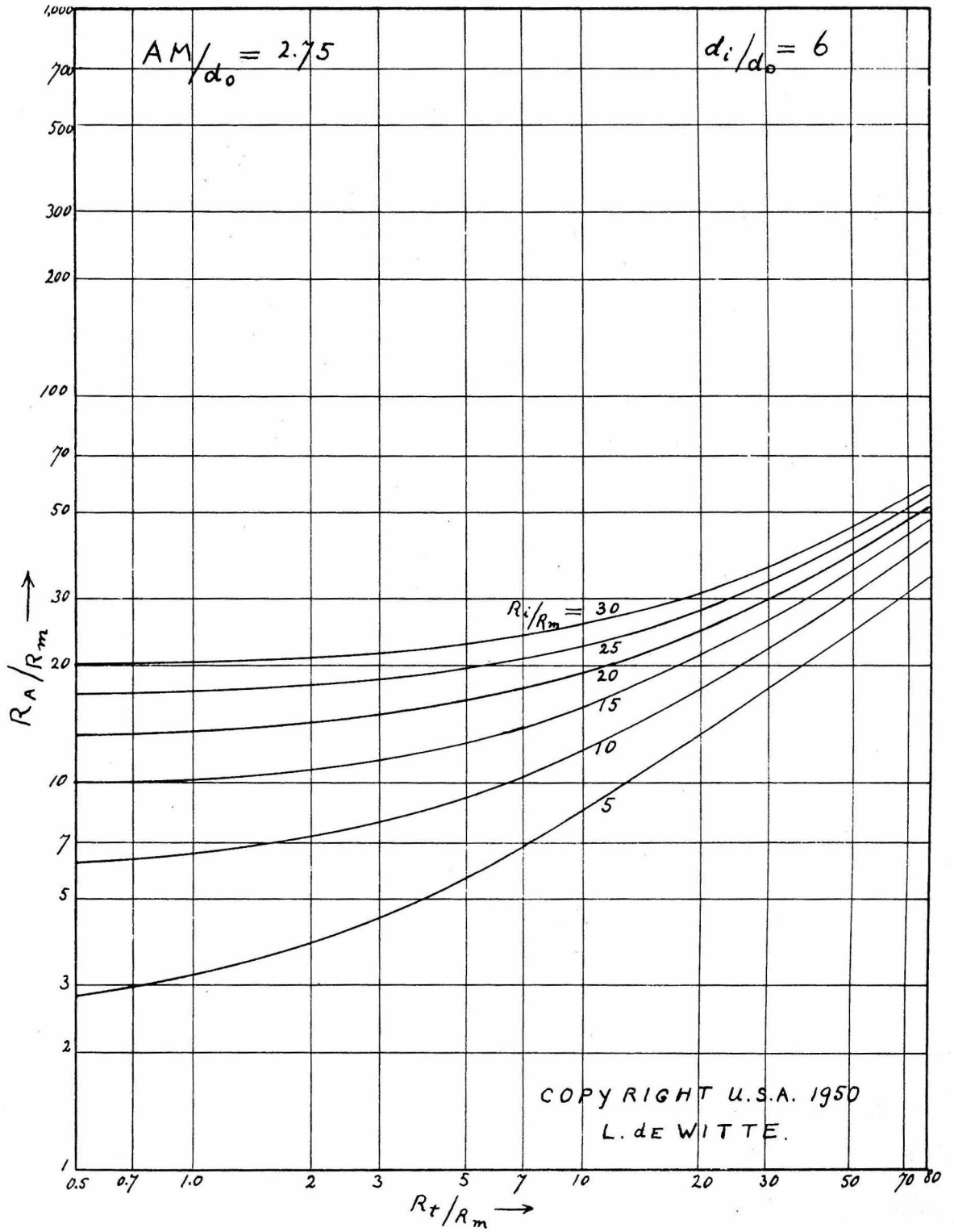


Fig. II-7

Let us first assume $d_1 = 6 d_0$, and suppose that the computed true resistivities, using this assumption, show $R_1 < R_t$.

For the values of R_1 and R_t as determined we then find the apparent resistivity which the short normal device should register, using the charts for $d_1 = 6 d_0$ made up for the short normal device.

This computed value of R_a is then compared with the apparent resistivity actually measured with the short normal device. Let us assume that we find the computed R_a to be larger than the measured R_a . Table II-D shows that for this case the actual $d_1 >$ assumed d_1 .

Our next assumption therefore will be $d_1 = 8 d_0$. For this assumption we now repeat the entire interpretation procedure. If this time we find that for the short normal device the computed R_a is smaller than the measured R_a , we know that now the actual $d_1 <$ assumed d_1 and therefore $6 d_0 < d_1 < 8 d_0$.

If we want great precision in the determination of d_1 we may interpolate d_1 between the values of $6 d_0$ and $8 d_0$ using the differences found in the computed and measured values of R_a as a basis for the interpolation.

The value of d_1 thus determined indicates the set of charts to be used for the computation of the final values of R_1 and R_t .

Usually we will be able to make a rough first estimate of the amount of filtration from the apparent resistivities of the short normal and the long normal device, especially if R_1 and R_t are sufficiently different, as can be judged from the apparent resistivities for the short lateral and the long normal.

Much infiltration will result in larger differences between the short normal and the long normal than little or no infiltration.

If there is no infiltration, the above interpretation procedure will result in $R_1 = R_t$ for any assumed invasion diameter.

As will be seen later it is possible that $R_1 = R_t$ in cases where invasion is present, as for instance when a water sand is invaded by a mud filtrate of the same resistivity as the connate water, or when in an oil horizon the opposite effects of the oil replaced by water and the saline connate water replaced by the less saline mud filtrate are equal.

In such cases a study of the S.P. curve and (or) the invasion of neighboring formations will often give clues as to whether invasion is present or not.

TABLE II-D

$R_1 > R_t$	$R_1 < R_t$
computed $R_a >$ measured R_a actual $d_1 <$ assumed d_1	computed $R_a >$ measured R_a actual $d_1 >$ assumed d_1
computed $R_a <$ measured R_a actual $d_1 >$ assumed d_1	computed $R_a <$ measured R_a actual $d_1 <$ assumed d_1

The above described method gives us as final answer the quantities R_t , R_1 and d_1 .

R_t is used directly in the quantitative determination of the fluid content of formations.

In later parts of this thesis it will be outlined how we may use R_1 to help solve other unknown factors in fluid content determinations.

PART III

Experimental Equipment

The technique employed in the laboratory investigations on the character of the infiltrated zones around drill holes, in porous reservoir rocks, makes use of two distinct sets of apparatus. The first set is used to saturate, infiltrate or flush sandstone samples, while the second set consists of an arrangement which enables us to measure the resistivity of the cores. The investigations were carried out using sandstone samples from outcrops of formations which are known to be oil-bearing in other parts. These samples were saturated with mixtures of crude oil, gas and water of varying salinity. After saturation, they were infiltrated by fresh water and the changes in resistivity, and relative saturation of the above components were registered.

Also a standard type of drilling mud was filtrated through typical samples and the resistivities of the sample containing the mud filtrate and of the effluent filtrate were measured.

Infiltration Equipment

The equipment used to saturate, infiltrate or flush the sandstone samples employed apparatus as indicated below:

The samples were mounted in the bottom part of a cylinder of a standard 100 pound baroid wall-building tester (9).

The necessary pressure was supplied by a large size nitrogen bottle, equipped with a regulation pressure reducing valve and a 300 pound outlet valve in line with the latter.

To insure accurate measurements of the pressure applied a 160 pound pressure gauge, with 3" dial, was installed near the inlet of the baroid tester.

The filtrate was collected in a 100 cc graduated cylinder, for the flushing experiments on water sands, while for experiments of longer duration a 250 cc bottle with rubber stopper, filter funnel and capillary air vent were used, to minimize evaporation.

The samples were shaped to fit the inside of the baroid tester by cutting them to the approximate proportions with a diamond saw and grinding them to a good cylindrical shape with a rough carborundum grinder and (or) a rotary wire brush. The final size of the cores was approximately 2.8" diameter x 2" height. The inside diameter of the wall building tester is 3", so that sufficient clearance existed for mounting and insulating.

Before mounting the cores they were first coated with castolite, a normally thermo-setting casting plastic, to which a cold-setting promoter had been added. The plastic was allowed to harden at room temperature.

In this way a very firm band with the core was obtained, while the rapidly setting action of the cold-setting promoter limited infiltration to a single granular layer.

After hardening of this first coating the bottom edge of the core was sealed to the inside of the baroid cylinder, with a coldwater putty, in such a way that the lower surface of the core was flush with the lower rim of the cylinder. The cylinder was then placed upright and the annular space between the core and the inner wall of the cylinder was filled with castolite, which was cured for approximately 45 minutes at

175°F.

The drilling muds used were samples of aquagel, seogel and natural clays, obtained from the Baroid Sales Division of Los Angeles. The proportions were weighed with an ordinary balance (accuracy .05 gram) and mud weight was measured with a baroid mud balance. The muds were mixed with a high speed Hamilton Beach soil dispersion mixer.

To obtain oil or gas saturations in the cores, comparable to those occurring in thick reservoir horizons, the samples were first 100% saturated with water and then oil or gas was forced in, by the capillary pressure method. For this purpose special adapters were machined to hold a porous porcelain diaphragm and to fit the baroid cylinders; details of this equipment and the procedure used, are described in a second thesis by the author (10).

General Circuit for Resistivity Measurements

The resistivity measurements were carried out with a separate set of apparatus.

Fig. III-1 gives the general lay-out of the measuring circuit used. The circuit consists of a four-electrode arrangement, comprising two current electrodes and two potential "pick-up" electrodes and apparatus to measure the current, through the current electrodes, and the corresponding potential difference between the pick-up electrodes, with a minimum of distortion in the potential distribution in the sample.

The current was supplied by a Hewlett-Packard 1 Watt audio oscillator. For reasons, to be outlined later, a frequency of 1000 cycles/sec. was used. In series with the current electrodes a group of standard resistors respectively of 10 Ω , 100 Ω , 1,000 Ω and 10,000 Ω ,

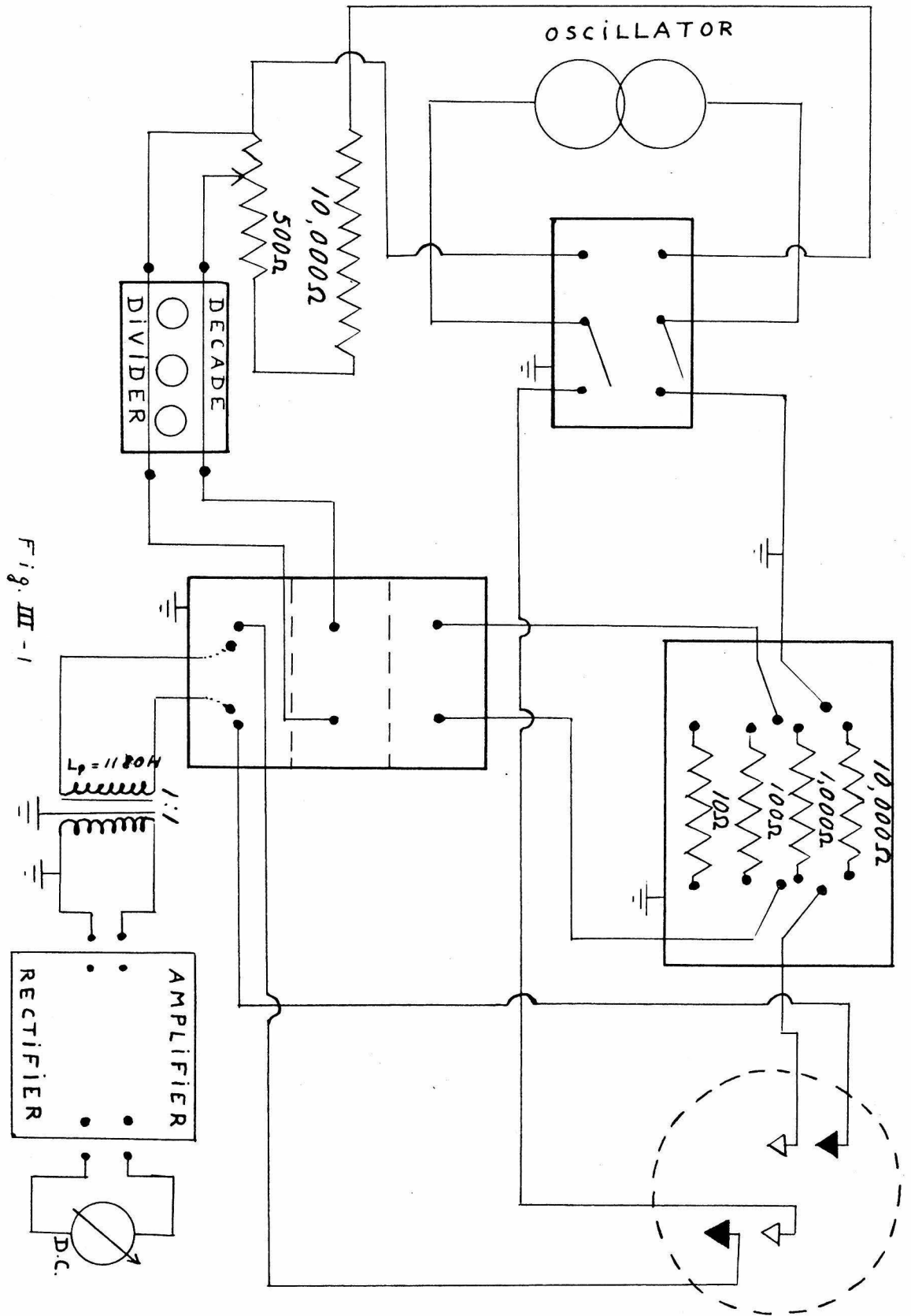


Fig. III - 1

one of which could be plugged into the circuit at a time. The resistors were all standard A.C., non-inductively wire wound, resistors with an accuracy of 0.25%. The group of resistors were mounted in a grounded chassis and the plugs were shielded chassis plugs. A third plug carrying two separate leads made connections with both ends of the resistors in their respective positions, enabling measurement of the voltage drop across the resistors.

To eliminate spurious affects in the circuit caused by capacitive and inductive coupling, between elements of the circuit and also to avoid pick-up of 60 cycle "noise" all leads had to be carefully shielded, and all shielding connected to a common ground. This however introduced new difficulties as capacitive coupling between wire and its own shielding would cause deviation in part of the current and inaccuracies in the measurements, as well as distortion of the potential distribution between the electrodes. For this reason amphenol polyethylene cables were used for all leads. The cables were of the armoured, single conductor type (RG-62/u). These cables have a capacitive coupling between wire and braid of $13.5 \mu\text{F}$ per foot. This was found to be still too high for our requirements and therefore the original wire of the cable was pulled out and replaced by No. 40 wire. This cut the capacitive coupling down to approximately $3 \mu\text{F}$ per foot, which was small enough for our purpose.

In order to measure the small voltages across the potential electrodes and the standard resistor in the current circuit, accurately, an amplifier-rectifier combination was used. The input leads to the amplifier could be plugged into one of three positions on a central switch box, thus connecting with the potential electrodes, the resistor in the current

circuit, or the output terminals of a decade divider used for calibration.

The voltages to be measured were of the order of 0.01 Volt A.C. They were amplified approximately 800 times and then rectified by a peak voltage rectification arrangement. The amplifier will be discussed in more detail. The final D.C. current was measured with a sensitive research test meter on the 100 A scale.

As, for resistivity measurements, we are only interested in the ratio of the voltage across the potential electrodes (ΔV) and the corresponding current (I). The actual amplification did not have to be determined and only linearity of the test meter reading had to be checked or calibrated.

To calibrate, the output, of the oscillator, was put across a potentiometer consisting of two wire wound resistors of respectively 10,000 ohms and 500 ohms. From the latter one fixed and one variable contact, taking about 1/100 of the total voltage across the potentiometer, were connected with the input terminals of a decade voltage divider. The input impedance of the decade divider was 10,000 ohms while the output impedance varied up to 10,000 ohms. Three dials in series enabled us, to divide the input into one thousandth, one hundredth, and tenth parts. The output was connected with the central switch box as indicated before.

To calibrate, the oscillator output would be varied so as to give a 100 μ A reading, with the decade divider shorted out. Then using the different dials the voltage was divided into equal parts of the original and the corresponding test meter readings were noted. Then a table was made up of test meter readings and corresponding proportional parts. The stability of the amplifier with time was very good so that new calibrations were only made every two weeks. All experimental readings

were corrected using the above calibration tables.

The Amplifier Rectifier System

Fig. III-2 schematically represents the amplifier and rectification circuit. The amplification circuit consists of three stages. The first stage is a medium μ twin triode (6J6), with a cathode follower arrangement, to provide a high input impedance.

To compute the real input impedance of the cathode follower arrangement we will use notations as indicated in Fig. III-3.

The input impedance is defined as: $R_1 = \frac{U}{I}$

$$U = U_1 + U_2 \quad \text{and} \quad I = \frac{U_1}{R_1}$$

$$\text{so that} \quad R_1 = \frac{U}{U_1} \cdot R_1 \quad (3-1)$$

If we neglect the influence of R_3 we can write for the plate current:

$$i_p = \frac{\mu U_1}{R_2 + R_p}$$

$$\text{while} \quad U_2 = i_p R_2 = \frac{\mu R_2}{R_2 + R_p} \cdot U_1 \quad (3-2)$$

From (3-1) and (3-2):

$$R_1 = \left[1 + \frac{\mu R_2}{R_2 + R_p} \right] R_1$$

In our case, with $R_p = \frac{7100}{2} = 3550$, $\mu = 38$ and $R = .5 \text{ Meg}$
we find $R_1 = 7.75 R_1 = 5.3 \text{ Meg}$.

The approximate gain of the first stage is calculated as follows:

$$K_1 = \frac{U_2}{U} = \frac{U_2}{U_1 + U_2} = 0.885$$

The second stage consists of a high μ twin triode (7 F 7). The two stages have a capacitance-resistance coupling.

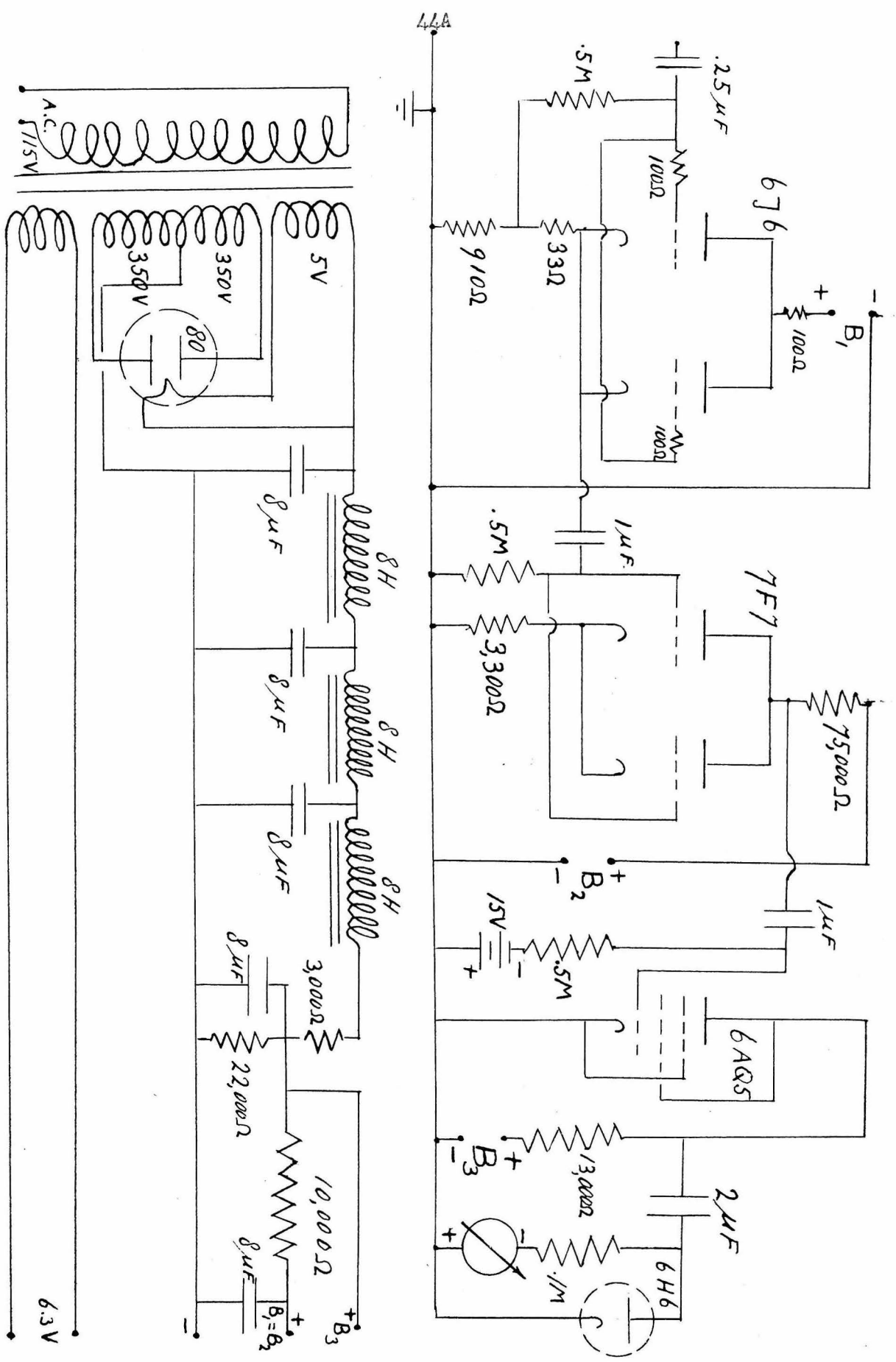


Fig. III - 2

For the two parts of the 7 F 7 coupled in parallel the plate resistance is 22,000 ohms while $\mu = 70$. With a load resistor of 75,000 ohms this would give a gain of $\frac{70 \times 75,000}{75,000 + 22,000} = 54$.

However, the cathode resistor of 3300 Ω gives negative feed back, the portion fed back being 0.042. The overall gain therefore is:

$$K_2 = \frac{54}{1 + 54 \times .042} = 16.5$$

The final stage of amplification consists of a 6 AQ 5, beam power amplifier. The suppressor grid is connected to the cathode while the screen grid is connected to the plate. The plate voltage E_3 is approximately 275 V. The load resistor is 13,000 ohms. Under these operating conditions the tube characteristics are approximately:

Plate resistance (r_p) 58,000 ohms

Transconductance g_m 4,000 mhos.

$$\mu = g_m \times r_p = 232$$

The quiescent grid voltage is maintained at - 15 V by a bias battery. The gain for the third stage is computed as:

$$K_3 = \frac{232 \times 13,000}{58,000 + 13,000} = 42.5$$

The output of the power amplifier is connected to a peak voltage rectification circuit as shown in Fig. III-2. This circuit contains a 6 H 6, twin diode, low voltage rectifier in parallel with a 0.1 Meg. resistor and a sensitive multimeter. The combination is in series with a 2 μ F capacitor.

The diode will only conduct current when the plate is positive with respect to the cathode. The electrons going from the cathode to

the plate will charge up the capacitor, with the positive and negative sides as indicated in Fig. III-4a. The capacitor then gives a continued slow discharge through the .1 Meg. resistor and the meter.

The charge on the capacitor will keep the anode from becoming positive during most of the A.C. cycle. Only when the positive voltage peak of the A.C. voltage becomes larger than the slowly decreasing negative charge of the capacitor plate, the tube will conduct, recharging the capacitor to the peak voltage level.

The variation of the direct voltage across the meter and the bleeding resistor, will therefore be as indicated on an exaggerated scale in Fig. III-4b. With the capacitor and bleeding resistor sufficiently large, these variations become completely negligible. Fig. III-4a also indicates the direction and path of the D.C. current which of course is opposite to the direction in which the electrons travel.

As indicated by Fig. III-1, the input to the amplifier goes via an input transformer. The transformer has a 1:1 ratio and serves merely to isolate the floating ground of the electrode system from the grounded common level of the amplifier. The amplifier was grounded in order to prevent spurious oscillations generated by the tubes on small fluctuations of the bias voltages, random "noise" picked up by the leads, or induction from the filament connections.

As the impedance between the potential electrodes is in some cases of the order of $50,000 \Omega$ the input impedance of the transformer must be at least several Megohms to keep the error introduced by current drawn by the measuring system, below a few per cent. As the total input impedance of the transformer may be represented by the equivalent

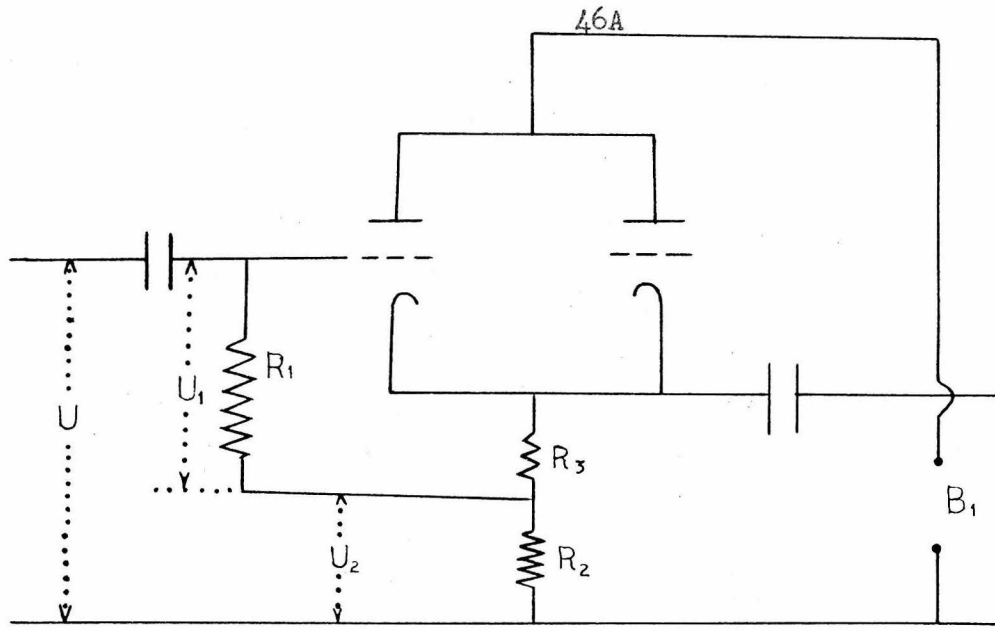


Fig III - 3

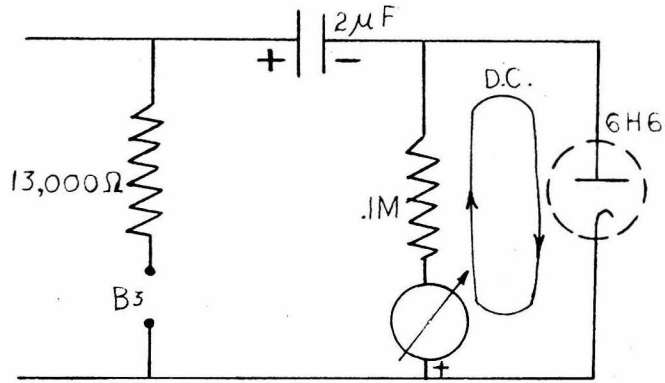


Fig. III - 4a

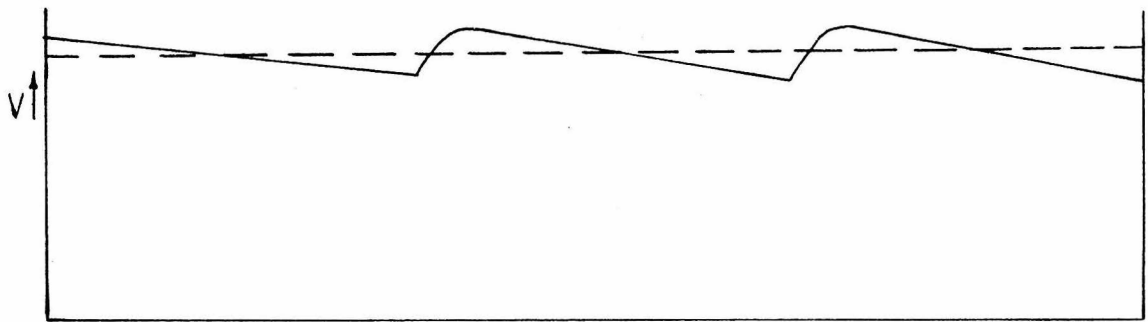


Fig III - 4b.

impedance of the primary with open secondary, in parallel with the load impedance of the secondary, the impedance of the primary must also be several Megohms.

To meet these requirements and also to have sufficient shielding, a special transformer was built by the Pasadena Transformer Engineers Inc. with a primary inductance of 1180 H. For the specifications of this input transformer and the computation of the inductance of the primary see appendix paragraph B. In order to have a sufficiently high primary impedance the frequency used for the measurements was chosen at 1000 cycles. A higher frequency would make capacitive and inductive coupling of some parts of the circuit to ground large enough to cause noticeable inaccuracies. A lower frequency would make the input impedance of the amplifier too small.

At 1000 cycles the primary impedance equals:

$$Z_p = 2 \pi f L_p = 7.45 \text{ Megohms}$$

The secondary load impedance was 5.3 Megohms. Therefore the total input impedance for the transformer with its secondary connected to the first stage of the amplifier is:

$$Z_t = \frac{1}{j/Z_p + 1/Z} = 4.5 \text{ Megohms}$$

For an impedance of 50,000 ohms between the potential electrodes the current drawn by the amplifier will be 1% of the total. This is within the permissible limits of accuracy.

The power supply to the amplifier is taken from a power pack of standard design as shown in Fig. III-2.

The transformer has a center tapped main secondary coil giving

350 V on each side. In addition two small coils give 5 V for the filament of the rectifier tube and 6.3 V for the filaments of the amplifier tubes.

The rectifier tube is a No. 80 full-wave rectifier. To insure that the A.C. component in the output will be absolutely negligible, a filter arrangement with three 8H chokes and three 8μ F capacitors is installed. Each of the three choke-capacitor combinations cuts the A.C. component to about 3% of the value put in.

Finally in order to minimize feedback through the power pack, which might lead to disturbing generations of oscillations in the amplifier, a low impedance path is provided for A.C. across the output terminals, by two 8μ F capacitors.

The voltage B_3 when providing the plate voltage for the 6AQ5 tube, that is, with a 71,000 ohms load across the output, is approximately 300 V, giving an operating plate voltage of 250 V for the beam power amplifier. Similarly B_1 under load conditions is approximately 150 Volts, giving operating plate voltages of 120 V for the 6J6 and 90 Volts for the 7F7.

The supply leads to the amplifier are shielded with 1/2" copper braid.

In order to make the operating conditions as stable as possible the A.C. supply for the power pack and the audio oscillator is obtained via a line voltage stabilizer set at 115 Volts, output voltage, by means of a Variac potentiometer.

While assembling the equipment the behavior of all parts of the circuit was carefully checked with an oscilloscope, to insure that no spurious oscillations were present and that unwanted capacitive and

inductive coupling between circuit elements were negligible at all times.

The Electrode Arrangement

As stated before, the resistivity measurements had to be made on the bottom face of cylindrical cores having a diameter of approximately 2.8".

In choosing an electrode arrangement suitable for such measurements the following factors have to be considered:

1. The formulae used for surface measurements of resistivities are all derived for semi-infinite media.

The cores of which the resistivity has to be measured are limited both in depth (or height) and in diameter. The influence of the walls on the potential distribution for a given current are directly dependent upon the spacing and arrangement of the electrodes.

2. In the resistivity formulae it is also assumed that the electrodes are "point electrodes." The error made due to the physical dimensions of the electrodes depends upon the ratio of the distance between current electrodes and potential electrodes and the diameter and amount of penetration of the electrodes.

3. In order to make good contact with the samples the electrodes must be pushed firmly onto the face of the core so that they will penetrate a small amount between the sand grains.

Electrodes of too small a diameter will be flexible and will be bent sideways by the sand grains. This would continuously change the distance between the points of contact and using predetermined formulae for a supposedly fixed electrode arrangement would give appreciable errors.

The smallest diameter that could be used for firm electrodes that

would not be bent by grains of well cemented sandstone was found to be 0.03". Penetration of the electrodes below the surface might be up to 0.05" to make a good contact. For hemispherical electrodes, the error made by assuming the electrodes to be point electrodes will be 1% or less, if the distance at which the measurements are made is larger or equal to 20 times the radius of the electrodes. This gives a lower limit of 0.3" for the distance, the potential electrodes may be separated from the current electrodes.

To estimate the influence of penetration of the electrodes into the medium of which the resistivity is to be measured, on the accuracy of the computation using formulae for point electrodes, the following derivation was made:

Suppose we have a cylindrical electrode of negligible diameter and length B (see Fig. III-5). For an element of length db of the electrode, we may apply the usual formula for point electrodes if db approaches zero. Taking into account the image above the surface we have for a buried point electrode $\varphi = \frac{2I\rho}{4\pi r} = \frac{I\rho}{2\pi r}$ where φ is the potential at a distance r and ρ is the resistivity of the semi-infinite medium.

The potential due to db at a point p, at the surface at a horizontal distance x from the axis of the electrode, will be:

$$d\varphi_p = \frac{I}{2\pi r} \cdot \frac{db}{B}$$

so that

$$\varphi_p = \int_0^B \frac{I\rho}{2\pi B} \frac{db}{r} = \frac{I\rho}{2\pi B} \int_0^B \frac{db}{(B^2 + x^2)^{1/2}}$$

$$= \frac{I\rho}{2\pi B} \left[\ln \left\{ b + (b^2 + x^2)^{1/2} \right\} \right]_0^B$$

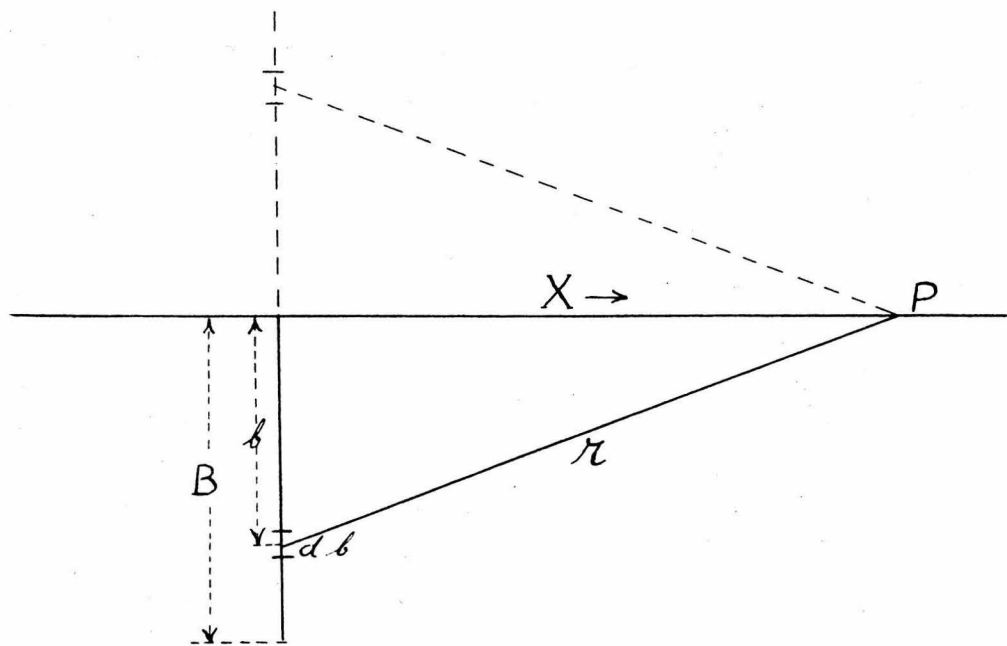


Fig. III - 5

$$\begin{aligned}\varphi_p &= \frac{I_c}{2\pi B} \left[\ln \left\{ \frac{B}{X} + \left(\left(\frac{B}{X} \right)^2 + 1 \right)^{1/2} \right\} \right] \\ &= \frac{I_c}{2\pi X} \cdot \frac{X}{B} \cdot \ln \left\{ \frac{B}{X} + \left(\left(\frac{B}{X} \right)^2 + 1 \right)^{1/2} \right\}\end{aligned}$$

The potential at p due to a point electrode at the surface, emitting the same current would be: $V_p = \frac{I_c}{2\pi X}$

The error as a percentage of V_p therefore is:

$$\Delta V_p = 100 \left[1 - \frac{X}{B} \ln \left\{ \frac{B}{X} + \left(\left(\frac{B}{X} \right)^2 + 1 \right)^{1/2} \right\} \right]$$

Fig. III-6 represents ΔV_p as a function of B/X . The actual potential is always smaller than the potential due to a point electrode carrying the same current.

We see that for a penetration of 0.05" and $X = 0.3$ ", the error is less than 0.3%, so that if we use the lower limit of spacing imposed by the electrode diameter we can neglect the influence of penetration.

The minimum distance between the electrodes being fixed by the above considerations, we must find an arrangement for which the influence of the walls of the cylindrical cores will be as small as possible. It must be pointed out however that the influence of the walls gives a deviation from the formulae used, for which we can make corrections. On the other hand the error due to the deviation from the assumed point electrodes is very difficult to estimate quantitatively, due to the irregularity of the contact. Therefore in compromising between distance from the walls and mutual distance between the electrodes, we will allow a sufficient safety margin above the lower limit, established for the latter theoretically.

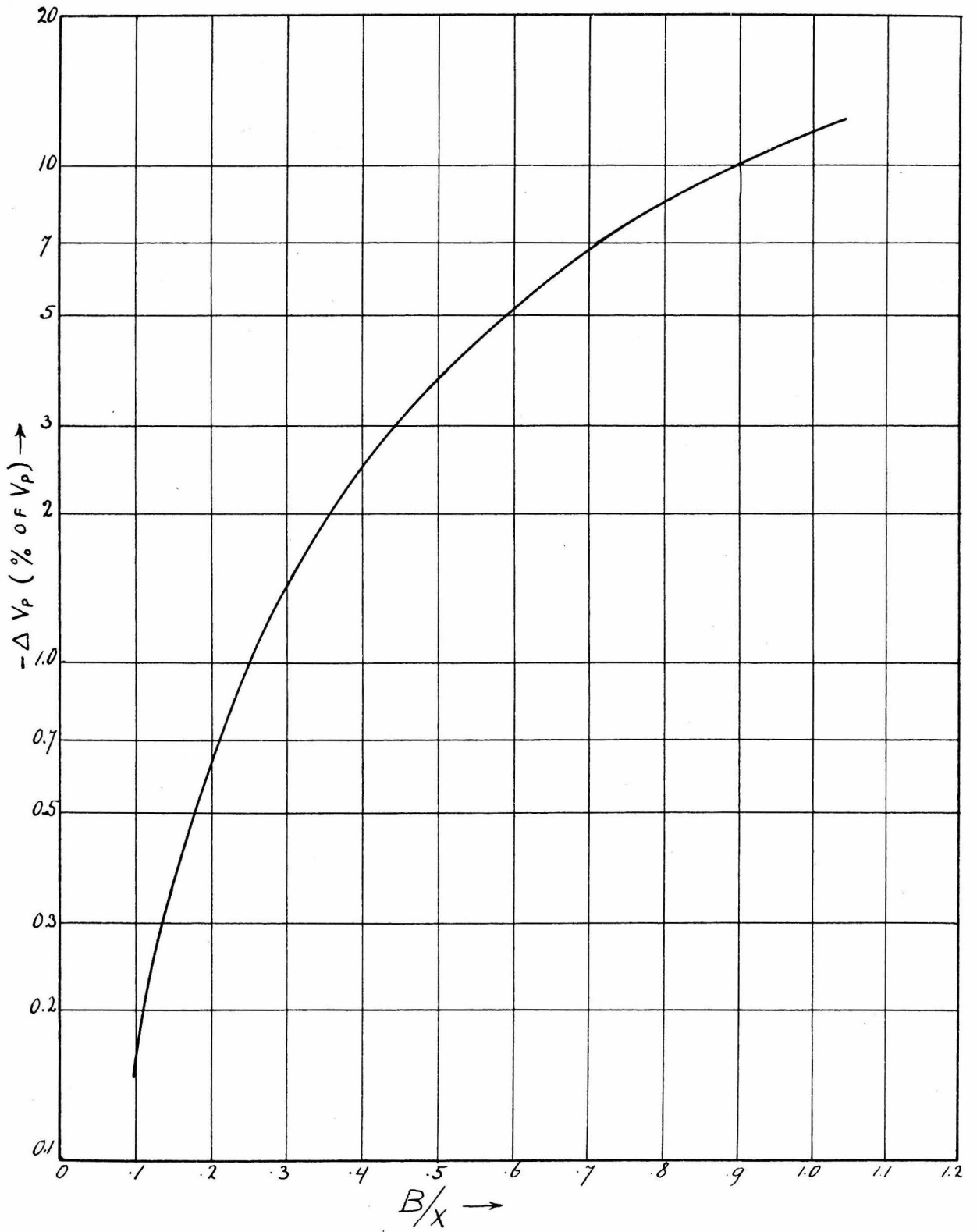


Fig III - 6

Considering possible arrangements that would fit within the circular area of the core-face, it is obvious that the Wenner arrangement, having equally spaced electrodes on a straight line does not make efficient use of the area available.

It seems logical therefore to choose an arrangement in which the current electrodes lie on a diameter of the circular area and the potential electrodes are placed symmetrically above and below that diameter.

In determining the optimum position of the potential electrodes, there is another important factor to be considered, namely the potential gradient in different parts of the field. In general, near the current electrodes the gradient is very steep and small fluctuations of the current or inaccuracies made in the determination of the distances between the electrodes will give relatively large errors in the measured voltages, when the potential electrodes are too close to the current electrodes.

Fig. III-7a gives the potential distribution, on the line connecting the two current electrodes. We see that to minimize the above difficulties the potential electrodes must be located in the central part between 30% and 70% of the distance AB, away from A, where the gradient is less steep.

When the potential electrodes are not located on the line AB we still can determine the zone where the potential gradient is small and about constant by projection of the limiting points P and Q along the equipotential lines through these points. Fig. III-7b shows the equipotential pattern due to two current electrodes and the area in

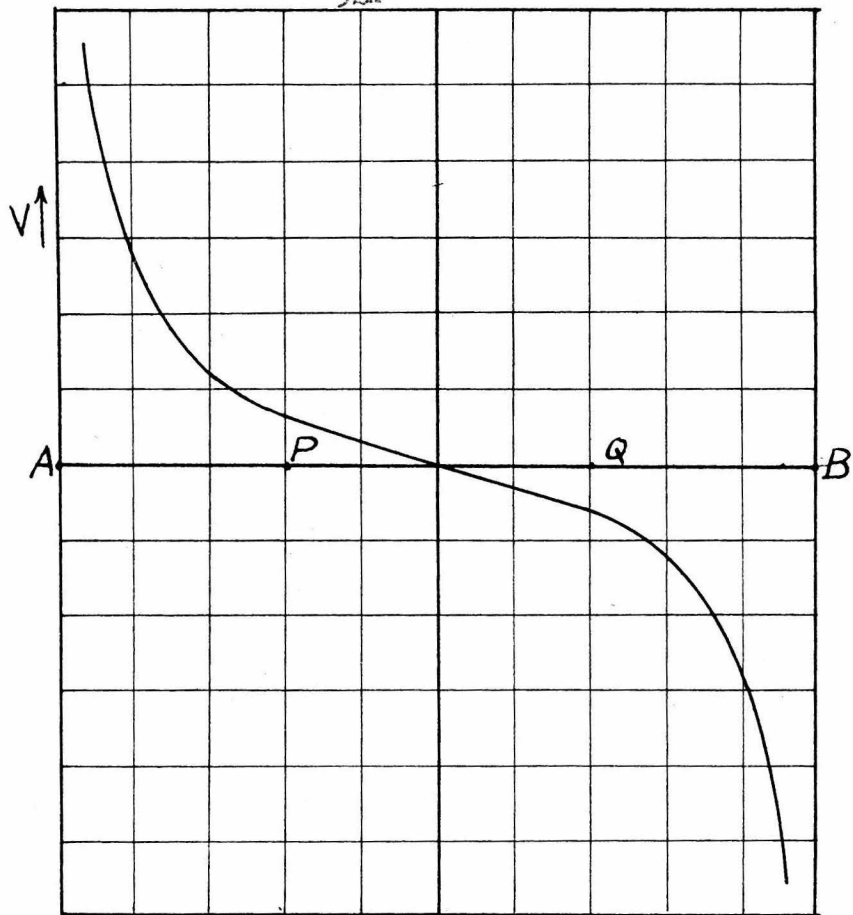


Fig. III-7a

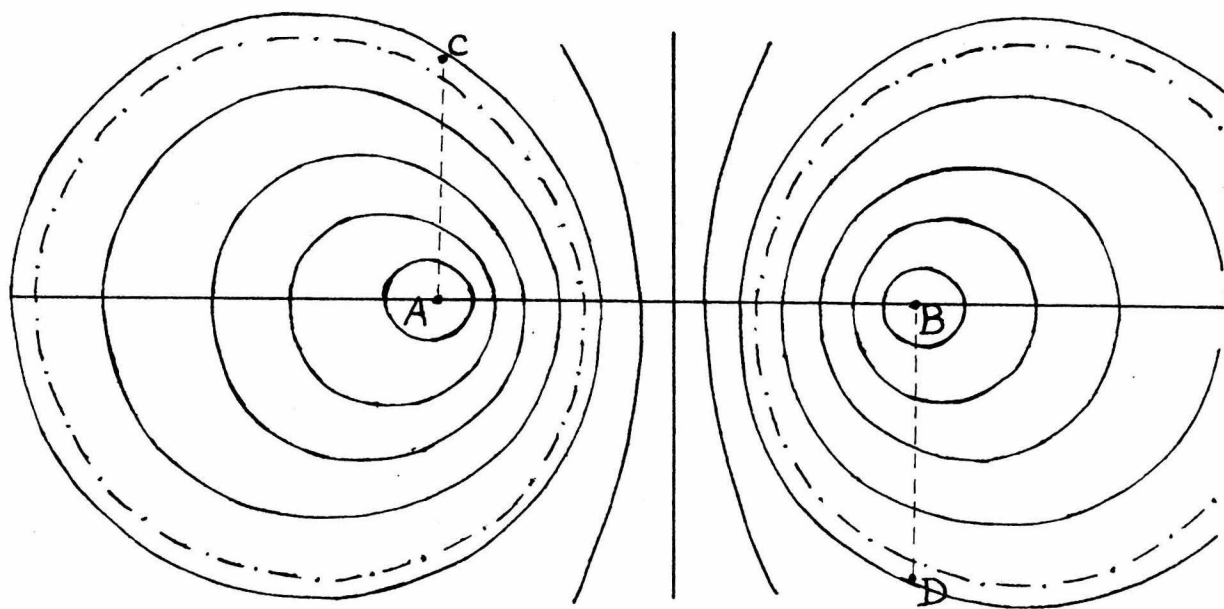


Fig. III-7b

which the potential electrodes preferably should be located (outside the dashed and dotted lines).

The requirements for the location of the potential electrodes can now be summed up as follows:

- 1) More than .3" from the current electrodes, preferably $AC = CD > .4"$.
- 2) Outside the zones of large potential gradient, e.g. outside dashed lines, in Fig. III-7b.
- 3) Far enough from the circular boundary of the cores to be only moderately affected by the distortion of the lines of current due to these boundaries.
- 4) Meeting the above three requirements the location should be chosen so as to give the largest possible potential drop for a given current so that inherent errors are, percentage wise, as small as possible.

As can readily be seen part of these requirements tend to move the locations C and D in opposite directions to those required by the other part. Therefore a compromising position must be found.

A good compromise is obtained by placing C and D on lines perpendicular to the diameter through A and B, just outside the dashed lines. This fulfills (1), the distance AC being approximately .45". It obviously satisfies (2), and there are a maximum number of equipotential lines between them, thus satisfying (4). The effect of the boundaries was determined experimentally and found of the order of 10% of the measured voltage. This means that if we can determine the correction factor for the boundary effect with an accuracy of 10% or less, we keep

the total error due to the boundaries below 1%.

The preferred positions of C and D are indicated in Fig. III-7b.

Based on the above principles two arrangements were tried out; one with $AB = .905''$ (hereafter referred to as arrangement No. I) and one with $AB = .624''$ (hereafter referred to as arrangement No. II).

Though No. II had slightly less influence of the walls, its sensitivity to the amount of contact area between the sample and the electrodes was considerably greater, making the accuracy with which measurements could be repeated smaller.

Therefore No. I arrangement was adopted for constant use, while No. II was kept for occasional double checks. For both arrangements empirical curves were made giving the effect of the boundary on measured resistivity as a function of the diameter and height of the sample.

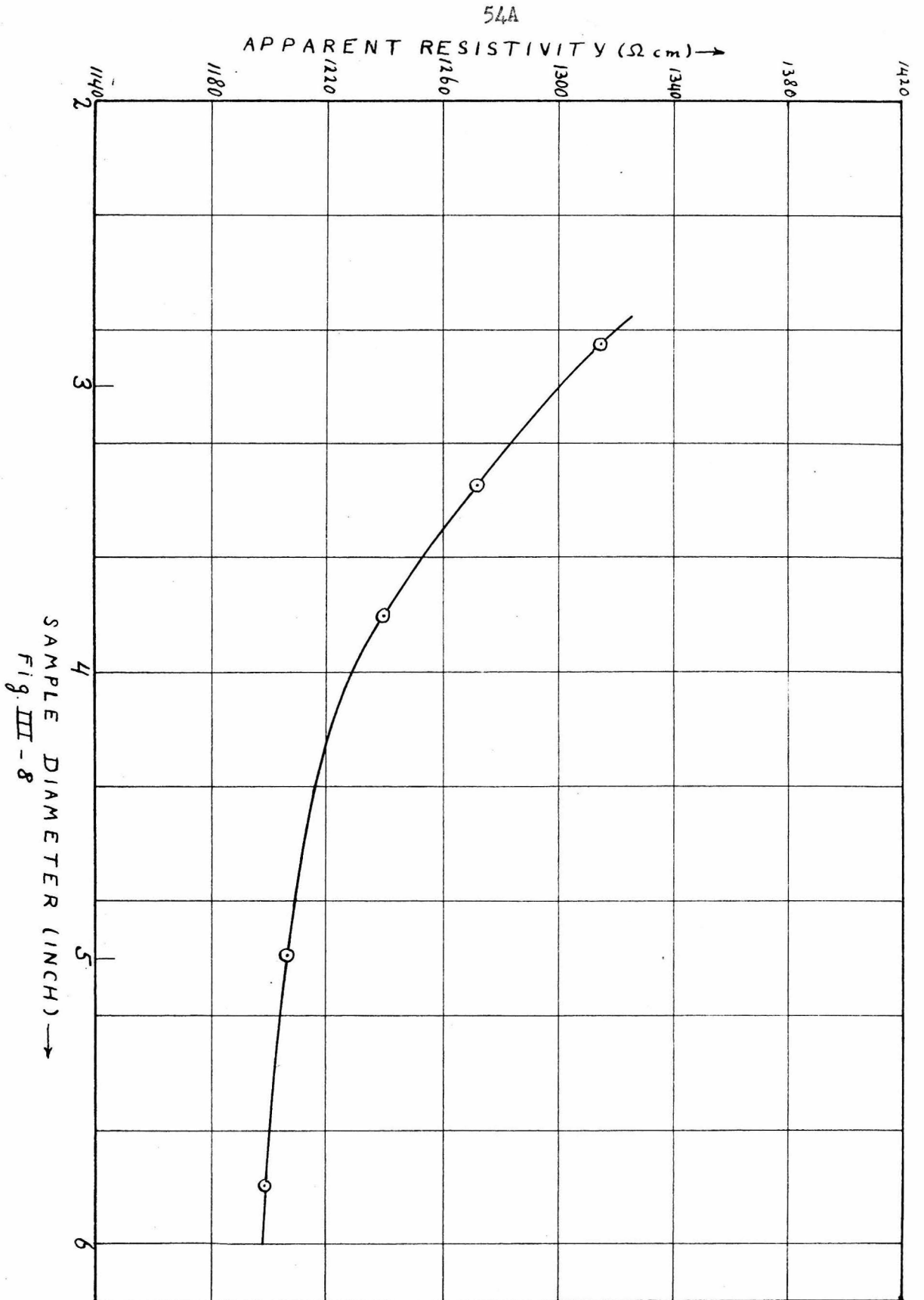
The correction to be applied for the affect of the core boundaries was determined experimentally. The empirical data were separated in two groups, one representing the affect of the cylindrical boundary of the core, the other giving the affect of the bottom.

The experiments were carried out in the following manner:

A series of cylindrical glasses varying in diameter from 5.8" to 2.85" were cut down to a height of approximately 2" and then filled with water of a given resistivity to the exact height of 1.9".

Then the electrodes were put, in a symmetrical, central position above the water level and lowered to make contact with the water, care being taken that the penetration was always close to 0.5". Then the apparent resistivities were measured and plotted against the diameter

54A



54B

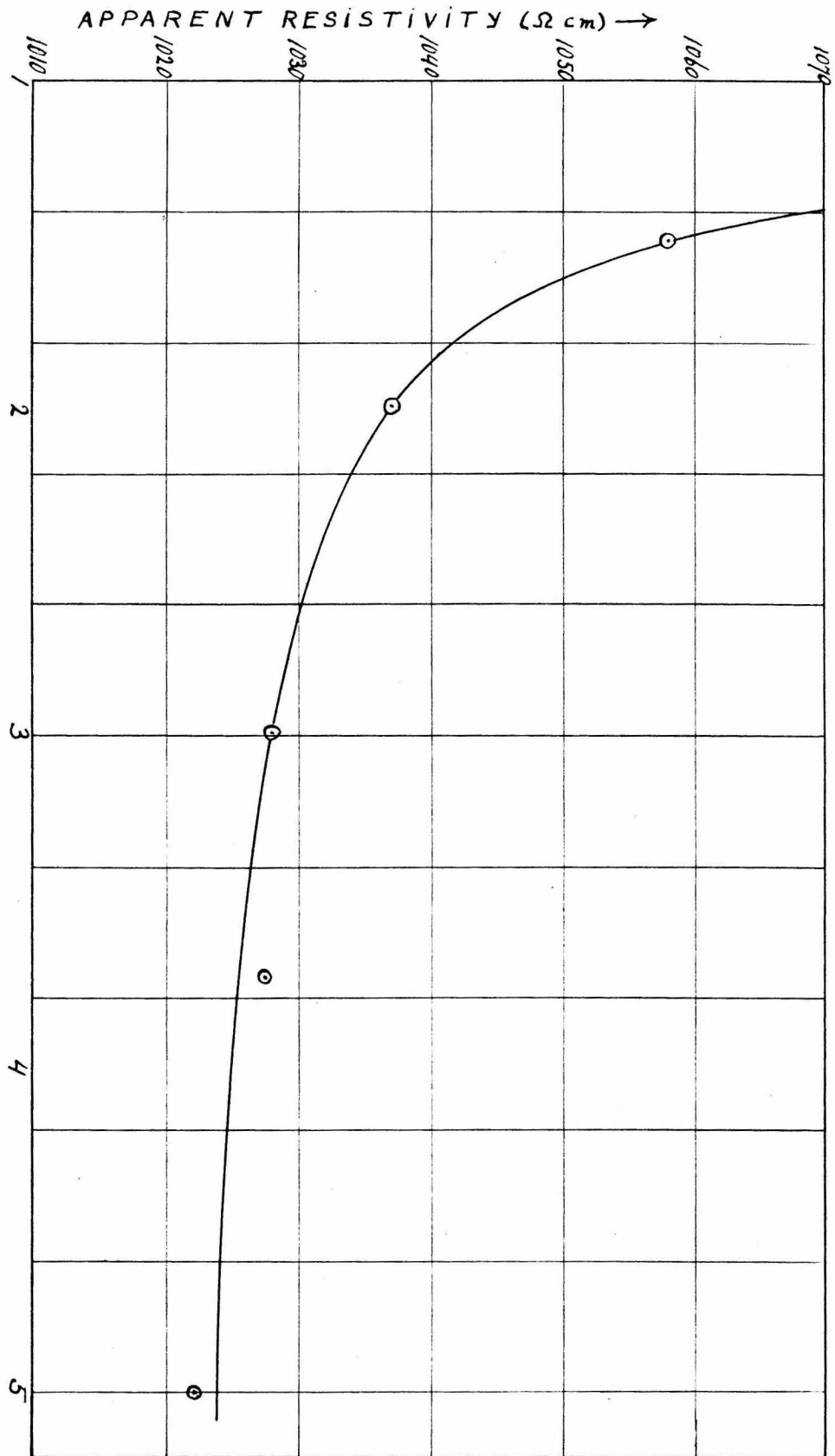


Fig. III - 9

of the glasses (I.D.). An example of the results obtained is given by Fig. III-8.

The same type of measurements were made with a series of glasses of the same diameter (2") and a height varying from 5" to 1.5" and the results were plotted giving the apparent resistivity as a function of the height of the glasses. (See Fig. III-9)

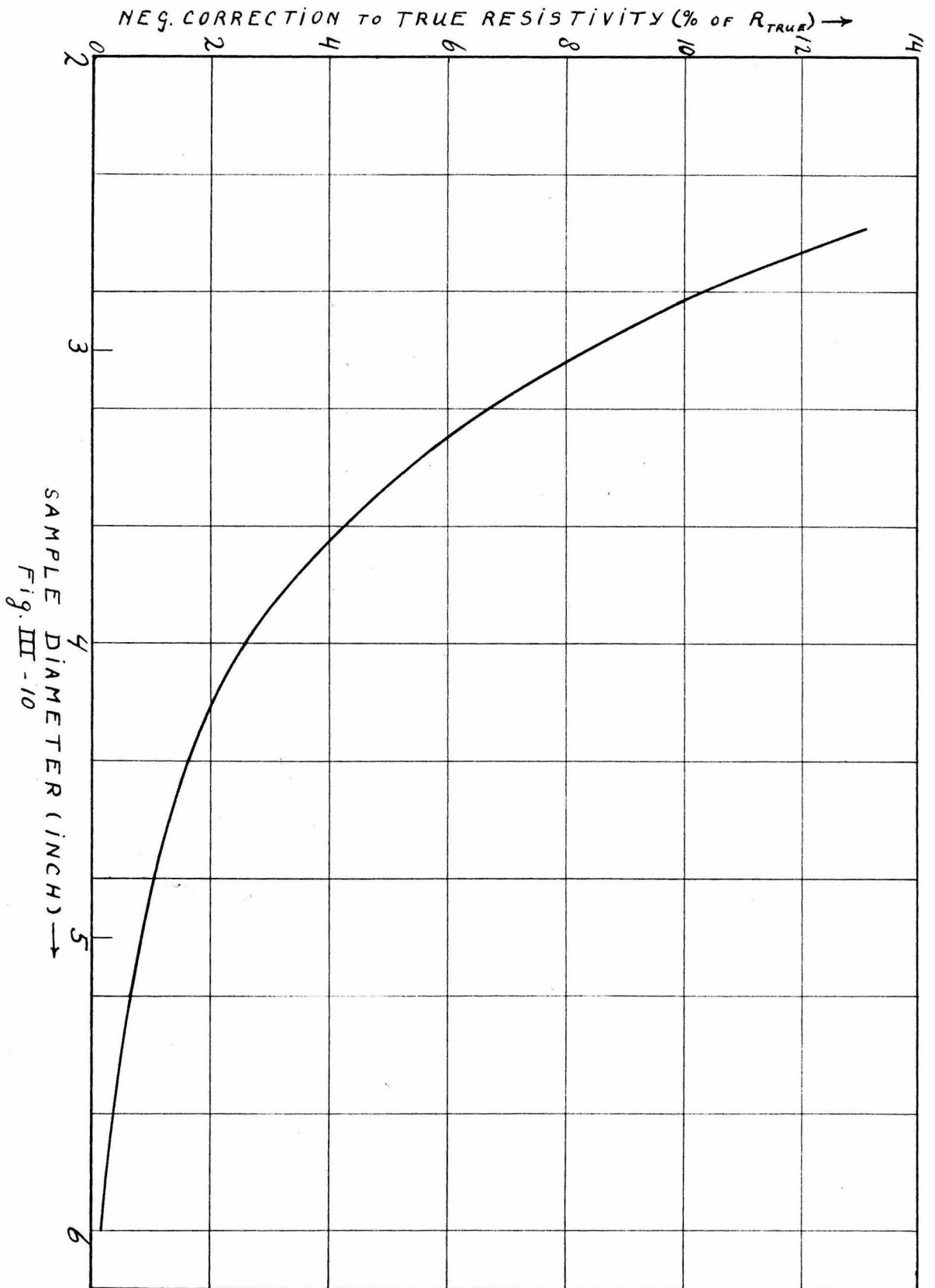
These measurements were repeated for various water resistivity over a range varying from 55 Ω cm to 15,000 Ω cm. The true resistivities were determined by measurements in a large container after preliminary measurements had shown that its walls had a negligible effect on the resistivity measured at its center.

From curves of the type of Fig. III-8 and Fig. III-9, the deviations were measured as a percentage of true resistivity. For a given height or diameter these deviations were independent of the water resistivity which also follows readily from the fact that in all cases the ratio of the resistivity outside the boundaries and the water resistivity is infinite. If beyond the boundaries is a medium of finite resistivity, ρ_2 , the effect on the apparent water resistivity is a

function of the factor $K = \frac{\rho_2 - \rho_1}{\rho_2 + \rho_1}$

However if $\rho_2 = \infty$ we have $K = \frac{1 - \rho_1/\rho_2}{1 + \rho_1/\rho_2} = 1 = \text{constant}$. The

deviations determined by a sufficient large number of experiments were averaged and then plotted as indicated by Fig. III-10 and Fig. III-11. The latter figures were determined for arrangement No. I and throughout the later experiments on the sandstone cores they were used to compute the correction factors to be applied to find the true resistivities of



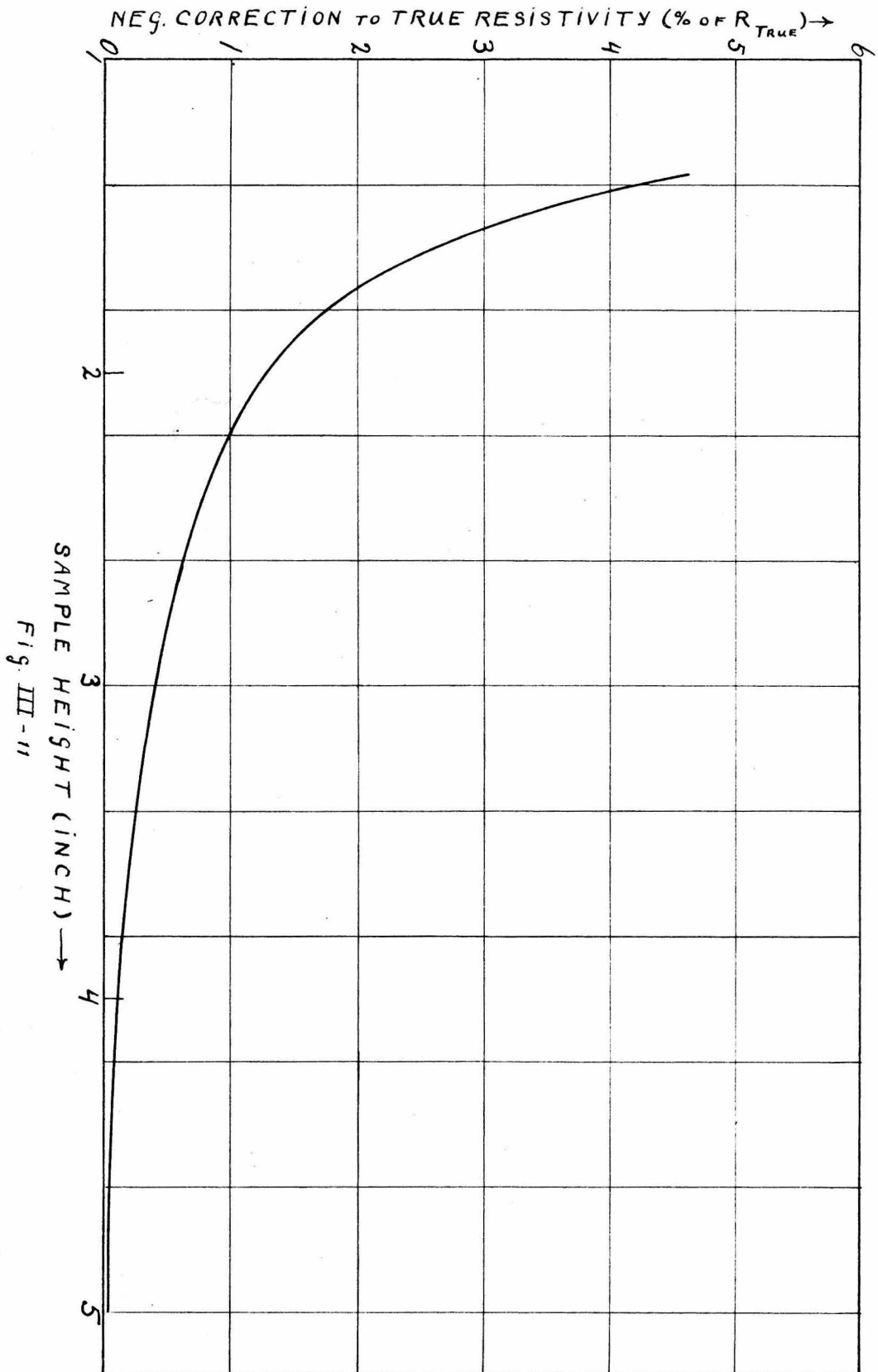


Fig. III-11

the cores.

Similar curves were made for arrangement No. II. To check whether the order of magnitude of the corrections agrees with what theoretically might be expected, we have calculated the effect of a straight boundary on a Wenner arrangement under the conditions of a similar resistivity ratio and relative distances.

The calculation was made using Tagg's formulae (11):

$$\rho_a = \rho_1 \left[1 + 4k \frac{d}{a} \left(\frac{1}{4d^2/a^2 - 4} - \frac{1}{4d^2/a^2 - 1} \right) \right] \quad (3-4)$$

Here ρ_a is the apparent resistivity, ρ_1 the water resistivity and $k = 1$. d = distance from center of electrode arrangement to the boundary = 1.5" for a sample of 3" diameter. $a = \frac{4B}{3}$ for the Wenner arrangement, so that $d/a = 4.5$. Substituting these values in (3-4) we have:

$$\rho_a = \rho_1 \left[1 + 18 \left(\frac{1}{6.8} - \frac{1}{9.8} \right) \right] = 1.09 \rho_1$$

This means a correction of 9% has to be made to obtain ρ_1 from ρ_a . This is of the same order of magnitude as the corrections determined experimentally for our arrangement. It must be pointed out however that the conditions of our tests are much different from the ones assumed for the above calculation, the most important fact being that in our case boundaries occur at both ends. This would double the correction to be applied. Our correction, though of the same order of magnitude, is considerably lower, which indicates clearly the advantage of our arrangement over a Wenner arrangement in the case of circular boundaries.

The electrode sets were constructed in the following manner:

Steel nails of 0.5" length and .072" diameter were soldered onto the bottom end of small tie points. Then the plastic top of the tie-point was fitted into a piece of steel tubing (O.D. = .462") flush with the rim of that tubing. The lower part of the tie point was centered by a snugly fitting lucite collar, while the space in between was filled up with a mixture of beeswax and rosin. The bottom part of the steel tubing was sealed around the nail with shellac, thus providing at all points a firm connection and good insulation between the electrode and the steel shielding. The end of the nail was filed to a blunt point, thus decreasing the diameter at the point of contact with the surface of the sample to approximately .03". The end of the electrodes protruding below the shielding was about .35" long.

The four electrodes were placed into a piece of 1/2" thick lucite (4" x 5") and cemented in place by Duco cement, the distances being approximately as indicated before.

After the electrodes were thus firmly sealed in their permanent places, the exact distances between the centers of the electrode points were measured with a micrometer. These measurements are listed below for arrangements I and II, and were used to compute the resistivity measured in terms of current and voltage drop.

Arrangement I (Fig. III-12):

$$\begin{array}{llll} AC = .446" & BD = .486" & AB = .905" & CD = 1.283" \\ AD = 1.040" & BC = .975" & & \end{array}$$

$$\Delta V = \frac{I\rho}{2\pi} \left\{ \left(\frac{1}{.446} + \frac{1}{.486} \right) - \left(\frac{1}{1.040} + \frac{1}{.975} \right) \right\} \frac{1}{2.54}$$

$$\text{or } \rho = \frac{\Delta V}{I} \times 6.744 \text{ } \Omega \text{ cm}$$

Instead if I , the voltage drop $(V)_I$ across a standard resistor R_I in the current circuit was measured so that we can substitute

$$I = \frac{(\Delta V)_I}{R_I} \text{ which gives:}$$

$$\rho = \frac{\Delta V}{(\Delta V)_I} \times R_I \times 6.74 \text{ } \Omega \text{ cm}$$

For arrangement II:

$$AC = .423'' \quad DB = .478'' \quad AB = .607'' \quad CD = 1.124''$$

$$AD = .759'' \quad BC = .801''$$

$$\text{For these distances } \rho = \frac{\Delta V}{(\Delta V)_I} \times R_I \times 8.45 \text{ } \Omega \text{ cm}$$

The electric connections with the rest of the circuit were made by single pole plugs, fitting the tie points. They were soldered onto the electrode leads and fitted with shellac into steel tubing of .462" I.D.

The braid shielding of the leads was connected to the steel electrode shielding by 1/2" steel braid clamped over the upper part of the steel tubing.

The protruding edge of the plug shielding fitted tightly over the shielding of the tie points, thus making a good connection electrically.

The plug-in system was made in order to facilitate interchanging arrangements No. I and No. II.

Electrolyte Resistivity Cell

To follow the changes in resistivity of the effluent water, which was necessary in some of the experiments, the apparatus described before had to be adapted to measure the resistivity of small quantities of electrolytes.

This was done in the following manner:

A small cylindrical glass container of 1.5" diameter and 0.4" depth

was placed concentrically inside a larger shallow beaker of similar shape and approximately 3 inches in diameter.

The upper edge of this beaker was cut off straight and fitted snugly in a groove cut in the lucite plate in which the electrodes are mounted. This groove was concentric with the geometric center of the electrodes. The height of the larger beaker was chosen such that upon placing the rim of the beaker in the circular groove, the points of the electrodes would just reach into the smaller container. To make a measurement the latter would be filled with a carefully measured quantity (12 cm^3) of the electrolyte of which the resistivity was to be determined, and the points of the electrodes would be dipped into the liquid by placing the lucite plate over the rim of the larger beaker, fitting the latter in the circular groove of the plate.

To insure that the position of the electrode points, with respect to the small container and the fluid level, was identical for all measurements, a mark on the large beaker was lined up with a mark on the lucite plate when placing the beaker in position and the entire system was leveled using a two dimension spirit level, placed on the lucite plate.

Because of the fixed configuration the resistivity of the electrolyte to be determined is equal to the apparent resistivity as measured in the small container times a constant correction factor, which corresponds to the cell-constant of a Kohlrausch cell.

This constant was determined by measuring the apparent resistivity of electrolytes of which the actual resistivity was found by measurements on large quantities (approx. 500 cc) using our conventional measuring system.

PART IV

Experimental Procedure

The larger part of the experiments were carried out with samples taken from outcrops of formations that are oil bearing in nearby regions.

Prominent among these are the following types:

- 1) A very pure quartzitic sandstone (Berea formation, lower Mississippian, Ohio)*
- 2) Sandstone from the Pico formation (lower Pliocene, California)
- 3) Sandstones from the ^{Modelo}/~~Modello~~ formation (upper Miocene, California)

Other types of sandstone used were:

- 1) Saugus (Pliocene - land laid)
- 2) A very tight Mesozoic sandstone, probably Jurassic, from outcrops near Redlands, California.

Thinsection (point-counter) analyses and sieve analyses of most of the sandstones used are given in another theses by this author (10).

To start an experiment, a cylindrical core of approximately 2.8" diameter and 2" height would be mounted in the bottom part of a cylinder of a baroid wall-building tester as described in Part III. Care had to be taken that the flat surfaces were left free and clean.

After mounting the core, the cylinder plus core would be weighed on a balance, accurate to one-tenth of a gram. The cylinder would then be placed in the baroid tester and dry CO₂ gas was forced through the core for about one-half hour. For this purpose a top lid of the baroid

* Obtained by the courtesy of the Union Oil Co., Production Department, Whittier, California.

tester was connected to a 40 lb. carbon dioxide bottle. The carbon dioxide would effectively replace all of the air present in the interstices of the core. After this a measured amount of water would be forced, repeatedly through the core until the resistivity of the core as measured with the four electrode system would no longer change indicating that no more gas was being removed from the core. To allow any trapped CO₂ to be completely dissolved in the water, the flushing was interrupted frequently for several hours. When resistivity became constant it was assumed that the core was 100% saturated with water. At this time the cylinder was weighed again and the difference, equalling the difference in dry and wet weight, of the core, in grams was taken to be equal to the porosity, in cubic centimeters. Using the predetermined dimensions of the core the porosity as percentage of total volume was easily computed. For several cores these porosity determinations were checked against values of porosities found from thinsections by the point counter method, and it appeared that the latter values were often a few per cent larger. This is probably due to isolated pores (non-effective porespace) which show up in the sections, but not in the measurements by imbibition. Apart from this deviation overall agreement was very satisfactory.

During flushing the water was forced through the core using nitrogen gas from a large nitrogen bottle. Rather than changing connections, two separate lines for the baroid tester were used, one permanently fitted to the connection of the carbon dioxide bottle, the other connected to the nitrogen bottle.

All core resistivities were measured by the four electrode system

and amplifying circuit described in Part III. Electrolyte (water) resistivities were measured in the same way if sufficient quantities were available. For quantities smaller than 300 cc, the electrolyte resistivity cell was used.

The permeability was determined by measuring the amount of water that would flow through the core in a measured length of time under a measured pressure gradient (approximately 5 psi per inch).

The baroid tester was always used, complete with a copper screen and two rubber gaskets at the bottom and one rubber gasket at the top, to seal the lid.

After the above preliminary measurements were completed, oil, salt water or drilling mud could be placed in the upper part of the cylinder and forced to filtrate through the core.

The oil saturations, however, were mostly obtained by the capillary pressure method, using special adapters to fit the baroid cylinders. (10)

Gas-oil or gas-water mixtures could be created in the core by letting nitrogen gas escape through the core (with no liquid in the upper part of the cylinder).

As described in Part III, the drilling muds were mixed from dry powders of aquagel, zeogel, kaoline, baroid and natural clays (obtained by courtesy of the Baroid Sales Division, Los Angeles, California).

The mixing was done with a high speed soil dispersion mixer, using mixing times of approximately one hour. This gave sufficiently stable muds for our purposes. (12)

As the filtration of drilling mud is a slow process taking approximately 24 hours to obtain 100 cm of effluent filtrate from the core,

the filtrate was collected in a glass bottle by a filter funnel, the bottle being closed by a rubber stopper to minimize evaporation. After given amounts of filtration the pressure was released and the resistivity of the core measured.

Additional measurements were made of the resistivity of the effluent filtrate at different times, using the electrolyte resistivity cell.

When obtaining oil saturations by the capillary pressure method, differential pressures across the oil-water interfaces up to 25 psi were used. At this pressure the "irreducible" water saturation was approached very closely for most of the samples used. The extracted water was measured in a small graduate cylinder connected by a rubber hose and glass tubing to the outlet of the baroid tester. At the end of the extraction an additional check on the amount of water extracted was made by weighing the cylinder containing the core together with the remaining oil and the adapter.

Comparison with a similar weight measurement before the extraction gave an accurate check on the amount of water removed. The volumetric and weight measurement gave very close agreement differences averaging not more than 1% of the computed saturation.

Finally upon completion of the oil saturation the resistivity of the core was measured.

After the required oil saturation was reached, the sample could be flushed with water and the resistivity change measured at regular intervals. Also the amounts of oil and water in the effluent mixture are measured volumetrically as accurate as possible.

When carrying out resistivity measurements on the cores, the pointed

electrodes, were brought into good contact with the surface of the sample by pressing firmly downward on the lucite plate, supporting the electrodes. Care had to be taken that the pressure was applied evenly.

All voltages were measured on the same scale of the multimeter. Always the largest one of the voltages between the potential electrodes and across the standard resistor in the current circuit, was measured first and adjusted by the output regulator of the oscillator to read at the top part of the multimeter scale. Then, without any changes to the main circuit, the amplifier input was changed to the other voltage via the central switch board. After reading the second voltage, the amplifier would be plugged back to the first one and another reading was taken of the first voltage. The two readings for the first voltage were averaged and the obtained value used together with the second voltage reading. This procedure was used to allow for small changes in the current electrodes during the measurement.

The entire measurement was always repeated for a lower oscillator output, thus obtaining two independent readings for the voltage-current ratios, used for the resistivity computations.

PART V

Theory of the Displacement of the Non-Wetting
Phase by Water During Radial Infiltration

The mechanism of fluid displacement in sands has been treated for the case of uni-directional flow by Buckley and Leverett (13).

A brief outline will be given of the part of their discussion that is of interest to our case, whereupon derivations will be made to apply to the case of radial infiltration.

For simplicity we will confine our reasoning to the case of an oil sand being flushed by water; but the same principles apply equally well to gas sands.

The net rate of accumulation of the displacing fluid which is equal to the net oil displacement will be proportional to the difference between the rate at which the displacing fluid enters any given volume of the sand and the rate at which it leaves that same volume.

Confining our attention to a unit volume of the sand and denoting the total fluid flow through this volume in cm^3/sec by p , and the fractions of the fluid flow comprising of water when entering and leaving the volume respectively by a and a' we have:

Entering the unit volume: $ap \text{ cm}^3$ of water per second

Leaving the unit volume: $a'p \text{ cm}^3$ of water per second

Remaining in the unit volume: $p(a - a') = \Delta ap \text{ cm}^3$ of water per second

Δa is the rate of accumulation of the water in the unit volume.

If S_w is the water saturation and θ denotes time we may write therefore:

$$\frac{\partial S_w}{\partial \theta} = \frac{\Delta S_w}{\varphi} \quad \text{where } \varphi \text{ is the fractional porosity.}$$

If u indicates length in the direction of the fluid flow we can write the following material balance:

$$\left(\frac{\partial S_w}{\partial \theta} \right)_u = \frac{-q_T}{A \varphi} \left(\frac{\partial f_w}{\partial u} \right)_\theta \quad (5-1)$$

Here we have replaced a by the infinitesimal ratio $\frac{\partial f_w}{\partial u}$, where f_w is the fraction of the flow comprising the displacing fluid ($f_w \equiv a$). And instead of p (the flow through 1 cm² cross-sectional area) we write the ratio of the total flow, q_T over the total cross-sectional area (A).

Equation (5-1) may be transformed in the following manner:

Let $\frac{q_T}{A \varphi} = \lambda$ We then may write:

$$\left(\frac{\partial S_w}{\partial \theta} \right)_u = -\lambda \left(\frac{\partial f_w}{\partial S_w} \right)_\theta \left(\frac{\partial S_w}{\partial u} \right)_\theta \quad (5-2)$$

As will be shown later f_w is a function of S_w only when we neglect capillary and gravitational forces. Therefore

$$S_w \equiv S_w(u, \theta)$$

We now impose the additional condition $S_w = \text{constant}$ with time, that is we concentrate our attention upon the progression of the locus of points for which S_w has a certain constant value.

This implies that:

$$\frac{dS_w}{d\theta} = \left(\frac{\partial S_w}{\partial \theta} \right)_u + \left(\frac{\partial S_w}{\partial u} \right)_\theta \left(\frac{\partial u}{\partial \theta} \right)_{S_w} = 0 \quad \text{or} \quad \left(\frac{\partial u}{\partial \theta} \right)_{S_w} = - \frac{\left(\frac{\partial S_w}{\partial \theta} \right)_u}{\left(\frac{\partial S_w}{\partial u} \right)_\theta}$$

Substituting the expression for $\left(\frac{\partial S_w}{\partial \theta} \right)_u$ from (5-2) we have:

$$\left(\frac{\partial u}{\partial \theta}\right)_{S_w} = \lambda \left(\frac{\partial f_w}{\partial S_w}\right)_{\theta} = \frac{q_T}{A \phi} \left(\frac{\partial f_w}{\partial S_w}\right)_{\theta} \quad (5-3)$$

For the case of uni-directional flow the locus of points for which S_w constant, is a plane perpendicular to the direction of flow.

Equation (5-3) states that the rate of advance of such plane where a certain fixed saturation prevails, is proportional to the change in composition of the flowing stream, caused by a small change in saturation of the displacing fluid.

Neglecting the effects of capillarity and gravity, f_w is related to the properties of the system in the following manner:

$$f_w = \frac{K_w/\mu_w}{K_w/\mu_w + K_o/\mu_o} = \frac{1}{1 + \frac{K_o \mu_w}{K_w \mu_o}} \quad (5-4)$$

where K_w and K_o are the relative permeabilities of the sand to water and oil respectively while μ_w and μ_o are the viscosities of the water and the oil.

Relation (5-4) follows directly from the definitions of relative permeabilities.

A representative value for the absolute viscosity of a 30° A.P.I. gravity oil under reservoir conditions is 2 centipoises so that $\frac{\mu_w}{\mu_o} \approx \frac{1}{2}$ if we assume $\mu_w = 1$ centipoise. Using equation (5-4) we can

determine f_w as a function of S_w from the relationships of relative permeabilities to water saturation, which have been determined experimentally both for oil and gas-water mixtures, for various unconsolidated sands and for consolidated sandstones (14, 15, 16, 17).

Referring back to equation (5-3) the basic relation between the

position along the path of flow, saturation and time may be written as

$$\Delta u = \frac{Q_T}{A} \left(\frac{d f_w}{d S_w} \right) \Delta \theta$$

or in terms of total amount of displacing fluid entering the system (Q_T):

$$u = \frac{Q_T}{A} \frac{d f_w}{d S_w} + C \quad (5-5)$$

For $Q_T = 0$ we have $u = (u_{S_w})_0$ so that $C = (u_{S_w})_0 =$ distance at which a given S_w occurs initially.

Displacement in the Case of Radial Flow

Consider a sector of a cylindrical slab of permeable rock into which radial infiltration takes place with its apex at the center of the drill hole. Let the intersected surface area of the boreface be 1 cm^2 . If the radial flow per 1 cm^2 of the boreface is again $p \text{ cm}^3/\text{sec}$, we see that $p \text{ cm}^3$ of fluid flow through any concentric section of our sector in one second. The sector as described above is shown in Fig. V-1.

We now consider a small section of the sector, of which the center is at a distance of $u \text{ cm}$ from the boreface and which width and height are both 1 cm . The curved boundaries of this section will vary from $\frac{(r_0 + u - \frac{1}{2})}{r_0}$ to $\frac{(r_0 + u + \frac{1}{2})}{r_0}$ where r_0 is the drill hole diameter.

The volume of this section is $\frac{\pi(r_0 + u + \frac{1}{2})^2 - \pi(r_0 + u - \frac{1}{2})^2}{2 r_0} = \frac{r_0 + u}{r_0}$. Again if a and a' indicate the fractions of water in the influent and effluent mixtures and $\Delta a = a - a'$ we have:

In $\frac{r_0 + u}{r_0} \text{ cm}^3$ remain $\Delta a p \text{ cm}^3$ of water per sec. so that

$$\left(\frac{\partial S_w}{\partial \theta} \right)_u = \frac{\Delta a p}{\varphi \left(\frac{r_0 + u}{r_0} \right)} \quad \text{or} \quad \left(\frac{\partial S_w}{\partial \theta} \right)_u = \frac{-Q_T}{A \varphi} \left(\frac{\partial f_w}{\partial u} \right)_\theta \frac{r_0}{r_0 + u} \quad (5-6)$$

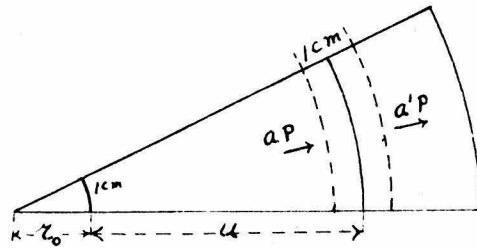


Fig. V-1

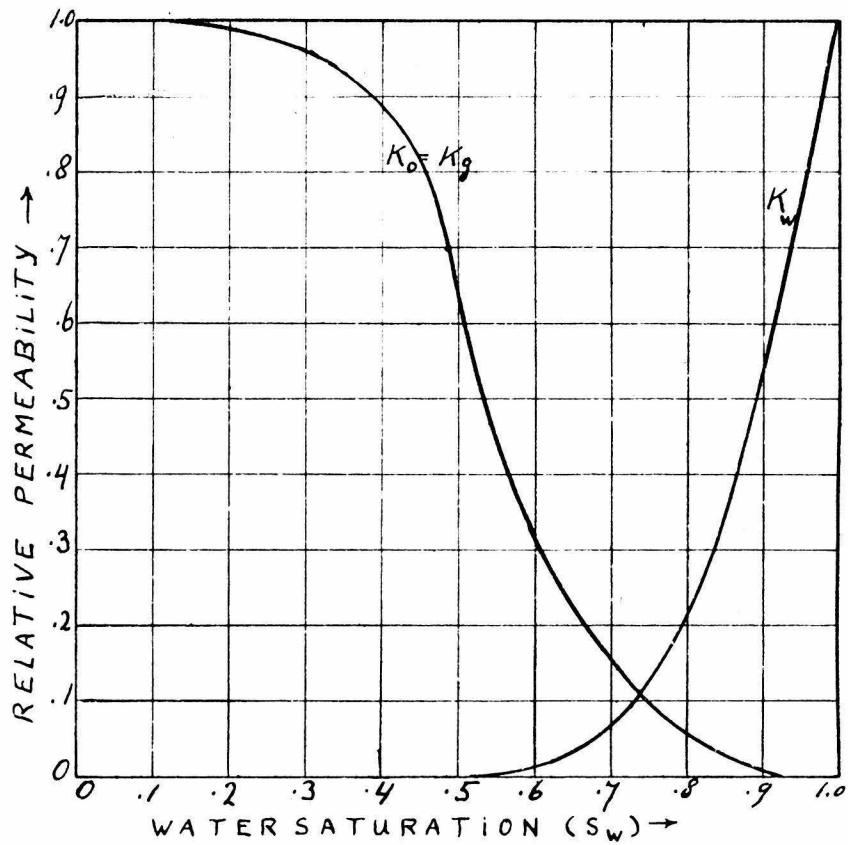


Fig. V-2
(AFTER BOTSET)

The minus sign is necessitated by the fact that f_w decreases with increasing u .

A is the surface of the boreface of the sandsection under consideration.

In a similar manner as described for the case of uni-directional flow, equation (5-6) may be transformed into:

$$\left(\frac{\partial u}{\partial \theta}\right)_{S_w} = \frac{q_T}{\varphi A} \left(\frac{\partial f_w}{\partial S_w}\right)_{\theta} \frac{r_0}{u + r_0}$$

or in terms of the total amount of water infiltration:

$$\int_0^u (u + r_0) du = \frac{r_0}{\varphi A} \left(\frac{\partial f_w}{\partial S_w}\right)_{\theta} \int_0^{\theta} q_T d\theta$$

$$\text{or } \frac{u^2}{2} + u r_0 + C = \frac{r_0}{\varphi A} \left(\frac{\partial f_w}{\partial S_w}\right)_{\theta} Q_T \quad (5-7)$$

For $Q_T = 0$, that is before infiltration has started, S_w will be equal to the connate water saturation of the undisturbed formation and will be the same for all radial distances from the boreface. The discontinuity at the boreface may be replaced by a continuous increase of S_w from its actual value in the formation to 1.0 between $u = +0$ and $u = -0$. All values of S_w that will be found within the infiltrated zone after infiltration has taken place for a given length of time, may therefore be assumed to exist initially in the interval between $u = +0$ and $u = -0$. From the initial condition $u_{S_w} = 0$ for $Q_T = 0$ we find from equation (5-7) that $C = 0$ so that we may write: $u^2 - 2 u r_0 - 2P = 0$

$$\text{with } P = \frac{r_0}{\varphi A} \left(\frac{d f_w}{d S_w}\right)_{\theta} Q_T$$

$$\text{This gives } u = \frac{-2 r_0 \pm (4 r_0^2 + 8P)^{\frac{1}{2}}}{2}$$

and as u is always positive this becomes:

$$u = (r_0^2 + 2 p)^{\frac{1}{2}} - r_0 \quad (5-8)$$

For a given Q_f we can calculate therefore at which distance from the boreface an arbitrary saturation will prevail, if the initial saturation and the relative permeability versus saturation relationships are known.

Rose (18) has shown that the relative permeability characteristics for both wetting and non-wetting phase, are dependent only on the saturation values at which the respective relative permeabilities become zero. These values in turn are closely related to the bound water content of the formations. We may assume therefore that all rocks with the same bound water content, have roughly the same relative permeability saturation characteristics and it seems likely therefore that there exists a fixed relationship between the saturation distribution in the infiltrated zone and the bound water content of the formation.

The above assumptions are supported by the work of Tixier (19) who obtained a reasonable correlation between the average water saturation in the infiltrated zone and the original water content of the formations, from field studies in the Rocky Mountain oil fields.

For thick oil sands the initial connate water content is approximately equal to the irreducible or bound water saturation in the entire section, except for a transition zone near the bottom of the sand.

Unfortunately data in the literature giving relative permeabilities and bound water contents are very scarce.

Some data are given in a paper by E. R. Brownscombe et al (20) and some information could be assembled from independent papers on experiments performed on the same type of sandstone.

As a first example we will use the data published on Nichols Buff sandstone.

The relative permeability relationships were experimentally determined by Botset (16) and are reproduced in Fig. V-2.

Fig. V-3 gives f_w for $\frac{\mu_w}{\mu_o} = \frac{1}{2}$ and $\mu_w/\mu_o = .06$

while Fig. V-4 gives $\frac{d f_w}{d S_w}$ versus S_w for the same two cases. Rose estimates the bound water content for the Nichols Buff sandstone to be approximately .35 .

From Figs. V-3 and V-4 and using equation (5-8) we can compute the infiltrated zone saturation distribution assuming the initial connate water content to be equal to the irreducible water saturation $(S_w)_o = .35$. As we are considering only the effects of lateral invasion the initial saturation is constant for all values of $u > 0$.

From evaluation of experimental results to be described later, we know that an infiltration of 25 cm^3 through each cm^2 of the boreface represents an average amount of infiltration in most cases. For the sake of simplicity we will assume that

$$r_o = 10 \text{ cm } (d_o \approx 8") \quad \text{and} \quad \phi = .25$$

$$\text{We have then:} \quad u = (100 + 2P)^{\frac{1}{2}} - 10$$

$$\text{and} \quad P = \frac{10}{.25} \times \frac{25 d f_w}{d S_w} = \frac{1000 d f_w}{d S_w}$$

$$\text{or} \quad u = 10 \left(1 + \frac{20 d f_w}{d S_w} \right)^{1/2} - 10 \quad (5-8a)$$

The saturation distribution for this case is now computed graphically by taking u as abscissa and S_w as ordinate.

The initial distribution is thus represented by a straight horizontal

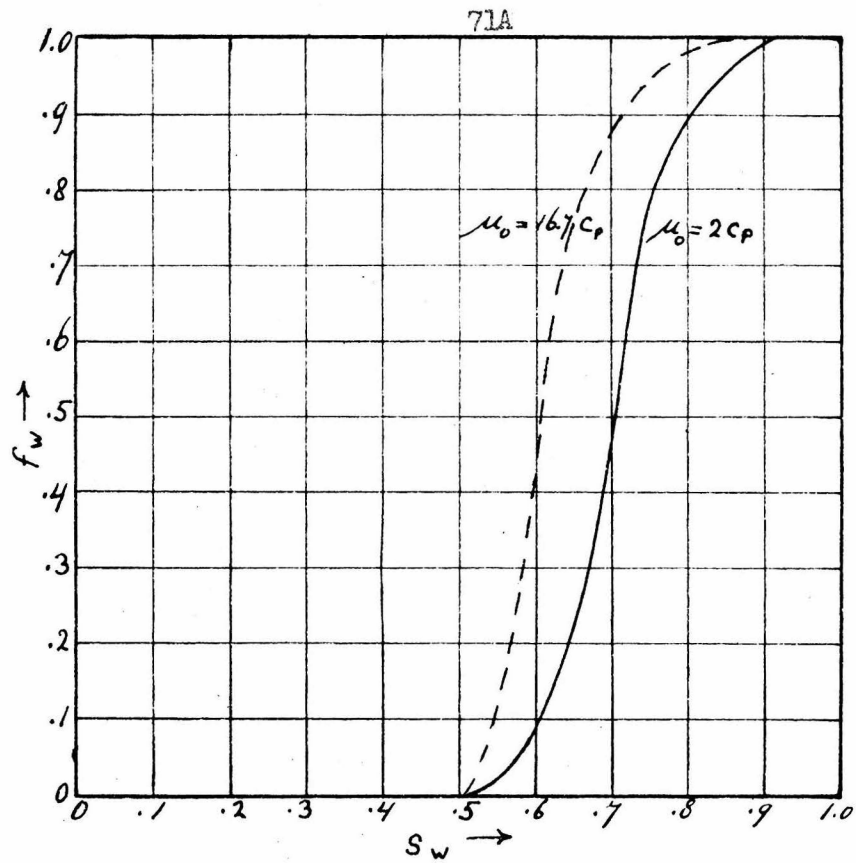


Fig. V-3

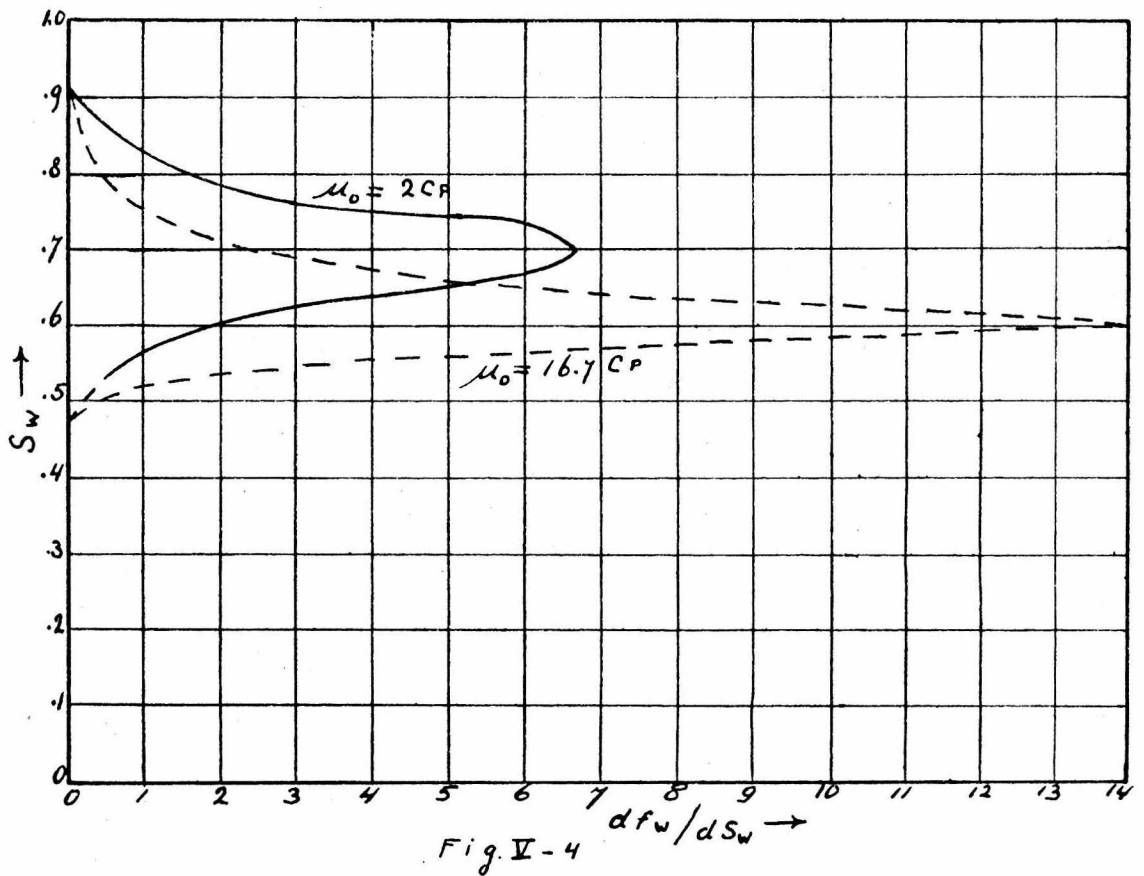


Fig. V-4

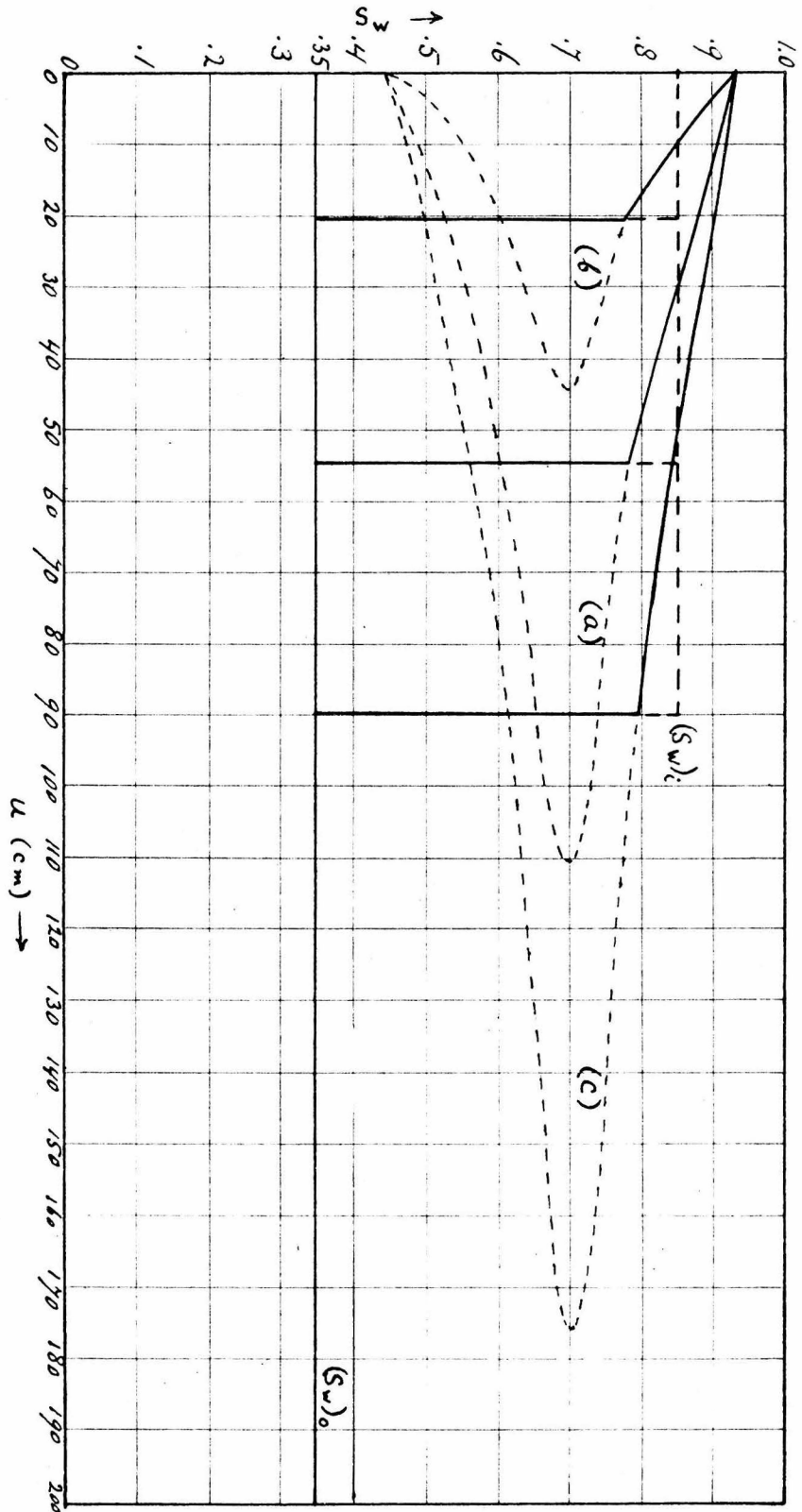


Fig. V-5

line ($S_w = .35$) from $u = 0$ to $u = \infty$ and a straight vertical line ($u = 0$) from $S_w = .35$ to $S_w = 1.0$. For all values of S_w we now calculate u from equation (5-8a). The resulting saturation distribution is plotted by laying off from any point S_w on the initial curve a distance equal to u on a line parallel to the abscissa. The resulting curve is shown in Fig. V-5.

We see that the curve for S_w and u is multiple valued for all values of u .

Buckley and Leverett obtained a similar result for the case of uni-directional flow. Obviously this result is a physical impossibility. As pointed out by Buckley and Leverett, the correct interpretation is that a portion of the curve is imaginary and that the real saturation versus distance graph is discontinuous with a discontinuity at a certain point u_1 .

To find u_1 we must make a new material balance based on the fact that in the sector under consideration the total inflow equals the fractional increase in water saturation times the pore volume in which the increase takes place.

The latter part of the equality may be represented by

$$\int_0^{u_1} A \frac{r_0 + u}{r_0} \cdot \phi \cdot \Delta(S_w)_u \, du$$

and we have therefore

$$\int_0^{u_1} \frac{r_0 + u}{r_0} \cdot \Delta(S_w)_u \, du = \frac{Q_w}{A \phi} = \frac{25}{.25} = 100$$

The integrand is plotted and u_1 is determined such that the area under the curve between the ordinates $u = 0$ and $u = u_1$ equals 100.

Due to effects of capillarity the actual saturation graph will have no sharp discontinuity but the corners will be somewhat rounded. The discontinuity (or the steep part) of the saturation distribution curve coincides with what is termed the outer boundary of the invaded zone and the radius of the invaded zone equals $r_0 - u_1$.

We see that the saturation in the invaded zone is not constant, but varies with the radial distance from the boreface. For practical purposes however, it may be approximated by a constant saturation of intermediate magnitude. In our example this value would be at $S_w = .85$.

It might be expected that the degree of infiltration will influence the average saturation within the invaded zone. To check this possibility the saturation distribution will be computed for two other invasion diameters.

We will first compute the distribution in the case of little infiltration. Let $\frac{(Q_T)_2}{A} = 5 \text{ cm}^3$ then $\frac{(Q_T)_2}{A \phi} = 20$ and $P = 200 \frac{d f_W}{d S_w}$ so that $u = 10 \left(1 - 4 \frac{d f_W}{d S_w} \right)^{1/2} - 10$.

The resulting values for u are plotted in Fig. V-5 curve (b) and the relation:

$$\int_0^{u_2} \frac{r_0 + u}{r_0} \cdot \Delta (S_w)_u \, d u = \frac{(Q_T)_2}{A \phi} = 20$$

is solved graphically for u_2 .

We obtain $u_2 = 20.4 \text{ cm}$. This means $d_1 = 30.4 \text{ cm}$ and $d_1/d_0 = 3.04$.

We see that in this case the subordinate phase of displacement is more prominent, that is the saturation within the infiltrated zone changes more rapidly with radial distance than in the case of larger infiltration. Approximating the actual distribution again by a constant, $(S_w)_1$, we find

however that the average saturation has not changed appreciably and is still approximately .85 .

Finally we will compute the saturation distribution for large infiltration. Let $\frac{(Q_T)_3}{A} = 60$ so that $\frac{(Q_T)_3}{\phi A} = 240$ and $P = 2400 \frac{d f_w}{d S_w}$.

$$\text{This gives: } u = 10 \left(1 + 48 \frac{d f_w}{d S_w} \right)^{\frac{1}{2}} - 10$$

The resulting values for u are plotted in Fig. V-5, curve (c).

$$\text{From } \int_0^{u_3} \frac{r_0 + u}{r_0} \cdot \Delta (S_w)_u \, d u = \frac{(Q_T)_3}{A \phi} = 240$$

we find $u_3 = 90$ cm or $d_1 = 10 d_0$.

We observe that for large infiltration radii, the subordinate phase of displacement is really unimportant and the assumption of a constant infiltrated zone saturation is very reasonable. The average saturation still equals .85 .

The above computations lead us to the following conclusions:

The approximation of the infiltrated zone saturation distribution by a constant, for oil sands, is more accurate for large radii of infiltration, than for smaller ones.

The average saturation of the infiltrated zone of an oil sand $(S_w)_1$ is independent of the amount of infiltration.

Effect of the Viscosity of the Non-Wetting Phase

In the preceding paragraphs the residual saturation in the infiltrated zone was computed for a certain type of sandstone and a viscosity ratio $\frac{\mu_H}{\mu_0} = \frac{1}{2}$.

The latter is a good value for gas saturated crudes under average reservoir conditions. However, most of our laboratory investigations

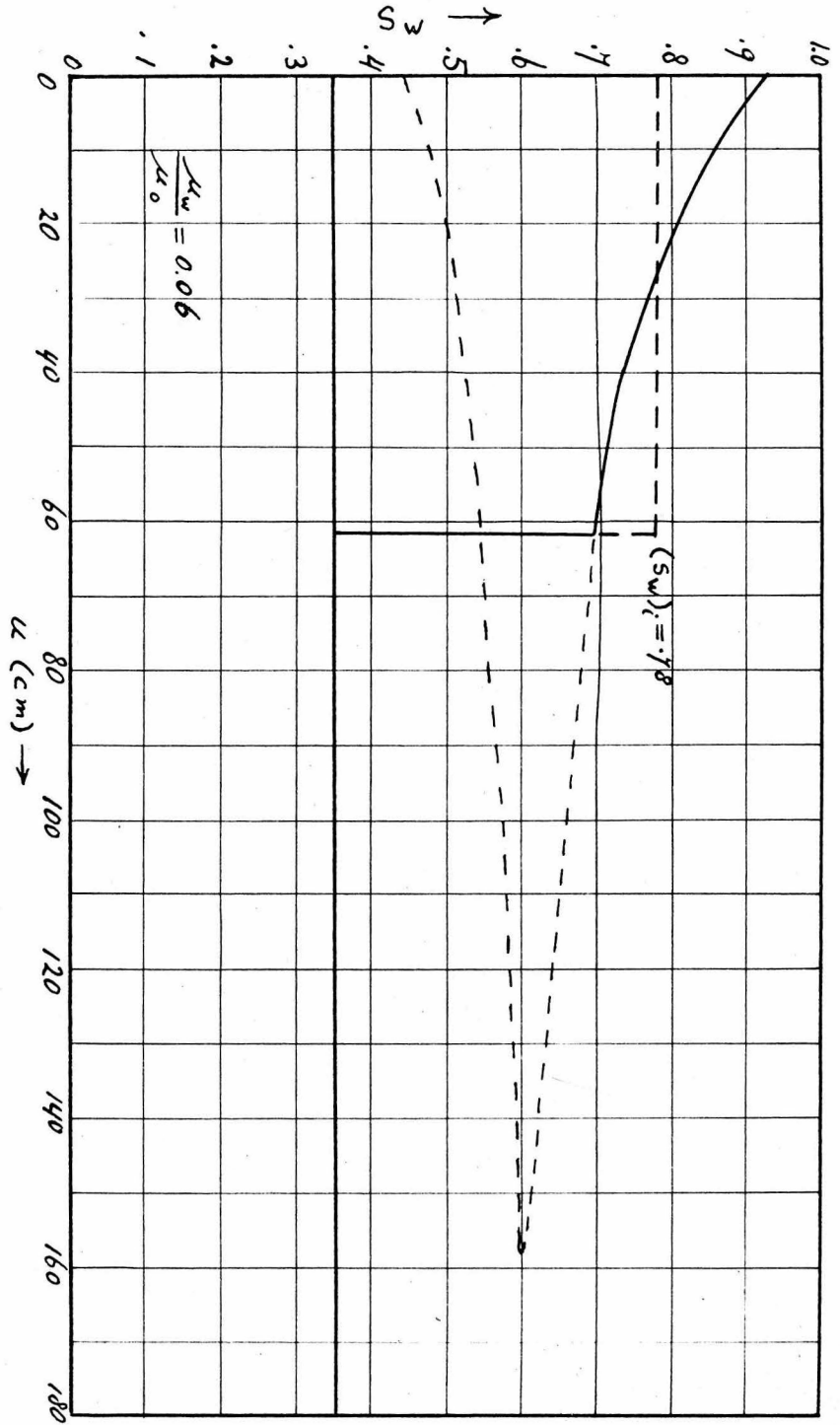


Fig. V - 6

were carried out using a 30.2° A.P.I. gravity oil at approximately 70° F and atmospheric pressure.

The viscosity of the oil under these conditions is in the neighborhood of 17 centipoises. This value was taken from a graph given by Beal (21) relating absolute viscosity to degrees of gravity for gas-free crudes at various temperatures.

In order to convert the laboratory data to reservoir conditions, we will compute the residual oil saturation for the same sandstone as above and a viscosity ratio

$$\frac{\mu_R}{\mu_0} = 0.06 \quad (\text{or } \mu_0 = 16.7 \text{ cp}).$$

$\frac{df_w}{dS_w}$ as a function of S_w is given in Fig. V-4.

As the influence of amount of invasion was shown to be negligible, we will only carry out the computation for average invasion $\left(\frac{Q_r}{A}\right) = 25$.

$$\text{For this case we had: } u = 10 \left(1 - 20 \frac{d f_w}{d S_w}\right)^{\frac{1}{2}} - 10$$

The corresponding saturation distribution is given in Fig. V-6. The location of the discontinuity (boundary of invaded zone) was found, by the method described before, to be 61.6 cm from the boreface.

We see that $(S_w)_1 = .78$ or almost 9% smaller than in the case of displacement of oil of 2 cp.

It must be pointed out here that the computation of saturation distributions by the above method depends strongly on the extreme values of the saturations at which the oil and water relative permeabilities become zero. These have heretofore not been determined with sufficient accuracy to make the above method of quantitative importance. However,

the method is very useful in outlining qualitative relationships.

Infiltration and Displacements of Non-Wetting Phase

In Gas Sands

In a gas sand the theoretical irreducible water saturation is probably smaller than for the same sand partially saturated with oil. However, in practice, capillary pressures are limited in magnitude and the actual water saturation prevailing in the larger part of a thick gas sand will be close to the irreducible or bound water saturation as defined in the case of an oil sand.

As pointed out by Rose (18), for a given reservoir rock, the gas-relative permeability, in the case of a gas-water system equals the oil-relative permeability in the case of an oil-water system. Also the water-relative permeability is independent of the nature of the non-wetting phase.

The computation of the saturation distribution upon invasion of a gas sand will furnish us therefore, additional information on the relationship between infiltrated zone saturation and non-wetting phase viscosities.

A representative value for the ratio of the gas-viscosity over the water-viscosity is: $\mu_g/\mu_w = 0.02$

This gives:

$$f_w = \frac{1}{1 + \frac{K_g \mu_w}{K_w \mu_g}} = \frac{1}{1 + 50 K_g/K_w}$$

The computed f_w is given in terms of its natural logarithm in Fig. V-7. The required values for K_w and $K_g = K_0$ were taken again from the relative permeability data for the Nichols Buff sandstone. (See Fig. V-2)

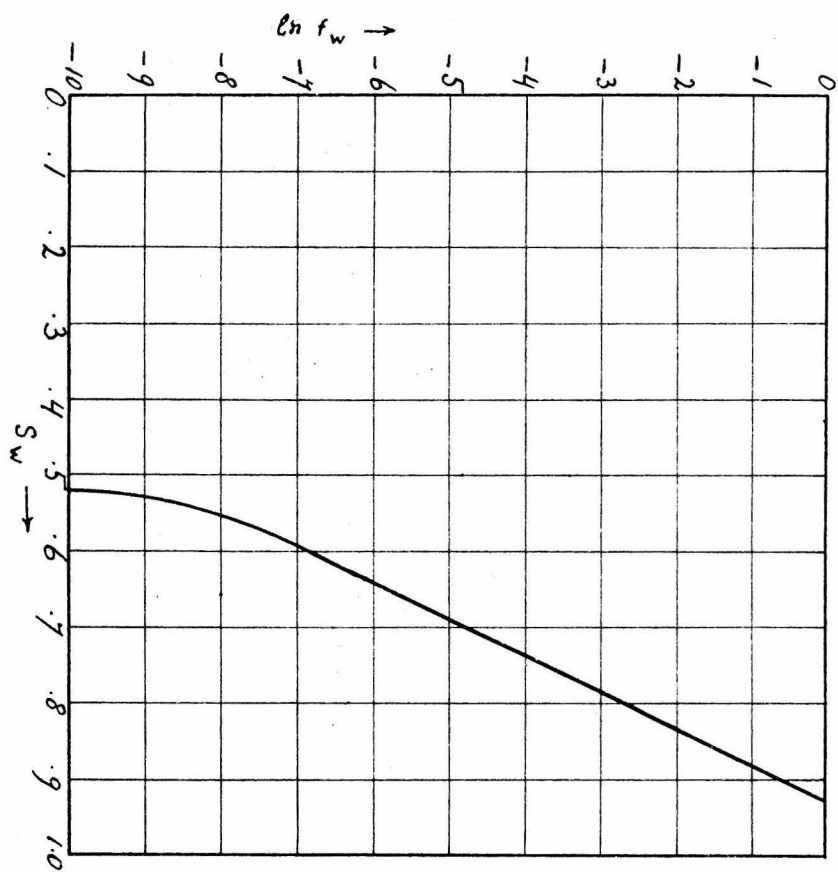


Fig. II-7

$\frac{d f_w}{d S_w}$ was computed using:

$$\frac{d \ln f_w}{d S_w} = \frac{d \ln f_w}{d f_w} \frac{d f_w}{d S_w} = \frac{1}{f_w} \frac{d f_w}{d S_w}$$

The values of the various quantities are tabulated in Table V-A:

TABLE V-A

S_w	f_w	$\ln f_w$	$\frac{d \ln f_w}{d S_w}$	$\frac{d f_w}{d S_w}$
.5	0	-8.1	30	.014
.55	.00046	-8.1	30	.014
.60	.0010	-6.9	20.7	.020
.70	.0083	-4.79	20.7	.172
.80	.0725	-2.61	20.7	1.50
.85	.187	-1.71	20.7	3.98
.88	.374	-1.08	23.3	8.73
.89	.454	-0.79	23.3	10.6
.90	.520	-0.65	24.0	12.5
.91	.71	-0.342	33.0	25.0
.92	1.00	0	0	0

Using again the formula: $u = 10 \left(1 + 20 \frac{d f_w}{d S_w} \right)^{\frac{1}{2}} - 10$

we find u as a function of S_w (See Fig. V-8).

For the distance of the discontinuity to the boreface we find

$$u_1 = 50.25 \text{ cm}$$

As the upper branch of the graph of $u = g(S_w)$ varies only between $S_w = .92$ and $S_w = .91$ the infiltrated zone saturation lies between these limits for all interior points of that zone, regardless of the

77A

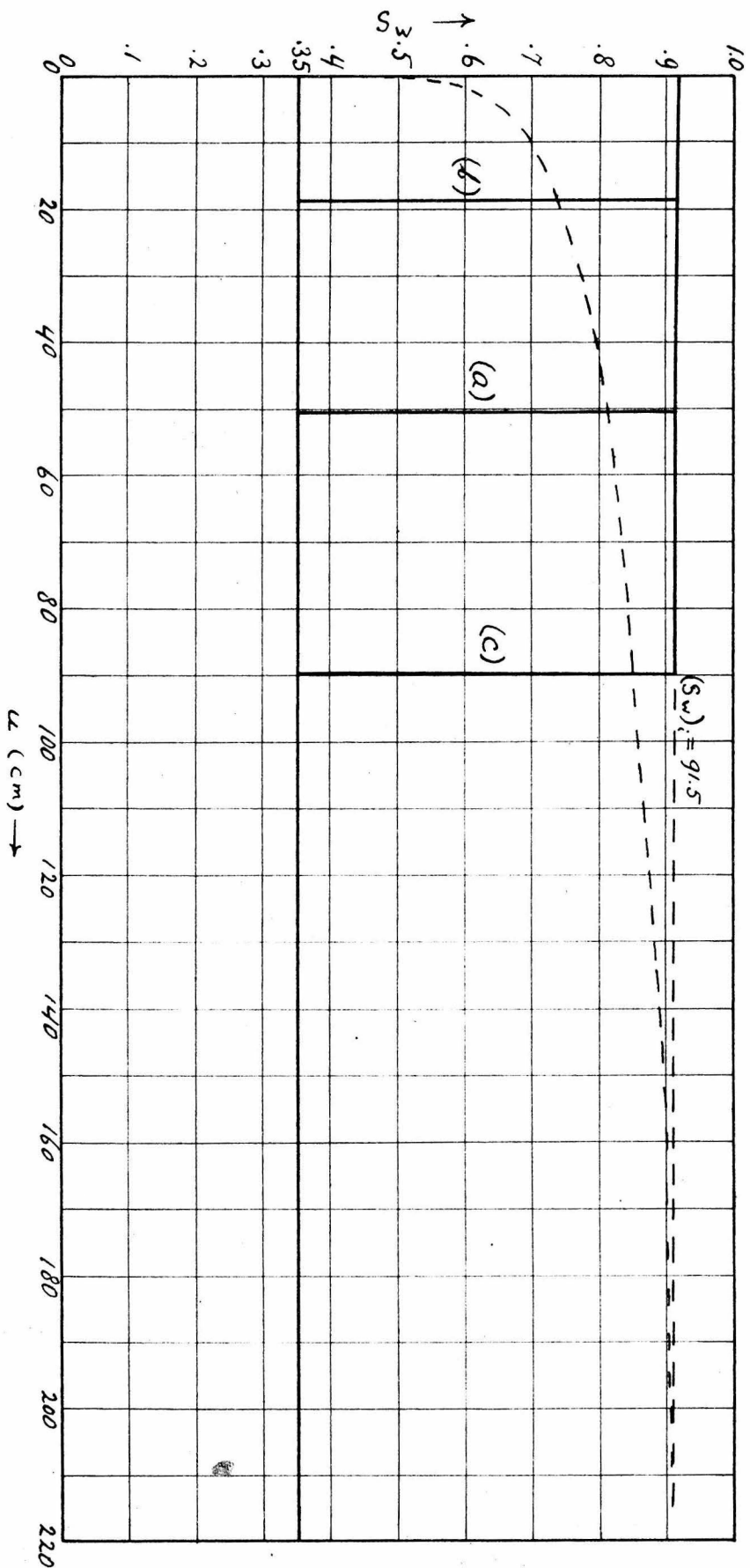


Fig. V - 8

amount of infiltration. Fig. V-8 shows the saturation profile for two other radii of infiltration, namely:

$$r_1 = 28.6 \text{ cm } (u = 18.6) \quad \text{and} \quad r_1 = 100 \text{ cm } (u = 90 \text{ cm})$$

For the relation between the water saturation of the infiltrated zone and the viscosity of the non-wetting phase, for Nichols Buff sandstone, the assembled data are given in Table V-B:

TABLE V-B

μ_o	μ_w/μ_o	$(S_w)_1$
16.7	0.06	.78
2	0.5	.85
0.02	50	.91

We see from Table V-B that the dependence of $(S_w)_1$ on the non-wetting phase viscosity is larger in the region of low viscosities (crude oils) than in the region of high viscosities (natural gases).

Influence of the Rate of Infiltration
on the Invaded Zone Saturation

For oil-water mixtures, Leverett (15) has demonstrated that the relative permeabilities depend to some extent on the factor $\frac{\pi N}{P D}$ where π is the displacement pressure of the sand to the non-wetting phase, N the length of the sample, $\frac{F}{N}$ the pressure gradient and D the average pore diameter.

This complex parameter can be reduced to a simpler form in the following manner.

As shown by Rose and Bruce (22) we may write for the displacement pressure:

$$\pi = \gamma \left(\frac{1}{k}\right)^{\frac{1}{2}} (k/f)^{-\frac{1}{2}}$$

where γ is the interfacial tension for the fluid system in question, k is the Kozeny constant of the rock, its specific permeability and f its fractional porosity.

For simplicity we write $\pi = C_1 \left(\frac{k}{f}\right)^{\frac{1}{2}}$ with C_1 depending only on the Kozeny constant and being therefore nearly constant for most clean sands.

The average pore diameter as used by Leverett was defined by

$$D = 5.63 \times 10^{-4} (k/f)^{\frac{1}{2}} \quad \text{or} \quad D = C_2 (k/f)^{\frac{1}{2}}$$

We have therefore:

$$\frac{\pi N}{P D} = \frac{C_1}{P/N C_2 (k/f)} = C_3 \frac{f}{P/N \cdot k}$$

Finally the quantity $k \times P/N$ is proportional to the rate of flow, F ,

so that $\frac{\pi N}{P D} \approx C \frac{f}{F}$.

The fractional porosity (f) of reservoir rocks will differ for various formations at most by a factor of two or three and plays therefore a minor role in the determination of the infiltration characteristics.

A quantitative analysis of the factors controlling the role of mud invasion, around bore holes was given by Williams (23).

The computations carried out by Williams showed that an average

value for the rate of mud infiltration (ν) into a permeable formation is 0.10 bbls/hr/ft (expressed as bbls of filtrate lost from the hole per hr., per foot of hole). Extreme values for this quantity are 1.00 and 0.01 bbls/hr/ft representing an extremely rapid and an extremely slow rate of infiltration.

The experiments and calculations by Williams also show that for a given speed of circulation of the drilling mud, the rate of radial invasion of the mud filtrate is independent of time. As the mudcake is very impervious, in comparison to the reservoir rocks, the rate of invasion is essentially only dependent upon the mudcake characteristics and the total differential pressure between the mud and the formation.

For radial flow, the cross-section perpendicular to the flow is proportional to the distance from the center of the hole. The rate of flow through a unit cross-section therefore is inversely proportional to the radial distance from the axis of the hole. Thus between the outer points of an infiltrated zone with a diameter 10 times the hole diameter and the points near the boreface, in the same zone, there exists a difference of a factor 10, in the rate of flow.

To obtain an estimate of the importance of the difference and variations in the rate of flow with regard to the saturation distribution in the infiltrated zone, we will use the experimental data given by Leverett (24).

These data represent the relations between f_w and S_w for pressure gradients ranging from 9 cm Hg/cm² to 0.06 cm Hg/cm² obtained on a sand of 1.04 darcies permeability. These values are equivalent to a water flow of .012 cm³ and $.82 \times 10^{-4}$ cm³ per cm² cross-section per second.

The infiltration rates as given by Williams, compare to this as follows for an 8" hole:

1 bbl/hr/ft of hole = $.166 \text{ cm}^3/\text{sec}/\text{cm}^2$ of boreface

0.1 bbl/hr/ft of hole = $.0166 \text{ cm}^3/\text{sec}/\text{cm}^2$ of boreface

0.01 bbl/hr/ft of hole = $.00166 \text{ cm}^3/\text{sec}/\text{cm}^2$ of boreface

At a distance of 9 times the radius of the hole from the boreface, these values become respectively:

$.0166$, $.00166$ and $1.66 \times 10^{-4} \text{ cm}^3/\text{sec}/\text{cm}^2$

We see that Leverett's data cover most of the range of actually occurring rates of infiltration.

Fig. V-9 gives f_w as a function of S_w for $F = .012 \text{ cm}^3/\text{sec}/\text{cm}^2$ and Fig. V-10 gives the same relationship for $F = .82 \times 10^{-4} \text{ cm}^3/\text{sec}/\text{cm}^2$ as presented by Leverett.

Figs. V-9 and V-10 also show $\frac{d f_w}{d S_w}$ as a function of S_w for both cases.

The water saturation distribution is again computed in the manner previously described, for average invasion diameter.

The results are shown in Fig. V-11. Curve (a) gives the saturation distribution for $F = .012$ and curve (b) shows the distribution for $F = .82 \times 10^{-4} \text{ cm}^3/\text{sec}/\text{cm}^2$.

The distribution graph for average infiltration rate for this particular sand, will be between the two curves just below curve (a).

We see that there is a marked difference between the average infiltrated zone saturations, for the two extreme cases (81.5% water saturation in case a) as compared to 72% for case (b).

Here again it must be stressed that these values only give an

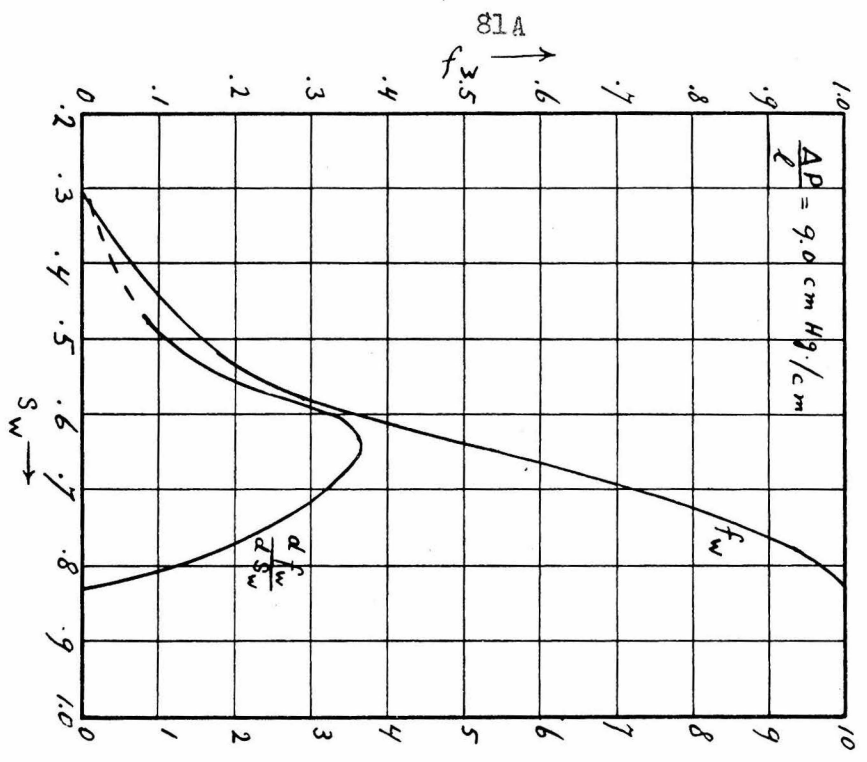


Fig. V-9

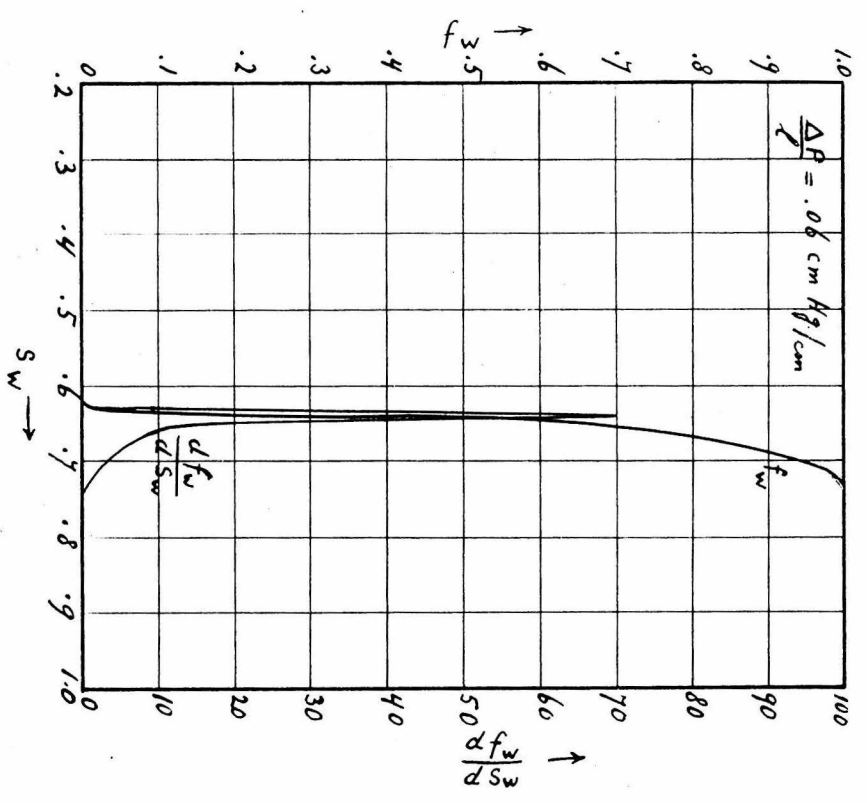


Fig. V-10

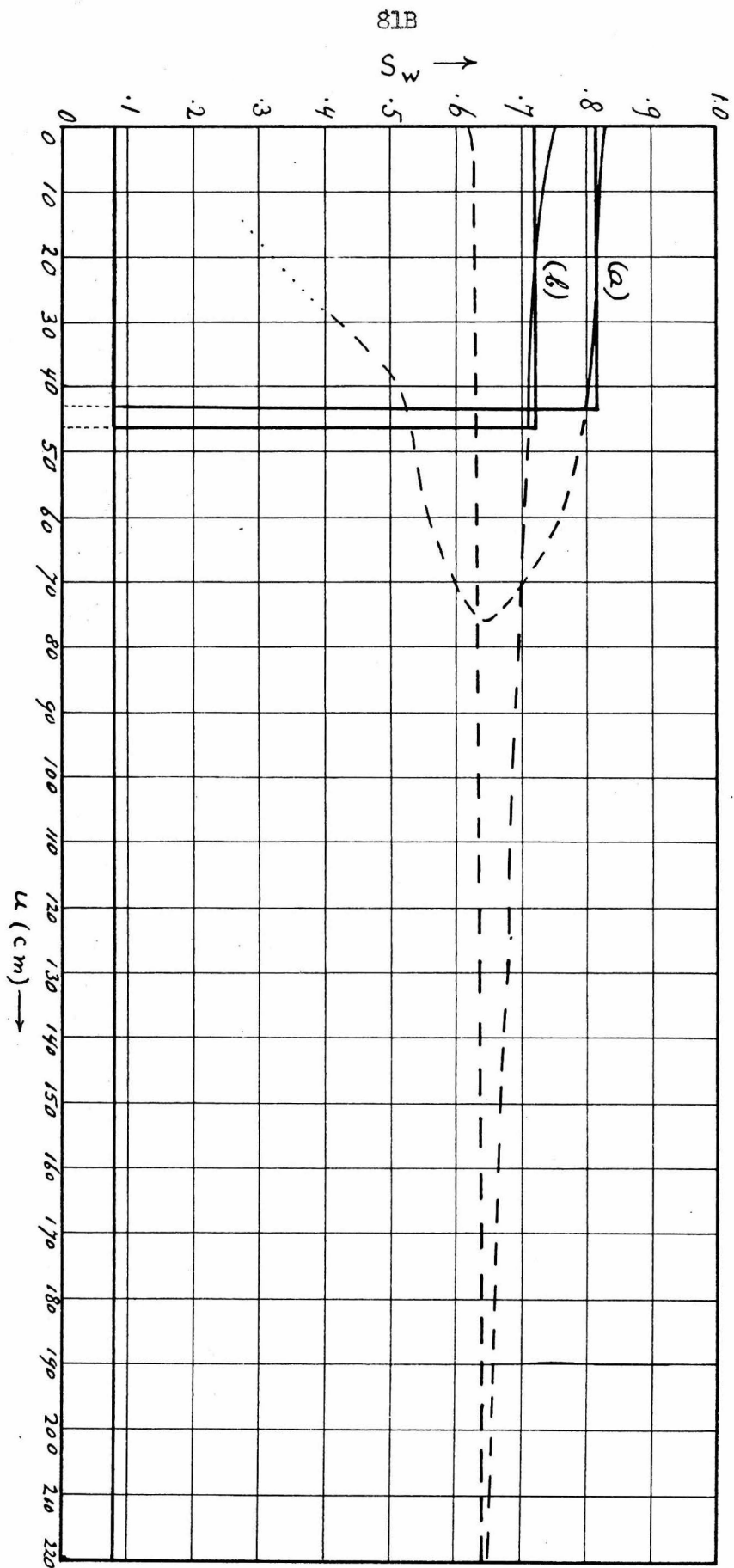


Fig. V-11

indication of the order of magnitude of the variations involved, but cannot be used for any further quantitative computations for consolidated sandstones.

In practice it is quite possible to estimate the rate of infiltration roughly as follows:

The radius of the infiltrated zone is found from the electrolog by the procedure outlined in Part II of this thesis.

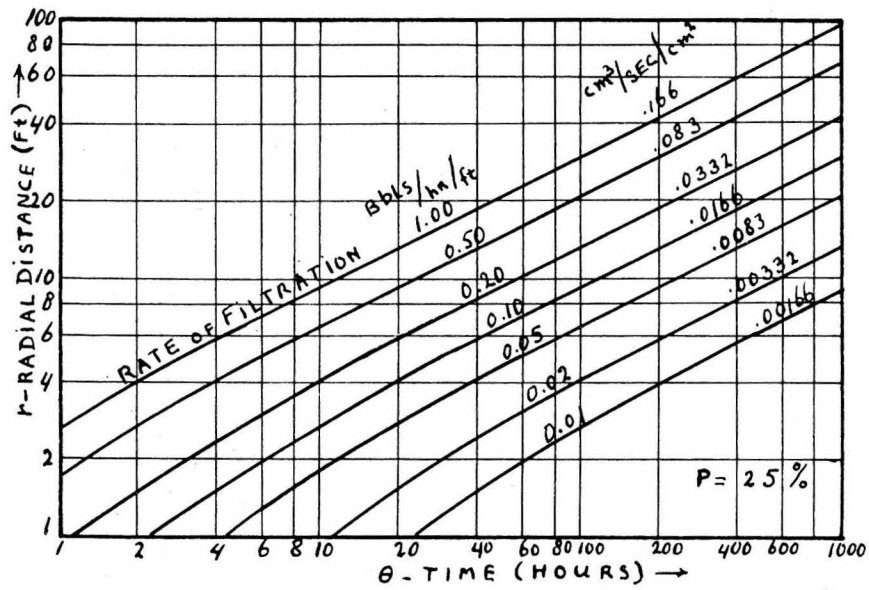
In addition the time in hours is estimated between the moment that the formation in question was first traversed by the drill, and the time that the electrolog is run.

This gives a relation between the distance penetrated by the filtrate and the time interval over which infiltration has been taking place.

Williams calculated such relations for various rates of infiltration, and presented the results as a family of curves, giving the distance penetrated, in feet as a function of the time during which invasion takes place in hours (25).

A copy of these curves is shown in Fig. V-12, with the infiltration rate given both in bbls/hr/ft of hole and in $\text{cm}^3/\text{sec}/\text{cm}^2$ of boreface.

The curves were made up for a hole diameter of 8-3/4", which represents an average size hole. The variations in computed infiltration rates due to different hole diameters are not large enough to be included in our calculations.



DISTANCE OF PENETRATION OF PERMEABLE STRATA
 ASSUMING 80% FLUID DISPLACEMENT
 AFTER M. WILLIAMS (23)

Fig. V - 12

Basic Relations Between Resistivities and Fluid Contents
of Porous Rocks.

and their Application to Electrolog Interpretation

Resistivities of Watersands

Until recently it was generally accepted that when a porous rock was saturated 100% with an electrolyte, the over-all resistivity of the rock was proportional to the resistivity of the electrolyte.

Analytically this could be expressed as:

$$R_0 = F R_w \quad (6-1)$$

where R_0 is the resistivity of the rock, 100% saturated with the electrolyte of resistivity R_w . F was assumed to be a constant, independent of R_w and physically had the same meaning as the cell-constant in electrolyte conductivity measuring cells.

In the early part of the experiments connected with this work, it was noticed that when a sample was first saturated with an electrolyte of low resistivity and then flushed with large quantities of a more diluted electrolyte, the resulting resistivity invariably was lower than the value computed from (6-1). It was definitely established that during the flushing process the resistivity gradually increased due to replacement of the saline interstitial water by the fresher water. After a quantity of water equal to three to four times the total pore volume has passed through the sample, the sample resistivity starts approaching an asymptotic value. After twenty times the pore volume has passed through no further changes in the resistivity are noticed. It is the resistivity prevailing at this final stage to which we referred above as the resistivity after flushing.

To explain the fact that the resistivity obtained after flushing was smaller than the one computed from (6-1) we assumed that a part of the initial connate water was not removed from the sample, but stayed adsorbed on the surface of the solid framework of the rock. The fact that the process was not reversible, was explained by assuming a certain portion of salt ions being adsorbed at the rock surfaces, without the necessity of a "fixed" water layer. Thus the water could be replaced but a portion of the salt ions remained in the sample. Different rocks exhibited such phenomena to different extents: "clean" sandstones showed a very small retention; while shaley sands, or sandstones with a large portion of "fines" gave a much larger effect.

Tixier (19), comparing resistivities of infiltrated zones, with those of the undisturbed formations in the field, came to a similar conclusion, namely that part of the initial connate water was not removed upon invasion of the formation by mud-filtrate.

The above conclusions did not seem to be in agreement with the findings of Mergan, Muskat and Russell (26) who experimented on the mobility of interstitial water in sandstones, using both radioactive tracers and NaCl as indicators. They found that for the particular sandstone they were using, all of the connate water was replaced after approximately ten times the pore volume of the sample had been flushed through. The possibility existed, however, that the sandstone they used (Nichols Buff ss.) happened to be a particularly "clean sandstone" where the retention effect would be negligible.

This was shown not to be the case by Patnode and Wyllie (27) in a recent publication. These authors made a large series of flushing

experiments using NaCl as a tracer and amongst the samples studied were sandstones of the same formation (Nichols Buff) as those used by Morgan, Muskat and Russell. Patnode and Wyllie attributed the apparent decrease in the formation factor with increasing interstitial water resistivity to the influence of conductive solids, which are present in most sandstones.

To prove that complete replacement of interstitial water takes place upon flushing with sufficient quantities of other aqueous solutions, they measured resistivities of an artificial core made up from alundum which contained no conductive solids. They found that for this case no lowering of the formation factor took place with increase in water resistivity and accepted this as proof of the complete replacement of interstitial waters in porous media, upon flushing.

It must be pointed out here that the alundum core can be compared to a completely clean sand, which would have no retention of connate water in any case and the experiment therefore proves nothing about the mobility of the connate water in sands in general.

In order to decide definitely whether or not connate water and the salt ions originally present are completely displaced upon flushing in average sandstones the following experiments were made:

Two samples of sandstones for which the apparent variations in formation factor had been found to be especially large were first saturated with a concentrated NaCl solution, of approximately 1M. After they had been completely saturated, fresh or less saline water was forced through and the resistivity of the effluent mixture was measured, with the electrolyte resistivity cell described in Part III.

The effluent water obviously is a mixture of the replaced original interstitial water and the water used for the flushing. By measuring its resistivity at intervals and knowing the resistivity of the two components we can calculate the fractions of each component in the following manner:

The concentration of a mixture of two electrolytes of given concentrations is given by:

$$\bar{C} = X_1 C_1 + X_2 C_2$$

Where \bar{C} , C_1 , and C_2 are the concentrations of the mixture and the two components respectively; X_1 and X_2 are the amounts of the components (1) and (2), expressed as fractions of the total volume. Obviously

$X_1 = 1 - X_2$, so that we have:

$$\bar{C} = X_1 C_1 + (1 - X_1) C_2$$

We now assume that the resistivity of an electrolyte is inversely proportional to its concentration. This holds true for dilute solutions, and is a fair approximation for concentrated solutions. We may then write:

$$\frac{1}{R_0} = \frac{X_1}{R_1} + \frac{1 - X_1}{R_2}$$

$$\text{or } R_0 = \frac{R_1 R_2}{R_1 - X_1 (R_1 - R_2)} \quad (6-2)$$

Here R_0 is the resistivity of the electrolyte mixture.

The volume fraction of the mixture represented by solution (1) is:

$$X_1 = \frac{R_2/R_0 - 1}{R_2/R_1 - 1} \quad (6-3)$$

Using formula (6-3), the amount of displaced connate water was computed in each case.

The results are summarized in Table VI-A.

TABLE VI-A

Symbols used:

v_1 = successive quantities of effluent mixture in cm^3 .

R_0 = resistivity of effluent mixture in $\Omega \text{ cm}$.

X_1 = fraction of original interstitial water in the effluent mixture.

$\sum (X_1)_1 v_1$ = total amount of original interstitial water displaced
(in cm^3)

S_1 = amount of original interstitial water still retained in sample,
as a percentage of the total porespace.

V_t = total accumulative amount of effluent mixture (cm^3).

I. Saugus ss. $P = 21.5 \text{ cm}^3 = 11.15\%$ $K = 5.32$ milli darcys
 $(R_w)_1 = 12.3 \Omega \text{ cm}$ $(R_w)_2 = 1950 \Omega \text{ cm}$

v_1	R_0	X_1	$(X_1) v_1$	V_t	$\sum (X_1)_1 v_1$	S_1
25	20.8	.603	15.08	25	15.08	29.9
25	69.4	.172	4.29	50	19.37	9.9
25	303.4	.0346	0.86	75	20.25	5.8
54	488	.0190	1.03	129	21.28	1.02
78	1160	.0041	.32	207	21.60	--

II. Modelo shaley sandstone:

$P = 32.5 \text{ cm}^3 = 15.04\%$ $K = 1.47$ milli darcys
 $(R_w)_1 = 11.9 \Omega \text{ cm}$ $(R_w)_2 = 106.6 \Omega \text{ cm}$

v_1	R_0	X_1	$(X_1) v_1$	V_t	$\sum (X_1)_1 v_1$	S_1
47.5	21.26	.47	22.5	47.5	22.5	30.8
50	50.55	.119	5.95	97.5	28.45	12.5
105	84.4	.029	3.26	202.5	31.71	2.4
140	102.5	.005	0.70	342.5	32.41	0.28
79	103.7	.0037	0.29	421.5	32.70	--
14.5	106.6	0.00	0.00	436	32.70	--

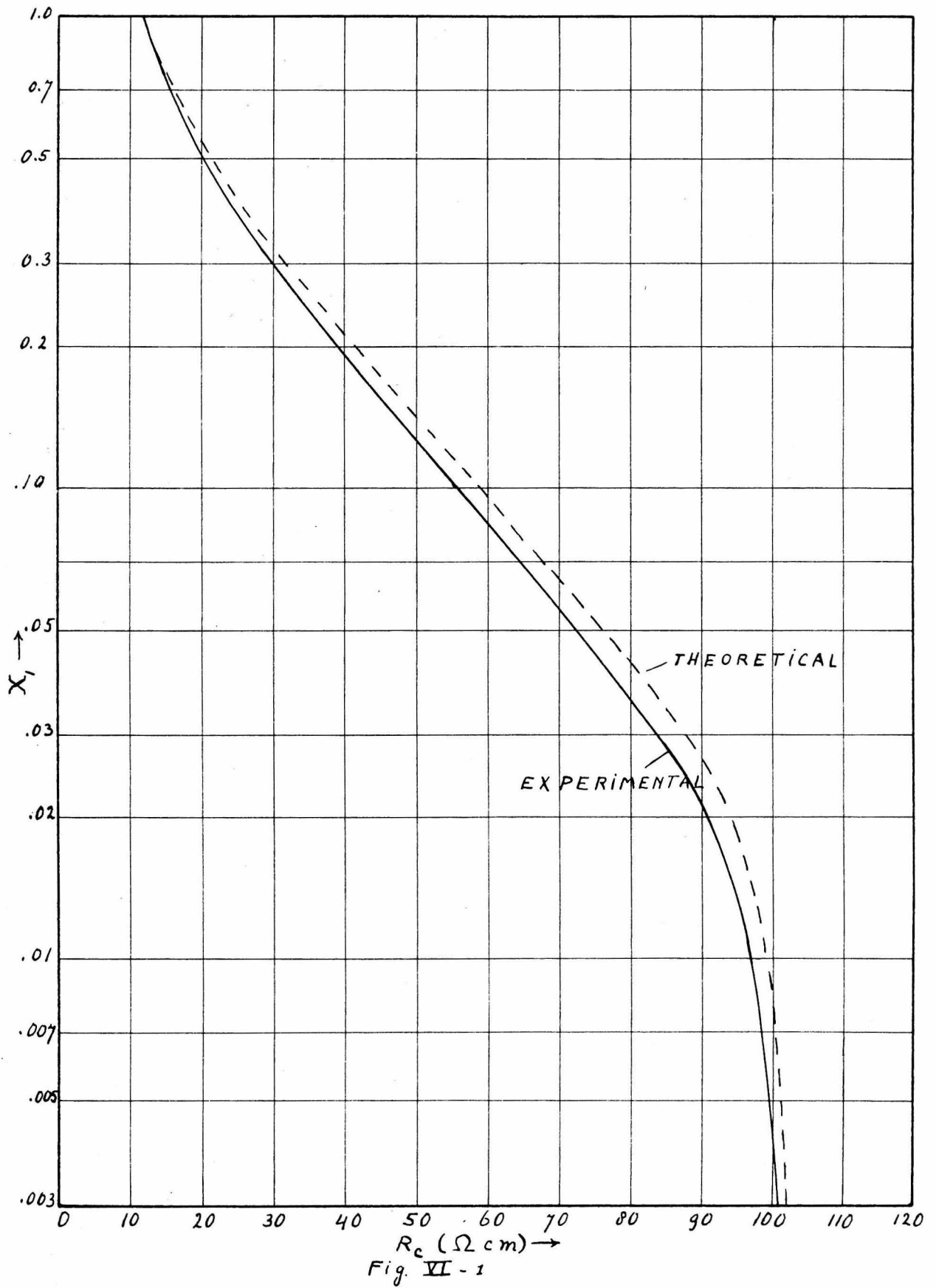
The examples show clearly that the interstitial water is completely replaced after ten times the pore volume has passed through the sample.

In the first examples, apparently some pollution took place and R_0 probably is too low in the last two stages.

In the second example, both solutions were rather concentrated to reduce effects of possible pollution of the effluent mixture. In order to avoid errors by using formula (6-3) an experimental graph of X_1 versus R_0 was made up, and used to find X_1 for the effluent mixtures. This graph is shown in Fig. VI-1. Also shown is the curve corresponding to computed values of X_1 using formula (6-3).

We see that even for concentrated solutions formula (6-3) gives fairly accurate results.

The results shown in Table VI-A definitely make the salt water retention hypothesis untenable. The explanation of the apparent decrease of the formation factor with increasing water resistivity offered by Patnode and Wyllie is a very logical one. In addition, these authors demonstrated that the conduction by part of the solids in reservoir rocks could be treated quantitatively for the case of water sands. The overall



resistivity of a water saturated sandstone was expressed in the form:

$$\frac{1}{R} = \frac{1}{\rho_f} + \frac{1}{\rho_w} = \frac{1}{\rho_f} + \frac{1}{F R_w} \quad (6-4)$$

Here ρ_f equals the resistivity of the conductive solids, as distributed, and ρ_w the resistivity of the water as distributed. $\rho_w = F R_w$ where R_w is the "bulk" water resistivity and F the formation factor, which would be found if none of the solids were conductive.

Formula (6-4) implies that the water saturated rock has an equivalent circuit consisting of two parallel resistances, one representing the resistance of the water phase and the other equal to the total resistance of the conductive solids, as distributed.

Physically this would be true, if the water and conductive solids were electrically insulated one from the other and both offered a continuous path for the current. This is not the case in a water saturated sandstone. On the contrary, the conductive solids and the water are everywhere in contact with each other and petrographic studies of thinsections of sandstones strongly suggest that in general the conductive solids do not form continuous layers or films over the sandgrains, but occur mostly in isolated small quantities randomly distributed throughout the rock.

Patnode and Wyllie proved that if the unknowns of equation (6-4), F and ρ_f , were solved from two measurements of R for corresponding values of R_w , one could calculate R for any other arbitrary value of R_w . The calculated R 's were compared with measured values and a very good agreement was obtained. This was taken by Patnode and Wyllie as a proof that formula (6-4) correctly represents the current conduction through

water saturated sandstones. Actually the above results only show that the conductivity of a watersand may be represented by an equation of the type $\frac{1}{R} = z - \frac{y}{R_w}$. The experiments of Patnode and Wyllie give us no conclusive information regarding the quantities z and y .

The same authors studied the behavior of mud slurries with regard to current conduction and found the empirical formula:

$$\frac{1}{R} = \frac{N^X}{R_f} \left(1 - \frac{1}{F}\right) + \frac{1}{F R_w} \quad (6-5)$$

where R_f is the bulk resistivity of the conductive solids, N is the fraction of conductive solids by volume and $X \approx 1$.

This again is of the type $\frac{1}{R} = z + \frac{y}{R_w}$, and we can assume that for rocks the quantity $\frac{1}{\rho_f}$ is the equivalent of the combination $\frac{N^X}{R_f} \left(1 - \frac{1}{F}\right)$.

It was also found that for slurries containing only conductive solids, there is a linear relationship between the percentage of solids $(1-P)$ and the conductivity of the solid phase $(1/\rho_f)$. Here P denotes the volume fraction of water, which is equivalent to the porosity in the case of a water sand.

This suggests that a homogeneous mixture of conductive solids and an electrolyte behaves exactly as a mixture of two electrolytes. For the latter we had derived the expression:

$$\frac{1}{R_0} = \frac{X_1}{R_1} + \frac{X_2}{R_2}$$

Applying this formula to a mixture of conductive solids and water we obtain:

$$\frac{1}{R_0} = \frac{X_f}{R_f} + \frac{X_w}{R_w} = \frac{1 - X_w}{R_f} + \frac{X_w}{R_w}$$

where X_f and X_w are the volume fractions of the conductive solids and the water respectively.

Rearranging gives:

$$R_0 = \frac{R_w R_f}{R_w - X_w (R_w - R_f)} \quad (6-6)$$

It seems reasonable to assume that the combination of randomly distributed conductive particles and water in a sandstone, behaves the same with respect to current conduction, as a slurry made up of the same amount of similar conductive solids and water.

The resistivity in the rock is then equal to F times the resistivity of the slurry (or the equivalent combination of conductive solids and water). Here F must be defined as the formation factor which we would find, if the conductive solids were replaced by water of the same type as that occupying the porespace.

The overall resistivity of the rock now becomes:

$$R = F R_0 = \frac{F R_w R_f}{R_w - X_w (R_w - R_f)} = \frac{F R_w R_f}{(1 - X_w) R_w + X_w R_f} \quad (6-7)$$

Letting $F R_f = l$, $X_w R_f = m$ and $1 - X_w = n$ we have:

$$R = \frac{R_w}{nR_w + m}$$

or $\frac{1}{R} = \frac{n}{l} + \frac{m}{R_w} = \frac{1 - X_w}{F R_f} + \frac{X_w}{F R_w} \quad (6-8)$

We see that (6-8) again is of the form $\frac{1}{R} = s + \frac{Y}{R_w}$ and therefore agrees with the experimental results of Patnode and Wyllie. Moreover formula (6-8) is also applicable to slurries containing both conductive and

non-conductive solids. F then represents the effect of the non-conductive solids on the resistivity of the system.

Patnode (28) found that for slurries which contain only solids of high resistivity (essentially non-conductive solids) the empirical relation $F = P^{-1.6}$ exists, where P is the volume fraction of water.

Assuming that the combination of conductive solids and water is equivalent to that of an electrolyte mixture this same relation should hold also for slurries and rocks containing conductive solids, if F is defined as in equation (6-7).

If we have two values of R for two corresponding values of R_w , we may solve equation (6-8) for the two unknown quantities $\frac{1 - X_w}{F R_f}$ and $\frac{X_w}{F}$. The resulting expressions for these quantities will be the same as those found by Patnode and Wyllie for $\frac{1}{\rho_f}$ and $\frac{1}{F}$.

We find:

$$\frac{X_w}{F} = \frac{(R_w)_1 (R_w)_2 [(R_o)_1 - (R_o)_2]}{(R_o)_1 (R_o)_2 [(R_w)_1 - (R_w)_2]} \quad (6-9)$$

$$\text{and } \frac{1 - X_w}{F R_f} = \frac{(R_w)_1 (R_o)_2 - (R_w)_2 (R_o)_1}{(R_o)_1 (R_o)_2 [(R_w)_1 - (R_w)_2]} \quad (6-10)$$

where $(R_o)_1$ and $(R_o)_2$ are the resistivities of the sandstone completely saturated with water respectively of a resistivity $(R_w)_1$ and $(R_w)_2$.

Once $\frac{X_w}{F}$ and $\frac{1 - X_w}{F R_f}$ are determined we can calculate any value of R_o resulting from any water resistivity, R_w or vice versa. In all the above expressions X_w is the volume fraction of water in the combination of conductive solids and water. Similarly $1 - X_w = X_f$ is the volume fraction of conductive solids in the same combination. If P_f denotes the amount

of conductive solids as a fraction of the total rock volume we then may write:

$$X_w = \frac{P}{P + P_f} = \frac{1}{1 + p_f} \quad \text{where} \quad p_f = \frac{P_f}{P}$$

$$\text{and } X_f = 1 - X_w = \frac{P_f}{P + P_f} = \frac{p_f}{1 + p_f}$$

Two experimental checks were made of the above formulae for overall resistivity using the same sandstones for which the mobility of the interstitial water was determined.

I. Saugus ss. $K = 5.31$ m. darcys $P = 11.15\%$

(Sample S-3)

$$(R_w)_1 = 12.3 \, \Omega \text{ cm.}$$

$$(R_o)_1 = 549 \, \Omega \text{ cm.}$$

$$(R_w)_2 = 156,300 \, \Omega \text{ cm.}$$

$$(R_o)_2 = 4025 \, \Omega \text{ cm.}$$

$$\frac{1 - X_w}{F R_f} = \frac{12.3 \times 4025 - 156,300 \times 549}{549 \times 4025 (12.3 - 156,300)} = .248 \times 10^{-3}$$

$$\text{Similarly } \frac{X_w}{F} = .0193 \quad \frac{F}{X_w} = 51.8$$

$$\text{This gives: } \frac{1}{R} = .248 \times 10^{-3} + \frac{.0193}{R_w}$$

$$\text{For } (R_w)_3 = 342.7 \text{ we obtain: } (R_o)_3 = 3282 \, \Omega \text{ cm.}$$

$$\text{The measured value was } (R_o)_3 = 3230 \, \Omega \text{ cm.}$$

II. Modelo shaley sand (Sample M-4)

$$K = 1.47 \text{ m. darcys} \quad P = 15.04\%$$

$$(R_w)_1 = 11.9 \, \Omega \text{ cm.}$$

$$(R_o)_1 = 367.7 \, \Omega \text{ cm.}$$

$$(R_w)_2 = 1024 \, \Omega \text{ cm.}$$

$$(R_o)_2 = 2876 \, \Omega \text{ cm.}$$

$$\frac{1 - X_w}{F R_f} = .32 \times 10^{-3}$$

$$\frac{X_w}{F} = .0286$$

$$\text{so that } \frac{1}{R} = .32 \times 10^{-3} + \frac{.0286}{R_w}$$

For $(R_w)_3 = 106.6 \ \Omega \text{ cm}$, we find $(R_o)_3 = 1700 \ \Omega \text{ cm}$.

The measured value was $(R_o)_3 = 1646 \ \Omega \text{ cm}$.

As stated before, the experiments of Patnode and Wyllie carried out on a much larger scale, all verify the validity of a relation of

the type $\frac{1}{R} = a + \frac{Y}{R_w}$ for the case of watersands.

Resistivity of Oil and Gas Sands

Before the idea of current conduction by part of the solids in porous rocks was introduced, the relation between rock resistivity and hydrocarbon content was generally given by an empirical formula of the type:

$$S_w = \left(\frac{R_o}{R}\right)^{1/n} \quad (6-11)$$

$$\text{or } R = R_o (S_w)^{-n} \quad \text{and} \quad \frac{1}{R} = \frac{(S_w)^n}{R_o}$$

This relation was first given general significance by the work of Archie (29), who found experimentally $n \approx 2$.

Since Archie's work, several other investigators carried out extensive experiments using many types of rocks and found that the value of n will vary considerably for different types of sandstones.

n was believed to have a specific value for any given rock.

Dakhnov (5, 30) obtained from experimental data $1.7 < n < 4.3$.

Bailey and others (31) found $1 < n < 2.5$.

All these experiments were made on sandstones of which the content of conductive solids was unknown and completely neglected. It is obvious that, if the effect of conductive solids is neglected and Archie's

formula applied as such, the apparent values of n will not only vary from rock to rock, but also will depend upon the water salinity.

Computations from our experimental data indicate, however, that Archie's formula does apply, with n equal to or nearly equal to 2 in cases where the influence of conductive solids is negligible or small, because of the high salinity of the interstitial water.

Table VI-B shows examples of these data.

TABLE VI-B

Sample	No.	P(%)	K n. darcys	S_w	R_w Ω cm	R_o Ω cm	R Ω cm	n
Berea ss	(0-7)	27.3	22.0	.19	40.7	568	14860	1.96
" "	(0-8)	28.9	40.2	.188	30.3	404	11470	2.0
Pico ss	P-4a	33.3	318	.295	36.1	386	4550	2.02
" "	P-4b	28.4	390	.21	35.9	271	7610	2.14
Saugus ss	S-3h	10.6	2.67	.675	38.2	1548	3478	2.06

The deviations from the value of $n = 2.0$ may be partly due to combined experimental errors and the influence of conductive solids. Even if these would be eliminated it would not be likely that n would have a completely constant value, but the variations in n will in general be small. Considering the enormous differences between the types of sandstones used in obtaining the data of Table VI-B, and the relatively small variations in n , it is believed that most of the anomalous values of n found by the aforementioned authors, are due to neglecting the influence of the conductive solids.

To take the effect of conductive solids into account, we must go back to the expressions for R in terms of F , R_w and the amount and (or) resistivity of the conductive solids.

It is in trying to expand these formulae to include the presence of hydrocarbons that the differences between the equations of Patnode and Wyllie and those resulting from the assumption of a homogeneous mixture of the conductive media become evident.

If one assumes an independent conduction through the conductive solids as suggested by the formula:

$$\frac{1}{R_0} = \frac{1}{\rho_f} + \frac{1}{F R_w}$$

the presence of oil would not have any effect on that part of the total conductivity represented by $1/\rho_f$.

It is obvious that the conduction through the water is influenced by the presence of oil in the same way as in the case where none of the solids are conductive. This means the term $\frac{1}{F R_w}$ is replaced by

$$\frac{(S_w)^n}{F R_w} .$$

Again combining the two conductivities for the parallel paths we obtain:

$$\frac{1}{R} = 1/\rho_f + \frac{(S_w)^n}{F R_w} \quad (6-12)$$

The outcome of experiments to test formula (6-12) proved the assumption of an independent conductive path through the solids untenable.

The evidence to that effect will be illustrated by an example:

A sample of Berea sandstone was saturated with water of two

different salinities successively and F and ρ_f were computed, using equation (6-4), after the resistivities were measured in both cases.

The following data were obtained:

$$\begin{aligned} (R_w)_1 &= 13.6 \quad \Omega \text{ cm.} & (R_o)_1 &= 190 \quad \Omega \text{ cm.} \\ (R_w)_2 &= 1009 \quad \Omega \text{ cm.} & (R_o)_2 &= 8500 \quad \Omega \text{ cm.} \end{aligned}$$

This leads to $F = 14.1$ and $1/\rho_f = .0000476$ or $\rho_f = 21,000 \quad \Omega \text{ cm.}$

The sample was then saturated with crude oil by the capillary pressure method until an oil saturation of 0.70 was obtained. This means $S_w = .22$.

The resistivity of the sample was now found to be 82,800 $\Omega \text{ cm.}$

Applying formula (6-12) gives:

$$\frac{1}{82,800} = \frac{1}{21,000} + \frac{(.22)^2}{14.1 \times 1009} \quad \text{which makes } n \text{ imaginary.}$$

Physically, the above result means that, assuming an independent continuous path through the conductive solids, the conductivity of the conductive solids as distributed would be larger than the combined conductivity of the entire system, which of course is not possible.

This forces us to abandon the concept of a network of conductive solids with an independent resistivity of the conductive solids as distributed.

The alternative hypothesis of homogeneous mixture of the conductive media leads to the following relations:

For a water sand we have, as described before:

$$R_o = F R_w$$

Assuming now that the influence of the non-conductive solids and hydrocarbons on the conductive mixture is the same as the influence on the water conductivity (as distributed) in the absence of conductive

solids we obtain:

$$S_w = \left(\frac{R_0'}{R}\right)^{\frac{1}{2}} = \left(\frac{F R_0'}{R}\right)^{\frac{1}{2}}$$

Here $R_0' \neq R_0$, as in the case of oil saturation the amount of interstitial water in the rock is diminished, while the content of conductive solids stays the same. Therefore the proportions of the two components in the "slurry" are different in the two cases.

We can write the above expressions as follows:

$$R_0' = \frac{F R_f R_w}{R_w - X_w' (R_w - R_f)} \quad (6-13)$$

$$\text{or } F R_0' = R S_w^2 = \frac{F R_f R_w}{R_w - X_w' (R_w - R_f)} \quad (6-14)$$

$$\text{Here } X_w' = \frac{P S_w}{P S_w + P_f}$$

In the case of a water sand we had $X_w = \frac{P}{P + P_f}$ which gives

$$\frac{P_f}{P} = \frac{1}{X_w} - 1 .$$

$$\text{Substituting gives } X_w' = \frac{S_w}{S_w + 1/X_w - 1} \quad (6-15)$$

Referring back to the parameters $l = F R_f$, $m = X_w R_f$ and $n = 1 - X_w$

we have

$$\left(\frac{P}{P_f}\right) \frac{X_w}{1 - X_w} = \frac{l/n}{l/m R_f} = \frac{m}{n R_f} \quad \text{or} \quad X_w = \frac{m/n}{R_f + m/n}$$

$$\text{Similarly } X_w' = \frac{m/n}{m/n + R_f/S_w}$$

If we have two equations of the type

$$(R_0)_1 = \frac{F R_f (R_w)_1}{(R_w)_1 - X_w [(R_w)_1 - R_f]} \quad (6-16)$$

where the respective values of $(R_0)_1$ and $(R_w)_1$ are known we can solve for the ratios ρ/n and ρ'/n from which we obtain n/ρ .

Combining one of the equations (6-16) with equation (6-14) we have for the case that R_w is the same in both expressions:

$$R_0 \left[R_w - X_w (R_w - R_f) \right] = R S_w^2 \left[R_w - X_w' (R_w - R_f) \right]$$

Substituting the expressions for X_w and X_w' and rearranging, we obtain:

$$\frac{\rho/n}{R_f + \rho/n} R_0 - \frac{\rho/n R S_w^2}{\rho/n + R_f/S_w} = \frac{R_0 R_w - R S_w^2 R_w}{R_w - R_f} \quad (6-17)$$

This is a cubic equation for S_w and S_w could be found if R_f is known.

R_f is the bulk resistivity of the conductive solids occurring in reservoir rocks. In general, these consist mostly of argillaceous materials, combined with substances like limonite, etc. The bulk resistivity of such material must have a value within a definite rather limited range, comparable with the bulk resistivities of shales. As pointed out by Patnode and Wyllie, the actual resistivity of neighboring shales might be a good approximation except for cases where the content of limonite and similar substances is large. We might therefore assume a value of R_f within its probable range and solve for S_w .

As the error in R_f may be appreciable, it is of importance to know how sensitive equation (6-17) is to variations in R_f .

To demonstrate the effect of such variations, equation (6-17) was applied to the case of the Berea sandstone (sample O-10), and solved for S_w , assuming values of R_f respectively of 10, 50, and 100 Ω cm. These values are representative for the range of values of the

resistivities of shales.

For our example we had:

$$a/n = \frac{21,000}{14.1} = 1490$$

$$R_w = 1009 \ \Omega \text{ cm.}$$

$$R_0 = 8500 \ \Omega \text{ cm.}$$

$$R = 82,800 \ \Omega \text{ cm.}$$

Substituting these values in equation (6-17) gives us three values for S_w , of which two are negative and therefore of no physical meaning. The third value is the actually prevailing water saturation.

The following values were obtained:

R_f (Ω cm)	S_w
100	0.245
50	0.227
10	0.210

The experimentally determined value of S_w (obtained both volumetrically and by weighing) was .220 .

This demonstrates that even with a large uncertainty in R_f , the "homogeneous mixture" hypothesis leads to formulae that approximate actual conditions well enough for all practical purposes. The results obtained also prove that a rough estimate of R_f gives a fairly accurate value for S_w .

Knowing the actual value of S_w we are in a position to compute the true value of R_f . This is most easily done graphically. Using this procedure we find $R_f = 33 \ \Omega$ cm.

The discussed experiments and derivations serve to outline the general relations between the resistivity and the fluid content of porous rocks.

Application of the Derived Formulae to Electrolog Interpretation

In practice, the electrolog gives us for each formation two quantities; namely, the true resistivity of the undisturbed formation, and the resistivity of the infiltrated zone.

In some cases, however, the upper part of a formation may be saturated with oil or gas and the lower part with water. This is often the case in wells at the periphery of a field or structure where the oil-water interface cuts the tilted beds. Where we have such a combination of an oil zone and a water zone in the same reservoir rock, the electrolog furnishes us four quantities; namely, the true resistivities of the oil sand and of the watersand, and the invaded zone resistivities for both zones.

The fact that both zones are in the same reservoir rock is concluded from the self potential curve of the log, which shows the combination as one unit.

Fig. VI-2 gives a somewhat idealized example of the electrolog curves for such combination.

From the values of R_2 and R_1 of the water zone and the R_2 of the oil zone, S_w may be calculated following the procedure outlined for the example of the Berea sandstone, after having assumed a value for R_f .

Using the additional equation furnished by the measurement of R_1 of the oil zone it is possible, however, to compute the actual value of R_f , if we know the relation between S_w and $(S_w)_1$, the water saturation of the infiltrated zone. It was shown by Tixier (19) that the latter relation is of the form $(S_w)_1 = S_w^{\frac{n}{2}}$, where $n \approx 2$. The details of this relation will be discussed in the next part of this thesis.

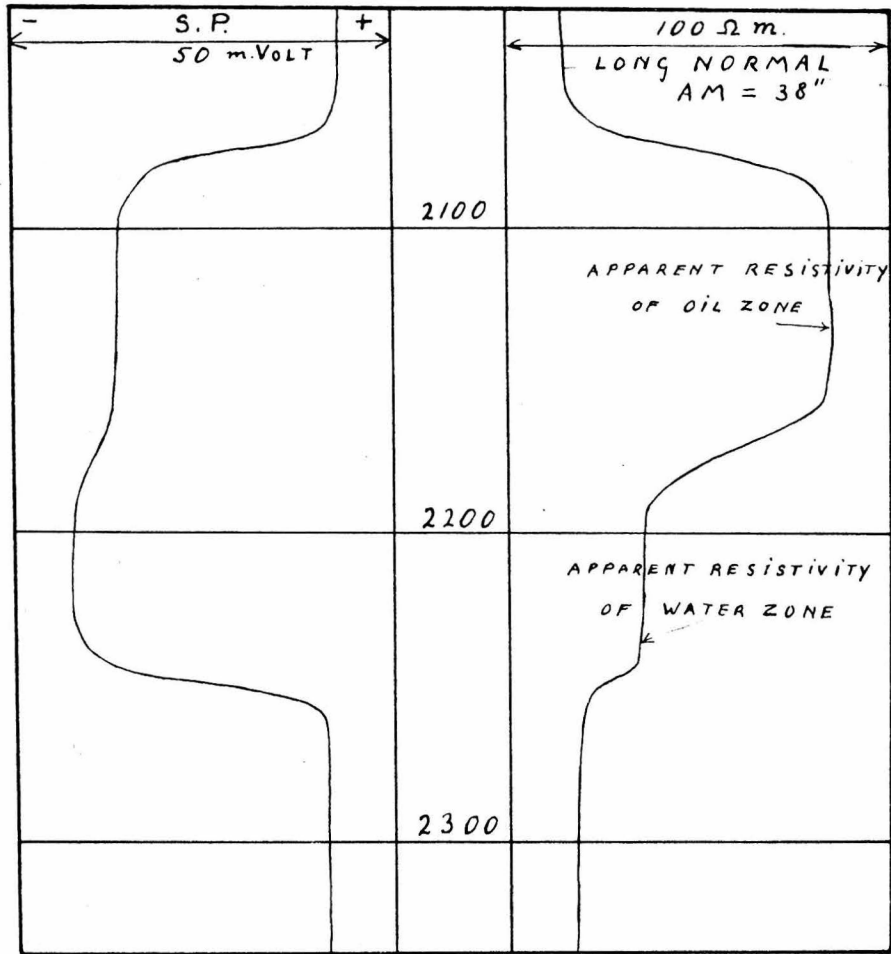


Fig. VI - 2

Summarizing the relationships for the case where we have a distinct oil zone and water zone in the same rock unit we have:

From the R_1 and the R_t of the water sand, denoted respectively by $(R_1)_1$ and $(R_t)_1$ we find from equations (6-9), (6-10) and the definitions of m and n :

$$N = m/n = \frac{R_w R_{mf} [(R_t)_1 - (R_1)_1]}{R_w (R_1)_1 - R_{mf} (R_t)_1} \quad \text{or} \quad 1/N = \frac{(R_{mf}/R_w) R_t - R_1}{R_{mf} (R_1 - R_t)} \quad (6-18)$$

where R_{mf} is the mud filtrate resistivity.

Denoting the R_1 and R_t of the oil zone by $(R_1)_2$ and $(R_t)_2$ we may write the equation (6-17) as:

$$\frac{m/n}{R_f + m/n} (R_t)_1 - \frac{m/n}{m/n + R_f/S_w} (R_t)_2 S_w^2 = \frac{(R_t)_1 R_w - (R_t)_2 S_w^2 R_w}{R_w - R_f} \quad (6-19)$$

$$\frac{m/n}{R_f + m/n} (R_t)_1 - \frac{m/n}{m/n + R_f/(S_w)^2} (R_t)_2 S_w = \frac{(R_t)_1 R_w - (R_t)_2 S_w R_w}{R_w - R_f} \quad (6-20)$$

Assuming values of R_f we can plot S_w as a function of R_f for relations (6-19) and (6-20). The actual R_f and S_w are found as the respective values at the intersection of the two graphs.

In most cases, however, there is no distinct separation between a water and an oil horizon in the same rock unit and we do not know whether the rock contains any hydrocarbons or not. In these cases we must try to solve for S_w . If $S_w = 1$ we have a water sand, if $S_w < 1$ we have an oil or gas sand. As we cannot solve for m/n directly we must go back to the original relations for X_w' of the undisturbed formation and X_w'' of the infiltrated zone.

On page 98 we showed that

$$I_w' = \frac{N}{N + R_f/S_w} \quad \text{with} \quad N \equiv n/n$$

If we use again $(S_w)_i^2 = S_w$ we have for the invaded zone

$$I_w'' = \frac{N}{N + R_f/(S_w)_i} = \frac{N}{N + R_f/(S_w)^{\frac{1}{2}}}$$

Using a probable value for R_f , for instance $R_f = 30 \Omega \text{ cm}$ and substituting the above expressions in equation (6-14) we obtain:

$$R_t (S_w^2) = \frac{30 F R_w}{R_w - \frac{N}{N + 30/S_w} (R_w - 30)} \quad (6-21)$$

$$\text{and } R_1 S_w = \frac{30 F R_{mf}}{R_{mf} - \frac{N}{N + 30/(S_w)^{\frac{1}{2}}} (R_{mf} - 30)} \quad (6-22)$$

As was shown on page 98

$$\frac{P}{P_f} = \frac{N}{R_f} \quad \text{or} \quad 1/N = \frac{P_f}{P} \quad \frac{1}{R_f} = \frac{P_f}{R_f} \quad (6-23)$$

with $p_f = P_f/P$.

In equation (6-23) p_f denotes the amount of conductive solids per unit pore space, while R_f is nearly a constant. This suggests that N is related to the electrochemical formation coefficient, C . The latter quantity was introduced and discussed in detail in a thesis by this author (32) on the characteristics of electrochemical potentials encountered in drill-holes.

Fig. VI-3 shows the relation between values of N and C determined for various sandstones. Although the number of points given in VI-3 is small, the great differences in the types of sandstones tested make it quite evident that the correlation represents a general relationship.

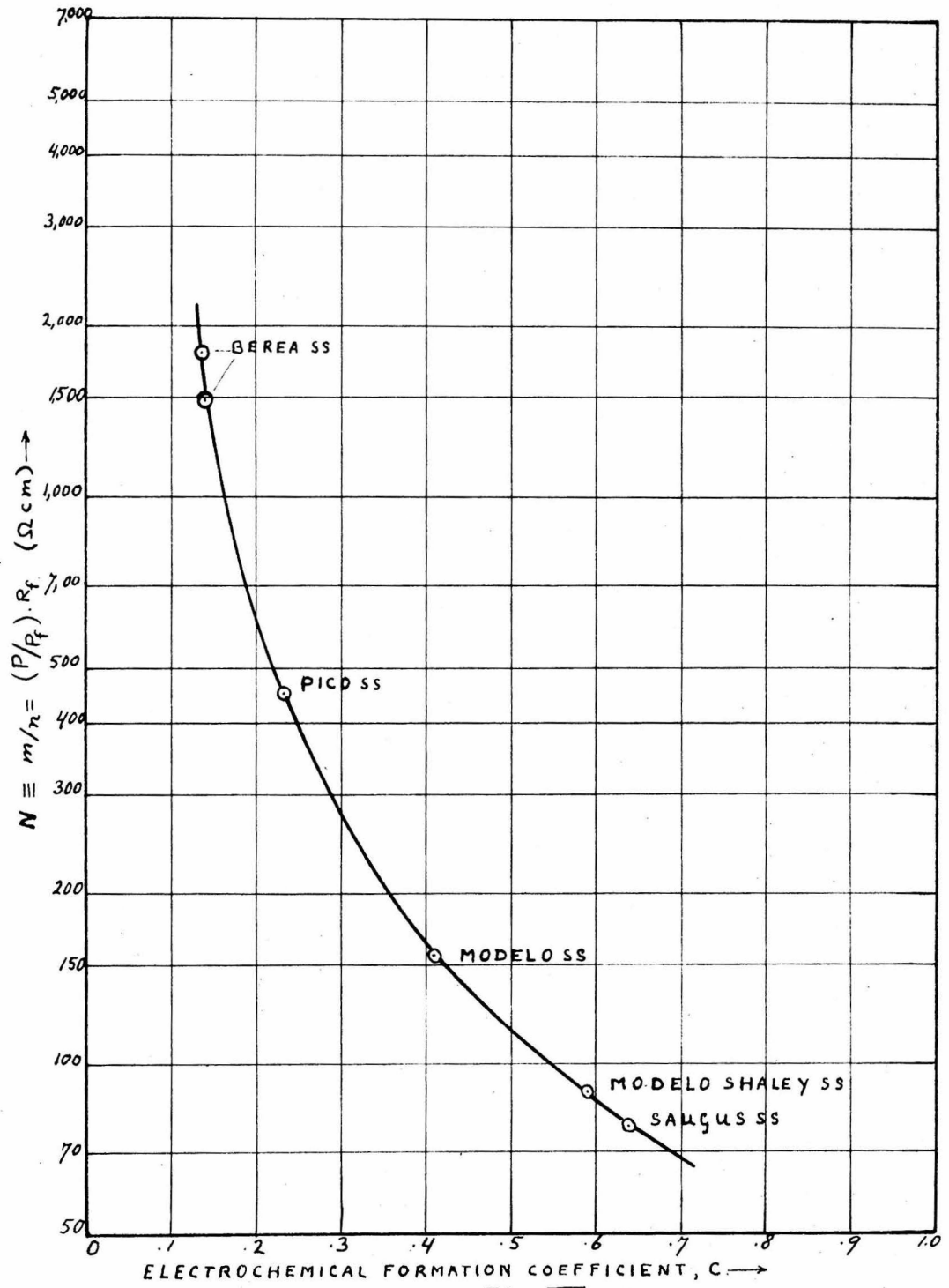


Fig. VI - 3

In the above mentioned thesis it was also shown, how using the relation between N and C , and data obtained from the self potential curves registered on the electrologs, we can determine both N and R_w for water sands.

For all the horizons in a particular well that are typically water-bearing R_w may be computed. For all horizons that might be suspected to contain hydrocarbons the value for R_w is interpolated between those for the nearest water sands and N is determined using the self potential kick for the formation in question.

Equation (6-21) and (6-22) then permit us to compute S_w and F , which is most easily done graphically.

F is of importance for the determination of porosity using the empirical formula

$$F = p^{-1.6}$$

Knowing the porosity and the oil saturation ($S_o = 1 - S_w$) we can calculate the total amount of oil present per acre foot of the oil horizon.

PART VII

Experimentally Determined Characteristics of the Infiltrated
Zones of Permeable Formations

1) Resistivity profilesa) Water sands

In the preceding parts of this thesis, some of the factors governing the characteristics of the infiltrated zones of permeable formations have been discussed. The primary purpose of this section is to determine the actually existing resistivity distributions in the invaded zones, as functions of the radial distance from the boreface.

As outlined in Part IV all experiments were performed on relatively small cylindrical samples, with a controlled initial fluid content which were submitted to uni-directional invasion by the infiltrating water. In most of the experiments, water of a given salinity was used to invade the samples, instead of actual drilling muds. This was done to avoid the retarding action of the mudcakes formed on the face of the samples.

At the beginning of the experimental work drilling muds of various compositions were forced through samples of Berea and Pico sandstones.

These experiments showed that all colloidal material from the muds were sieved out, at the face of the sandstones or in the first few centimeters of the rock. The filtrates obtained through cores of 2" length were in all respects (resistivity and absence of colloidal material) identical to filtrates obtained through Whatman #52 filter paper. This means that for all practical purposes no errors are introduced by using simple aqueous solutions instead of drilling muds, in experiments on

the changes in resistivities and fluid contents of rocks upon invasion.

After any arbitrary amount of fluid had passed through the sample the resistivity of the sample could be measured, and in this way graphs were made up, showing the sample resistivity as a function of the amount of fluid passed through the sample.

In the case of radial infiltration around a drill hole, the amount of fluid passed through a unit cross-sectional area perpendicular to the direction of flow will be a function of the radial distance from the boreface. Therefore the resistivities of our samples after various amounts of flushing by the infiltrating water, correspond to the resistivities of points at various distances from the boreface, in the actual invaded zones of permeable formations. Unfortunately the relations are complicated by the influence of the longitudinal dimensions of the cores.

The resistivity measurements do not represent the conditions at a single point, but give a weighted average for the entire core. The weighting is a function of the electrode spacing and the distance from the face of the core, at which the measurements are made.

Measurements of the content of the flushed out connate water in the effluent mixture, however, provide us a means of approximating the average amount of connate water left in the core. We also know the amount of filtrate passing through the upper face of the core and the amount of filtrate in the effluent which equals the amount that passed through the lower (out-flow) face. These values may be combined to give an average amount of filtrate passed through the core. We can plot therefore the average amount of connate water retained in the core, as a

function of the average amount of filtrate passed through.

Fig. VII-1 shows this relation for the Saugus ss. From the data the corresponding sample resistivities may be calculated, using the methods outlined in Part VI of this thesis:

$$\begin{aligned} (R_w)_1 &= 39.8 \quad \Omega \text{ cm.} & (R_o)_1 &= 1362 \quad \Omega \text{ cm.} \\ (R_w)_2 &= 993 \quad \Omega \text{ cm.} & (R_o)_2 &= 4700 \quad \Omega \text{ cm.} \end{aligned}$$

From these values we obtain:

$$\frac{X_w}{F} = .02163 \qquad \frac{1 - X_w}{F R_f} = .191 \times 10^{-3}$$

so that $1/R = .191 \times 10^{-3} + \frac{.02163}{R_w}$

For the mixture of initial connate water and invading water in the core

R_w is found as:

$$R_w = \frac{(R_w)_1 (R_w)_2}{X_1 (R_w)_2 + (1 - X_1) (R_w)_1} = \frac{39,500}{993 X_1 + 39.8 (1 - X_1)}$$

where X_1 is obtained from Fig. VII-1.

The resulting values of R for various amounts of filtrate passed through the sample are plotted in Fig. VII-2.

Also shown in Fig. VII-2 are three points representing direct measurements of the sample resistivity for given amounts of influent filtrate. We see that taking the measured resistivity of the sample as average sample resistivity and the influent filtrate as average amount of flushing, does not introduce any serious errors.

Once the variation of the resistivity with amount of filtrate passed through the sample has been determined, the changes in resistivity as a function of the radial distance r from the boreface, in

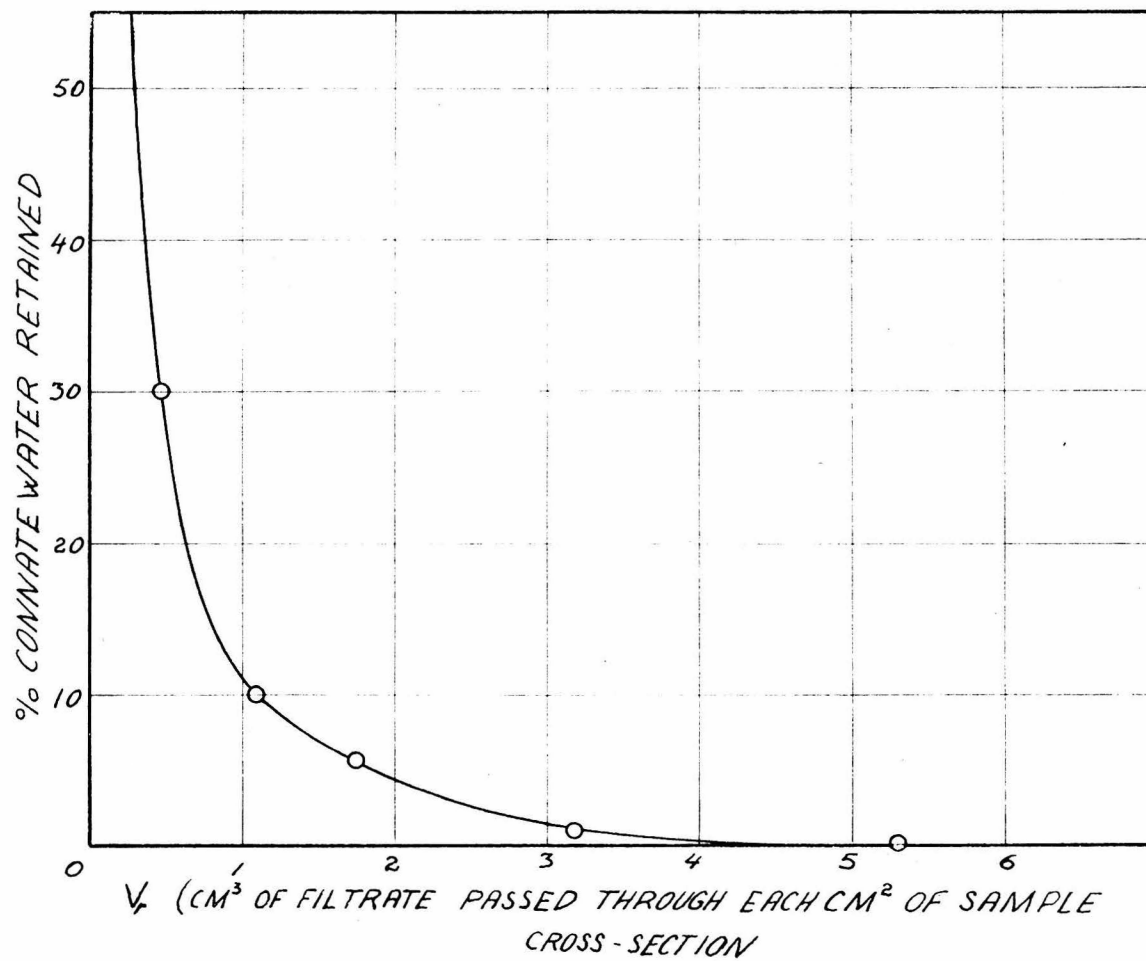


FIG VIII-1

107B

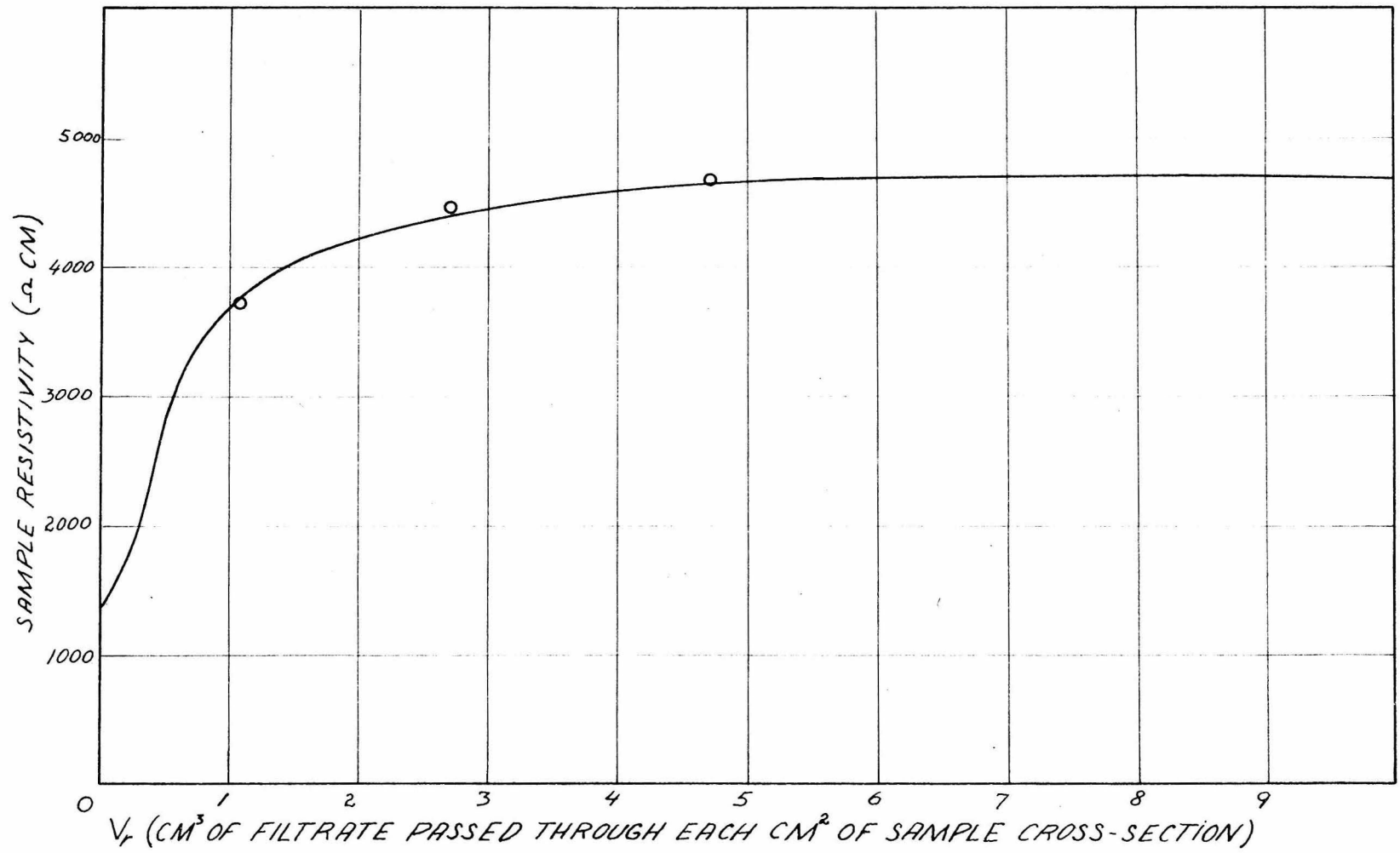


FIG VII-2

the case of radial infiltration, may be computed in the following manner:

Consider a slice of 1 cm. thickness of the borehole and infiltrated zone. In this slice we will limit our attention to a sector, corresponding to 1 cm. circumference of the drill hole cross-section. (See Fig. VII-3). The intersection of this sector with the boreface has a surface area of 1 cm². We now divide this sector into volumes V_1, V_2 , etc., by arches concentric with the borehole, corresponding to equal increments in r . In each of these volumes we assume the amount of invading liquid retained to be constant. If the amount of invading liquid retained in volume V_1 is denoted by X_1 , in volume V_2 by X_2 , etc., we first assume that $X_1 = (X)_{r_0}$, $X_2 = (X)_{r_1}$, etc. This means that in each volume we make X equal to its actual value at the inner boundary of the volume.

Using this assumption we have:

$$\text{Amount of invading liquid remaining in } V_1 = \frac{r_1^2 - r_0^2}{2 r_0} \cdot \varphi \cdot (X)_{r_0}$$

Where φ is the fractional porosity and $\frac{r_1^2 - r_0^2}{2 r_0} =$

$$\frac{1}{2\pi r_0} \times \pi (r_1^2 - r_0^2) = V_1$$

If $(v)_{r_0}$ is the total quantity entering the sector through its 1 cm² cross-section at the boreface we have:

$$\text{Flowing into } V_2: (v)_{r_0} = \frac{r_1^2 - r_0^2}{2 r_0} \cdot \varphi \cdot (X)_{r_0}$$

and the amount of invading liquid per cm² of the inner boundary of V_2 is:

$$(v)_{r_1} = r_0/r_1 \left[(v)_{r_0} - \frac{r_1^2 - r_0^2}{2 r_0} \cdot \varphi \cdot (X)_{r_0} \right]$$

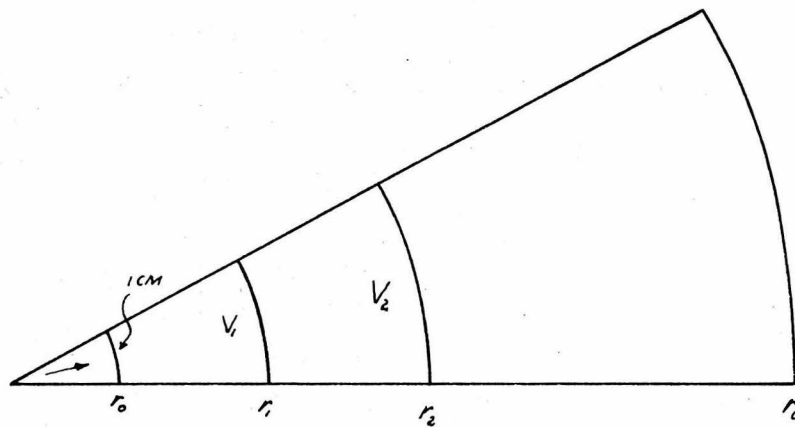


FIG VIII-3

$(v)_{r_3}$, etc.

The general formula for v_r becomes:

$$\frac{r_{n+1}}{r_0} (v)_{r_{n+1}} = \frac{r_n (v)_{r_n}}{r_0} - \frac{(r_{n+1})^2 - (r_n)^2}{2 r_0} \cdot \varphi (X)_{r_n} \quad (7-1)$$

$(X)_{r_n}$ is found from Fig. VII-1 corresponding to an amount $(v)_{r_n}$ of invading liquid, which was determined from the preceding equation.

In this manner we find v_r as a function of r . Another approximation of this relation can be made by assuming $X_1 = (X)_{r_1}$; $X_2 = (X)_{r_2}$ etc., that is by making X in each volume equal to its actual value at the outer boundary of the volume.

The actual conditions will result in a relation which falls in between the two approximations determined above.

Fig. VII-4 gives v_r as a function of r , calculated in the above manner, showing both the bracketing values and the averaged relationship. The latter is used for further computations.

We now have v_r as a function of r and the resistivity R as a function of v_r . Combining the two relations gives R as a function of r , which means the actual resistivity in the infiltrated zone as a function of the radial distance from the center of the hole.

Fig. VII-5 shows this actual resistivity distribution. We see that the resistivity in the infiltrated zone is not constant throughout the entire zone, and that the outer boundary is not a sharp discontinuity in the resistivity distribution. For all practical purposes we may however replace the transition zone by two parts of constant resistivity separated by a discontinuity as indicated by the dashed line in Fig. VII-5.

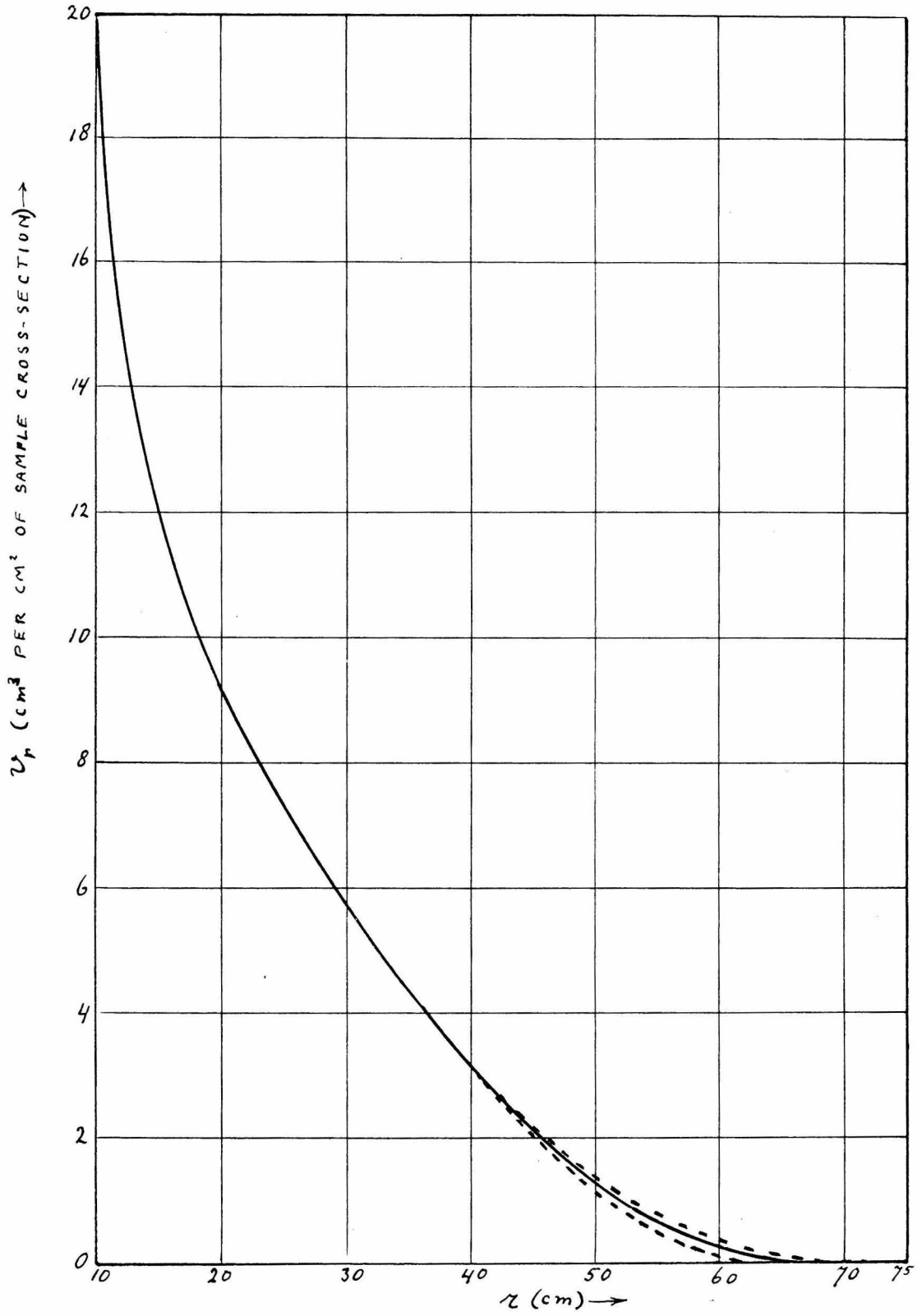


Fig. VII-4

109B

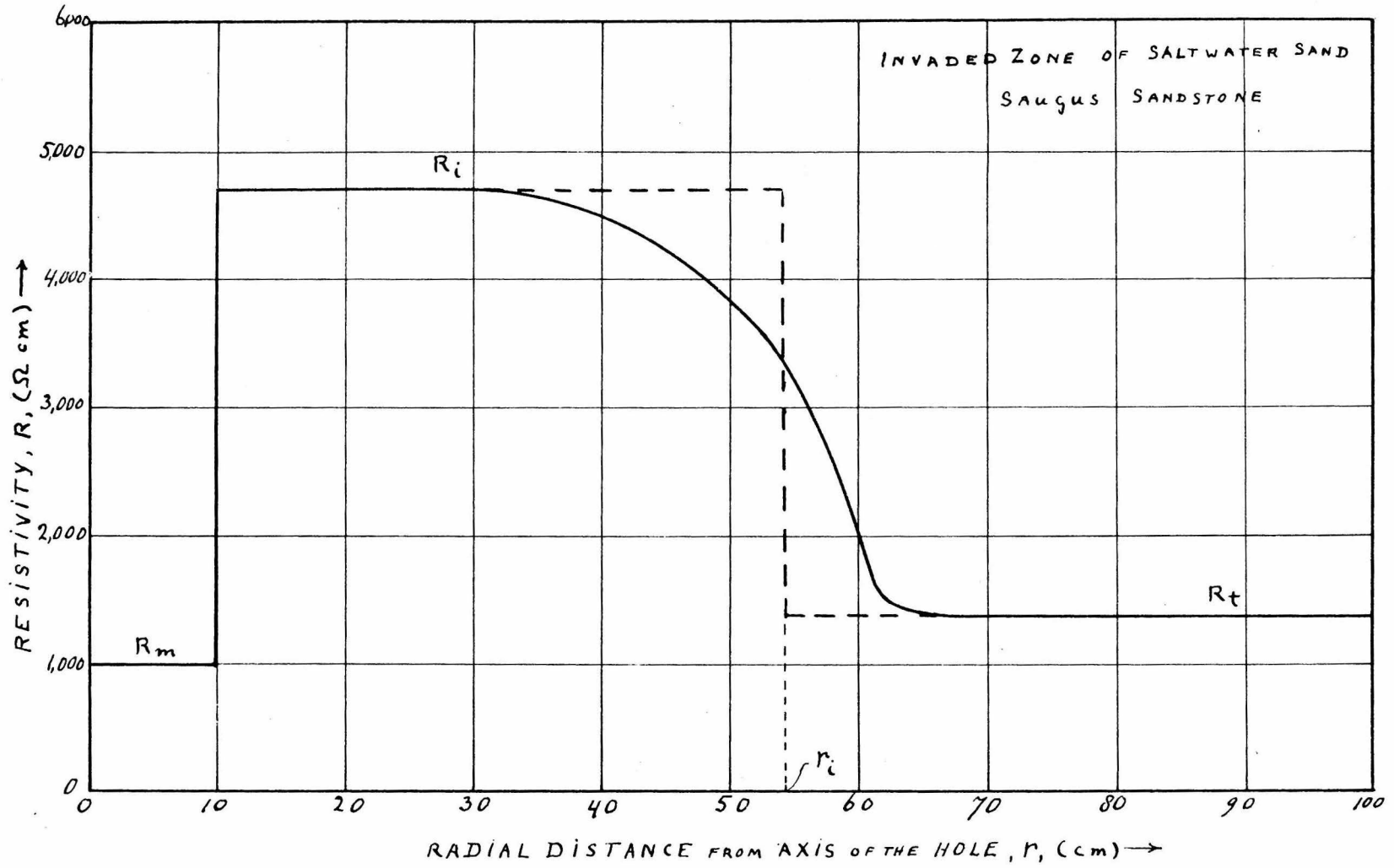


Fig. VII - 5

The radius of the infiltrated zone, as determined with the aid of apparent resistivity curves, by the method described in Part II of this thesis, represents the distance from the axis of the hole to this hypothetical discontinuity. In Fig. VII-5 the radius of infiltration, r_1 , equals 54.5 cm. As we had assumed $r_0 = 10$ cm. we have in this case $r_1 = 5.45 r_0$. This represents an average amount of infiltration.

For larger amounts of infiltration the transition zone remains practically unchanged, while the zone of constant resistivity becomes larger. In such cases, the approximation made by representing the actual resistivity distribution by a constant R_1 , becomes better.

For smaller radii of infiltration the zone of constant resistivity becomes smaller and the approximation used for purposes of interpretation becomes less accurate.

In the case of invasion of a fresh water sand by a more saline mudfiltrate, the resistivity distribution exhibits the same characteristics as those shown in Fig. VII-5, except that the true resistivity is larger than the infiltrated zone resistivity. The transition zone is therefore represented by an upward curve. All remarks made regarding the approximation of the actual resistivity by a constant resistivity, R_1 , apply also in this case.

The displacement of the connate water by the mudfiltrate can be regarded in part as a piston mechanism, where the filtrate pushes a fraction of the connate water ahead of itself. However, an important part of the removal of the connate water is due to diffusion of the salt ions into the mudfiltrate. It would be logical to assume that the non-bound connate water is removed by the piston mechanism of the

invading fluid, especially in the larger pores. The bound water gives off its salt ions by diffusion into the less saline filtrate.

To check these assumptions, the influence of the rate of invasion on the character of the transition zone was determined experimentally. The results are shown in Fig. VII-6, which gives the amounts of connate water, replaced by the filtrate, as a function of the amount of filtrate passed through the sample, for the Saugus sandstone.

We see that the smaller the pressure gradient for a given sample, or the smaller the rate of flow during infiltration, the more rapid the replacement of the connate water takes place.

This means that for slow rates of infiltration the transition zones of the resistivity profiles of the invaded zones, will be relatively less important.

In practice the pressure gradients encountered during the infiltration of permeable formations are mostly smaller than the gradient under which invasion took place in the experimental case, worked out and shown in Figs. VII-1 through VII-5. In this case the pressure gradient was 43 psi/inch.

The transition zones of the resistivity profiles will therefore in general be smaller than the one shown in Fig. VII-5 and the approximation made by assuming $R_1 = \text{constant}$, will be better than in our example.

The removal of salt ions by diffusion into the mudfiltrate for a given amount of filtrate passed through a unit volume of rock depends more directly on the rate of flow of the filtrate than on the pressure gradient.

This means that in very permeable sands the rate of removal of the

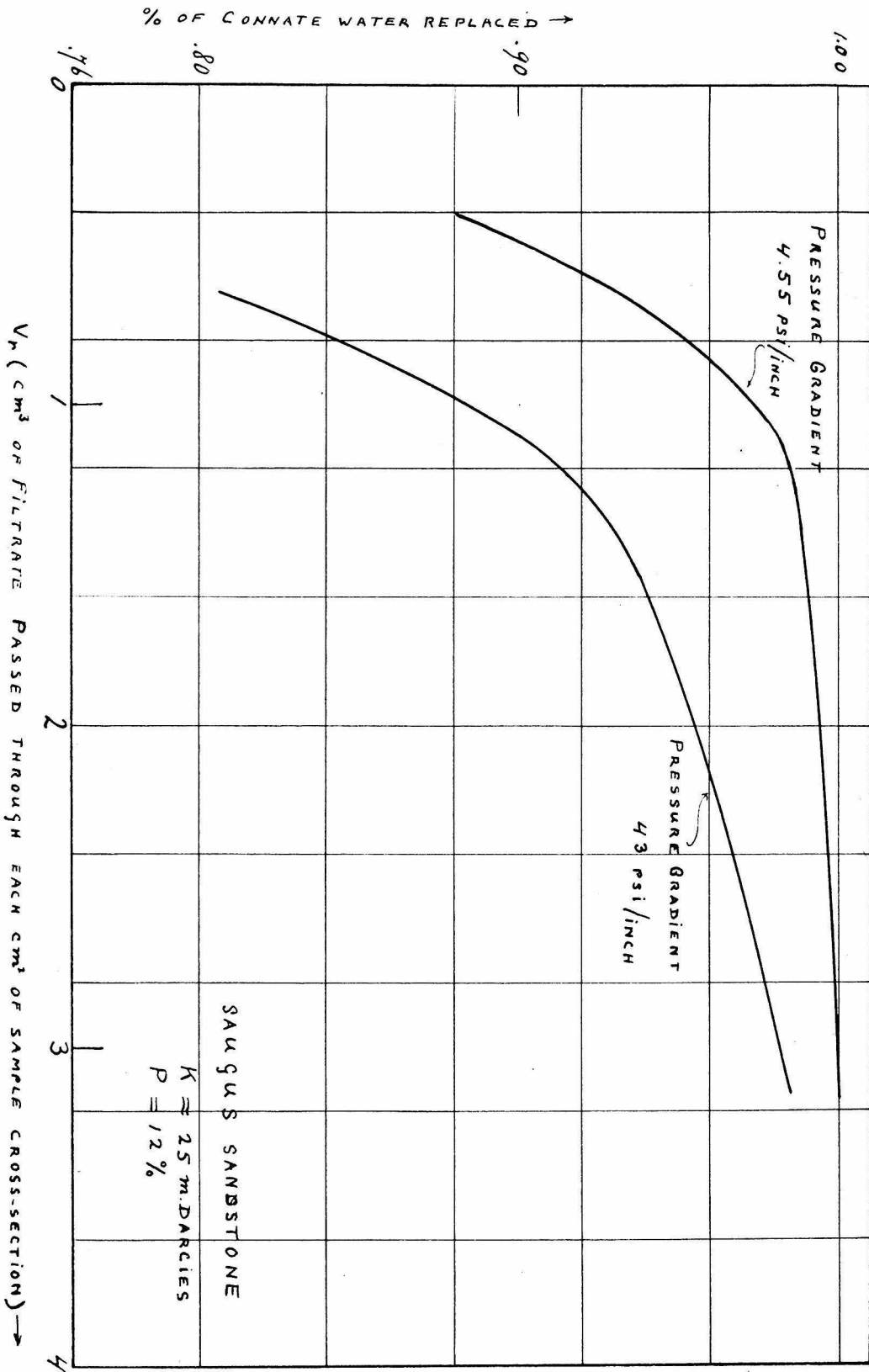


Fig. VII-6

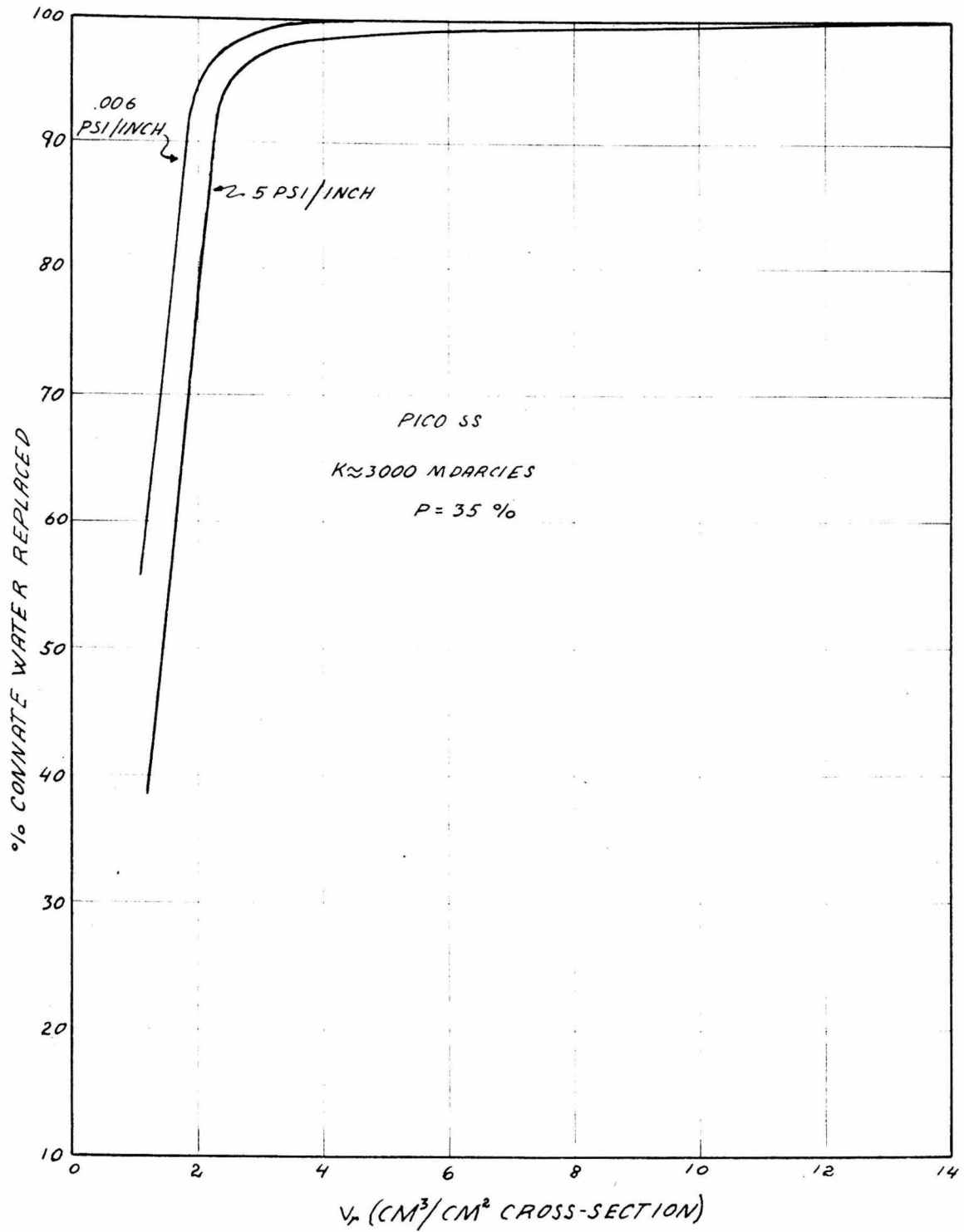


FIG VII-7

salt ions from the bound water will be slower than in a relatively tight sand. However this effect is partly offset by the fact that there exists a rough correlation between percentage of bound water and permeability of sediments.

The more permeable formations will have less bound water and larger pores and therefore the amount of salt ions to be removed strictly by diffusion will be percentagewise smaller.

In order to obtain a clear indication of the overall effect of permeability on the replacement rate of the connate water, experiments were made on a very permeable Pico sandstone ($K \approx 300$ m. darcys) and the results were compared with those obtained for the Saugus ss ($K \approx 2.5$ m. darcys).

Fig. VII-7 gives the % connate water replaced as a function of v_r for two different pressure gradients for the Pico sandstone.

Comparison with Fig. VII-6 shows that for the same pressure gradient the connate water replacement is more rapid in the less permeable sand.

b) Oil sands

The resistivity distribution in the invaded zones of oil sands depends upon two factors. The first is the displacement of part of the oil by the invading fluid; the second factor is the replacement of the connate water by the mudfiltrate.

As the displacement of the oil does not depend upon the resistivity of the invading mudfiltrate, its effect on the resistivity can be found by using a mudfiltrate of the same salinity as the connate water.

We can further simplify the procedure of obtaining the relation between amount of oil displaced, and radial distance from the boreface,

by using very saline connate water and mud filtrate, so that we may use Archie's formula to relate the oil saturation and the resistivity at any point.

In Part V it was shown on theoretical grounds that the oil saturation in the infiltrated zone is related to the bound water content of the rock and also that the oil displacement depends upon the oil viscosity and the rate of infiltration. These relations will be checked quantitatively in the following sections. At this stage however we want to obtain primarily a qualitative picture of the resistivity distribution in the invaded zone as a function of radial distance from the boreface.

Fig. VII-8 and Fig. VII-9 represent the resistivity variation with amount of filtrate passed through each cm^2 of cross-sectional area perpendicular to the flow, respectively for a sample of Saugus ss (S-4a) and a Berea ss (O-9).

In Part VI of this thesis it was shown that for sufficiently small values of the water resistivity we may apply Archie's formula directly to calculate the water saturation. The samples used to demonstrate this fact were all saturated under high capillary pressures and contained practically only their bound water. During the process of invasion the water content is increased and the effect of conductive solids on the resistivity should therefore become even smaller. For these reasons it is quite safe to find the water saturation at the respective stages of invasion using Archie's formula, with the resistivity index $n = 2$. The water resistivities were $28.2 \ \Omega \text{ cm}$. in the case of the Saugus ss and $27.2 \ \Omega \text{ cm}$ for the Berea ss. The connate water in both cases was

113A

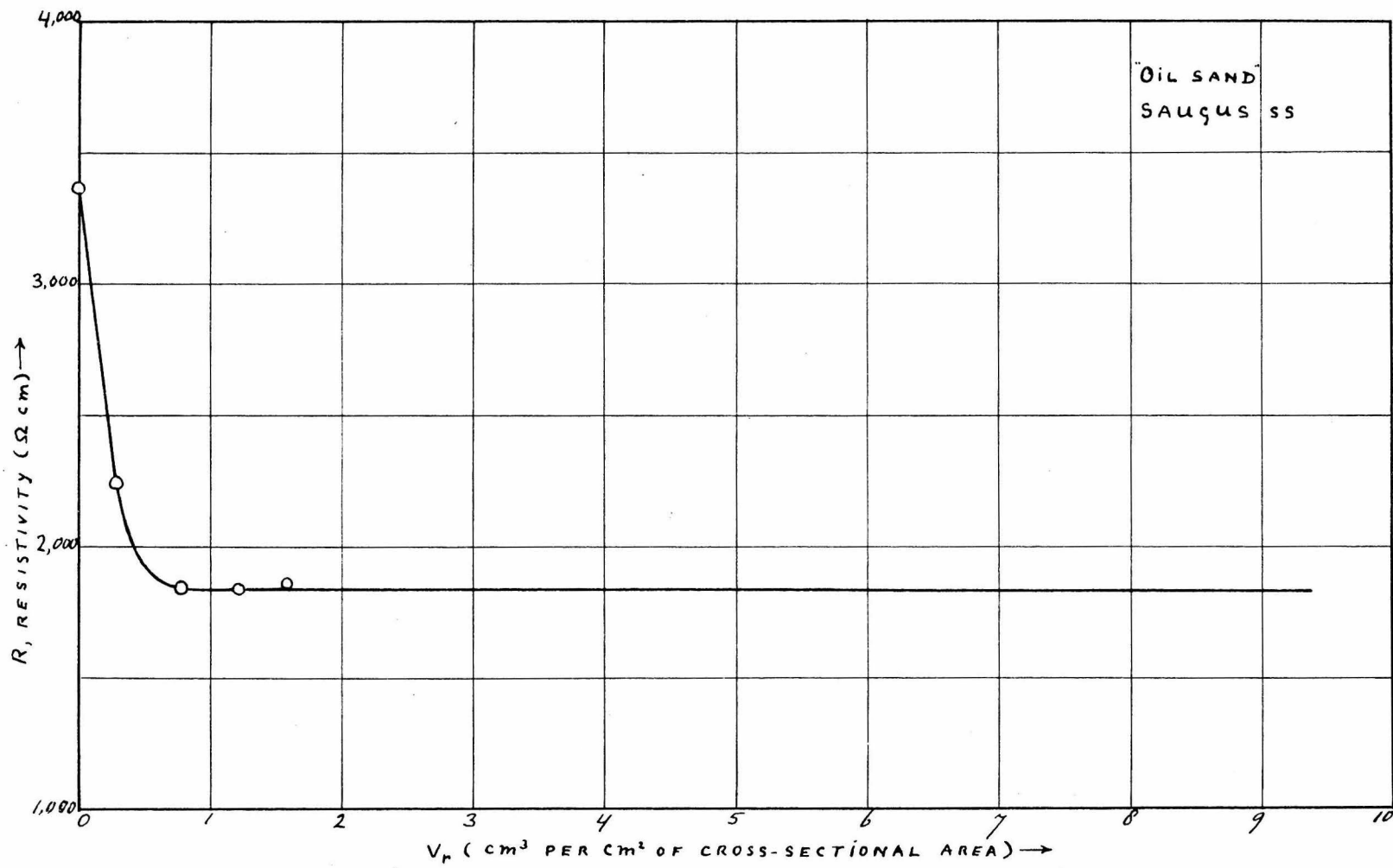


Fig. VII - 8

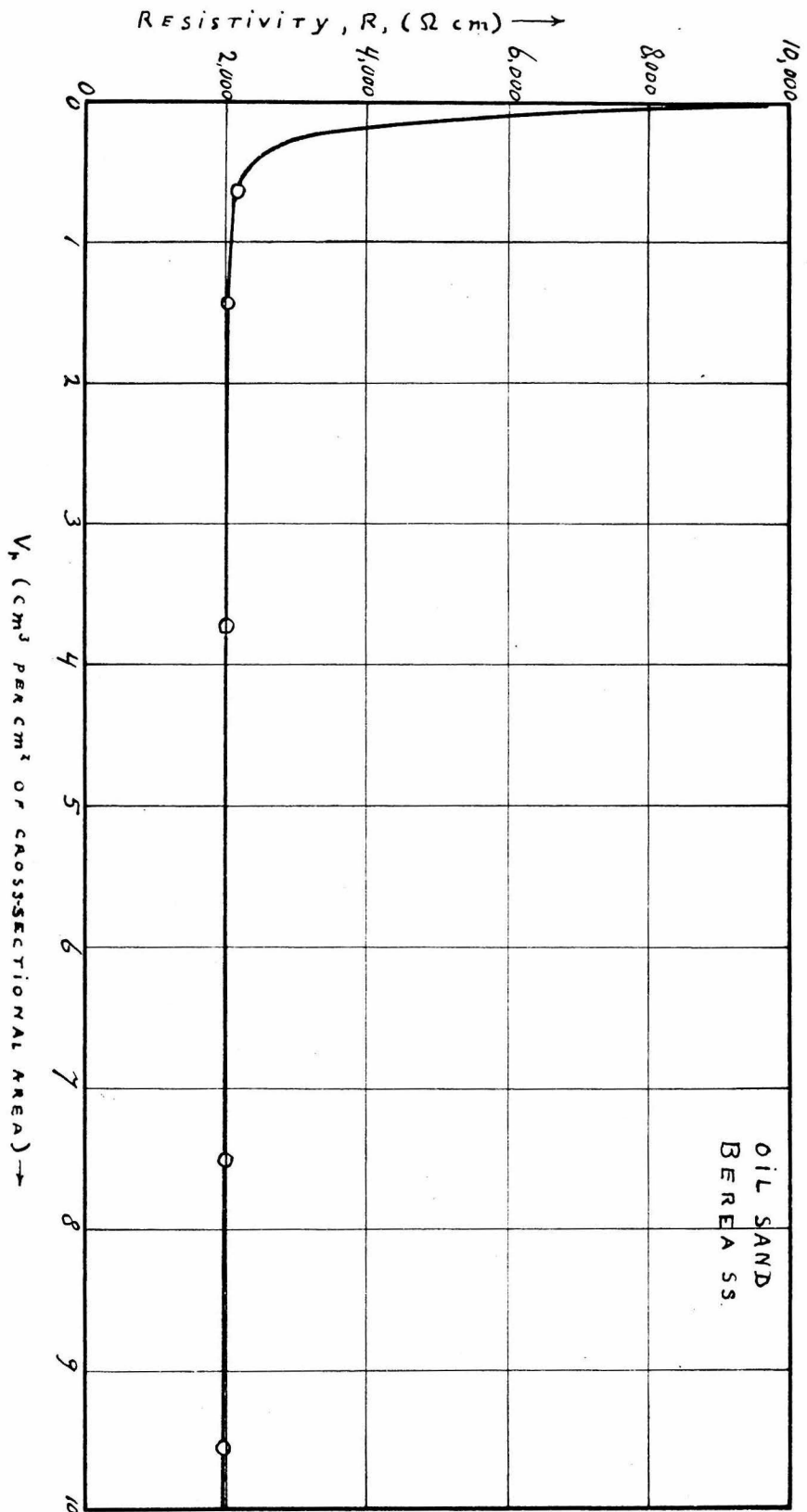


Fig. VII-9

identical with the invading water.

From the computed water saturations, we easily find the amounts of oil removed, which equal the amounts of filtrate retained as fractions of the total pore space, for each amount of infiltration at which a resistivity measurement of the sample was made. These fractions are shown as a function of v_r in Fig. VII-10, curves (a) and (b).

Using the data of Fig. VII-10 and formula (7-1) we can again plot v_r versus r . These plots are shown in Fig. VII-11.

Finally combining the data of Fig. VII-11 and Fig. VII-8 we can plot the resistivity as a function of the radial distance from the boreface, for the invaded zone of the Saugus ss. Combining the data of Fig. VII-9 and Fig. VII-11 we obtain a similar plot for the Berea sandstone. The computed resistivity distributions are shown for the Saugus ss and the Berea sandstone, respectively in Fig. VII-12 and Fig. VII-13.

We see that for sandstones of high bound water content ^{C_w} and low porosity, as in the case of the Saugus ss, the transition zone of the resistivity profile is quite important.

On the other hand, for sands of low bound water content and high porosity, the transition zone becomes completely negligible.

Again for larger infiltration radii for a given sandstone the constant part of the resistivity profile becomes relatively more important, while for smaller radii of invasion the approximation of the resistivity distribution by a constant R_1 becomes poorer.

As stated before, the above two cases only represent the effect of oil displacement in the infiltrated zones on the resistivity, as the

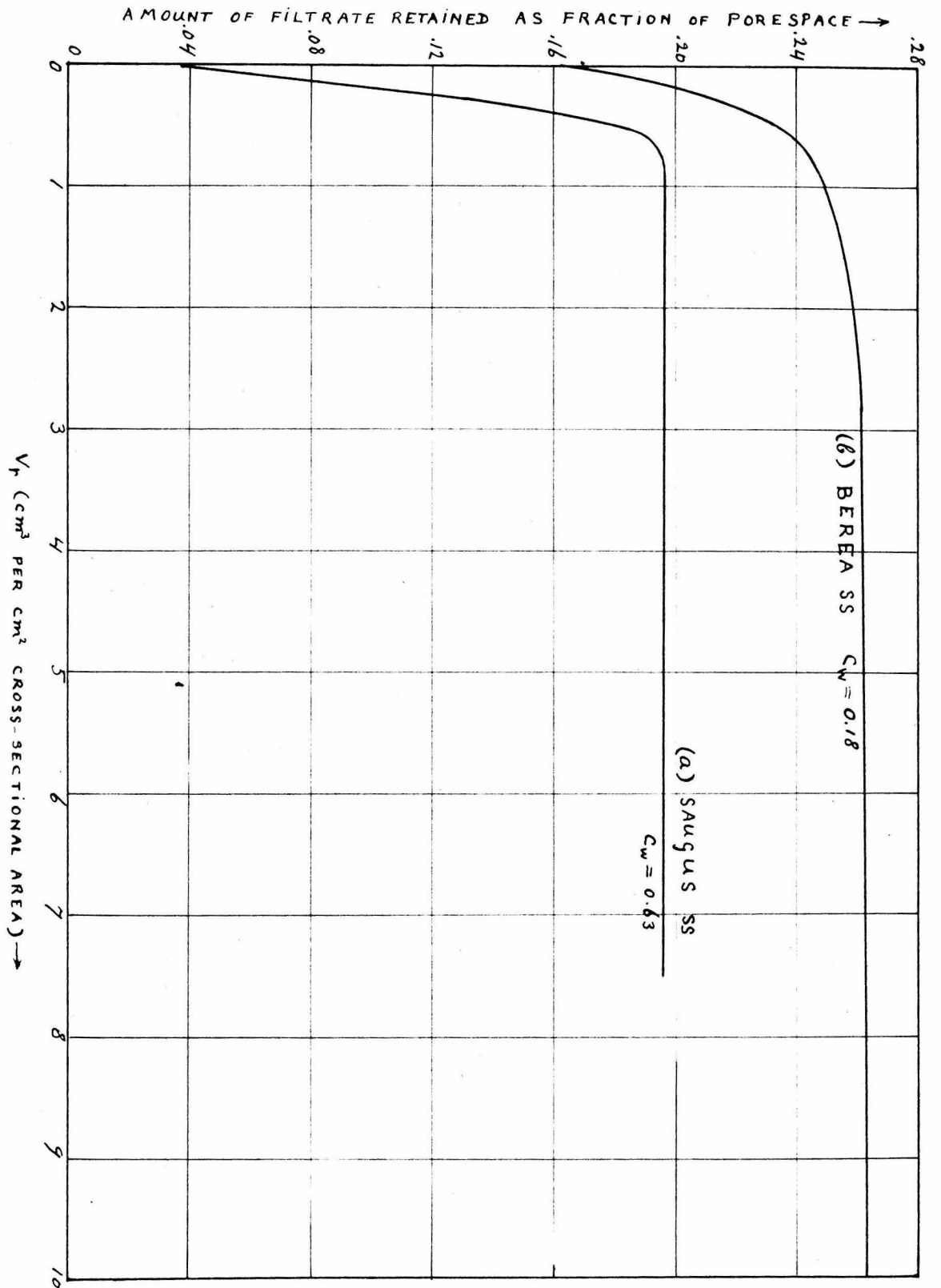


Fig VII - 10

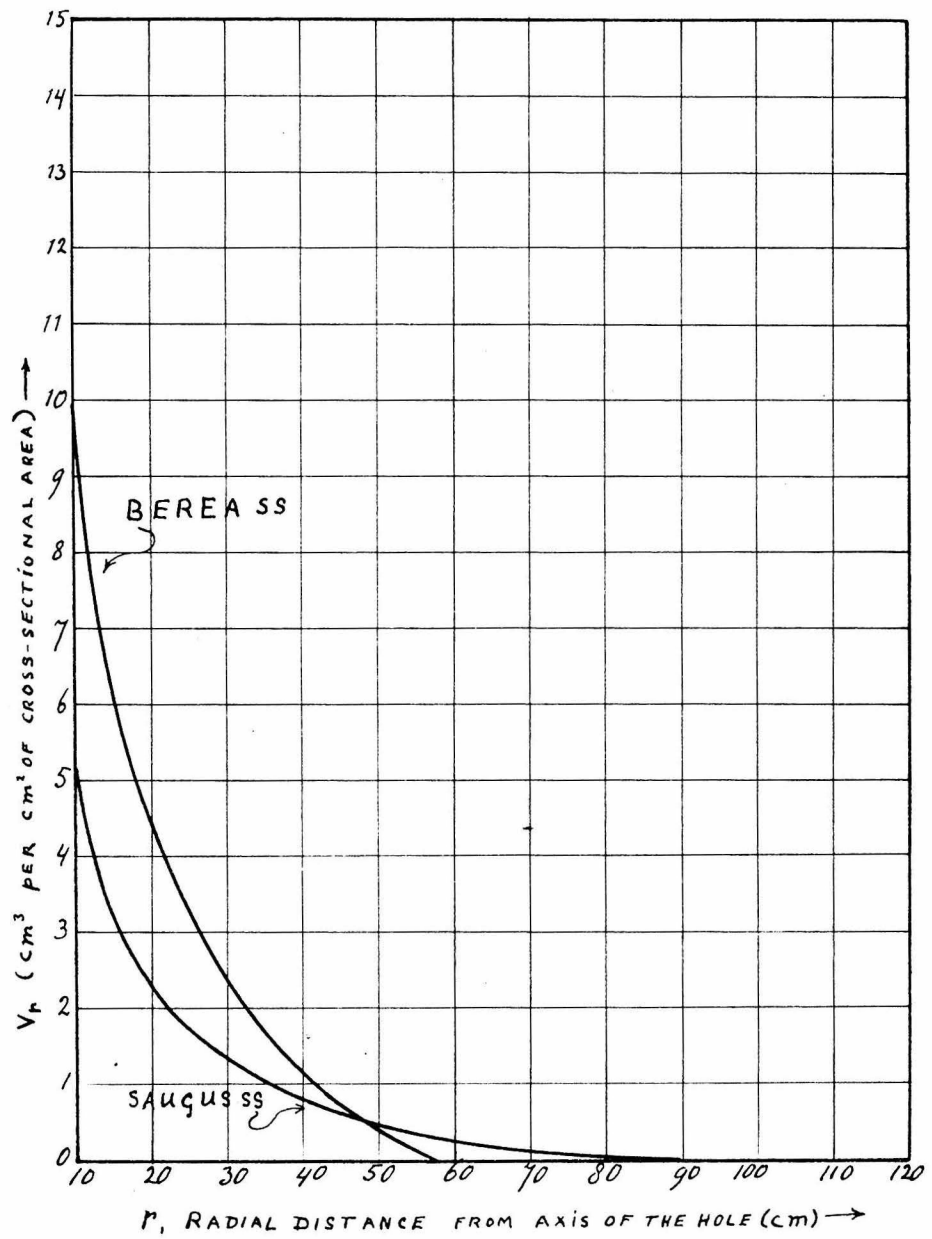


Fig. VII - 11

117C

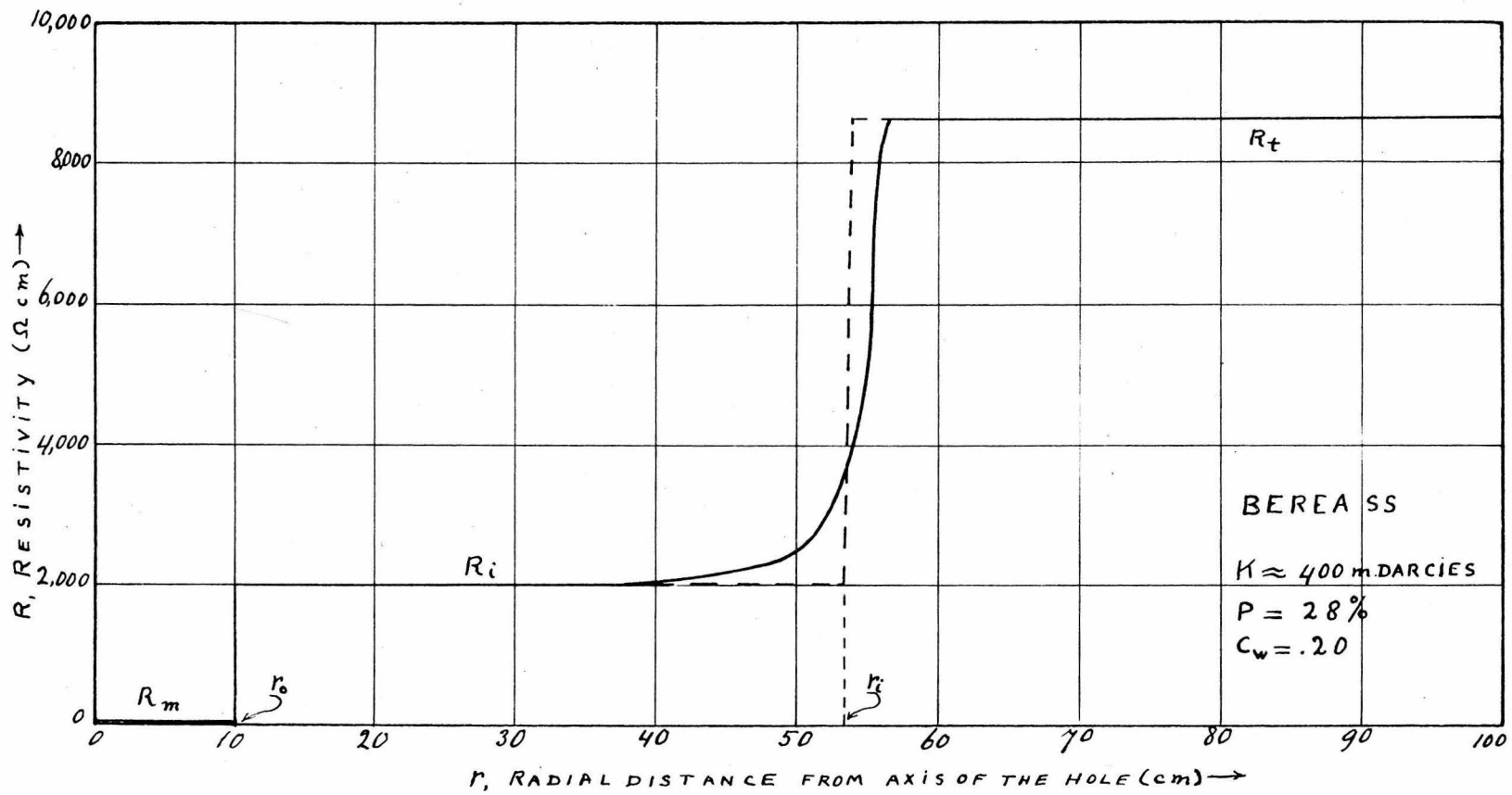


Fig. VII-13

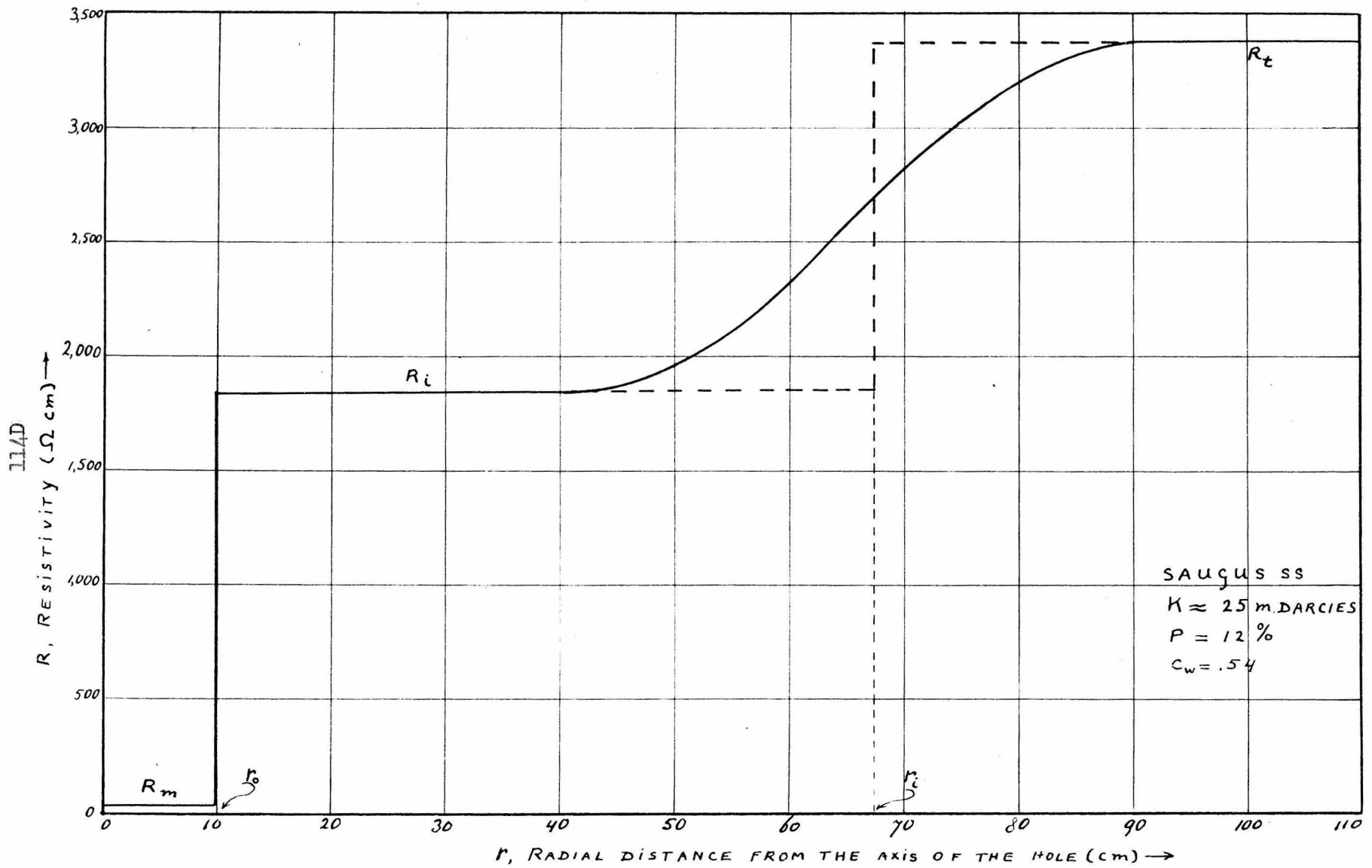


Fig. VII - 12

invading fluid was made identical to the connate water.

If, as is usually the case, the mud filtrate is less saline than the connate water, we have superimposed on the effects of oil displacement the resistivity changes due to replacement of the connate water by the mud filtrate.

The two effects are of opposite sign, and often are of almost equal magnitude, so that for many oil sands the resistivity of the infiltrated zone does not differ much from the true resistivity of the formation.

The computing of the resistivity distribution in the invaded zone in this case is quite complicated. The simultaneous change in oil content and interstitial water composition makes it impossible to compute the amount of filtrate retained in the core from single resistivity measurements.

For these reasons an experiment was performed using a Berea sandstone sample identical to those used in the preceding experiments. This sample was saturated with oil to an oil saturation of approximately 79%, which is the same saturation as prevailed initially in the preceding experiment where the invading water was identical to the connate water.

As the oil displacement does not depend upon the salt content of the invading water, we may use the graph for the Berea sandstone in Fig. VII-10 to determine the amount of oil displaced or the corresponding water-saturation for any amount of infiltration. The amounts of oil displaced for various amounts of infiltration (v_f) are denoted by $(x_f)_{oil}$ and listed in Table VII-A, together with the corresponding water saturations (S_w) and the measured resistivities of the sample (R).

To find the total amount of infiltrating fluid retained in the sample, we have to add onto the amount retained by displacement of oil the quantity retained by replacement of the original connate water. To find this latter quantity we must calculate the interstitial water resistivity after various amounts of infiltration. The water resistivity then serves as an indication of the fraction of the interstitial water consisting of the invading fluid and the fraction consisting of the original connate water.

To calculate the water resistivity Archie's formula may only be applied where the interstitial water resistivity is sufficiently low, as was pointed out before. As soon as part of the original saline connate water is replaced by mud filtrate this holds no longer true and we have to use formula (6-14) to calculate the interstitial water resistivity.

Equation (6-14) relates the water resistivity to the other parameters involved in the following manner:

$$R S_w^2 = \frac{F R_f R_w}{R_w - X_w' (R_w - R_f)}$$

where

$$X_w' = \frac{m/n}{m/n + R_f/S_w}$$

We found previously that for the Berea sandstones $R_f \approx 33 \Omega \text{ cm}$. It remains therefore to determine the values of F and m/n for the sample in question. This is done by measuring the resistivity of the sample when 100% water saturated for two different water resistivities.

m/n is found from equations (6-9) and (6-10) as:

$$m/n = \frac{(R_w)_1 (R_w)_2 [(R_o)_1 - (R_o)_2]}{(R_w)_1 (R_o)_2 - (R_w)_2 (R_o)_1}$$

Also we have from equation (6-9):

$$\frac{I_w}{F} = \frac{(R_w)_1 (R_w)_2 [(R_o)_1 - (R_o)_2]}{(R_o)_1 (R_o)_2 [(R_w)_1 - (R_w)_2]} \quad \text{with} \quad I_w = \frac{m/n}{m/n + R_f}$$

which gives us the value of F.

Using the relations the following results were obtained:

$$\begin{aligned} (R_w)_1 &= 10.6 \quad \Omega \text{ cm} & (R_o)_1 &= 182 \quad \Omega \text{ cm} \\ (R_w)_2 &= 1131 \quad \Omega \text{ cm} & (R_o)_2 &= 11,310 \quad \Omega \text{ cm} \\ I_w/F &= 0.0577 & m/n &= 1554 \\ F &= 16.98 & I_w &= .98 \end{aligned}$$

Using these data we obtain the values of R_w from equation (6-14).

Finally the fraction of invading fluid in the interstitial water is found using equation (6-2) and the computed values of R_w .

Equation (6-2) may be written as:

$$1 - X_1 = X_2 = \frac{1 - R_1/R_o}{1 - R_1/R_2}$$

where R_1 , R_2 and R_o are respectively the resistivities of the original connate water, of the invading fluid, and of the interstitial water mixture upon invasion. X_1 and X_2 are respectively the fraction of connate water and of invading fluid in the interstitial water.

$$R_1 = 12.2 \quad \Omega \text{ cm}; \quad R_2 = 955 \quad \Omega \text{ cm}.$$

Table VII-A lists the computed values of X_2 . Multiplying these with the corresponding values of the water saturation, S_w , we obtain the amount of invading fluid retained, as a function of the porespace. This quantity is denoted by $(X_f)_t$ and is also tabulated in Table VII-A.

TABLE VII-A

v_F	R Ω cm	$(x_F)_{oil}$	S_w	I_w'	R_w	X_2	$(X_F)_t$
0	5010	0	.202	.907	12.2	0	0
0.223	2750	.205	.407	.95	26	.537	.219
0.473	2690	.232	.434	.953	29.6	.590	.240
0.696	5510	.242	.444	.955	66.9	.820	.368
1.002	14,910	.249	.451	.955	213	.966	.436
1.560	20,940	.255	.457	.956	380	.981	.448
2.090	21,300	.258	.460	.957	393	.983	.452
2.480	21,640	.268	.462	.957	413	.985	.455
8.000	24,000	extrapolated					.462

The initial water saturation, before flushing was started, was calculated to be .202 using equation (6-17). Using Archie's formula gave $S_w = .206$, which is a very good approximation as would be expected for the very low resistivity of the connate water.

Having determined the amounts of infiltrating fluid, $(X_F)_t$, as a function of the amount of infiltration, v_F , we can again compute the resistivity distribution for the infiltrated zones of any arbitrarily chosen invasion diameter, in exactly the same manner as described for the case of invasion of a salt sand.

Fig. VII-14 shows the measured values of R, as a function of v_F , while Fig. VII-15 gives the actual resistivity profile for the invaded zone of an oil sand with saline connate water.

We see from Fig. VII-14 that upon invasion the resistivity first

118A

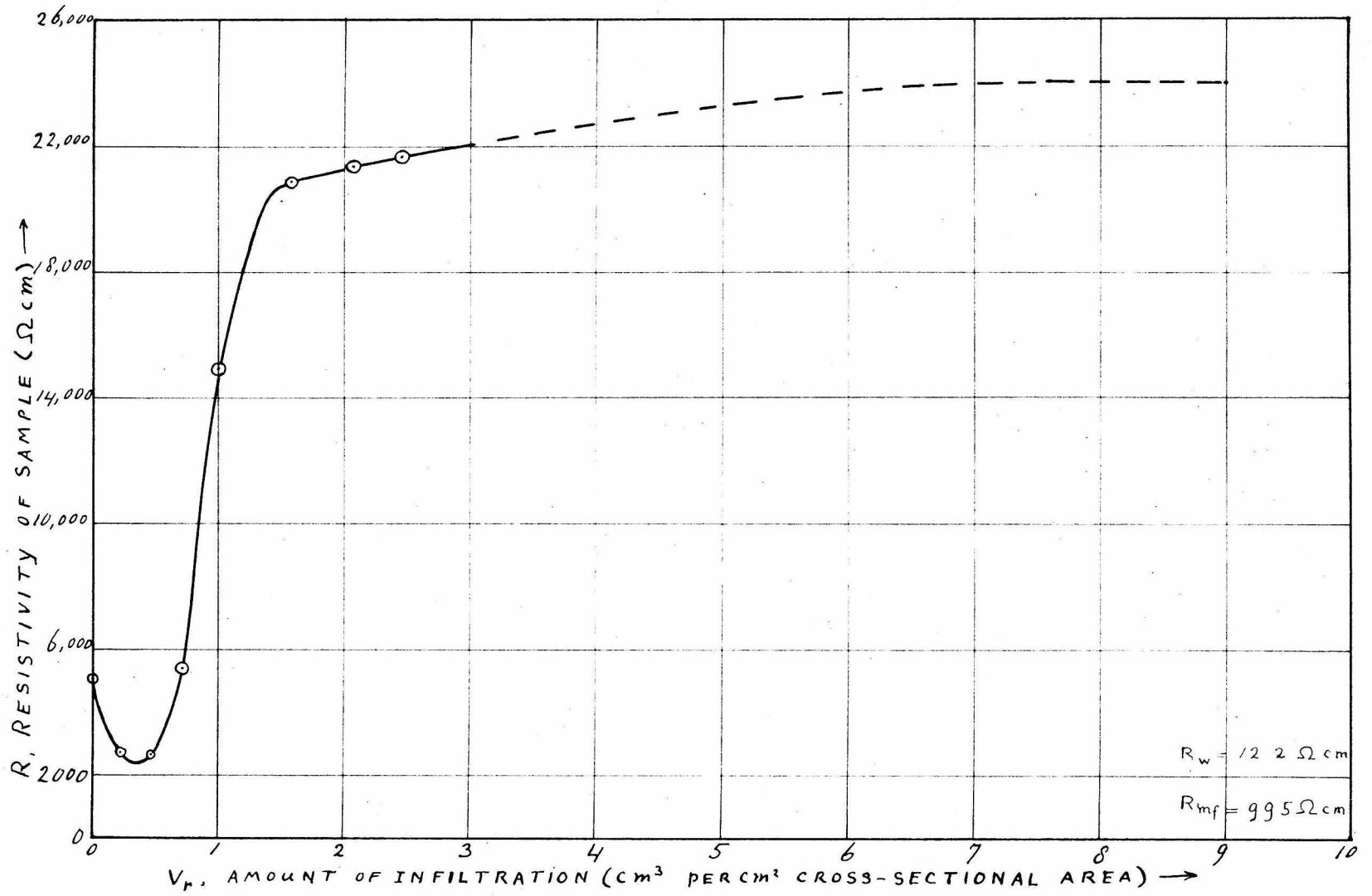
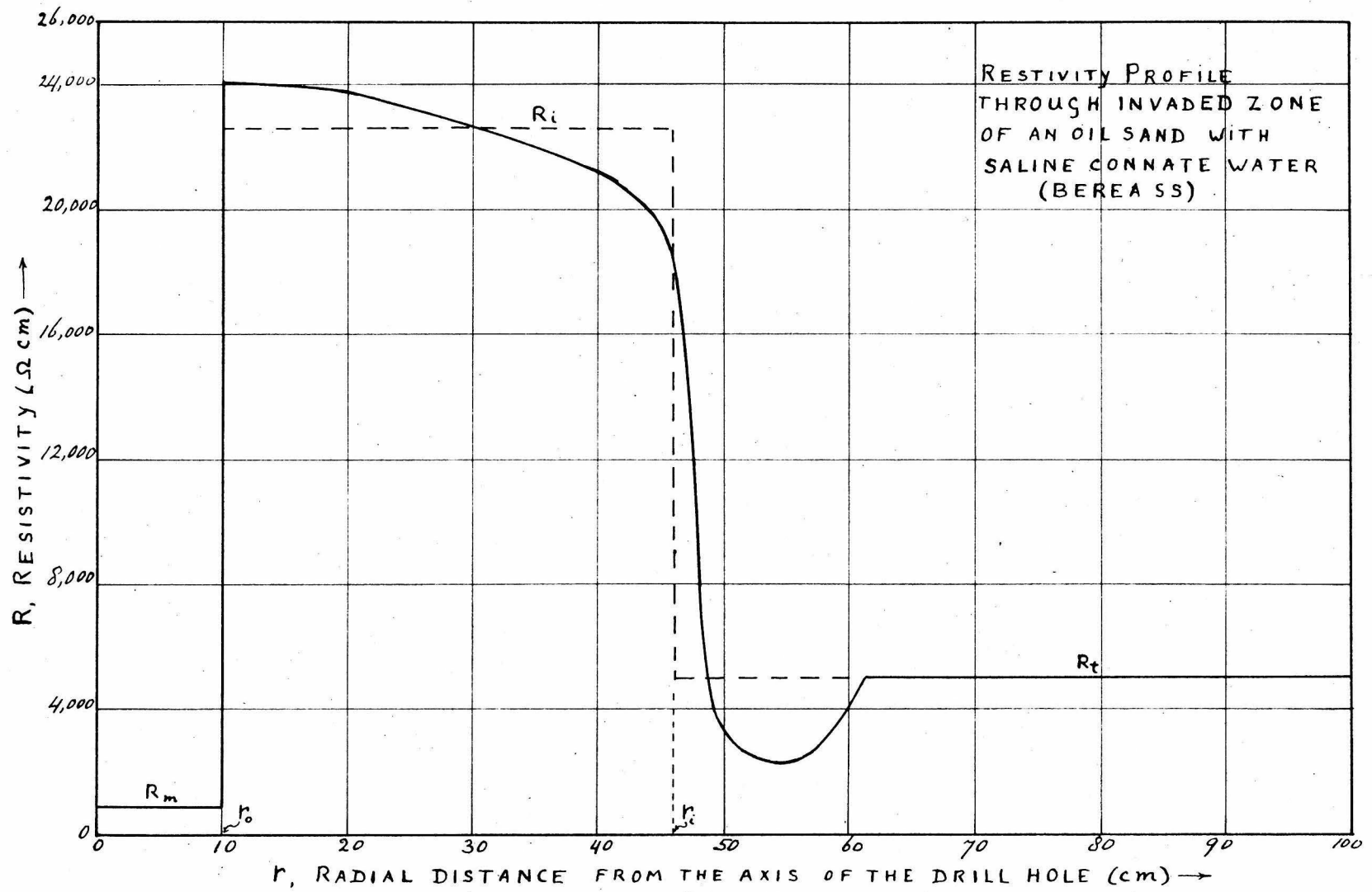


Fig. VII-14



decreases, goes through a minimum and then sharply increases. This is caused by the fact that the oil is removed more rapidly than the connate water. The replacement of oil by the invading water decreases the resistivity. However as soon as the larger part of the saline connate water starts being replaced by the less saline mudfiltrate, the resistivity rises sharply.

As shown in Fig. VII-15 the infiltrated zone resistivity may be much higher than the true formation resistivity, if the salinity contrast between the connate water and the mudfiltrate is large enough. In our example, $\frac{R_{mf}}{R_f} = 78.5$. In many practical cases the contrast will be much smaller and R_i and R_t may be very nearly equal. If the mudfiltrate is as saline as the connate water or more saline, the infiltrated zone resistivity will naturally be smaller than the true resistivity. However these cases will be exceptions rather than the rule.

c) Gas sands

In Part V of this thesis some computations on the saturation distribution in the invaded zones of gas sands, based on published relative permeability data, were carried out. The results showed an almost constant saturation throughout the entire infiltrated zone. It was pointed out however that the relative permeability data are not reliable close to the points where the permeability of one of the phases approaches zero. In the case of gas sands, because of the low viscosity of the gas compared to the water, very small values of the relative permeability to gas are still of noticeable importance in determining the amount of gas that will be displaced upon invasion by water.

Experimentally determined saturation distribution data for a gas

sand showed that indeed the relative permeability relations are not reliable for gas displacement computations. The experiment on the character of the infiltrated zone of gas sands was carried out in exactly the same manner as that described for the case of an oil sand. The sample used was Berea sandstone which contained a very small fraction of bentonite. The gas used was nitrogen gas. By the capillary pressure method water from the core was displaced by gas until a gas saturation of .506 was reached.

The resistivity of the connate water was made low so that Archie's formula could be applied with fair accuracy and the invading water was made identical to the connate water. Resistivity measurements gave for the 100% water saturation sand $(R_0)_1 = 182 \ \Omega \text{ cm}$ and at $S_g = .506$ we found $R = 752 \ \Omega \text{ cm}$.

Applying Archie's formula gives $S_g = 1 - S_w = .48$. Or using

$(S_w)^n = \frac{(R_0)_1}{R}$ we find $n = 1.95$. We see that Archie's formula with $n = 2$ gives us a reasonable approximation of S_w for gas sands as well as for oil sands, if the effect of conductive solids may be neglected.

Resistivity measurements for a different value of the connate water resistivity and application of equations (6-9) and (6-10) gave

$$\frac{1}{R_0} = 0.372 \times 10^{-4} + \frac{0.0577}{R_w}$$

For the gas displacement experiment we had $R_w = 10.6 \ \Omega \text{ cm}$, and we see that in this case the factor representing the influence of the conductive solids is indeed negligible.

The sample resistivity is given as a function of the amount of invading water passed through the sample in Fig. VII-16.

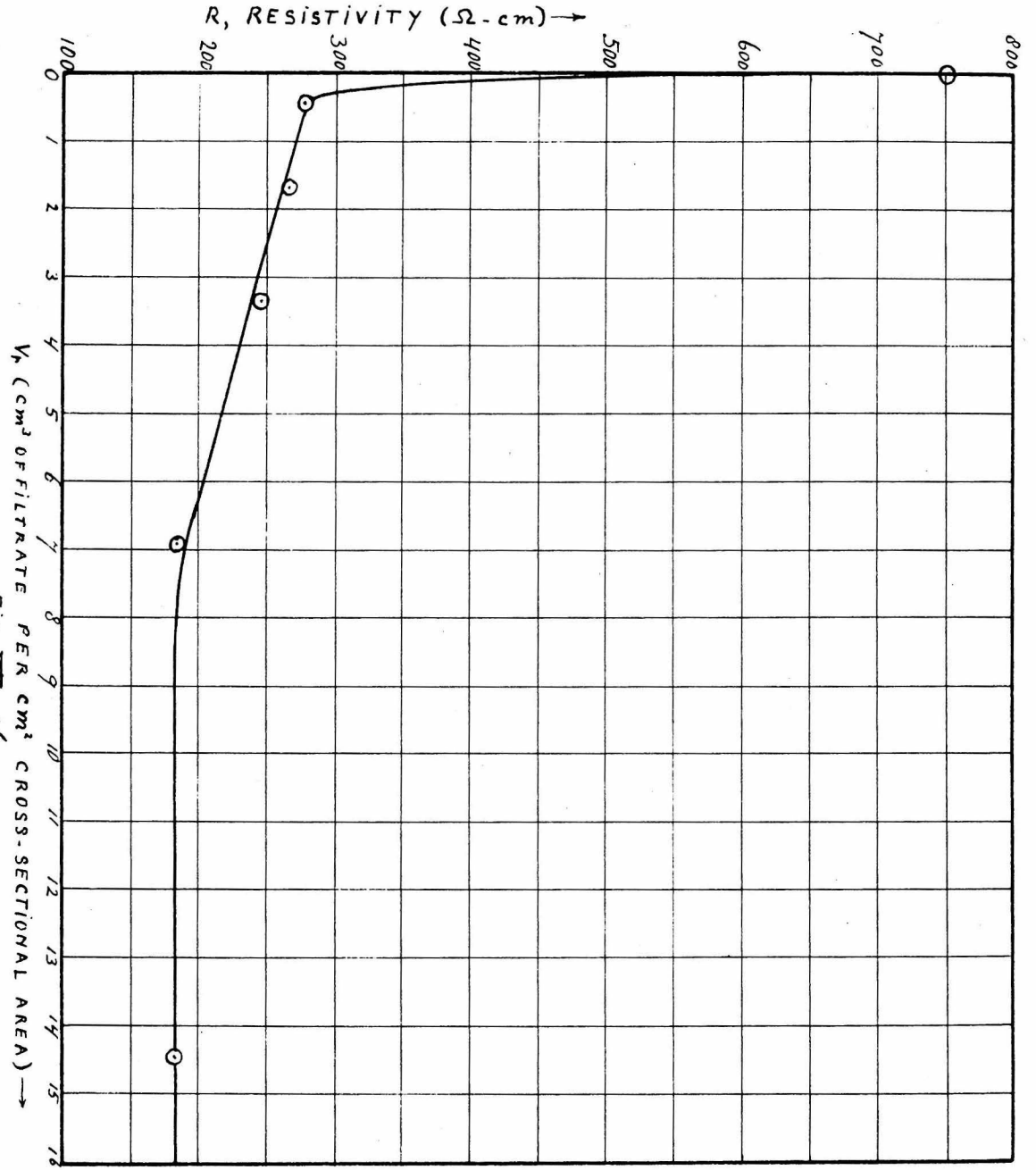


Fig. VII-16
 V_f (cm^3 OF FILTRATE PER cm^2 CROSS-SECTIONAL AREA) \rightarrow

Using the same procedure as described for the case of an oil sand with invading water resistivity equal to the connate water resistivity, the resistivity distribution in the invaded zone, as a function of the radial distance from the center of the borehole, is computed again. The result is shown in Fig. VII-17

We see that the resistivity is not constant, as was concluded from the relative permeability data, but varies with the radial distance, r .

The total magnitude of the variation however is small enough so that, approximation by a constant resistivity, R_1 , may still be applied.

Other measurements were made using the same sample but different initial gas saturations.

It was found that the initial gas saturation for a given sample has little or no effect on the resulting saturation upon infiltration.

The water saturation in the invaded zone in this experiment varies from .81 to 1.00 with an average at approximately .90 .

We found that for oil of 17 cp viscosity the invaded zone of the Berea ss had a water saturation of approximately .48 . This illustrates clearly the influence of the viscosity of the nonwetting phase upon the resulting saturation of the invaded zones.

2) Relation between the water saturation of the invaded zone and of the undisturbed formation in oil and gas horizons

From computations based on resistivity log data, Tixier (19) showed that a relation exists between the amount of oil retained upon invasion of an oil sand and the amount of oil initially present in the sand.

That such relation should exist was explained in Part V of this thesis by the fact that the oil retained upon flushing depends upon the

121A

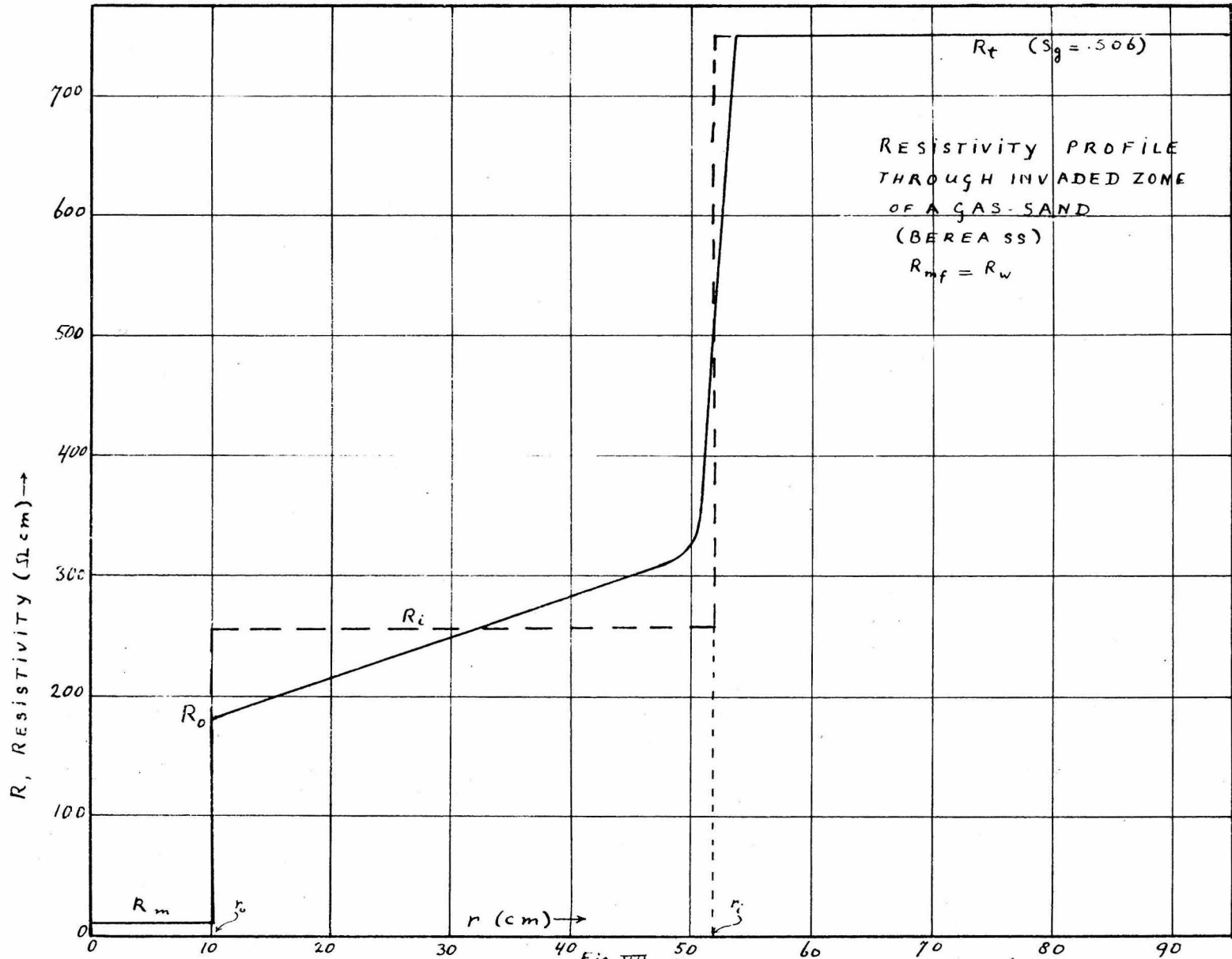


Fig. VII - 17

relative permeability of the formation to oil and water at various saturations. The latter are related to the capillary characteristics of the rock and those in turn determine the bound water content or the initial oil saturation in the horizon in question.

Tixier found that the above relation could be approximated by $(S_w)_i^n = S_w$ with $n \approx 2$ where $(S_w)_i$ and S_w denote respectively the water saturation in the infiltrated zone and in the undisturbed formation.

In Part V we showed however that the saturations prevailing in the infiltrated zones depend upon the rate of flow of the invading fluid and the viscosity ratio of the oil and the water.

To obtain a quantitative estimate of the magnitude of the various factors involved, a series of experiments was carried out in which the effects of each factor were studied keeping all other factors constant. In all cases the bound water content was determined from the capillary pressure-saturation relationships. To facilitate the interpretation of the measurements, water of low resistivity was used and the infiltrating fluid was always identical to the initially present connate water. Under these conditions the water saturation upon flushing could be determined by measurement of the sample resistivities and application of Archie's formula.

The main series of experiments was carried out with oil of 30.2° A.P.I. gravity at approximately 70°F, having a viscosity of close to 17 centipoises.

The pressure gradient during the flushing was kept at approximately 2 psi/cm.

The average pressure gradients encountered during infiltration of

porous horizons around drill holes are mostly smaller (0.1 - 1 psi/cm).

The relation between $(S_w)_i$ and (S_w) under the above conditions was investigated for four types of sandstone, namely a Saugus ss, a Berea ss and two types of Pico ss.

The relation is represented graphically in Fig. VII-18, graph I. We note that on a log-log scale the relation may be represented by a straight line, which for the particular conditions in question approaches very closely the graph for the relation $(S_w)_i^2 = S_w$ (graph II).

The effect of the pressure gradient during infiltration upon the invaded zone saturation was found by flushing a sample of Pico sandstone under various pressure gradients and computing the resulting values of $(S_w)_i$ from resistivity measurements. The applied gradients were respectively 0.1, 1 and 22 psi/inch. The results are shown by points 1, 2 and 3 respectively in Fig. VII-18.

On the assumption that for any pressure gradient the relation $(S_w)_i^m = S_w$ holds true, graphs have been drawn through points 1 and 3, to apply respectively to the cases where invasion took place under a gradient of 0.1 psi/inch and 22 psi/inch.

Unless specific information is at hand on permeabilities and rates of infiltration, the relation $(S_w)_i^2 = S_w$ will have to be used for the interpretation procedures as outlined in Part VI.

To find the effect of the viscosity of the non-wetting phase on the resulting infiltrated zone saturations, $(S_w)_i$ was determined for a Pico sandstone sample saturated with kerosene (45° A.P.I. gravity, viscosity 3 centipoises). The following results were obtained:

$$R_w = 20.5 \ \Omega \ \text{cm}$$

$$R_0 = 318.3 \ \Omega \ \text{cm.}$$

After saturation with kerosene under a capillary pressure of 25 psi, the resistivity was found to be 3244 Ω cm. Using Archie's formula this gives $S_w = .313$. (By volumetric measurement we found $S_w = .28$).

After flushing with 500 cm of water, identical to the interstitial water (water resistivity = 20.5 Ω cm) under a pressure gradient of 2 psi/cm, the resistivity of the sample was found to be 593 Ω cm.

Using again Archie's formula we obtain $(S_w)_i = \left(\frac{318.3}{593}\right)^{\frac{1}{n}} = .732$.

The corresponding point is plotted in Fig. VII-18. Assuming again that the relation $(S_w)_i^n = S_w$ applies also in this case, graph III is drawn to represent the relation between $(S_w)_i$ and S_w for $\mu_o/\mu_w = 3$. (Here μ_o and μ_w denote respectively the viscosity of the oil and that of the water).

For graph III we find $n \approx 4$. We see that the variation of n with the value of μ_o/μ_w is quite large. Lack of knowledge of the viscosity ratio under reservoir conditions may therefore introduce considerable errors in computations of water saturations of formations based on assumed values of n .

It is realized that the data presented in Fig. VII-18 are too few to be relied upon for precise evaluation of the combined effects of viscosity ratios and pressure gradients on the invaded zone saturations.

Taking into account the lowering of oil viscosity with temperature and amount of dissolved gas and the lowering of the water viscosity with temperature as described by Beal (21) it seems reasonable to use the relation $(S_w)_i^n = S_w$ with $n = 2$ in regions where the surface gravity of the oil is smaller than 30° A.P.I., and to use $n = 3$ where the surface gravity of the oil is larger than 30° A.P.I.

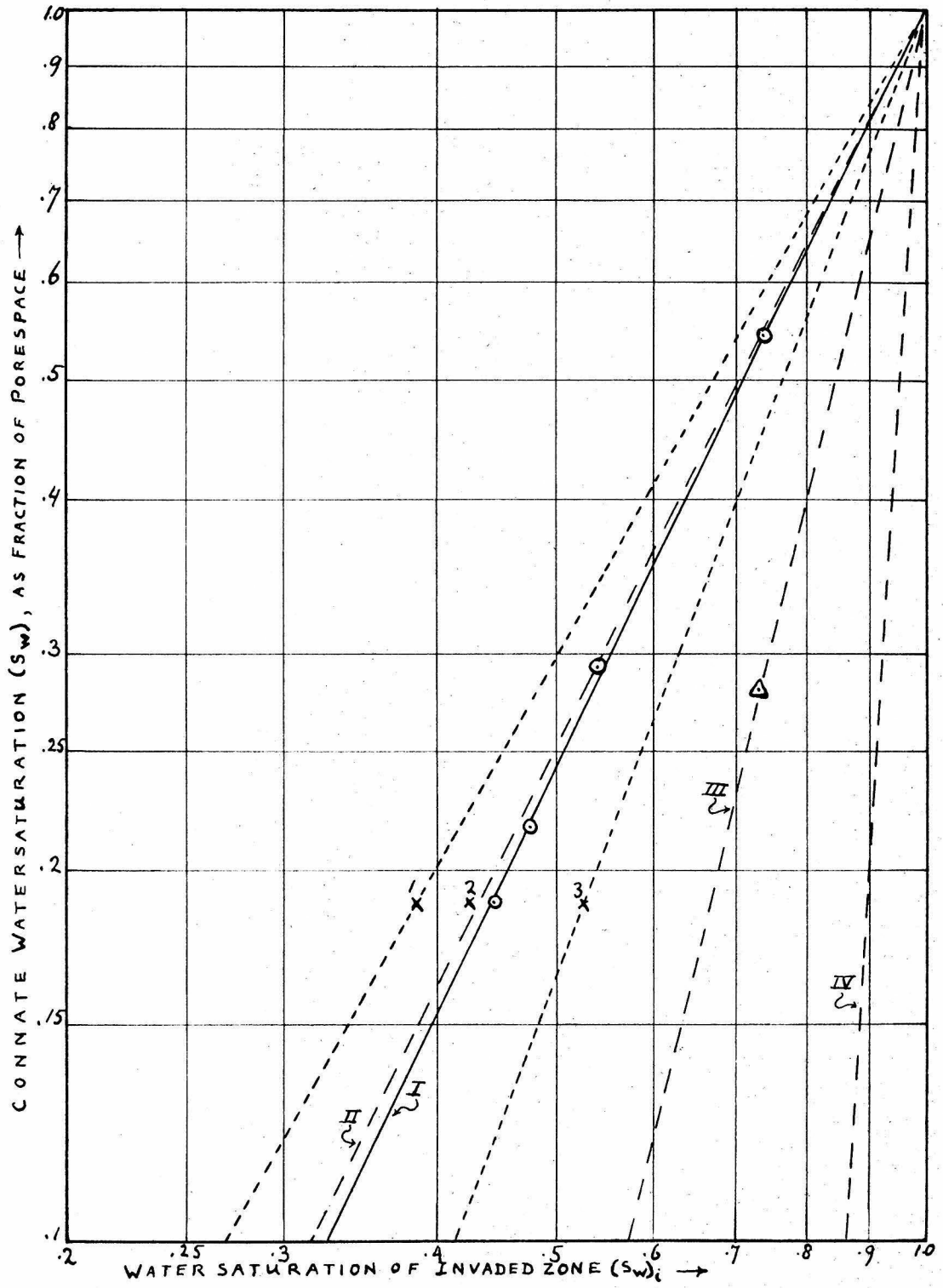


Fig. VII - 18

As described in the section on the resistivity profiles through invaded zones of gas sands, the water saturation in such zones varies continuously with the radial distance from the boreface. For gas sands we have to use therefore the concept of average invaded zone saturation. Based on the data obtained in the preceding section for the Berea sandstone, graph IV of Fig. VII-18 has been drawn to represent roughly the relation between the water saturation of the invaded zones and those of the undisturbed formations, for gas sands.

REFERENCES

1. W. R. Smythe: *Static and Dynamic Electricity*, New York, McGraw-Hill Book Co., Inc., 1939, 169.
2. W. R. Smythe: *loc. cit.* (1) p. 195.
3. V. A. Fock: *Theory of the Determination of the Resistivity of Beds by Electrologging*. State Technical Theoretical edition USSR (1933).
4. L. M. Alpin: *A Theory of Electrical Well Logging*, USSR (1938).
5. V. N. Dakhov: *Well-logging, Interpretation of Logs*, Moscow (1941), reprinted in 1945.
6. H. G. Doll, J. C. Legrand, E. F. Stratton: *True Resistivity Determination from the Electric Log - Its Application to Log Analysis*. *Oil and Gas Journal*, September 20, 1947, 297.
7. Schlumberger Well Surveying Corporation, Houston, Texas, *Resistivity Departure Curves*, (1947).
8. H. Guyod: *Electric Log Interpretation*. *Oil Weekly*, December 17, 1945.
9. *Drilling Mud* (National Lead Company publication) May, 1940, p.4.
10. L. de Witte: *Factors Governing Accumulation of Oil and Gas in Stratigraphic Traps*. Thesis - California Institute of Technology, 1950.
11. G. F. Tagg: *The Earth Resistivity Method of Geophysical Prospecting - Some Theoretical Considerations*. *The Mining Magazine*, 43, (1930), 150.
12. W. E. Bergman, P. G. Carpenter, H. B. Fisher: *The Preparation of Drilling Muds for Laboratory Investigations*. *Oil and Gas Journal*, (August, 1943), 196.
13. S. E. Buckley and M. C. Leverett: *Mechanism of Fluid Displacements in Sands*. *A.I.M.E. Transactions* 146 (1942), 107 - 116.

14. R. D. Wyckoff and H. C. Botset: The Flow of Gas-Liquid Mixtures through Unconsolidated Sands. *Physics* 7 (1936), 325.
15. M. C. Leverett: Flow of Oil-Water Mixtures through Unconsolidated Sands. *A.I.M.E. Transactions* 132 (1939), 149.
16. H. C. Botset: Flow of Gas-Liquid Mixtures through Consolidated Sands. *A.I.M.E. Transactions* 136 (1940), 91.
17. M. C. Leverett and W. B. Lewis: Steady Flow of Gas-Oil-Water Mixtures through Unconsolidated Sands. *A.I.M.E. Transactions* 142 (1941), 107.
18. W. Rose: Theoretical Generalizations Leading to the Evaluation of Relative Permeability. *Petroleum Technology*, May 1949, 111.
19. M. P. Tixier: Electric Log Analysis in the Rocky Mountains. *Oil and Gas Journal*, June 23, 1949.
20. E. R. Brownscobe, R. L. Slobod and B. H. Candle: Relative Permeability of Cores, Desaturated by Capillary Pressure Method. *A.P.I. Division of Production, Los Angeles Meeting, May 13 - 14, 1949.*
21. C. Beal: The Viscosity of Air, Water, Natural Gas, Crude Oil and its Associated Gases at Oil Field Temperatures and Pressures. *A.I.M.E. Transactions*, 165, (1946), 94 - 115.
See also M. Muskat: *Physical Principles of Oil Production.* p. 97, fig. 24E. McGraw-Hill, 1949.
22. W. Rose and W. A. Bruce: Evaluation of Capillary Character in Petroleum Reservoir Rock. *Journal of Petroleum Technology*, May 1949, 127.
23. M. Williams: Radial Filtration of Drilling Muds. *A.I.M.E. Transactions* 136 (1940), 57.

24. M. C. Leverett, Op. cit. (18) fig. 7, curves a and c, pg. 159.
25. M. Williams, Op. cit., fig. 8.
26. F. Morgan, M. Muskat and R. C. Russell: Some Experiments on the Mobility of Interstitial Waters. A.I.M.E. Transactions 170 (1947), 51.
27. H. W. Patnode and M. R. J. Wyllie: The Presence of Conductive Solids as a Factor in Electric Log Interpretation. Journal of Petroleum Technology, February, 1950, pg. 47.
28. H. W. Patnode: Relationship Between Mud Resistivity and Mud Filtrate Resistivity. Journal of Petroleum Technology, January, 1949.
29. G. E. Archie: Electrical Resistivity Log as an Aid in Determining some Reservoir Characteristics. A.I.M.E. Transaction 164 (1945), 322.
30. H. Guyod: Electrical Logging Developments in the U.S.S.R. World Oil, August 1948, pg. 120.
31. C. R. Bailey, H. L. Bilharty, H. F. Dunlap and E. Shuler: The Relation between Electrical Resistivity and Brine Saturation in Reservoir Rocks. Petroleum Technology (October, 1949), 259.
32. L. de Witte: Experimental Studies on the Characteristics of Electrochemical Potentials Encountered in Drill Holes. Thesis - California Institute of Technology, Pasadena, 1950.

APPENDIX

A) Derivation of the Expression for the Inverse Distance from the Origin in Terms of Modified Bessel functions.

By substitution we can prove that

$$R = \int_0^{\infty} e^{-v \cosh \varphi} d\varphi$$

is a solution of the modified Bessel equation

$$\frac{d^2 R}{dv^2} + \frac{1}{v} \frac{dR}{dv} - \left(1 + \frac{R^2}{v^2}\right) R = 0$$

Substitution gives (for $n = 0$):

$$\begin{aligned} & \int_0^{\infty} \cosh^2 \varphi e^{-v \cosh \varphi} d\varphi - \frac{1}{v} \int_0^{\infty} \cosh \varphi e^{-v \cosh \varphi} d\varphi \\ & - \int_0^{\infty} e^{-v \cosh \varphi} d\varphi = 0 \end{aligned} \quad (A-1)$$

Using $\cosh^2 \varphi - \sinh^2 \varphi = 1$ or $\cosh^2 \varphi - 1 = \sinh^2 \varphi$ and combining the first and third terms gives:

$$\begin{aligned} & \int_0^{\infty} \left[\sinh \varphi e^{-v \cosh \varphi} d \cosh \varphi \right] = \text{(by partial integration)} \\ & = \left[-\frac{\sinh \varphi}{v} e^{-v \cosh \varphi} \right]_0^{\infty} + \frac{1}{v} \int_0^{\infty} \cosh \varphi e^{-v \cosh \varphi} d\varphi \end{aligned}$$

of which the first part equals zero and the second part equals the second term of (A-1) except for the negative sign. This makes the left hand member of (A-1) equal zero and proves that

$\int_0^{\infty} e^{-v \cosh \varphi} d\varphi$ is a solution of the modified Bessel equation of zero order.

However, any such solution must be of the form

$R = A I_0(v) + B K_0(v)$ and since the integral is zero when $v = \infty$ it cannot contain $I_0(v)$ and it must be of the form $B K_0(v)$, so that we have:

$$B K_0(v) = \int_0^{\infty} e^{-v} \cosh \varphi \, d\varphi$$

Let $v = kr$, multiply both sides by $\frac{2}{\pi} \cos kz$ and integrate from $k = 0$ to $k = \infty$.

$$\frac{2}{\pi} B \int_0^{\infty} \cos kz K_0(kr) \, dk = \frac{2}{\pi} \int_0^{\infty} \cos kz \left(\int_0^{\infty} e^{-kr} \cosh \varphi \, d\varphi \right) dk$$

We integrate the right hand side first with respect to k using:

$$\int_0^{\infty} e^{ax} \cos px \, dx = \left| \frac{e^{ax} (a \cos px - p \sin px)}{a^2 + p^2} \right|_0^{\infty} = \frac{-a}{a^2 + p^2};$$

with $a = -r \cosh \varphi$ and $p = z$

This gives: $\frac{2}{\pi} \int_0^{\infty} \frac{r \cosh \varphi}{z^2 + r^2 \cosh^2 \varphi} \, d\varphi$ and as $\frac{d \cosh^2 \varphi}{d \varphi} = 2 \cosh \varphi \sinh \varphi$

we may write:

$$\begin{aligned} \frac{2}{\pi} \int_0^{\infty} \frac{r \cosh \varphi \, d\varphi}{z^2 + r^2 \cosh^2 \varphi} &= \frac{1}{\pi r} \int_0^{\infty} \frac{d(\cosh^2 \varphi)}{(\cosh^2 \varphi - 1)^{\frac{1}{2}} (z^2/r^2 + \cosh^2 \varphi)} \\ &= \frac{1}{\pi r} \int_{(1+z^2/r^2)}^{\infty} \frac{d(\cosh^2 \varphi + z^2/r^2)}{[\cosh^2 \varphi + z^2/r^2 - (1 + z^2/r^2)]^{\frac{1}{2}} (z^2/r^2 + \cosh^2 \varphi)} \end{aligned}$$

Using

$$\begin{aligned} \int_p^{\infty} \frac{dx}{x(c+bx)^{\frac{1}{2}}} &= \left[\frac{2}{(-c)^{\frac{1}{2}}} \tan^{-1} \left(\frac{c+bx}{-c} \right)^{\frac{1}{2}} \right]_p^{\infty} = \\ &= \frac{2}{(-c)^{\frac{1}{2}}} \left\{ \frac{\pi}{2} - \tan^{-1} \left(\frac{c+bp}{-c} \right)^{\frac{1}{2}} \right\} \end{aligned}$$

with $b = 1$ and $a = -(1 + z^2/r^2)$, the above expression becomes:

$$\frac{2}{(1 + z^2/r^2)^{3/2}} \times \frac{1}{\pi r} \left\{ \frac{\pi}{2} - \tan^{-1} \left(\frac{-(1 + z^2/r^2) + (1 + z^2/r^2)^{1/2}}{1 + z^2/r^2} \right) \right\} =$$

$$= \frac{2}{\pi r} \times \frac{\pi}{2} \times \frac{1}{(1 + z^2/r^2)^{3/2}} = \frac{1}{(r^2 + z^2)^{3/2}} = \frac{1}{\bar{r}}$$

So we have:

$$\frac{1}{\bar{r}} = \frac{2}{\pi} B \int_0^\infty \cos(k z) K_0(k r) d k$$

where \bar{r} is the inverse distance from the origin.

To evaluate B, we differentiate both sides with respect to z, multiply by r and integrate from r = 0 to r = ∞. This gives after rearranging:

$$-\frac{2B}{\pi} \int_0^\infty \frac{\sin k z}{k} \int_0^\infty k r K_0(k r) d(k r) d k = - \int_0^\infty \frac{z r d r}{(z^2 + r^2)^{3/2}}$$

and as $\int_0^v v K_0(v) d v = -v K_1(v)$ and $K_0' = -K_1$

this becomes:

$$\frac{2B}{\pi} \int_0^\infty \frac{\sin k z}{k} \left[k r K_0'(k r) \right]_0^\infty d k = \left[\frac{z}{(z^2 + r^2)^{3/2}} \right]_0^\infty$$

The limits for $k r K_0'(k r)$ are evaluated as follows:

From $K_0(v) = A \int_0^\infty e^{-v \cosh \varphi} d \varphi$ we have

$$K_0'(v) = \frac{d K_0(v)}{d v} = -A \int_0^\infty \cosh \varphi e^{-v \cosh \varphi} d \varphi$$

This is zero for $v = \infty$ because v appears in the integrand in the form $v e^{-av}$ with $a > 1$. For the other limit we use an expression derived from the definitions of K, I, Y and J:

$$K_0(v) = -1/\beta Y_0(j v) + j \pi/2 J_0(j v)$$

or $K_0(v) = -I_0(v) \ln(\alpha v) + v^2/2^2 + \frac{v^4}{2^4 (2!)^2} (1 + \frac{1}{2}) +$

$$+ \frac{v^6}{2^6 (3!)^2} (1 + 1/2 + 1/3) + \dots$$

Upon differentiating we find that the only term in $v K_0'(v)$ that does not contain the factor v is $I_0(v)$ and as $I_0(v) = 1$ for $v = 0$, also $v K_0'(v) = 1$ for $v = 0$ as all other terms vanish. We have therefore: $v K_0'(v) = 0$ for $v = \infty$ and $v K_0'(v) = 1$ for $v = 0$.

Hence $\left| k r K_0' k r \right|_0^\infty = -1$ and our equation becomes:

$$\frac{2B}{2\pi} \int_0^\infty \frac{\sin k z}{k} dk = 1 \quad \text{or} \quad \frac{2B}{\pi} \cdot \frac{\pi}{2} = 1 \quad \text{which gives } B = 1.$$

This means that the final formula for the inverse distance from the origin is:

$$\frac{1}{r} = \frac{2}{\pi} \int_0^\infty \cos(k z) K_0(k r) dk$$

B) Specifications of the Input Transformer and Computation of its Primary Inductance.

Specification No. 4088H

Primary and secondary balanced and each consisting of two turns in series having 3000 windings. (This means 6000 windings each for primary and secondary).

Core: #44 Allegheny Ludlum mu metal (initial permeability 15,000).

Lamination No. ei-21; $\frac{1}{2}$ " lamination stack.

Cross section $\frac{1}{2}$ " x $\frac{1}{2}$ " Stacking factor .90 .

Shielding: 4 copper and 4 mu metal shields. Steel outer case; electrostatic shield between primary and secondary.

The impedance of the primary with open secondary is computed as follows:

The induced voltage due to a sinusoidal varying flux,

$$\varphi = \varphi_0 \sin 2\pi f t, \text{ is:}$$

$$e = 10^{-8} \frac{N d\varphi}{dt} = 2\pi f N \varphi_0 10^{-8} \cos 2\pi f t.$$

Here N is the number of windings and f is the frequency. The rms value

of the voltage is: $E = \frac{2\pi}{2} f N \varphi_0 10^{-8} = 4.44 f N \varphi_0 10^{-8}$ Volts. In

the primary coil, the impressed and induced voltage are equal if we neglect the resistance and core losses, and the flux can be found from the impressed voltage:

$$\varphi_0 = \frac{10^8 E}{4.44 f N}$$

where f = 1000 cycles.

With E between 0.1 and 0.01 volts and N = 6000 we have

$$\varphi_0 = \frac{10 E}{4.44 \times 6000 \times 1000} = 0.038 \text{ to } 0.38 \text{ maxwells.}$$

The corresponding flux density is found from $B = \varphi/A$ gauss, where A equals the cross sectional area of the core in cm^2 times the stacking factor: $A = .90 \times 1/4 \times (2.54)^2 = 1.45$

This gives: $B = .0262$ to $.262$ gauss.

From the normal magnetization chart for μ metal (from the Allegheny Ludlum catalogue) we find that for these flux densities, the permeability μ equals 15,000 cgs units.

By definition $L = 10^{-8} N \frac{d\varphi}{dI}$ where I is the current.

We had $\varphi = BA = \mu HA$ where H is the magnetizing force which equals $\frac{F}{l}$ oersteds, with l denoting the equivalent flux path. F , the magnetomotive force is given in cgs units by $F = \frac{4\pi NI}{10}$ gilberts.

This gives us $= \frac{4\pi NI}{10} \frac{\mu A}{l}$

Substituting this in the above expression for L we have:

$$L = \frac{0.4 \pi N^2 \mu A}{l \times 10^8}$$

For the ei-21 lamination the equivalent flux path is 8.26 cm.

$$L = \frac{1.26 \times (6000)^2 \times 15,00 \times 1.45}{8.26 \times 10^8} = 1188 \text{ Henrys}$$

The value found experimentally in the transformer engineers' laboratory was $L_p = 1170 \text{ H}$.